Supramolecular Systems for Diol and Fluoride Recognition

Xu, Suying

Award date:
2014

Awarding institution:
University of Bath

Supramolecular systems for diol and fluoride recognition

Su-Ying Xu

A thesis submitted for the degree of Doctor of Philosophy

University of Bath

Department of Chemistry

January 2014

COPYRIGHT

Always Do Your Best. Your best is going to change from moment to moment; it will be different when you are healthy as opposed to sick. Under any circumstance, simply do your best and you will avoid self-judgment, self-abuse and regret.

--Miguel Angel Ruiz

Contents

Abstract

Determination of a target molecule is of great importance both in industrial applications and human health. For a long time, this has attracted the extensive attention of researchers to develop new strategies. One of the vigorous sub-branches lies in supramolecular field. its ability to mimic a natural occurring event and unearth the mode of interaction for a targeted molecule. By varying the structure of a probe, researchers could rationally design synthetic sensors with selective binding affinity to target molecules and also satisfy different requirements for a certain application by combining different functional groups.

The growing incidence of diabetes has promoted scientists to develop new effective strategies for early and quickly monitoring saccharide concentration. Interest in boronic acid-based saccharide probes has dramatically increased in the past several decades due to the unique properties of forming boronate esters with *cis*-diols. Previous work in James group demonstrated that by the introduction of a proximal amine group, the binding between boronic acid and saccharide can occur at neutral, *i.e.*, physiological pH and the binding between boronic acids and saccharides can induce fluorescent "turn-on" responses.

Acrylamide hydrogels with boron-additives have potential applications in separating saccharides and recognising glycation process in electrophoresis. Two monoboronic acid-based gel monomers **27** and **28** with different fluorophores have been synthesised and analysis measurements were carried out both in hydrogel, as well as in solution.

As a Lewis acid, the strong binding affinity between boron and fluoride was also extensively explored to develop fluoride sensors. By investigating boron-containing 1,8-naphthalimide derivative **33**, it is found that the binding between boron and fluoride could induce a red-shift of absorption (about 20 nm) with obvious colour changes and unique changes of NMR chemical shift. By comparison with control compounds (**34** and **35**), it was found that the addition of the boronic acid moiety would improve the selectivity, though at the expense of loss of sensitivity towards anions.

Traditional molecular recognition is mainly based on host-guest interaction, where a synthetic host molecule could selectively interact with a guest molecule *via* weak and

generally reversible interactions. The reaction-based sensing strategy is a new strategy in designing a high sensitivity probe toward a specific analyte, in which an irreversible reaction is normally utilised. Boronic acid moieties were extensively used both in exploring saccharide sensors and organic synthesis (Suzuki Homocoupling reaction). Here these two aspects were combined together to develop a Suzuki Homocoupling reaction-based saccharide sensing strategy. Different boronic acid substrates were employed and the sensing mechanism was investigated

Furthermore, as a collaboration project, colorimetric enantioselective recognition of chiral secondary alcohols was achieved *via* hydrogen bonding to a chiral metallocene containing chemosensor (**38** and **39**).The observed enantioselectivity of **38** could partly be due to the steric effect of the formed hydrogen bond complexes and the distance to the chiral centres.

Acknowledgement

First I would like to thank Prof. Tony James from University of Bath in UK and Prof. Yun-Bao Jiang from Xiamen University in China. Without their good collaborations, I would not get the chance to study in University of Bath. It is their kind guidance and support that help me to overcome the difficulties I met during the last four years. I am also very grateful for financial support from China Scholarship Council (CSC) and University of Bath Full Fees Scholarship.

Many thanks also go to members in Tony's group for their help both in daily life and academic research. It is the first time that I have been so far away from home and also the first time I have been abroad. They are always ready to help me in every aspect: Dr. Steve Flower and Winson who picked me up on the first day I arrived in UK. They gave me the first great welcome and lots of help in later life. Sabrina, just like my sister, helps me to learn how to carry out the scientific research in a proper way and get me familiar with the lab. I do believe difficulties will make us stronger and better. I hope she will have a great life in the future. Joshua helped me from the time I left China and gave me a lot of guidance on my experiments when I started my PhD. Owen, Kate and David are never hesitated to help me to get used to the life here and also tell me lots of interesting culture about UK. Thanks also go to Tomoki, silent but warm-hearted Post-doc. He taught me a lot on how to be effective in research. Thanks also go to the new comers: first year PhD students Chris, Jessie and Shawn. It is all the group members that give the group a sense of home.

I owe my thanks to people I met in Jiang's group. Yi-Bin and Yu-Feng led me to have the first taste of research when I was an undergraduate. It's at that time when I got the feeling of being a scientist. Dong-Hua and Jin-song gave me lots of help on my project and lots of tips for forming good habits when doing

research. Many thanks will go to Jiang-Shan, who gave me lots of advice until now. You all are my life-long friends.

Thanks also go to all the staff in Department of Chemistry making everything go smoothly in research activities. Special thanks go for John helping me analysing NMR spectra; Dan Pantos for giving me advice in tackling problems; Prof. Frank Marken for helping in doing electrochemistry and Dr. Toby Jenkins for offering me a chance to attend the "bio-nano summer school", which is a fantastic experience.

To BoBo, Le, Wei and Junzhe, those past and present friends I met in Bath, lots of great memories in my life are accompanied by you, especially thanks for BoBo bringing me lots of delicious food; All of you make my life in Bath full of joy and happiness. I am very thankful to friends I met in UK. Qinquan Gao offered me a great chance to be involved in the Xiamen university alumni association in UK and also gave lots of help whenever I went to London. I so much appreciate knowing you.

Finally, I want to give my special and most grateful thanks to my family. Without their continuous support and understanding, by no means, could I go through the ups and downs of the past 26 years. Most grateful thanks to my mum, giving me the chance to come to the wonderful world, showing me the road to knowledge and supporting me without any spare efforts. It's my most regret not having you to see what I am today. You are always living in my heart. I love you more than I can say.

Abbreviations

Å	Ångström
AIBN	2,2'-azobisisobutyronitrile
AIE	aggregation induced emission
Alloc	allyloxycarbonyl
Ar	aryl
APS	ammonium peroxydisulfate
ARS	Alizarin Red S
AuNPs	gold nanoparticles
BASE	boronate affinity in saccharide electrophoresis
BBV	bis-boronic acidappended benzyl viologen
b. p.	Boiling point
bp	by product
br	broad
Boc	*tert*-butoxycarbonyl
°C	degree Celsius
$CDCl_3$	deuterated chloroform
cm^3	cubic centimetre
cm^{-1}	wave numbers
Con A	Concanavalin A
COSY	correlated spectroscopy
CPK model	space filling model
δ	chemical shift in parts per million
Δ	heat
2D	two dimensional
D	deuterium (^2H)
d	doublet
dL	decilitre
DCM	dichloromethane
dm^3	cubic decimetre
DMSO	dimethyl sulfoxide
DMF	dimethylformamide

ds	doublet and singlet
e^-	electron
ELISA	enzyme-linked immunosorbent assay
ESI-MS	Electrospray Ionization Mass Spectrometry
Et	ethyl
EtOAc	ethyl acetate
EtOH	ethanol
eq.	Equivalent
FASE	fluorophore-assisted carbohydrate electrophoresis
FLAB	fluorophore linker boronic acid biotin
FRET	Froster resonance energy transfer
g	gram
GOx	glucose oxidase
h	hours
hib	*Haemophilusinfluenzae* type b
$h\nu$	incident light
HEPES	*N*-(2-hydroxyethyl)-piperazine-*N*'-2-ethanesulfonic acid
HOMO	highest occupied molecular orbital
HPTS	8-hydroxypyrene-1,3,6-trisulfonic acid trisodiumsalt
I	fluorescence intensity
IDA	indicator displacement assay
I/I_0	relative fluorescence intensity
ICT	internal charge transfer
J	coupling constant
k	rate constant
K	stability constant
K_a	acidity constant
K_a'	acidity constant of complexed boronic acid
K_{obs}	observed stability constant
K_{tet}	ligand – tetrahedral boronate anion stability constant
K_{trig}	ligand – trigonal boronic acid stability constant
kJ	kilojoules
λ	Wavelength
λ_{em}	emission wavelength

λ_{ex}	excitation wavelength
L	Litre
LUMO	lowest unoccupied molecular orbital
µM	micromolar
µm	micrometre
µL	microlitre
µg	microgram
m	*meta*
m	unresolved multiplet / minutes
M^{-1}	cubic decimetres per mole
$[M]^+$	parent molecular ion
Me	methyl
MeCN	acetonitrile
MeOD	deuterated D4 methanol
MeOH	methanol
mg	milligram
MHz	megahertz
MLCT	metal-ligand-charge transfer
mm	millimetre
mM	millimolar
mmol	millimole
mol	mole
Ninhydrin	2,2-dihydroxyindane-1,3-dione
m. p.	melting point
NBS	*N*-bromosuccinimide
nm	nanometre
NMR	nuclear magnetic resonance
ns	nanosecond
o	*ortho*
p	*para*
PAGE	polyacrylamide gel electrophoresis
PBA	phenylboronic acid
PET	photo-induced electron transfer
pK_a	- log K_a

ppm	parts per million
q	quartet
QD	quantum dot
R^2	goodness of curve fitting
R_f	retardance factor
RET	resonance energy transfer
RIR	restriction of the intramolecular rotation
rt	room temperature
s	singlet / second
S_0	singlet electronic ground state
S_1	first singlet electronic excited state
S_2	second singlet electronic excited state
SPR	Surface Plasmon Resonance
t	triplet
T_1	first triplet electronic excited state
TBAB	*tetra*-*n*-butylammnonium bromide
TBACl	*tetra*-*n*-butylammnonium chloride
TBAF	*tetra*-*n*-butylammnonium fluoride
TBAF	*tetra*-*n*-butylammnonium iodide
TFA	trifluoroacetic acid
THF	tetrahydrofuran
TICT	twisted internal charge transfer
TLC	thin layer chromatography
TMEDA	*N*, *N*, *N'*, *N'*-tetramethylethane-1,2-diamine
TMS	tetramethylsilane
TPE	tetraphenylethene
UV	ultraviolet
wt%	weight percent

CHAPTER ONE

Introduction

1 Introduction

1.1 General introduction

Optical sensor

According to the IUPAC definition, a chemical sensor is a device which transforms chemical information into an analytically useful signal. Optical sensors, are molecules which would give optical changes when bound with a target molecule. UV-*vis* absorption and fluorescent emission are the most common optical tools for sensing. With regards to fluorescence, its high sensitivity, multiple parameters and simplicity attracted great efforts for developing a single molecule detection technique or technique for studying biological events. Here, the general sensing mechanisms involved in designing fluorescent sensors will be introduced.

Saccharides and its interactions with boronic acid moiety

Together with nucleic acids, proteins and lipids, saccharides, commonly known as carbohydrates, are four of the main kinds of biomolecules.[1] There are four major roles of saccharides: a) they are an energy source and the oxidation of them serves as the central energy-generating pathway in most non-photosynthetic cells.[2] b) glycans (carbohydrate polymers) play a vital role in cell membrane structure as well as providing a protective element. A rigid structure can be formed when saccharide molecules combine together. c) by combining with proteins or lipids, carbohydrate polymer complexes act as identification tags, a crucial feature in cell-cell recognition. Furthermore, their information-carrying potential is expected to be much higher than that of nucleic acids of equivalent molecular weight. d) carbohydrate-based therapy is an important field, which has already benefited many people. A bacteria called *Haemophilusinfluenzae* type b (*Hib*) has affected thousands of children a few decades ago, and was eventually eliminated by a sugar-based vaccine.[3] However, the complex

structures of carbohydrates make them hard for scientists to synthesise and analyse, which confines the research on carbohydrates to a small niche.

The simplest carbohydrate is a monosaccharide, consisting of a single polyhydroxyl aldehyde or ketone unit. These monosaccharide could form disaccharides, oligosaccharides and polysaccharides through a characteristic linkage, namely glycosidic bonds. The most abundant monosaccharide is the six carbon sugar, D-glucose. According to the position of the carbonyl group, they can be classified as aldose (an aldehyde group) and ketose (a ketone group). One of the reasons why saccharide structure is so complicated is that saccharides with four carbons or more tend to form cyclic structures[1], in which the carbonyl group forms a covalent bond with the hydroxyl group along the chain. During this process, a hydroxyl group in two stereoisomeric forms is produced. Also, maturation takes place when saccharides are dissolved in aqueous solution. Taking D-glucose as an example, when dissolved in aqueous solution, the linear structure can produce two cyclic structures: furanose (five-membered ring) and pyranose (six-member ring), each cyclic structure giving rise to two stereoisomers, designated α and β . Thus, there are five configurations for D-glucose in aqueous solution in varying quantities (Scheme 1).[4] However, the six-membered aldopyranose ring is the most stable and predominate configuration in solution.

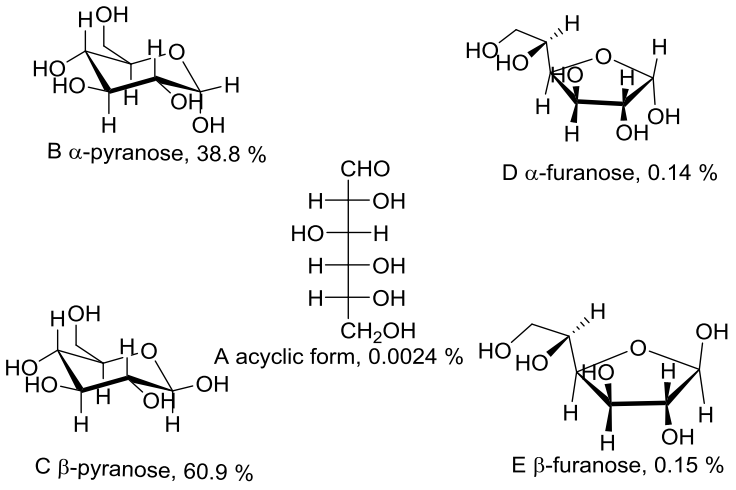

Scheme 1 D-Glucose in its various configurations and the percentage composition at equilibrium of each form of the sugar in D_2O at 27 ℃

Considering these different conformation structures in solution, it's not hard to imagine the difficulties faced by scientists when trying to analyse them. However, determination of saccharides is of great importance in various aspects like blood glucose monitoring[5] . The normal blood glucose level in the human body is between 4.4 and 6.1 mM (82 to 110 mg/dL). Blood sugar concentration deviation from the normal level usually is an implication of an underlying medical condition. Low levels (hypoglycemia) can cause fainting or death while persistent high levels (hyperglycemia) usually result in diabetes mellitus, which affect millions of people with complications such as heart disease, blindness, kidney failure and stroke.[6] Early diagnosis of cancer[7] is another issue researchers tried to achieve, as this could allow for better and successful therapy. Saccharides and their glycoconjugates regulate tumour proliferation and invasion, thus early detection is vital to reduce the morbidity and mortality caused by cancer. For decades, scientists have developed new methods for saccharide detection. Great progress has been achieved and some of these methods are now commercially available.

It's well known that boric acid can form a complex with diols, with hydroxyl groups in favourable 1,2- and 1,3- configuration, by means of which the structures of pyrannose and furanose forms of D-glucose were determined in 1913.[8] However it was not until 1959 that the first quantitative investigation into the interaction of boronic acid and polyols was reported.[9] Lorand and Edwards suggested a tetrahedral, rather than trigonal structure of boronic acid. The X-ray structure of unbound boric acid showed an O-B-O bond angle of 120.0°,[10] suggesting an sp^2 trigonal planar geometry. When under alkaline condition, the boronate anion is formed, which is in sp^3 geometry, with an O-B-O bond angle of 109.5°. Another investigation[11] gave the single-crystal X-ray structure of the diphenylboronic acid-fructose complex under non-basic conditions, which indicated an O-B-O bond angle of 113.65°. When forming boronate ester with saccharides under non-alkaline conditions, the compressed angle reduced to the value between the bond angles for sp^2 and sp^3 geometry. As it is known that the *s* orbital are closer to the nucleus than the *p* orbitals, thus *s* orbital shows more Lewis acidic characters than those in *p* orbitals. Due to orbital changes of boron atom from sp^2 to sp^3, the empty *p* orbital has some *s* orbital character, which has an increase of exposure of nucleus, resulting in increased boron acidity. The increased acidity of boron atom would strengthen interactions between boron atom and oxygen atom of the approaching

water, which in turn weakens the adjoining O-H bond, thus induces the liability of the acidic hydrogen. When diols interact with boron, the Lewis acidity of boron increases and B-O bond is strengthened, which in turn facilitates deprotonation, leading to the reduction in pK_a.[12] This result also explains why the K_{tet} is four orders of magnitude larger than K_{trig} as well as $pK_a > pK_a'$ in Scheme 2. Rehybridisation makes the boronate ester ring less strained and lowers the energy of the system, which is therefore more stable.

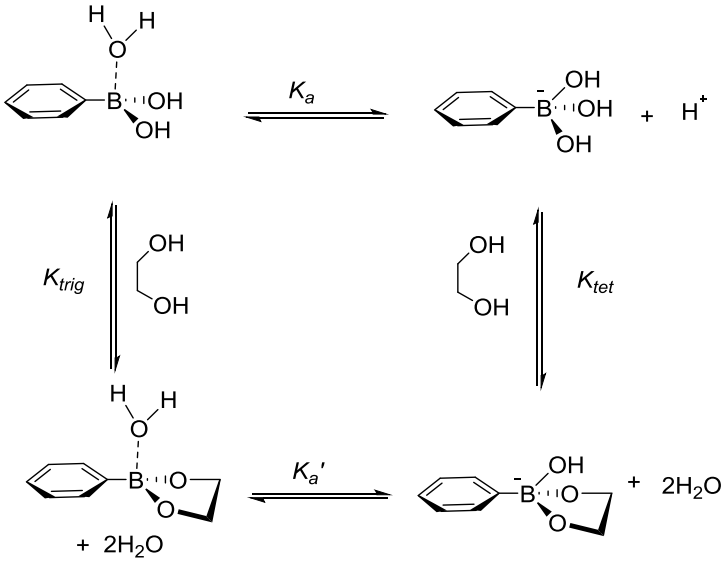

Scheme 2 The thermodynamic cycle of boronic acid with diol

The rapid and reversible interaction between boronic acid and diols offers a perfect platform for saccharide detection considering their numerous hydroxyl groups available on saccharide molecules. Thus many saccharide sensors have been developed taking this interaction as part of the fundamental design concept.

Fluoride and the interaction with boron compounds

Anion recognition is one of the most challenging issues for analytical chemists due to the complexity of their geometries, small charge to radius ratios and also heavy solvation.[13-15] All these factors result in anions having a weaker binding affinity than that of cations, which have smaller size and large charge values. Additionally, anions

are prone to be protonated and the binding strength and selectivity would also be strongly affected. Most of the reported anion sensors are synthetic host substrates, as the synthetic strategies could allow design of matching binding site geometry for specific anions. In this regard, several excellent reviews have summarised the development of anion chemosensors.[14, 16-18] Among these achievements, fluoride recognition has attracted considerable interest not only because of its unique properties, but also its vital importance in our daily life.

Fluoride anion has many applications in industrial areas and also used in toothpaste. Typical levels in the blood have been reported to be in the range of 20-60 $\mu g\ L^{-1}$, determined by using a fluoride selective electrode.[19] Fluoride used to be added to drinking water in the United States of America, as a way to prevent tooth decay. However, recent research results showed its duplicitous nature, as high levels would induce several human pathologies. Fluoride is also the hydrolysis product of UF_6 and phosphorofluoridate nerve agents, which could be tracked by monitoring fluoride concentration.[17] Fluorine is the most electronegative element, that is, a strong Lewis base, with hydration enthalpy as high as -504 kJ/mol. These unique properties make it possible to design highly selective fluoride chemosensors. Currently, fluoride concentrations are determined by using an LaF_3 containing electrode.[20] However, in some cases, it has its limitations such as direct visualisation of intracellular fluoride and other aspects.

Amide, urea, thiourea, guanidinium, or pyrrole functionalities are usually utilised in designing fluoride sensors due to their hydrogen bonding capacities with fluoride. Another alternative way is employing Lewis acidic receptors that can bind fluoride ions through covalent bonds. Boron is known for its electron deficiency, which could serve as an ideal candidate for fluoride recognition. Usually boron atoms exist in a sp^2 hybridised state, leading to a planar conformation, yet after binding with fluoride, the sp^2 hybridisation of boron converts to sp^3 hybridisation. Thus, the photophysical properties of the whole compound are greatly altered. Based on this change, many fluoride probes have been developed.

1.2 Concepts of fluorescence

1.2.1 Fluorescent spectroscopy

Electrons prefer residing in ground-state orbitals, those excited to the excited states will return to the ground states, accompanied by energy release. According to the different ways of energy release, those in the form of light, are called luminescence. Fluorescence occurs, accompanied by the transformation of an electron from its excited state (S_1) to its ground state (S_0). Another emission pathway, similar to that of fluorescence, where electrons are transferred from its triplet state (T_1) to the ground state, calls phosphorescence. Jabłoński diagrams (Scheme 3) showed the difference of these two pathways. Electrons will be excited to the excited states such as S_1 and S_2, after absorbing a certain wavelength of light. Then they quickly relax to the lowest vibrational level of S_1 through internal conversion. The decay of the excited electron from a singlet excited state (S_1) to the ground state (S_0), is a spin-allowed process as it has opposite spin to the electron in the ground-state orbital. Thus typical fluorescence lifetime is about 10 ns.[21] However, some excited electrons also undergo a spin conversion process and transfer to the first triplet state T_1. The decay from T_1 to S_0 is typically with longer lifetime as it is spin-prohibited. Some phosphorescence could last a few hours.

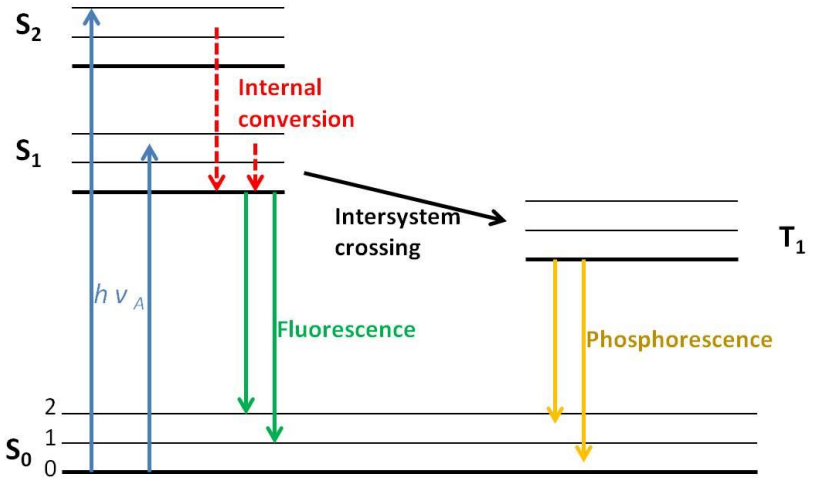

Scheme 3 Jabłoński diagram showing various energy transitions in common optical events.[21]

There are several unique characteristics of fluorescence, such as the Stokes shift, maximum emission wavelength, fluorescent intensity. Due to internal conversion, the wavelength where fluorescence emission occurs is often longer than that at which absorption happens. The wavelength shift is called Stokes shift. Another property of fluorescence is that the maximum emission wavelength remains the same when changing the excitation wavelength. As whichever level the molecule is excited to, internal conversion will quickly remove the excess energy and fluorescent emission always takes place at the lowest vibrational state of S_1 state. Since emission is the opposite process to absorption, the emission spectrum is often the mirror image of absorption, though there are some exceptions.

As for applying fluorescence in a sensing aspect, fluorescent intensity, wavelength shift, lifetime, anisotropy and quantum yield are the common used parameters. A linear relationship can be obtained by plotting the parameter changes *versus* analyte concentration. But fluorescence applications are not solely in the sensing aspect. By using near-infrared fluorophores, it is possible to achieve non-invasive monitoring or labelling.[22] Using fluorescence anisotropy changes, protein-protein interaction can also be investigated.[23]

1.2.2 Types of sensing mechanisms

The mechanisms used for sensing include internal charge-transfer (ICT)[24], photo-induced electron transfer (PET)[25, 26] and resonance energy transfer (RET). This thesis focuses on the applications of boron in the sensing field and thus the following examples are based on boron-containing sensors.

1.2.2.1 Sensing systems based on internal charge-transfer (ICT)

For the boronic acid-appended fluorescent ICT sensors, the receptor and fluorophore groups must be integrated so that there is overlap between them, shown in Scheme 4.

The added saccharides cause the changes of electronic properties of donor or acceptor, inducing a shift in emission wavelength, which are taken as a signal reporter together with the fluorescent intensity changes. The boronic acid moiety usually acts as an electron acceptor in its neutral form. However it would be switched to a donor group when in its anionic form (tetrahedral form) at a certain pH value.[27] When the fluorophore is the donor group, the boronic acid takes a role as the acceptor group. Along with a re-hybridisation of boron from sp^2 to sp^3, its acceptor ability is lost, leading to a loss of ICT process. The emission spectra would display a blue shift, upon binding with saccharides with an increase in fluorescent intensity. For fluorophores bearing an electron withdrawing group, the emission spectra changes are reversed.

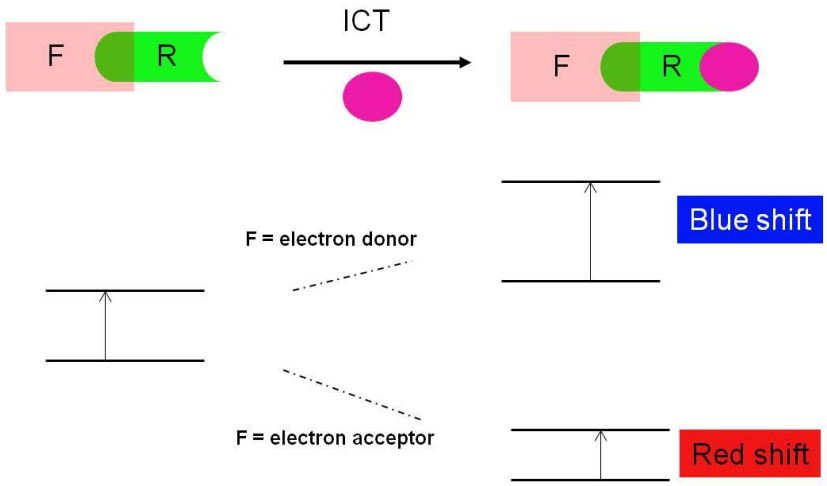

Scheme 4 Illustration of ICT sensing mechanism

The first ICT sensor for saccharides was developed by the Shinkai group,[28, 29] which achieved the recognition of saccharides at neutral pH in aqueous solution. The James group[30] further developed a D-glucose selective fluorescent ICT sensor (compound **1**), which exhibits a large change in the intensity as well as the wavelength of the emission maxima. A 45 nm blue shift of the emission wavelength was observed upon addition of D-glucose with an observed binding stability value of 140 mol^{-1} dm^3, two times larger than that with D-fructose.

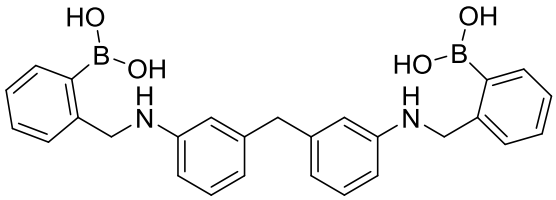

1

Lakowicz *et al* has done a lot of work on ICT-based fluorescent sensors. By following Shinkai's initial work, a series of stillbene based boronic acid analogues were synthesised and then further developed into probes taking diphenyloxazole as the reporter component.[31] When in its neutral form, compound **2** has maximum emission at 557 nm with a quantum yield of 0.03 and a monoexponential lifetime of 2.8 ns at pH 7. After combining with D-fructose, the maximum emission appeared at 488 nm, with a quantum yield of 0.95 and a monoexponential lifetime of 3.6 ns. Addition of saccharide also induce the conformation changes of compound **2**.

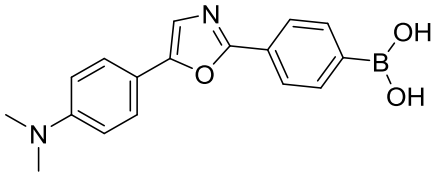

2

1.2.2.2 Sensing systems through photo-induced electron transfer (PET)

Another distinct design principle is photo-induced electron transfer (PET), which is characterised by the format of "fluorophore-spacer-receptor". This mechanism involves a one-electron reduction/oxidation process as the excess energy contained in a photo excited state fluorophore could induce such electron transfer. The excited fluorophore can be either an electron donor or electron acceptor, leading to a "switchable" nature of PET sensors. The direction of electron transfer is dominated by the oxidation and reduction potentials of its ground and excited states. The illustration shown in Scheme

5 is a “switch-on” sensor. The oxidation potential of the free receptor is less than that of the fluorophores in their excited states and an electron is released from the receptor to the fluorophore, leading to a quenched fluorescence, which could be described as an excited state deactivation pathway that quenches the fluorescence of the fluorophore. In terms of frontier molecular orbital theory, the highest occupied molecular orbital (HOMO) of the free receptor is higher in energy than the HOMO of the fluorophore. Upon photon excitation fluorescence is quenched by an electron transferring from the HOMO of the free receptor to the HOMO of the fluorophore. Yet, once bound to the analyte, the HOMO energy of the bound receptor is lower than the HOMO of fluorophore, resulting in a fluorescence recovery. The total result is that addition of an analyte can induce an increase fluorescence intensity of a fluorophore.

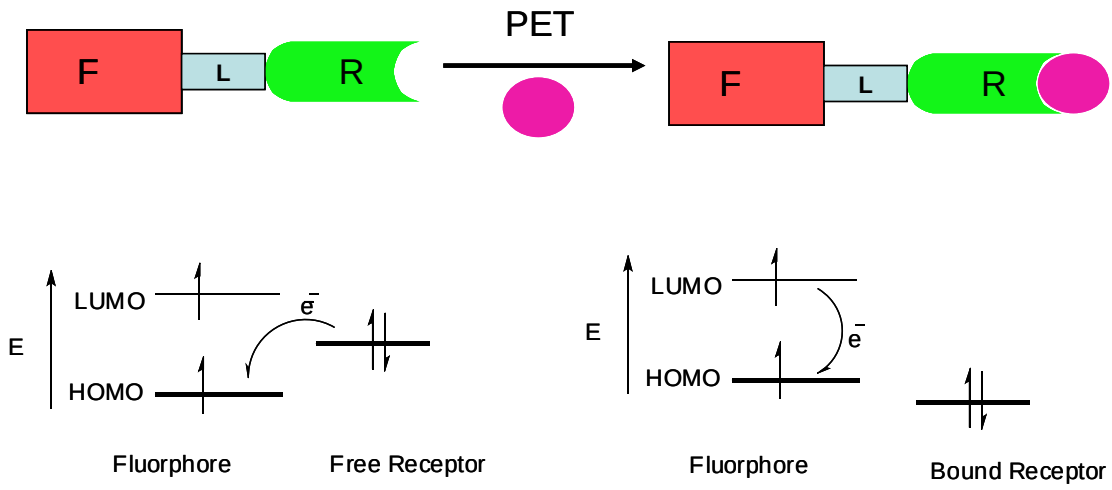

Scheme 5 Illustration of PET mechanism and interpretation by frontier molecular orbital theory

The initial work on saccharide recognition based on PET was carried out by Shinkai and James.[32] Compound **3** tolerated a broad pH range for saccharide sensing and a large increase in fluorescence upon adding saccharides. Before binding the saccharide, the lone pair electrons on the nitrogen atom have mostly quenched the fluorescence of the anthracene group due to PET process. Following the formation of boronic acid-saccharide complex, the boron-amine interaction was greatly enhanced, leading to reduced electron density around nitrogen atom, and thus inhibited the PET quenching

process. It's well known that monoboronic acid has an inherent trend in selectivity toward saccharide: D-fructose > D-galactose > D-glucose.[9] While glucose detection has more important meaning in clinical application, efforts have been long devoted to this goal. Based on the CPK molecular models, James *et al* rationally designed another probe **4** [33] as the first boronic acid-based fluorescent PET sensor with high selectivity toward D-glucose by introducing two binding sites and with proper space assignment. The conformation flexibility was much reduced once the boron-nitrogen bond formed, with two inwardly facing boronic acid groups resulting in a convergent binding cavity, elegantly positioned for binding 1,2- and 4,6-hydroxyls of glucose.

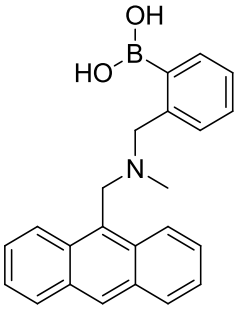

3

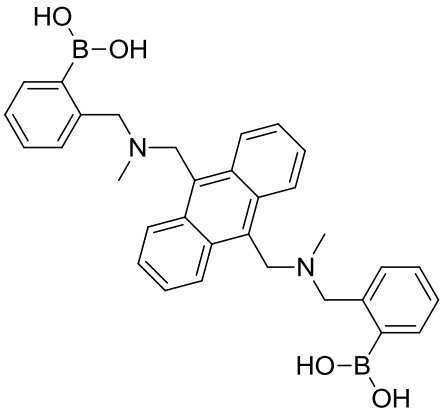

4

1.2.2.3 Förster resonance energy transfer (FRET) system

FRET, also known as fluorescence resonance energy transfer, is used to describe energy transfer between two chromophores. The two choromophores are generally

named after their functions, donor and acceptor. If the emission of the donor could be overlapped by the absorption of the acceptor, the donor choromphore, when in its electronic excited state, will transfer energy to the acceptor chromophore through non-radioactive dipole-dipole coupling (Scheme 6). This process results in a decrease in the donor emission intensity and/or excited relaxing time, accompanied by an increase in acceptor fluorescence intensity. [21, 34] The energy transfer efficiency is dependent on the inverse sixth power of the distance between donor and acceptor. This distance dependent process makes FRET a useful tool to investigate molecular level interaction as well. Meanwhile, the energy transfer could occur in an intramolecular or inter-molecular mode, shown in Scheme 6(a) and (b).

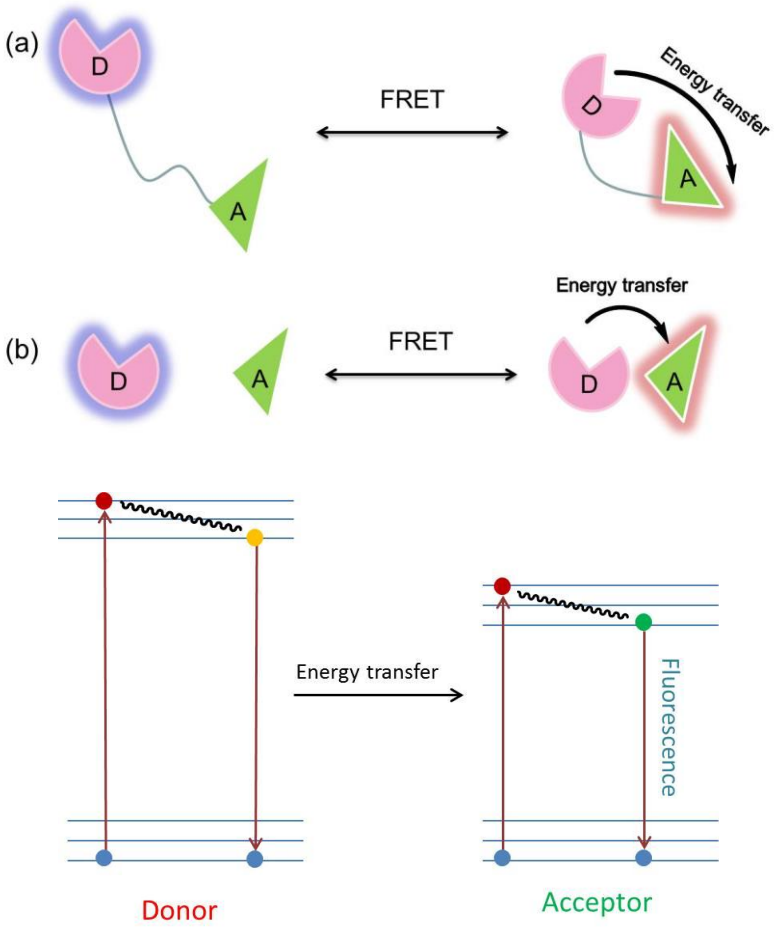

Scheme 6 Illustration of FRET systems and Jabłoński diagram of this process

A boronic acid-modified QDs based saccharide sensor *via* a FRET mechanism was developed by the Willner group.[35] Glutathione (GSH)-capped CdSe-ZnS QDs, covalently linked to 3-aminophenyl boronic acid, could form a boronate ester with ATTO-590-labeled-galactose, the formed complex leading to FRET from the QDs to the dye. After saccharide addition, competition occurred between the analyte and dye-labelled galactose, which facilitated the dissociation of the complex formed beforehand and thus reduced the FRET efficiency, that is, the increase of luminescence intensities of QDs and decrease fluorescent intensities of the dye, shown in Scheme 7. By using dopamine-functionalised-dye, dopamine sensing could be achieved. As for this strategy, improvement needs to be done to get the receptor selective to glucose without loss of the simplicity and efficiency of this method.

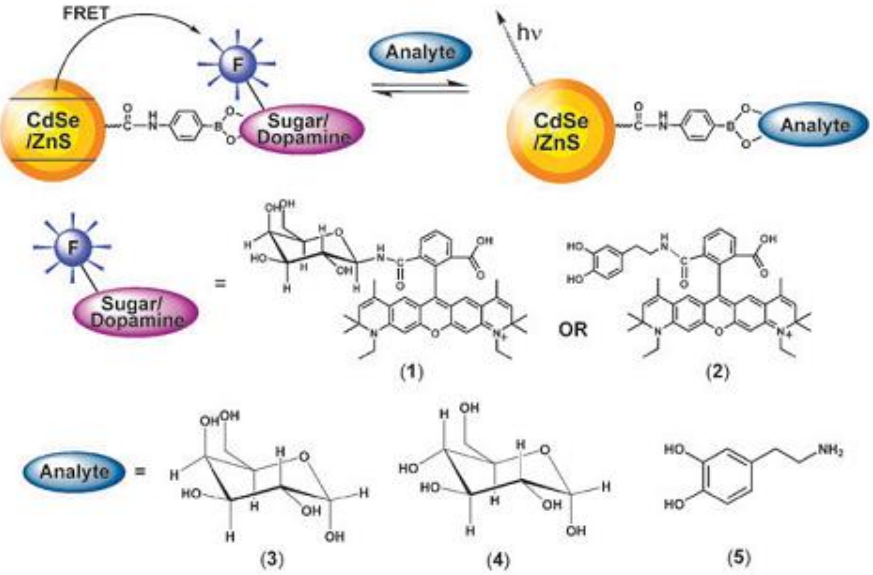

Scheme 7 Illustration of IDA based saccharide sensing using boronic acid modified-QDs and dye-labelled sugar *via* FRET (copyright)[35]

1.2.2.4 Alternative sensing mechanism

Except aforementioned mechanisms, other emissive phenomenons are also utilised in synthetic receptors, like metal-ligand charge transfer (MLCT), twisted intramolecular

charge transfer (TICT), aggregation-induced emission (AIE) and C=N isomerization, which could be ascribed to fluorescence changes *via* conformation restriction.[36, 37]

Another interesting example has been identified by Tang[38] and co-workers, who found a specific glucose sensing probe under a new concept. Tetraphenylethene (TPE) based diboronic acid (compound **5**) was synthesised. The binding between boronic acid unit and diol could activate the restriction of the intramolecular rotation (RIR), resulting in the aggregation of compound **5** and thus inducing aggregation-induced emission (AIE), non-emissive compounds becoming fluorescent when aggregated together. A proposed mechanism was that at high pH, the compound is non-emissive due to the dissolution by its charged boronate groups. Oligomerisation would occur with the continued increase of glucose since glucose tended to bind with two boronic acid units, thus acted as a linker between compound **5** molecules. Once the oligomer formed, RIR effect was greatly promoted. Saccharides, such as fructose and galactose, lack the ability to form oligomers, thus can hardly induce AIE phenomenon.

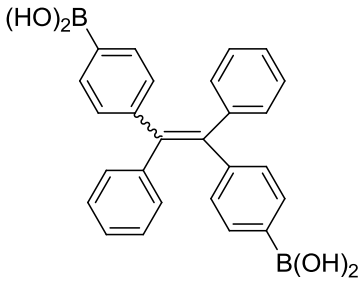

5

1.3 Saccharide recognition development

1.3.1 Previous work in the TDJ group

Our group is dedicated to developing strategies by applying the boronic acid moiety in various applications,[39] such as molecular recognition,[40-43] molecular self-assembly,[44]

chiral impurity determination,[45] electrochemical[46] and electrophoresis applications.[47] For all these aforementioned aspects, molecular recognition showed its prosperous development in recent decades, especially in saccharide recognition.

Our initial work[29, 32] has shown that the spacing of a diboronic acid sensor can provide an effective binding pocket for glucose. The linker length and conformational constraints have great impact on determining the specificity for glucose. Appleton and Gibson[48] first investigated this by varying the linker length between two boronic acid motifs and found that six- and seven- carbon linkers possessed the highest selectivity towards D-glucose. Our group has adopted a modular approach (Scheme 8) for the construction of saccharide sensors, which consists of three components: receptor unit, linker unit and fluorophore unit. By employing the modular approach, two *N*-methyl-*O*-(aminomethyl)phenylboronic acid groups remained the same while varying the methylene linker and fluorophores.[49] The linkers were varied from *n*-propylene (n = 3) to *n*-octylene (n = 8) and the compound with six carbons as the linker has the highest observed stability constants for D-glucose, which is consistent with previous results, reported by Appleton. By fixing the linker length while varying the fluorophores, it was found that the largest enhancement in observed stability was pyrene and naphthalene appended sensors, the former showing enhanced D-glucose selectivity and the latter D-galactose. The fluorophores have different hydrophobic ability and steric layout, which will directly influence the environment around the binding sites, thus affecting not only the emission wavelength but also the overall selectivity.[50]

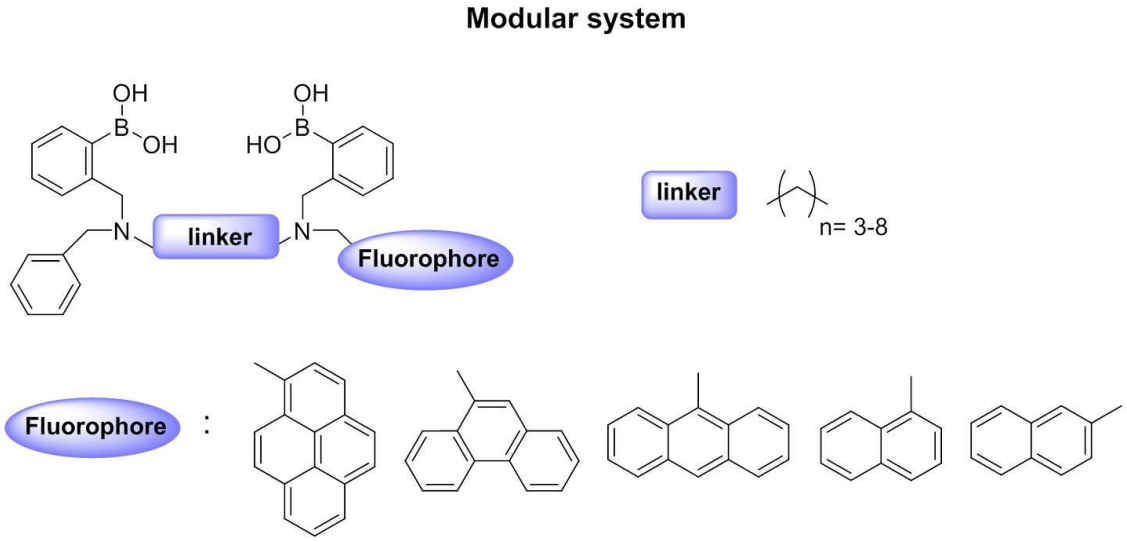

Scheme 8 Structures of modular sensor system

By applying modular design, another saccharide sensing platform[51] was built based on the fluorescence resonance energy transfer (FRET) mechanism. Results from compound **6** showed that in the presence of saccharide, when excited at 299 nm (phenanthrene), the fluorescence spectra showed the characteristic pyrene emission instead of emission at 369 nm, which means that the phenanthrene serves as the donor group and pyrene as acceptor.

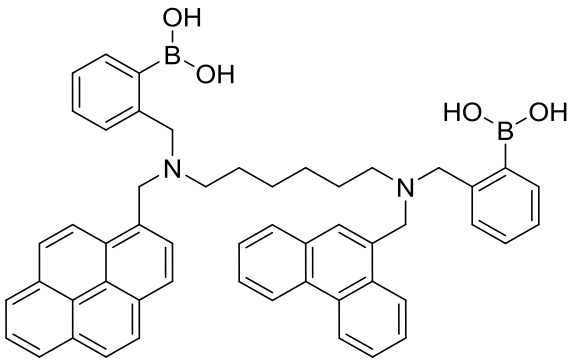

6

Following Shinkai's pioneering work on a synthetic colour sensor for saccharides,[52] Jame's group reported a series of azoboronic acid derivatives **7** with various

substitutions in order to modulate the electronics of the chromophore.[53] If large absorption shifts were observed after binding with saccharide, detection of saccharide would be achieved *via* universal indicator paper, similar to that of pH paper. Results showed that the binding constants increased as the Hammett – σ values for phenylazo-ring substituent reduced, the ring substitution becoming less electron-withdrawing. As for **7a**, the absorbance maximum shifted by 55 nm upon addition of saccharide. However, these sensors only worked well at the high pH value (11.32).

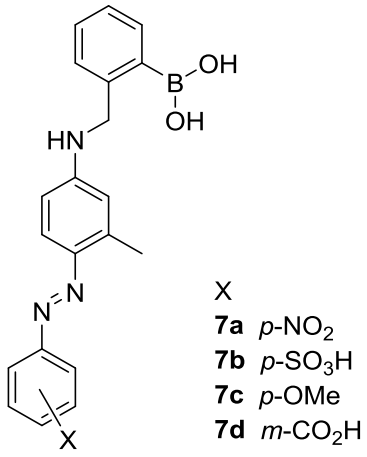

7

As most naturally occurring chemical species, including sugars and sugar acids, are chiral compounds, a chiral sensor is inherently better than that of an achiral one, since the chirality of analyte is another co-factor for discrimination. Thus our group designed chiral sensor **8** for sugar acids in 2004, such as tartaric acid, glucaric acid and gluconic acid, by cooperating a chiral centre near the binding site.[54] The enantioselectivities of tartaric acid is up to 550:1 and chemoselectivity up to 11000:1 with sensitivities in the micromolar range. And this selectivity is pH-dependent as well, higher pH values (8.3) giving higher enantioselectivity. Furthermore, the according monoboronic acid sensor was also synthesised, however, no enantioselectivity was observed, which indicated both the importance of the chiral centre and the modular construction of the binding sites are accounting for such high chemo- and enantioselectivity towards saccharide acids. Meanwhile, the same sensor was also used to investigate the responses to sugar alcohols.[55] It was found that this sensor shows excellent selectivity for six-hydroxyl sugar alcohols over those with five- or four-hydroxyl sugar alcohols. More importantly,

this probe can enantioselectively respond to six-hydroxyl sugar alcohols (D-mannitol and D-sorbitol) as the fluorescent enhancement is significantly different. The investigation of a monodentate sensor showed that two binding sites are necessary for high chemoselective binding in terms of sugar alcohols, which is attributed to the rigid linker and cooperative binding sites. As the binding pocket of **8** is rather crowded, 1:1 complex formation with bulky analytes such as monosaccharides is unfavourable. Also the steric requirements of sensor **8** also needed to be met in terms of the correct length of sugar alcohols, which is the reason why five- or four-hydroxyl sugar alcohols are not favourable.

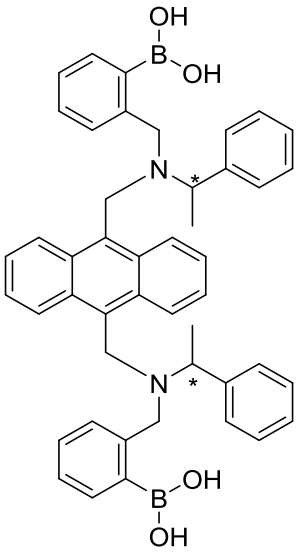

8 (R,R-**8** and S,S-**8**)

Based on the previously described modular approach of designing saccharide sensors, a molecular tweezers (**9**) design was thus postulated in 2009.[56] The two pyrene moieties have strong π-π stacking serving as a potential platform for enhancing selectivity. Thus two boronic acid groups were included, allowing either a 1:2 or 1:1 binding mode for each saccharide. Also, two hexamethylene linkers were also employed in order to introduce a degree of conformational flexibility into the system.

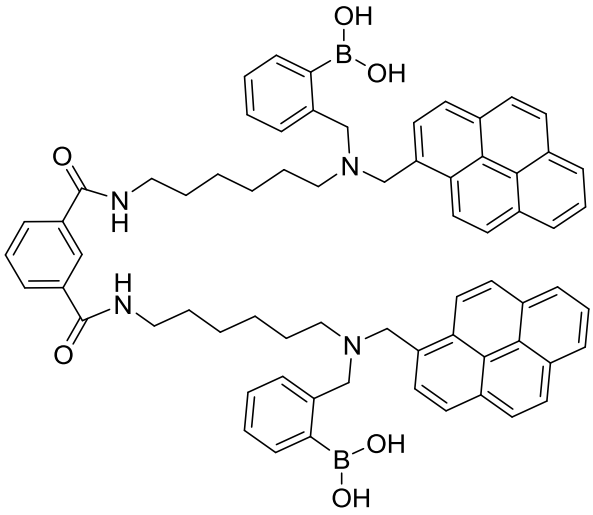

9

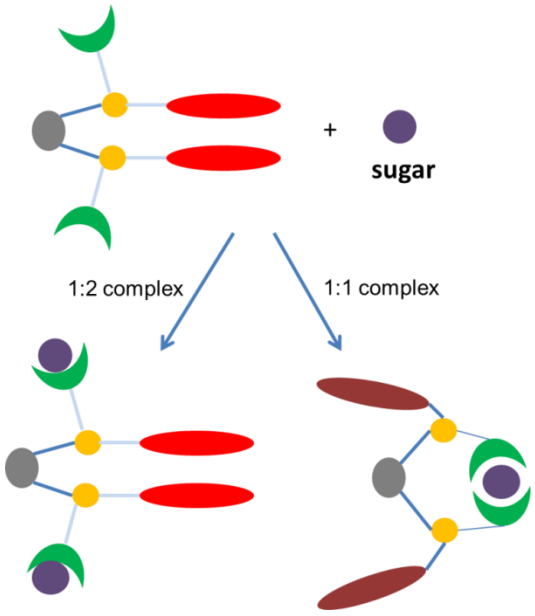

Scheme 9 Illustration of two different possible binding modes of molecular tweezers with sugars

Before addition of saccharides, compound **9** exhibits fluorescence emission at 470 nm, typical pyrene excimer emission due to the π-π interaction. There is an increased fluorescent intensity at 377 nm after addition of D-glucose, D-fructose, D-galactose and D-mannose. However, the fluorescent intensities at 470 nm showed different behaviours for different saccharides, it is invariant with the addition of D-fructose and decreases with increase of D-glucose and D-mannose. As for D-galactose, an initial quenching was observed at low concentration followed by fluorescence recovery when

concentration increases. This phenomenon could be attributed to the different binding modes (Scheme 9) between saccharides and compound **9**. A 1:1 cyclic complex was formed for D-glucose, D-mannose, formation of which would induce separation of the pyrene units, while only a noncyclic 1:2 complex forms for D-fructose without interfering with the excimer emission. As for D-galactose, it was believed that a 1:1 complex was formed at low concentration, followed by formation of 1:2 complex at higher concentration.

The indicator displacement assay (IDA) is an alternative method of probe design. In the traditional host-guest system, the host substrate is generally consisted of a receptor unit as well as a signal reporter unit. Yet, in an IDA system, the receptor and signal reporter are two separate units. Generally, these two units form a complex and addition of analyte would competitively bind with the receptor, which in turn releases the signal reporter, leading to the spectral changes of the signal reporter. Such a multi-component strategy simplifies the syntheses of probe and also allows for different indicators with same receptor. Boronic acids have previously been used in electrophoresis to separate saccharides.[47] Based on this work, hydrogels incorporating boronate units were reported to function as saccharide sensors. The sensing scheme was shown in Scheme 10. Polyacrylamide hydrogels were synthesised using acrylamide monomer, boronic acid containing acrylamide monomer and cross-linker reagent under initialising reagents of *N, N, N′, N′*-tetramethylethane-*1,2*-diamine (TMEDA) and ammonium peroxydisulfate (APS). Firstly the boron-hydrogel was incubated in Alizarin Red S (ARS) solution to generate the corresponding boronate ester. After washing off the excess ARS, the hydrogel was treated with different saccharides. The competitive binding results in release of ARS in solution. By recording the spectral changes of the hydrogel, the binding between the hydrogel and different saccharides were studied along with colour changes.

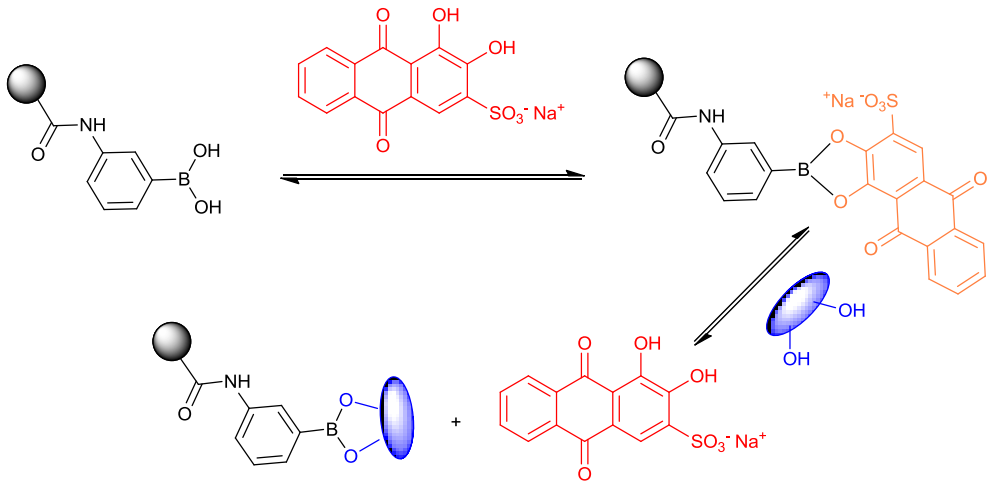

Scheme 10 Representation of boron-containing hydrogel for saccharide sensing

This IDA strategy was further used in a biotinylated boronic acid fluorophore conjugate to explore its possibility in saccharide sensing.[57-59] The molecule, coined FLAB (Fluorophore linker Boronic Acid Biotin), was initially studied for the attachment to streptavidin and the search for an effective diol quencher. It is expected that the FLAB would go through a FRET process with diol quencher *via* a boronate ester linkage. And the biotin terminal would render FLAB immobilised on the streptavidin modified gold surface, resulting in a Surface Plasmon Resonance (SPR) signal. Incubation of diol quencher with FLAB gave rise to both fluorescence quenching and a SPR response, indicating a dual response probe. It was further found that the fluorescent intensity of the bound complex could be recovered when a model saccharide was added due to the efficiency difference between static quencher (boronic ester) and dynamic quencher (free quencher). Furthermore, spectral changes could be observed by the naked-eye even on solid support.

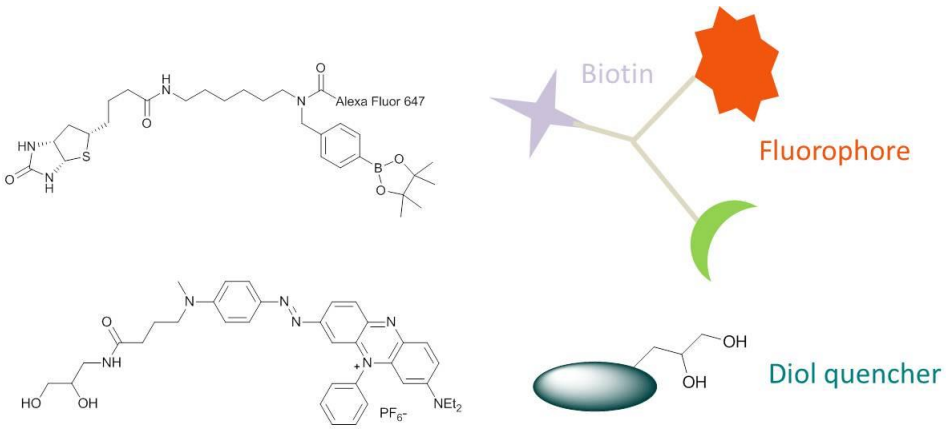

Scheme 11 Structure of biotinylated boronic acid conjugate and diol quencher

The exploration and application of boronic acid moiety in multiple scenarios are still underway in our group. Here are only selected examples of our achievements in saccharide recognition. Many novel sensing probes are under investigation currently. The current issues for saccharide sensing are how to construct a sensitive and *in vivo* platform which could be used for continuous monitoring saccharide levels.

1.3.2 Recent developments in saccharide sensing

Recently, new sensing protocols have been reported on saccharide recognition, most of which focus on using multiple interactions in one system or importing new signal reporters. Weak interactions, such as hydrogen bonding, π-π stacking and electrostatic interactions are often used separately or cooperatively in supramolecular sensing. Though the interaction strength is rather weak, when such weak interactions work together in a cooperative way they can achieve significant total effect. Some examples successfully employed the covalent bonding interaction (boronic acid-diol) and these weak interactions in a cooperative way.

Singaram's group used an array of six cationic bis-boronic acid appended benzyl viologens (BBVs), shown in Scheme 12, capable of sensing 12 different saccharides at a concentration of 2 mM. It was supposed that the ground-state complex between the

cationic BBV receptor and the anionic fluorescent dye, 8-hydroxypyrene-1,3,6-trisulfonic acid trisodium salt (HPTS), promoted the electron transfer from the dye to the receptor, leading to quenching the fluorescence of the dye. However, upon adding the saccharide, anionic boronate ester is formed, which reduces the net charge of the receptor, namely reducing the quenching efficacy, which induces the recovery of the fluorescence.[60] As the static quenching constants of HPTS with BBV receptors are one or two orders of magnitude higher than those of saccharides with BBV receptors, a ratio of 1:125:500 for the sensing ensemble HPTS / BBVs / saccharide was chosen to make sure the IDA works, which requires the affinity between the indicator and the receptor be comparable to be that between the analyte and the receptor.

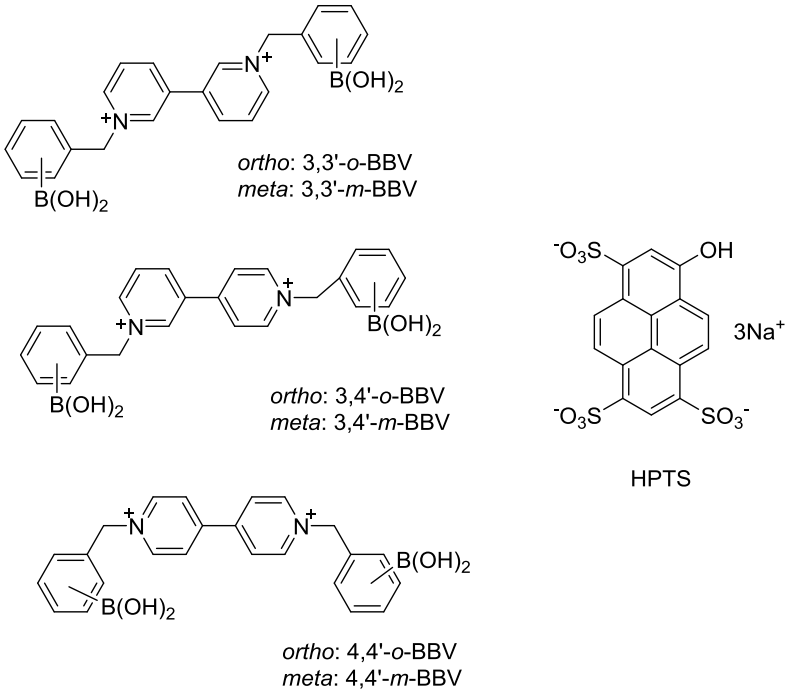

Scheme 12 Saccharide sensing ensemble of an array of six cationic bisboronic acid appended benzyl viologens and the anionic fluorescent dye, 8-hydroxypyrene-1,3,6-trisulfonic acid trisodium salt (HPTS)

As we know, D-glucose recognition is more important in terms of clinical applications and previous results showed that diboronic acid afforded better selectivity toward D-glucose. However, the extensive syntheses work has inspired researchers to search for alternative methods to achieve the selective recognition. There are two *cis*-diols,

suitable binding sites, which make it possible to form unique 1:2 complexes with boronic acid groups.

Hiroaki Tao *et al* [61] have cleverly used this property to design a novel fluorometric probe. Compound **10** can be preconcentrated along the polycation chain through electrostatic interaction, resulting in an increase of local concentrations of compound **10**, which induces the pyrene excimer emission. Addition of saccharides could continue to increase the excimer emission, of which glucose gave the maximum excimer emission when other parameters were fixed, which is attributed to the preference of glucose to form a 2:1 complex with compound **10**. This system circumvented the complicated organic synthesis without loss of selectivity for glucose.

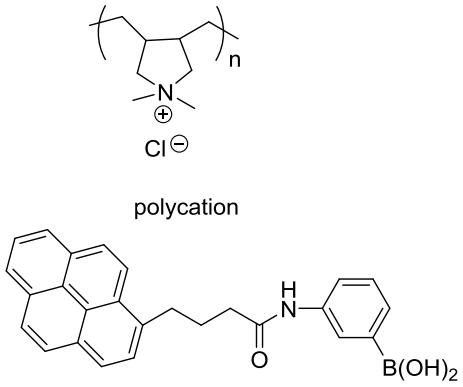

10

Yu *et al* [62] employed a similar strategy, however, in a different way by employing a water soluble polymer (**11**) with multiple boronic acid functional groups. Polymer **11** would be converted to a polyanion after binding with saccharides, which then induce the aggregation of positive charged fluorescent reporter. The aggregation as well as the strong π-π stacking interaction of pyrene would give rise to the excimer emission. D-glucose caused the most significant spectral changes, since one glucose molecule provides two pairs of diols to interact with two boronic moiety

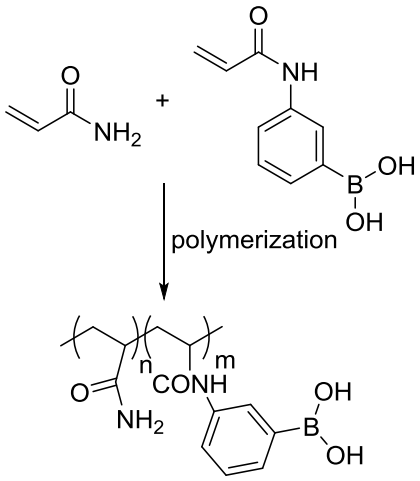

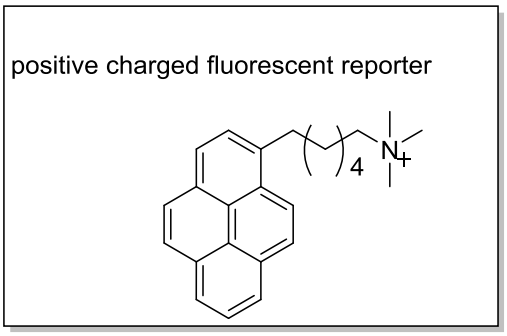

11

A two-component system with a platinum complex was successfully used to detect glucose.[63] In this report, a synthetic boronic acid polymer would become a polyanion once bound with saccharide *via* forming a boronate ester anion, which would draw the positively charged terpyridylplatinum(II) closer in terms of electrostatic interactions. Such interaction can result in aggregation of the complex with the help of metal-metal and/or π-π interaction. Thus, the spectroscopic and luminescence properties of this complex can change greatly due to these interactions, shown in Scheme 13. A 46-fold increase in emission intensity was observed by such a system upon glucose addition. Selectivity experiments showed that only glucose binding gave the most emission enhancement due to the fact that one glucose molecule will bind to two boronic-acid moieties, that is, one glucose offering two negative charges, more efficiently than those of other monosaccharides.

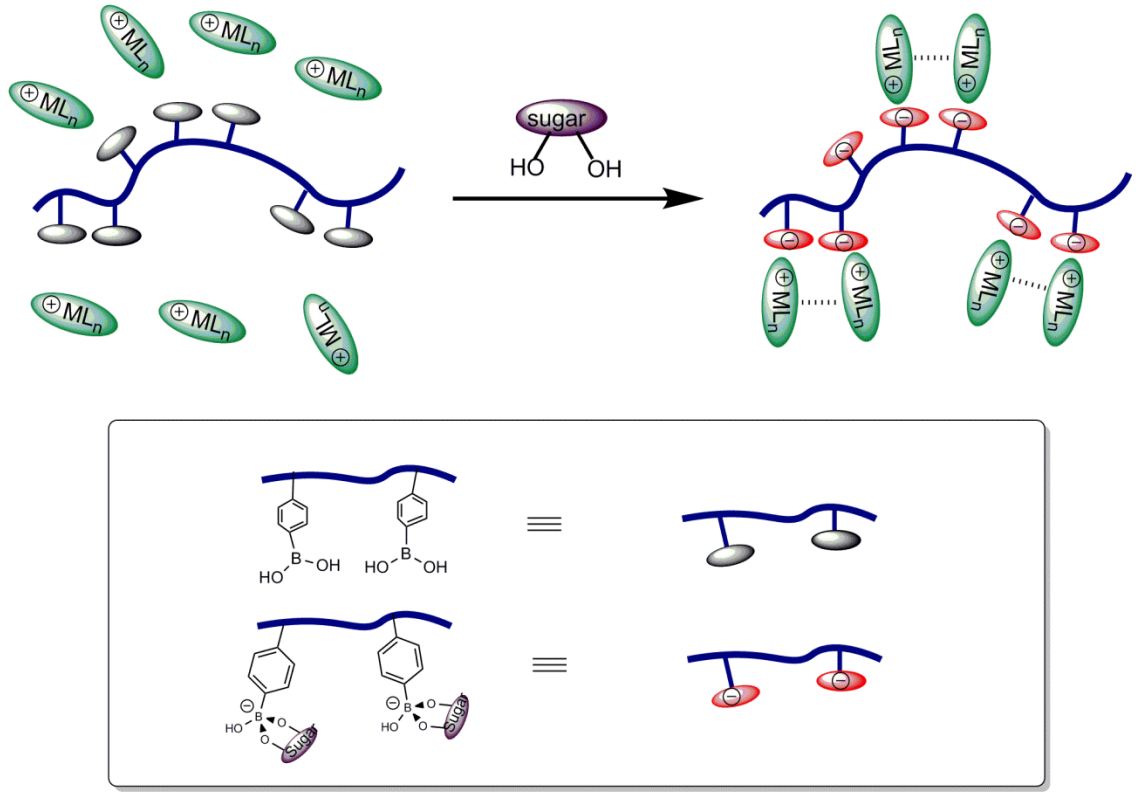

Scheme 13 Interpretation of saccharide sensing based on the aggregation of platinum complex onto boronic-acid polymer.

In terms of achieving a D-glucose selective system, Hayashita and co-workers have employed γ-cyclodextrin (γ-CD) to form inclusion complex with mono-boronic acid probe, resulting in D-glucose selectivity in aqueous solution. The compound (BA-azo) could successfully form 2:1 inclusion complexes with γ-CD,[64] shown in Scheme 14, resulting in two boronic acid groups behaving as covalently linked bisboronic acid compound. Results showed that the spacer between the boronic acid group and the benzyl azo group played a vital role in glucose selectivity.

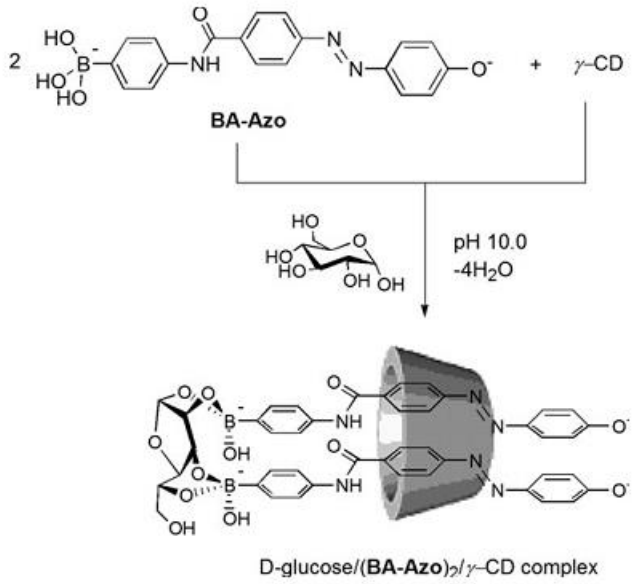

Scheme 14 The 2:1 inclusion complex formation of BA-Azo with γ-CD in presence of D-glucose (copyright)

Recently the Jiang's group has reported an amphiphilic monoboronic acid molecule (**12**), which could be selectively aggregated under guidance of D-glucose. The incorporation of a pyrene fluorophore and pyridinium moiety will endow compound **12** with an amphiphilic characteristic and also a strong π-π stacking interaction. The cationic pyridinium moiety affords a cation-π interaction, which could quench the fluorescence of the pyrene monomer. An excimer emission around 510 nm was observed upon addition of D-glucose with only slightly enhanced monomer emission. As for D-fructose, only modest enhancement of monomer emission was observed. Besides, dynamic light scattering measurement implied that aggregation is formed at pH > 9 for compound **12** without observed excimer emission. Addition of D-glucose could induce formation of aggregates with diameter *ca.* 2 μm along with significant increase of excimer emission. The binding behaviours of compound **12** with saccharides were illustrated as Scheme 15. It was also found that compound **12** could selectively respond to nucleosides, with nucleoside guanosine (G) showing the strongest binding affinity. Competitive experiments also demonstrated that in the presence of both D-fructose and D-glucose, addition of phenylboronic acid (PBA) would selectively bind with D-fructose.

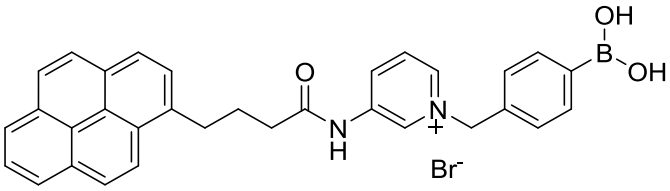

12

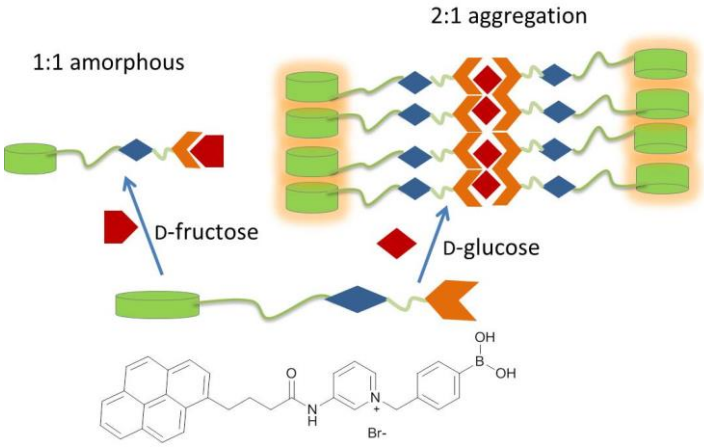

Scheme 15 Illustration of different binding modes between saccharides and compound **12**

1.3.3 Summary of saccharide recognition

The importance of monitoring saccharide level has promoted multiple strategies for tackling this issue.[65] The organic synthetic probes, generally employing the boronic acid moiety, have seen their flourishing development in recent decades as it has potential to monitor saccharides level by incorporating in fibre optic sensors, affording a minimal-invasive strategy.

Traditional organic sensors, solely relying on the interaction between boronic acid and diol, need sophisticated syntheses and suffer from low solubility. Recently, alternative methods including combining other weak interactions, showed multiple ways for developing saccharide sensors. These platforms reduced synthetic effort without decreasing the ability for selectively recognising saccharides. However, there is still a long way to go for these sensors to become practical.

1.4 The development of fluoride recognition

1.4.1 Brief classifications of fluoride sensing

Anions play an important role in fundamental biological processes and are important environmental contaminants. Therefore, the recognition of anions is a hot topic in analytical science. However, developing effective strategies for anion detection are more challenging than that for metal cations. The reason is that anions have a smaller charge to radius ratio and heavily solvation, which means electrostatic interactions are less effective, impairing the anion binding strength and selectivity.[13, 43]

Fluoride recognition has attracted considerable interest not only because of its unique properties but also its vital importance in our daily life. Fluoride salts can be used as phosphatase inhibitors.[66] Excess fluoride could cause fluorosis though low levels of fluoride anion could be used as a treatment for oral hygiene.[67, 68] The commercially available ion-selective electrode methods allow for fast determination of fluoride concentration. However, these systems, although well established, possess some disadvantages. As a membrane electrode containing single crystals of LaF_3, it is fragile and time consuming and produces large errors in the presence of other ions.

Optical methods received much attention due to their simplicity, low cost and reliability. Generally, the recognition of fluoride utilises the strong Lewis base and deprotonation character of fluoride. There are several reviews at hand that have summarised recent development on fluoride sensing.[14, 16-18, 43, 69-72] . The Lewis acid nature of boron allows it being a receptor for hard anions and also the hybridisation changes from sp^2 to sp^3 along with significant photophysical changes, make it suitable candidate for fluoride recognition. Recent achievements were divided into two groups: those fluoride sensors that do not have B-F coordination interactions and others sensors with B-F coordination for fluoride recognition.

1.4.2 Fluoride sensors without B-F coordination

Among these fluoride chemosensors, many of them are based on the hydrogen bonding interaction between a NH group and the fluoride ion with involvement of (thio)ureas,[73-77] amides,[78, 79] and pyrrole[80, 81] moieties. However, such sensors lose the sensing ability once in protic or polar solvents due to strong solvation effect. Recently, several chemodosimeters for fluoride anion were reported *via* deprotection reaction of a silyl group by utilising the strong affinity of silicon toward fluoride.[82-84]

The urea group possesses a bisamide moiety with two acidic NHs which have been taken as a good hydrogen bond donor for construction of anion receptors with two hydrogen bonds.[72] In 2005, Gunnlaugsson *et al* reported the first colorimetric naphthalimide-based ICT sensors **13**, which could be used in highly competitive aqueous media. Initial investigations were carried out in DMSO and upon addition of anions, like AcO^-, $H_2PO_4^-$ and F^- , the original absorption peak at 414 nm of **13a** decreased along with new absorption band at 350 nm and 560 nm, with two clear isosbestic points at 465 nm and 380 nm, respectively. Also a clearly visible colour change from yellow to deep purple was observed by naked-eye as well. Comparative experiments suggested that the thiourea moiety is essential to achieve successful anion sensing and colour changes. Both **13a** and **13b** showed similar results, indicating that the nature of the aromatic ring has little effect on the binding affinity. The most important results are that both anion sensing and colour changes could be obtained even in competitive aqueous buffer solution. Yet, the problem is the poor selectivity between anions.

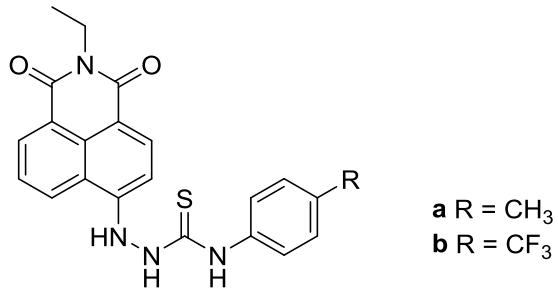

13a and **13b**

Bearing in mind that strong hydrogen bonding is good for anion sensing, amide, pyrrolic and indolic moieties were extensively explored as well, as they offer relatively acidic hydrogens. However, few pyrrolic based sensors performed well in polar solvents. Indolic NHs are ca. 100 times more acidic than pyrorolic NHs,[17] and thus with different affinities and selectivity properties towards fluoride and other anions. Gale's group reported sensor **14** in 2007, composed of an indolic moiety and pyridine unit, which showed a high selectivity for fluoride over other putative anion sensors. It was found that in DMSO- 0.5 % water system, the binding affinity to fluoride is two orders of magnitude larger than that of other anions. It is believed that the tendency for formation of a twisted conformation of compounds **14** in solution accounts for the high selectivity, as only the small fluoride ion could be more easily isolated from the solvent mixture. The assumption was also demonstrated by X-ray analysis of TBA[**14a**·F], TBA[**14a**·Cl],TBA[**14b**·F] and TBA[**14b**·Cl].

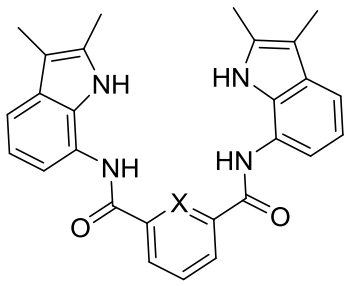

a X = N
b X = CH

14a and **14b**

The tendency of forming hydrogen bonds of fluoride was also employed with quantum dots (QD)and gold nanoparticles.[85] The emission of thioglycolic functionalised CdTe QDs was overlapped with the absorption of Au NPs, thus leading to an FRET process between QDs and Au NPs. It was assumed that in pH 5-7 the carboxyl group in thioglycolic acid and citric acid could be partly protonated and hydrogen bonds formed between the two weak acids when CdTe QDs and AuNPs were mixed together. A significant increase of the QDs emission was observed for the CdTe-AuNPs assemblies upon addition of F^-, resulting from the cleavage of hydrogen bond and recovery of photoluminescence of QDs (Scheme 16). Another point is that the ratio of QDs to

AuNPs is crucial for achieving the best signal responses for a given F^- concentration. The detection of fluoride could be achieved in pure aqueous media. These results shows a possible solution for detection of fluoride in a simple way.

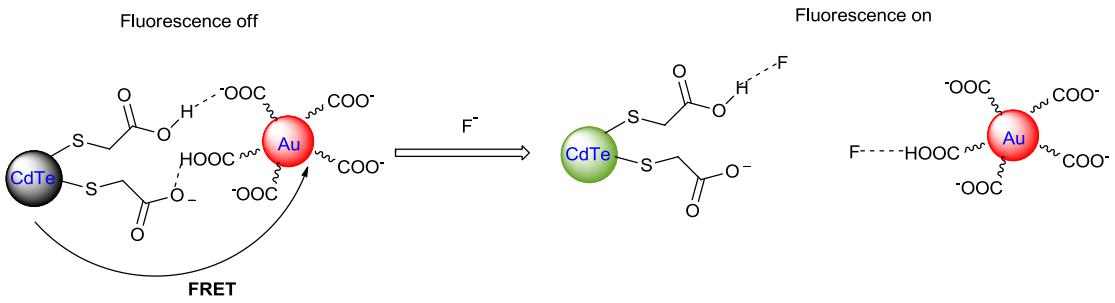

Scheme 16 Illustration of fluoride sensing mechanism of CdTe QD-AuNPs ensembles

Recently there are also quite a few fluoride sensors which were based on fluoride involved reaction. The chemical reaction based sensing probes, often referred to as "chemodosimeters", are a relatively new emerging methodology. In reaction-based sensing, fluoride has some unique and attractive features, including strong Lewis basic character and high affinity for silicon, making it possible to easily distinguish fluoride from other anions.

There are a number of chemodosimeters for fluoride exploiting its affinity for silicon.[86-91] The general structure and sensing mechanism of these sensors are similar and the differences are the fluorophores and silicon leaving groups (Scheme 17). Most of these investigations were performed in organic solvents, except for the one carried out by Zhang group.[87] The probe was comprised of a hydrophilic benzothiazolium hemicyanine dye and a lipophilic *tert*-butyldiphenylsilyl moiety, such system could be successfully employed in living cells.

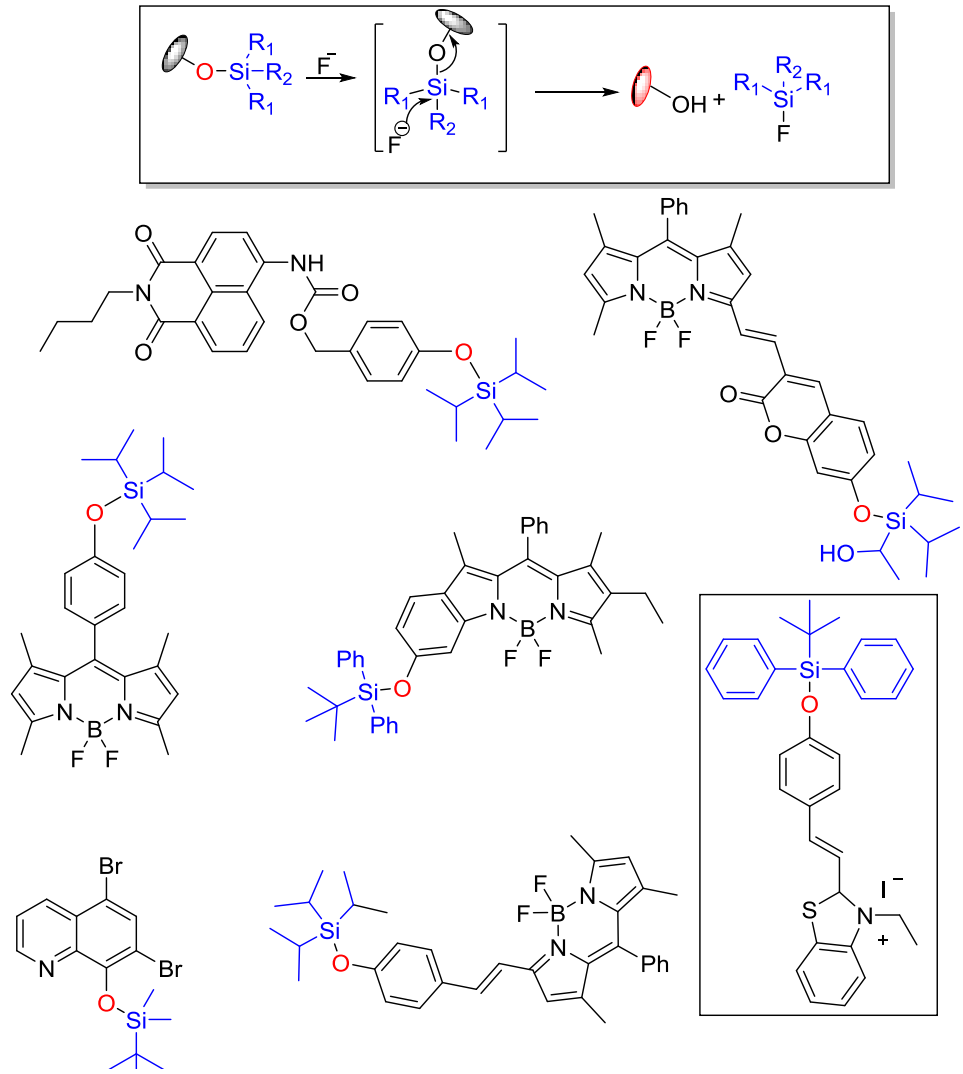

Scheme 17 Si-O cleavage strategy for fluoride sensing

Kumar and co-workers used a cascade reaction for fluoride sensing involving a Si-O cleavage reaction followed by cyclisation.[92] Compound 1**5a** underwent silyl ether deprotection with tetrabutylammonium fluoride in THF, followed by an irreversible cyclisation of the intermediate terphenyl **15b** to **15c,** producing a significant colour and fluorescent spectral change. Control experiments showed that increased negative charge on the phenolateoxygens of **15b** after deprotection of the silyl ether group offered optimal electron density to complete cyclisation.

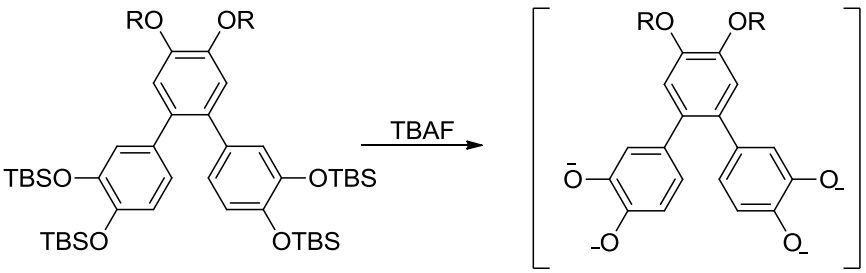

15a **15b**

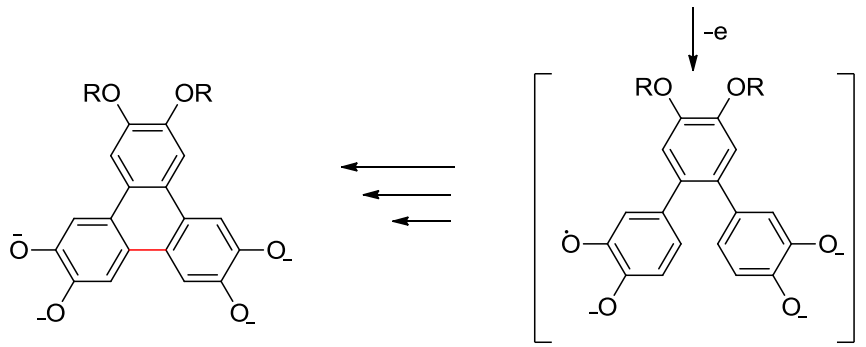

15c

1.4.3 Fluoride sensors with B-F coordination

Boron often exists in its sp^2 hybridisation and has an empty *p* orbital, leading to a planar conformation, which is ready to form a conjugated system. The Lewis acidic nature of boron makes it an ideal candidate for designing fluoride sensors. The first detailed study of Lewis acidic boron binding to fluoride ion was reported in 1985, which was tracked by NMR.[93] Later a theoretical investigation of organoboron macrocycles was performed by Jacobson and Pizer.[94] These calculations found that the nature of anion-boron interaction was more like a covalent bond than a purely ionic interaction, involving significant amount of charge transferred from anion to the host upon complexation. In 1995, Shinkai reported the first example of a fluoride concentration determining chemosensor by means of interaction between Lewis acidic boron and strongly basic fluoride.[95] Following this work, lots of results were reported, some of which were listed to outline the development of fluoride sensors based on boron-derivatives.

The Tamao group disclosed a series of new colorimeteric fluoride sensors based on boron-containing π-electron systems, as the unique empty *p* orbitals of boron enables extension of π-conjugation.[96] The binding of fluoride changed the sp^2 hybridisation of boron to sp^3, leading to the interruption of this conjugation system. The interaction was studied by UV-*vis* absorption in THF solution and upon complexation with a fluoride ion, the characteristic strong absorption band of compound **16a** at 470 nm disappeared, with new bands around 360 nm to 410 nm, corresponding to anthracene absorption bands. The colour changed from orange to colourless and the binding constant of compound **16a** for fluoride is $(2.8 \pm 0.3) \times 10^5$ M^{-1}. Compound **16b** has a more extended π electron system and is capable of binding with fluoride in a stepwise fashion as the four boron atoms have two different environments. Both sensors gave colour changes when bound with fluoride.

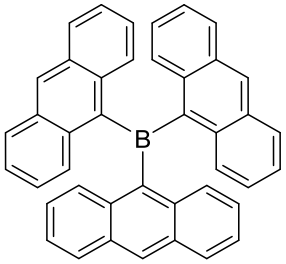

16a

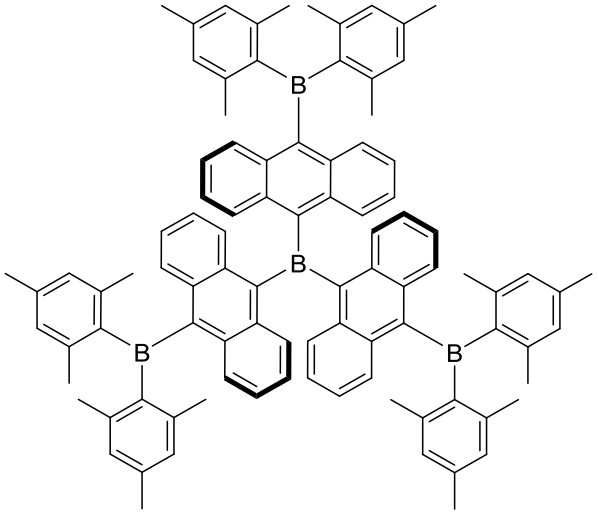

16b

The first fluorescent sensor for fluoride was developed in the James's group in 1998.[97] However, the spectra did not change much as only simple boronic acids were employed. Yoon's group reported a fluorescent turn-on fluoride chemosensor in 2006 by modifying fluorescein fluorophore with boronic acid moiety.[98] Compound **17** was obtained using a Mannich reaction between dichlorifluorescein and 2-methylaminomethyl boronic acid. It is worth noting that there is boronate formation between boron and adjacent phenolic oxygen atom in compound **17**. Before addition of

fluoride, the fluorescent intensities of compound **17** is weak due to the well- established nitrogen-benzylic based PET-quenching mechanism. It is believed that upon binding with fluoride, a strong hydrogen bond with phenolic hydrogen and benzylic nitrogen as well as fluoride was formed, which blocked the PET quenching process, resulting in the recovery of fluorescein emission.[11]B NMR spectra also confirmed the tetrahedral structure of boron after addition of fluoride. Based on this, a colorimetric sensing platform was obtained.

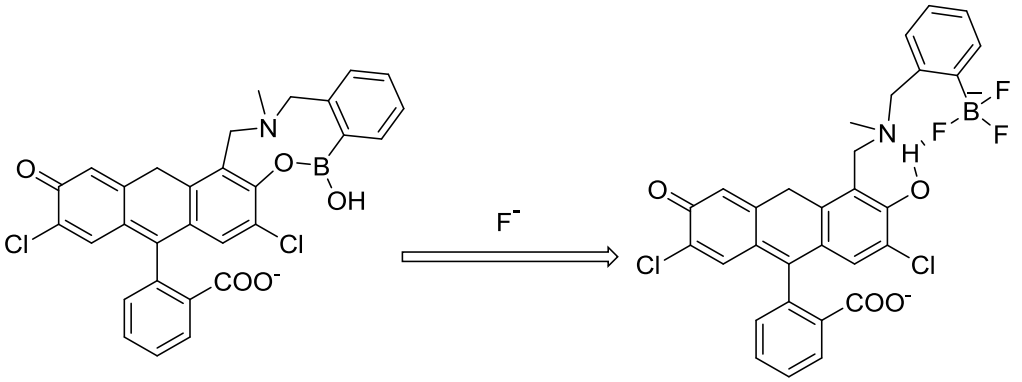

17a **17b**

Later James's group published another fluoride sensor with similar boronate structure, compound **18**. Probe **18** can selectively respond to chloride and fluoride. Upon addition of chloride, a decrease of fluorescence intensity was observed, which is due to the associative hydrogen bonding between chloride and two boronic acid groups, whilst a colorimetric changes was seen on addition of fluoride. The fluoride induced B-O bond cleavage and air oxidation of phenolate anion was demonstrated to account for this phenomenon. Meanwhile, the sensing mechanism was investigated by electrochemical analysis. In free form of compound **18**, an irreversible oxidation peak at 1.8 V *versus* SCE was exhibited. Addition of 0.2 mM TBAF caused a decrease in the peak at 1.8 V and a new peak at 1.5 V. When concentration of TBAF is higher than 0.4 mM, two new peaks at -0.3 V and +0.1 V were obtained, assigned to the oxidation of phenoxyldianion and a coloured phenoxyl diradical. However, *tetra-n*-butylammnonium chloride (TBACl) can't cause any oxidised fragments and colour changes. Thus the chloride is more like a water molecule and forms hydrogen bonds with four B-OH moieties from

two molecules **18**, which induced conformation change and disturbed the π systems, leading to decrease of fluorescent intensity.

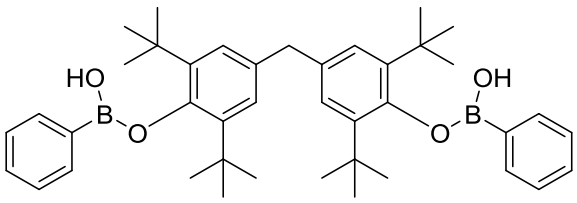

18

Our group recently prepared a fluorescent "turn-on" fluoride sensor using pyrene appended pyridylboronic acid derivatives(**19a-19c**) with variation of linker length.[99] All three compounds showed moderate fluorescence emission at 378 nm and 397 nm in dichloromethane, ascribed to pyrene monomer emission. Upon addition of fluoride, both the monomer emission and excimer fluorescence were observed, which suggests that the fluoride ion enhances the π-π stacking of pyrene unit. **19b** showed the strongest fluorescent enhancement of the excimer emission, implying that the ethylene linker between pyrene and pyridylboronic acid is optimal. Job-plot anaylsis revealed a 1:2 binding mode ([TBAF]: **19b**), which was also confirmed by MS. Thus it was proposed that two boron atoms chelate to a single fluoride anion, which in turn enhances the intermolecular π-π interaction. Other anions can hardly enhance pyrene excimer formation. Furthermore, **19b** could successfully extract fluoride from aqueous solution.

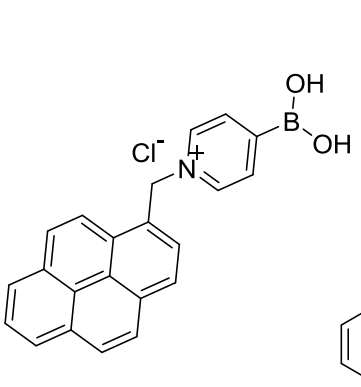

19a

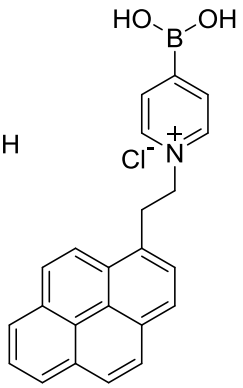

19b

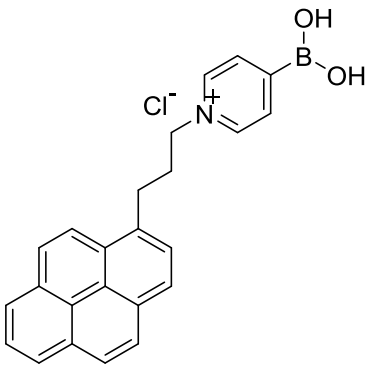

19c

By using diborane species, a rigid 1,8-naphthalene backbone with two proximal Lewis acidic sites, the Gabbaï group developed a series of ground-breaking sensors. Compound **20** serves as a colorimetric fluoride sensor with an association constant greater than 5×10^9 M^{-1} in THF. Absorption titration of compound **20** with fluoride showed a 1:1 binding along with a colour change from yellow to colourless. No changes were observed when other anions like chloride, bromide and iodide were added. The fluoride bridging intermediate complex was isolated, confirmed to be the bidentate binding mode. Most importantly, the complex is stable even in aqueous condition. It was assumed that steric effects are the driving force for such a high fluoride binding affinity. As fluoride binding induced hybridisation changes of boron, from sp^2 to sp^3, accordingly a coordination geometry change from trigonal planar to tetrahedral. Such changes allow aryl substituents to adopt a more divergent orientation and thus less sterically hindered compared with the starting diboranes.

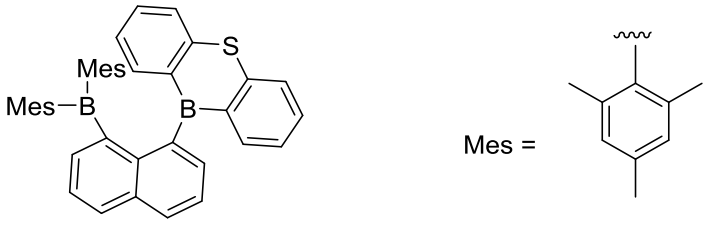

20

Inspired by this work, Gabbaï group extended the range of bidentate sensors by synthesising heteronuclear Lewis acid centres[100] or using hydrogen-bond donor derivatives. Then in an effort to achieve fluoride ion sensing in pure water, they employed a positive charged phosphonium moiety, trying to combine the B-F coordination interaction together with columbic effect. A series of compounds **21a-d** were obtained, which are water stable and react reversibly with water. Fluoride titrations were carried out in H_2O-MeOH (9:1 vol.) and the corresponding binding constants indicated that Lewis acidity of cationic boranes increase with their hydrophobicity. Especially for **21d**, the strong fluorophilicity allows it to bind to

fluoride ion below US Environmental Protection Agency's recommended maximum level for drinking water of 4 ppm.

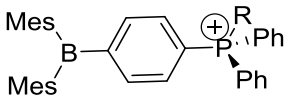

a R = Me
b R = Et
c R = *n*-Pr
d R = Ph

21

1.5 Suzuki-Miyaura coupling reaction and Tsuji-Trost reaction

1.5.1 Introduction of catalytic reaction based sensing

So far, the strategies for molecular recognition are based on analyte/receptor complexation, where one receptor unit combined with one analyte except those with two or more recognition sites. The binding event will induce readable changes, which is generally taken as the reporting signal and thus the target molecule could be recognised. As discussed before, depending on connection nature between receptor site and signal reporting site, such kind of sensors could be divided into two systems: a) host-guest approach, where the two sites were connected by covalent bonds; b) indicator-displacement assay, where these two sites interact with each other by weak interactions or reversible covalent bonds.

Though great progress has been achieved by the conventional molecular recognition strategies, it is hard to meet the increase demand for a more sensitive detection method. Progresses in the development of ELISA (enzyme-linked immuno sorbent assay) technology gave researchers clues to discover new sensing protocols. If one analyte could generate lots of signal reporters, then the sensitivity would be greatly improved.

Bearing this idea in mind, more and more catalytic reactions based sensing approaches have been developed, which were summarised in several reviews.[101, 102]

Such reaction involved sensing strategies, by their nature, often have high selectivity and sensitivity. The general design protocols are illustrated as in Scheme 18. One type of these probes employed the reaction where the analyte is one of the reagents to generate a new compound, like (a). The other type is that the analyte acts as a catalyst, which is involved in more than one reaction cycle, like (b). The latter one normally employed catalytic reaction, which could be further divided into two categories: 1) the analyte itself is the catalyst and a catalytic reaction is activated upon adding the analyte into the system. The products normally offer the signal output. 2) The recognition process and the signal output are separated. And the analyte sensing events affect the catalysis reaction, generating the reporting signal.

(a)

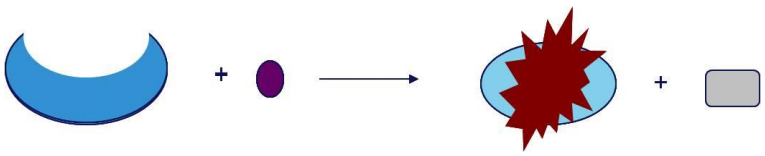

(b)

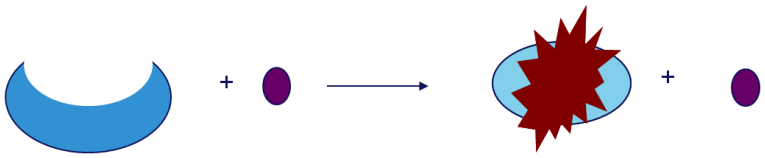

Scheme 18 Design protocols for reaction-based recognition

An interesting example[103] of molecule sensing based on catalytic reaction is shown in Scheme 19. The unique characteristic is that a self-catalysed reaction is involved, namely, the resulting products could, in turn, catalyse a reaction, which produces signal reporter. The analyte Pd (II) generated the first F^- ion in this system. The F^- ion catalysed the amplification reagent, generating colorimetric products and more F^-; the generated F^- ion then joining the next run to get more signal reporters (colorimetric

products), of which the total effect is that with a minimal amount of analyte, massive signal reporters were obtained. The F^- ion acted as a signal transduction reagent.

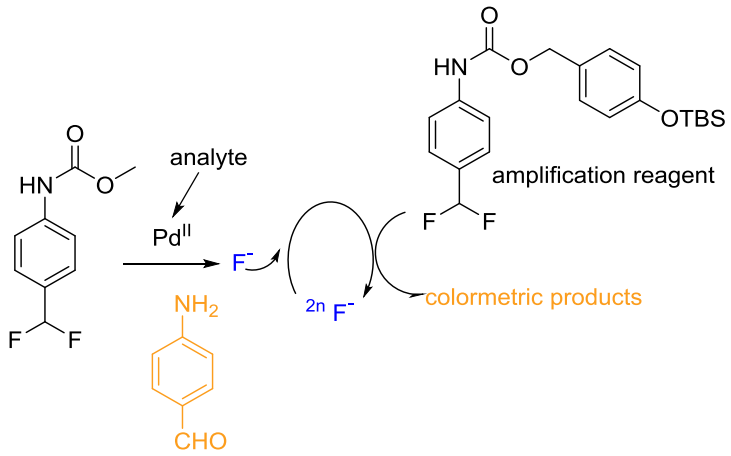

Scheme 19 The schematic illustration of two components system based sensing platform with involvement of an autocatalytic process.

Sensing based on catalytic reactions offers great opportunities to exploit more sensitive strategies. However, there are also some problems. First, the catalysts used are typically metal ions, that is, the choices of catalytic reactions are limited. It might be hard to find the relationship between a specific analyte and an according catalytic reaction. Second, the catalytic reaction often requires two or more components, which makes the sensing platform quite complicated. Third, some catalysts need high temperature or organic solvents in order to obtain high turn-over, which would be a drawback considering the practical application. Also, a multi-disciplinary background is needed in order to design elegantly protocols for sensing. For the approaches based on catalytic reactions, signal amplification is obtained since a catalyst itself is a signal amplifier in terms of chemical conversion.

1.5.2 Suzuki-Miyaura coupling reaction

After the first report of cross-coupling reaction of alkenylboranes and aryl halides *via* $Pd(Ph_3)_4$ catalysis in the presence of a base in 1979,[104] the so-called Suzuki-Miyaura coupling reaction has seen a dramatic increase in use over the past several decades[105-108] and the 2010 Nobel prize also went to Akira Suzuki *et al* for their contributions to Pd-catalysed cross coupling reaction in organic synthesis. The Suzuki-Miyaura coupling reaction is one of the most utilised methods for the introduction of a new carbon-carbon bond, though there are several other coupling reactions able to achieve this. The Suzuki-Miyaura coupling reaction received more attention as it has several advantages: the Suzuki-Miyaura coupling reaction can be carried out under mild conditions with easy removal of boron-containing by-products; the vast varieties of commercially available boronic acids are more environmentally friendly than other organic-metallic reagents;[109] a lot of functional groups could be tolerated by this coupling reaction, which is especially important for natural products synthesis.

There are generally two types of Suzuki-Miyaura coupling reactions, cross-coupling and homo-coupling. The homo-coupling reaction,[110] firstly discovered as the side-reaction of Suzuki cross- coupling, however, is now used as a useful strategy to get symmetrical products. The general illustration of Suzuki cross-coupling is shown in (reaction (**1)**).

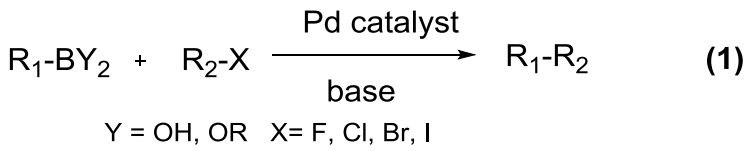

(1)

The classical mechanism cycle for Suzuki cross-coupling reaction could be depicted as Scheme 20, which includes four steps: (a) oxidative addition of organic halides to Pd^0; (b) transmetallation between boron compounds and the resulting complex from the first step; (c) isomerisation of *cis*- and *trans*-complex after transmetallation; (d) final product resulting from a reductive elimination step.

There have been a large number of studies on the catalytic process. Canary and co-workers observed the intermediates involved in Pd(0)-catalyzed Suzuki coupling

reaction by ESI-MS directly under reaction conditions,[111] which strongly supported the cyclic mechanism.

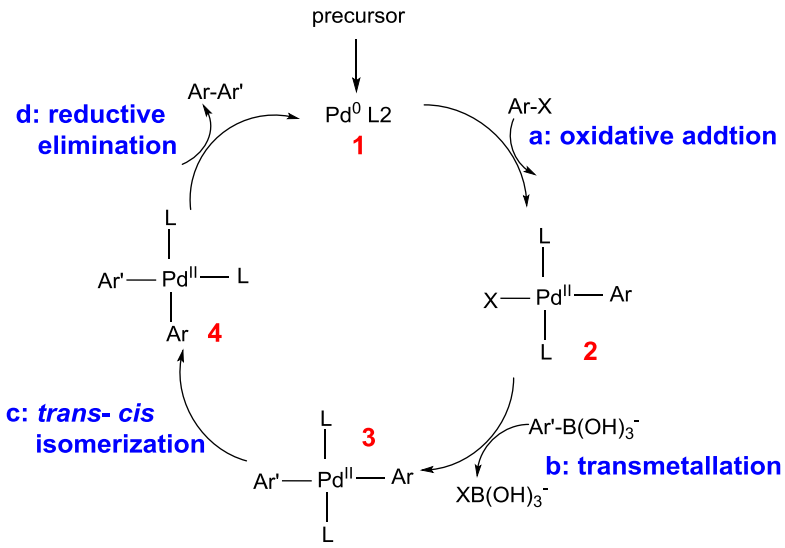

Scheme 20 Catalytic cycle for Suzuki-Miyaura type cross-coupling

$Pd(0)L_2$ could be obtained by ligand dissociation from the precursors of Pd(0)-phosphine complexes, or by the double transmetallation of the Pd(II) precursor salts and phosphines.[112]

The oxidative addition is usually taken as the rate-determining step. Several factors may affect the rate of this process. Both experimental and theoretical results show that the choice of X would greatly influence this process, liability towards oxidative addition in the order of ArI > ArBr >> ArCl.[113] Thus, the reactivity could be tuned by changing the substitution groups. Aryl halides with electron deficient groups have higher oxidative addition rates. Besides, the ligands of palladium could also affect the efficiency of the catalyst, electron-rich phosphines offering stronger activity. It's easy to understand since the oxidative addition could be explained as that the Pd^0 catalyst, carrying lone pair electrons, attacks the Ar group, thus the more electron-donating ability of the ligands offers more electron density of palladium.

A base is needed to increase the nucleophilicity of boron in order to facilitate transmetallation between boron and the positive metal centre since organoboron compounds are highly electrophilic. However, for different solvent systems, the preference of base is different. In THF/ H_2O system, stronger bases resulted in better yield, whereas K_2CO_3 and K_3PO_4 are more efficient in DMF. In fact, results showed that the cross-coupling reaction is in some degree pH dependent. An isomerisation between complex **3** (trans-$Pd^{II}L_2Ar`Ar$ in Scheme 20) and complex **4** takes place to make the following reductive elimination proceed smoothly.

The reductive elimination step is supposed to be facile. However, the natures of ligands also play an important role in this step. Stronger donor ligands make the metal centre more electron rich, which greatly promotes the oxidative addition, yet inhibits the reductive elimination step.

The Suzuki type homo-coupling (chemical equation (**2)**) is now attracting more and more attention for its usage in biphenyl syntheses.[110] Results found that when carried out the Suzuki cross-coupling, if not handled properly, for example, not under inert atmosphere, more homo-coupling products are generated.[114] This gave some clues to investigate the mechanism of Suzuki homo-coupling, which found that oxygen, solvent and other factors[115] seem to play very important roles.

$$ArB(OR)_2 \xrightarrow[base]{catalyst} Ar\text{-}Ar + 2"B(OR)_2" \qquad \textbf{(2)}$$

The general belief is that homo-coupling occurs in the presence of oxidants.[115-117] A proposed intermediate compound ArPd-[$OOB(OR)_2$](dppp) complex was involved in the reaction cycle,[118] followed by transmetallation with another $ArB(OR)_2$, generating Ar_2Pd(dppp). Adamo and co-workers[119] offered evidences for the involvement of peroxo complex of palladium both experimentally and theoretically, the proposed cycle shown in Scheme 21, the steps similar to that of cross-coupling. Two $ArB(OH)_2$ molecules are supposed to involve in, the first for activating peroxo complex of palladium and the other for transmetallation. They also explained the generation of phenols, usually the by-product of homo-coupling.

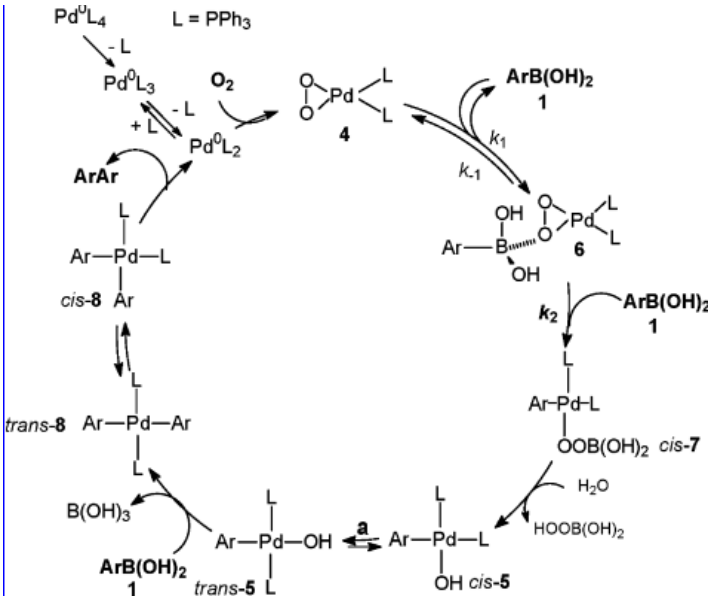

Scheme 21 Catalytic cycle of Suzuki homo-coupling copyright[120]

Overall there are many factors that affect the catalytic reaction. Great efforts have been devoted to investigate the effects of catalyst, ligands, bases, solvents as well as the additives. Current developments with new catalysts can carry Suzuki type reactions with unactivated aryl chlorides,[121] heterocycles[122] as substrates at room temperature with low loading of catalyst. Some other transition metals, like Au,[123] and Cu[124] are also reported to be a catalyst in Suzuki type coupling.

1.5.3 Tsuji-Trost reaction

The Tsuji-Trost reaction is a palladium-catalysed substitution reaction, named after Jiro Tsuji who first reported the method in 1965 and Barry Trost who extended the scope of this reaction.[125, 126] The total reaction is listed as chemical equation (**3)**: X stands for a leaving group, like halides, acetate or esters; NuH stands for the nucleophiles such as active enolates, amines or phenols. The product is generated by nucleophile replacing

the leaving group on the starting material, the proposed catalytic mechanism shown in Scheme 22.

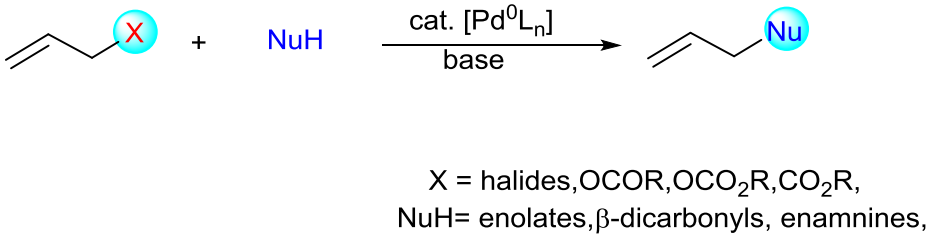

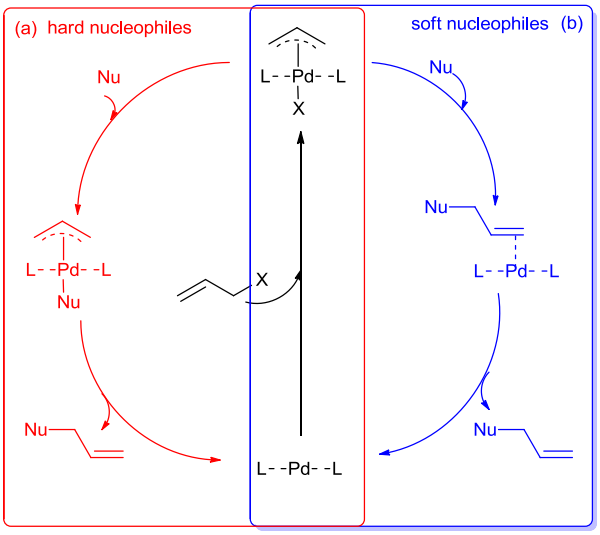

Scheme 22 Catalytic cycles of Tsuji-Trost reaction

Palladium catalyst goes through the oxidative addition with the nucleophile, which forms an η^2-π-allyl complex *via* coordination of Pd(0)-catalyst to the double bond. Depending on the nature of the nucleophile, there are two general classes of reaction types for Tsuji-Trost reaction. The "hard" nucleophiles were those derived from conjugate acids with pK_a > 25, whose catalytic mechanism shown in Scheme 22 (**a**).[127] The hard nucleophile first attacks the metal centre, followed by reductive elimination to afford the allylation product. Whereas the "soft" nucleophile was referred to that derived from corresponding conjugate acid with pK_a < 25 and would directly attach to the allyl unit. The final allylation product is generated from decomplexation of intermediate Scheme 22 (**b**).

Tsuji-Trost reaction found its application in many aspects, especially in making chiral compounds *via* achiral substrates and asymmetric allylic alkylation. Recently it also saw its potential in molecular sensing.[128]

1.6 Deduction of equations for calculating binding constants

1.6.1 Overview of binding constants determination

In the field of host-guest chemistry, binding constants are one of the important parameters to quantitatively determine the formed complex, a criterion for the evaluation of the host-guest complexation process, which is also known by the terms of formation constant, association constant or stability constant. The binding constants indicate the thermodynamic stability of the host-guest complex at a given solvent with a given temperature. Thus, thermodynamic parameters (enthalpy, entropy) and Gibbs free energy offer more suitable criteria for determining binding constants, given in Equation (1) to (3), where the binding constant K is correlated with those thermodynamic parameters. [129]

$$\Delta G = -RT ln K \qquad \text{eqn. (1)}$$

$$\Delta G = \Delta H - T \Delta S \qquad \text{eqn. (2)}$$

$$\ln K = -\frac{\Delta H}{R} * \frac{1}{T} + \frac{\Delta S}{R} \qquad \text{eqn. (3)}$$

At the same time, binding constants determination could also be achieved *via* titration of the guest molecule with the host molecule by means of UV-*vis*, fluorescence and NMR spectroscopy. Such analysis is based on the binding equilibrium model: Equation (4), with binding constant K presented by Equation (5), where H is host; G, guest; P, complex; *a*, *b*, stoichiometry numbers. During the binding process, the Law of conservation of mass is still applied, which could derive Equation (6) and (7), where

$[H]_0$ and $[G]_0$ are the initial concentrations of host and guest molecules; [H] , [G] and [HaGb], concentrations of host, guest and complex at equilibrium state.

$$a \cdot H + b \cdot G \leftrightarrow HaGb \qquad \text{eqn. (4)}$$

$$K = \frac{[HaGb]}{[H]^{a} * [G]^{b}} \qquad \text{eqn. (5)}$$

$$[H]_0 = [H] + a * [H_aG_b] \qquad \text{eqn. (6)}$$

$$[G]_0 = [G] + b * [H_aG_b] \qquad \text{eqn. (7)}$$

However, in order to calculate the binding constants, the stoichiometry of *a* and *b*, needs to be determined, which are commonly obtained by Job's plot analysis, which was carried out by fixing the total concentration of host and guest molecule while varying the ratio of these two components. If no specific binding ratio for a host-guest interaction, approximation strategy is often employed to get the binding constants. Here the deduction of binding constant calculating equation is discussed according to the requirement in this thesis.

1.6.2 Deduction of observed binding stability calculation equation for simple binding process

When performed the titration, concentration of the host molecule normally stay constant while keeping increasing the concentration of guest molecule. The signal of the system will change along with the formation of host-guest complex. Assuming the fluorescent intensity is the signal and guest molecule itself does not have fluorescence. Then the initial fluorescence intensity F_0 is only generated from host molecule, which is supposed to be proportional with the concentration of host molecule, shown in Equation (8), where k_H includes parameters like quantum yield, path length, molar absorptivity.

$$F_0 = k_H * [H]_0 \qquad \text{eqn. (8)}$$

Along with addition of guest molecule, the observed fluorescent intensity, then, included the formed complex as well as the fluorescence of free host molecule, represented as in Equation (9).

$$F = k_H * [H] + k_{HG} * [HG] \quad \text{eqn. (9)}$$

When excess amount of guest added, it is supposed that all the host molecules formed the complex, that is, $[HG] \approx [H]_0$ and then the final fluorescence intensity would mostly come from the fluorescence of the formed complex, as indicated in Equation (10).

$$F_{lim} = k_{HG} * [HG]_{lim} = k_{HG} * [H]_0 \quad \text{eqn. (10)}$$

From Equation (8) and (10), both k_H and k_{HG} could be obtained. As together with Equation (5) – (7), where taking *a* and *b* as 1, [*H*], [*HG*] would be represented in terms of K and [*G*]. Then all the variation factors (k_H, k_{HG}, [H], [HG]) in Equation (9) could be replaced and Equation (9) is rewritten as Equation (11).

$$k_H = \frac{F_0}{[H]_0}, k_{HG} = \frac{F_{lim}}{[H]_0}, [H] = \frac{[H]_0}{1+K*[G]}, [HG] = K * [G] * \frac{[H]_0}{1+K*[G]} \rightarrow\rightarrow$$

$$F = \frac{F_0}{[H]_0} * \frac{[H]_0}{1+K*[G]} + \frac{F_{lim}}{[H]_0} * K * [G] * \frac{[H]_0}{1+K*[G]}$$

$$F = \frac{F_0 + F_{lim}*K*[G]}{1+K*[G]} \quad \text{eqn. (11)}$$

Equation (11) is easy to be rewritten as Equation (12)

$$\frac{F}{F_0} = \frac{1+\frac{F_{lim}}{F_0}*K*[G]}{1+K*[G]} \quad \text{eqn. (12)}$$

Then suppose

$$y = \frac{F}{F_0}, X = [G], P_1 = K, P_2 = \frac{F_{lim}}{F_0}$$

Here we get the equation for calculating the observed binding stability of boronic acid based saccharide sensors.

$$y = \frac{1+P_1*P_2*X}{1+P_1*X} \quad \text{eqn. (13)}$$

Additionally, if the binding event occurred along with absorption changes of host molecule, then the similar deduction could afford Equation (14), similar to that of Equation (11).

$$A = \frac{A_0 + A_{lim} * K * [G]}{1 + K * [G]} \qquad \text{eqn. (14)}$$

Where A_0 is the initial absorption of host molecule, A_{lim} is the absorption when excess guest molecule added, *K* is the binding constant.

Accordingly, Equation (15) is easy to obtain by deducting A_0 from each side, which could be further derived into Equation (16), when y = A-A_0, b = A_{lim} – A_0, X = [G].

$$A - A_0 = \frac{A_0 + A_{lim} * K * [G]}{1 + K * [G]} - A_0 = \frac{(A_{lim} - A_0) * K * [G]}{1 + K * [G]} \qquad \text{eqn. (15)}$$

$$y = \frac{b * K * x}{1 + K * x} \qquad \text{eqn. (16)}$$

Equation (16) is often used for calculating binding constant based on absorption changes.

However, Equation (13) and (16) do not always fit well with the acquired titration profile, especially those with multiple binding ratios. At this point, modified equations are needed in order to get satisfactory binding constants.

1.6.3 Deduction of binding constant calculation equation for binding with 1:2 binding ratio

For the binding ratio larger than 1:2, the binding constant calculating equation would be very complicated. Here only the complex formed with a 1:2 binding ratio is discussed. The binding constants for the formation of complex with 1:2 binding could be listed as in Equation (17) and (18), where K_1 and K_2 are the separating binding constants, respectively.

$$G + H \leftrightarrow HG \qquad [HG] + [G] \leftrightarrow HG_2$$

$$K_1 = \frac{[HG]}{[H]*[G]}$$ eqn. (17)

$$K_2 = \frac{[HG_2]}{[HG]*[G]}$$ eqn. (18)

Similarly, Equation (19) could be acquired when absorbance or fluorescent intensity changes of host molecule is proportional to the guest molecule concentration.

$$A_0 = a * [H]_0$$ eqn. (19)

At certain concentration of guest, the total signal comes from three components and could be expressed in Equation (20).

$$A = a * [H] + b * [HG] + c * [HG_2]$$ eqn. (20)

where *a,b,c* are parameters, including the molar absorption coefficient/quantum yield of H, HG, HG_2.

In the presence of excess amount of analyte, free host molecule as well as the HG complex barely exist, where the signal of the system would only from the HG_2 complex. And the concentration of HG_2 is approximately the same as the initial concentration of host molecule, shown in Equation (21)

$$A_{lim} = c * [HG_2] \approx c * [H_0]$$ eqn. (21)

Together with Equation (22) and (23), it is able to get Equation (24), [130] which is the modified equation for determining binding constants with a 1:2 host to guest binding ratio.

$$[H]_0 = [H] + [HG] + [HG_2]$$ eqn. (22)

$$[G] = [HG] + 2[HG_2]$$ eqn. (23)

$$A = \frac{A_0 + [H]_0 * b * K_1 * [G] + A_{lim} * K_1 * K_2 * [G]^2}{1 + K_1 * [G] + K_1 * K_2 * [G]^2}$$ eqn. (24)

The Equation (13), (16) and (24) are the commonly used equations for calculating binding constants. Actually, for a certain type of host and guest molecules, the binding processes are not always occurred exactly as above deduced. The equation presented here is the simplified model for determining the binding constants. There are also some

processes, requiring other specific binding equations in order to obtain satisfactory results.

1.7 Summary of Chapter 1

Firstly, a brief introduction was given about saccharides and their function in various aspects, followed by the background information about the character of the boronic acid moiety and its unique interaction with diols, which have been extensively used in saccharide recognition. Later fluorescent techniques together with different types of fluorescence sensing mechanisms were presented.

Literature reviews were listed about the progress on saccharide detection based on boronic acid reported by our group and other groups.[131] [132, 133] The B-N interaction has been investigated in order to design more sensitive probes. Selectively recognition of D-glucose could be achieved if two boronic acid moieties were in a proper orientation. And the factors which affect the binding constants and selectivity were studied in detail in terms of modular sensor approach. Recent achievements on saccharide sensing based on weak interaction as well as boron acid-diol covalent interaction were also presented. A lot of monoboronic acid sensors were reported which can selectively bind with D-glucose, reducing the synthetic effort and with better solubility.

Furthermore, the progress about fluoride sensing was reviewed in terms of with and without B-F interaction probes. Fluoride is a Lewis base and able to form strong hydrogen bonds which can be extensively used in developing fluoride sensors. Meanwhile, two different palladium-catalysed reactions, Suzuki coupling reaction and Tsuji-Trost reaction, were introduced with the reaction mechanisms outlined at the same time.

At last, the deduction of equations for calculating binding constants, used in this thesis, were also presented.

CHAPTER TWO

Results and discussion

2 Results and discussion Boron-additive hydrogel for saccharide sensing

2.1 Overview of hydrogel based saccharide detection

2.1.1 Introduction of hydrogel

A hydrogel can be considered as a kind of material between liquid and solid state, exhibiting both liquid- and solid-like behaviours. Hydrogels have substantial internal structure and are often made from cross-linked water-soluble polymers that can hold water from 20% to 99% by weight,[134] which offers a natural advantage for storing or carrying active ingredients. Furthermore, various properties of hydrogels, like swelling, mechanical, permeation, surface and optical properties, offer many potential applications.[135] The so-called intelligent hydrogel is one example, capable of providing a volume change from their collapsed state to swollen, which can be seen as a signal response to external stimuli. The stimuli could be temperature, pH, ionic strength, concentration of organic solvent. Furthermore, the collapse / swollen changes are reversible. At this point, many pH,[136-138] temperature[139-141] and other stimuli sensors based on smart hydrogels have been developed and also the design of elegant drug delivery devices based on hydrogels also attract lots of attention.

According to the nature of cross-linkers, hydrogels are generally classified as physical and chemical hydrogels.[142] As the name suggests, the former type hydrogels are cross-linked by physical methods, namely non-covalent interactions, such as hydrogen bonding, π-π stacking, van der Waals forces, hydrophobic interactions, charge interactions and transition metal coordination *etc*. Such kind of hydrogels, also called supramolecular hydrogel, often take sol-gel transition as the signal reporter for sensing. Chemical hydrogel are cross-linked by covalent bonds in terms of interlinked

polymerisation, which are generally not able to go through sol-gel state transitions, yet with stronger mechanical strength.

The applications of hydrogels are various, depending on the properties of hydrogels. Those, sensitive to external stimuli, have the ability to indicate pH, temperature. Some are capable of responding to specific molecule, for example, glucose and can be used as biosensors or drug delivery devices. Some medical electrodes and contact lenses also use hydrogels.[143]

2.1.2 Hydrogel used for saccharide sensing and separation

As hydrogels with sensitive ingredients respond to external stimuli and also can behave as a drug carrier, they are believed to be the promising materials in maintaining blood sugar levels of diabetes patients, expecting them to work as an artificial pancreas. Various strategies have been reported based on such kind of materials. There are several types: a) enzyme modified hydrogel: glucose oxidase is encapsulated in a pH-sensitive hydrogel;[144] gluconic acid was generated after enzyme catalysis of glucose, which lowered the local pH in the microenvironment, resulting in pore size changes of the hydrogel and insulin release. b) lectin-modified hydrogel: lectins are natural receptors of carbohydrates, such as concanavalin A(Con A).[145] c) phenylboronic acid-functionalized hydrogel: phenylboronic acid is known to form cyclic esters with diols along with the decrease of pK_a of boronic acid.

As our group interests in the application of boronic acid moiety in various aspects, the progress on the boron modified hydrogels will be briefly summarised.

The first glucose-responsive hydrogel[146] was formed from the monomer of *N*-isopropylacrylamide crosslinked by *N*,*N*′-methylene-bisacrylamide with a fraction of phenylboronic acid as recognition moiety. Almost no release of insulin occurred when the glucose concentration was below 1 g/L whereas a large release was observed when glucose concentration increased to 3 g/L. When the immobilized phenylboronic acid in hydrogel binds with saccharide, a negative charge is induced. With addition of glucose, more of these anionic boronate complexes are formed, which are more hydrophilic than

the uncharged boronic acid, making the polymer more soluble and resulting in the release of insulin.

For such kind of gel, the changes in volume are the common parameters for monitoring the added saccharides, however, a bulky hydrogel, which has a low diffusion rate, leads to a slow response time. In order to tackle this issue, thin hydrogel film, or micro-, nano-hydrogels are made, which require special and expensive instruments to recognise the volume changes. One possible solution is to use a transducer, which could reflect the volume changes in an easy and convenient detectable way.[147] The interesting results were reported by Asher,[148, 149] who combined a polyacrylamide hydrogel with an embedded crystalline colloidal array (CCA) that diffracts light to report on its lattice space, and thus the volume of hydrogel. Glucose binding with phenylboronic acid induced the formation of boronate anions, which resulted in a Donnan potential, and an osmotic pressure that caused the hydrogel swell and red-shifted of Bragg diffraction.[149] This system was further improved by introduction of an amine group and PEG. Only glucose can self-assemble the system into a supramolecular complex, which is associated with cross-linking of the hydrogel and blue-shifted diffraction. As the glucose concentration of tear fluid is closely linked to that in blood, they used this new material for non-invasive glucose monitoring by using in contact lenses.[150] Zhang *et al* prepared an ultrathin film and successfully detected glucose concentration *via* shifts of Fabry–Pérot fringes.[151] Those aforementioned results rely on changes on either diffraction or reflection. Meanwhile, extensive efforts are devoted to fluorescent-based systems due to its unique advantages of fluorescence, like high sensitivity and multiple parameters to use. The Zhou group[152] reported a series of hybrid gels with imbedded fluorescent sensor, such as noble-metal nanoparticles; a boronic acid moiety was incorporated onto the polymer to afford a glucose responsive polymer hydrogel, which is also bound to fluorescent nanoparticles. The variation of glucose concentration would direct the behaviour of polymer hydrogel, which in turn tuned the optical behaviour of nanoparticles. They further used this disruption to regulate release of insulin, offering a state-of-art strategy for diabetes treatment.

Saccharides exist not only in the format of monosaccharides, oligosaccharides but also in glycoproteins, common biological components. Besides saccharide detection in human blood, boronic acid modified polyacrylamide hydrogels could also be used in

electrophoresis to separate oligosaccharides or detect glycated protein, which also known as non-enzymatic glycosylation, is an important biomarker for various disease states.[153] Polyacrylamide gel electrophoresis (PAGE) is a general separation matrix of biomolecules. Due to the electro neutrality of saccharides, the PAGE technique was further extended to FACE, the so-called fluorophore-assisted carbohydrate electrophoresis, [154, 155] where saccharides are modified with a fluorophore *via* the Schiff base formation reaction between aldehyde group on saccharide and amine group on fluorophore before separation. However, for saccharides with similar mass, structure and charge, the FACE strategy met its limit. Jackson and co-workers[47] improved the FACE method by developing a boronate affinity saccharide electrophoresis (BASE), which incorporated the specific carbohydrate affinity moiety (boronic acid) in a polyacrylamide gel. The BASE method was further investigated to separate glycated proteins,[156] which showed positive results and a potential application in identification of protein glycation.

2.2 Aim and Objective

Our group had prepared a dye displacement assay for saccharide sensing based on boronate hydrogel,[157] which gave inspiration to further extend this system by synthesising a fluorescent boronate-hydrogel. The binding between boronic acid and diols would directly induce the fluorescent change without adding another signal reporter component.

Previous results had demonstrated that boronic acid-modified acrylamide hydrogel could also be able to detect glycated protein in electrophoresis. Thus it was proposed that boronic acid-modified hydrogel has potential applications in directly visualising protein glycation under UV lamp other than staining procedures. PET sensors prepared in our group showed a fluorescent *turn-on* upon on complexation with saccharides. Bearing this in mind, it was proposed to further functionalise this structure with a methylacrylamide group to afford acrylamide monomers, which can be used in

electrophoresis. Different fluorophores were used in order to check the fluorophore effect on saccharide binding as well.

2.3 Syntheses of boron-modified acrylamide monomers

The proposed synthesis route is shown as Scheme 23.

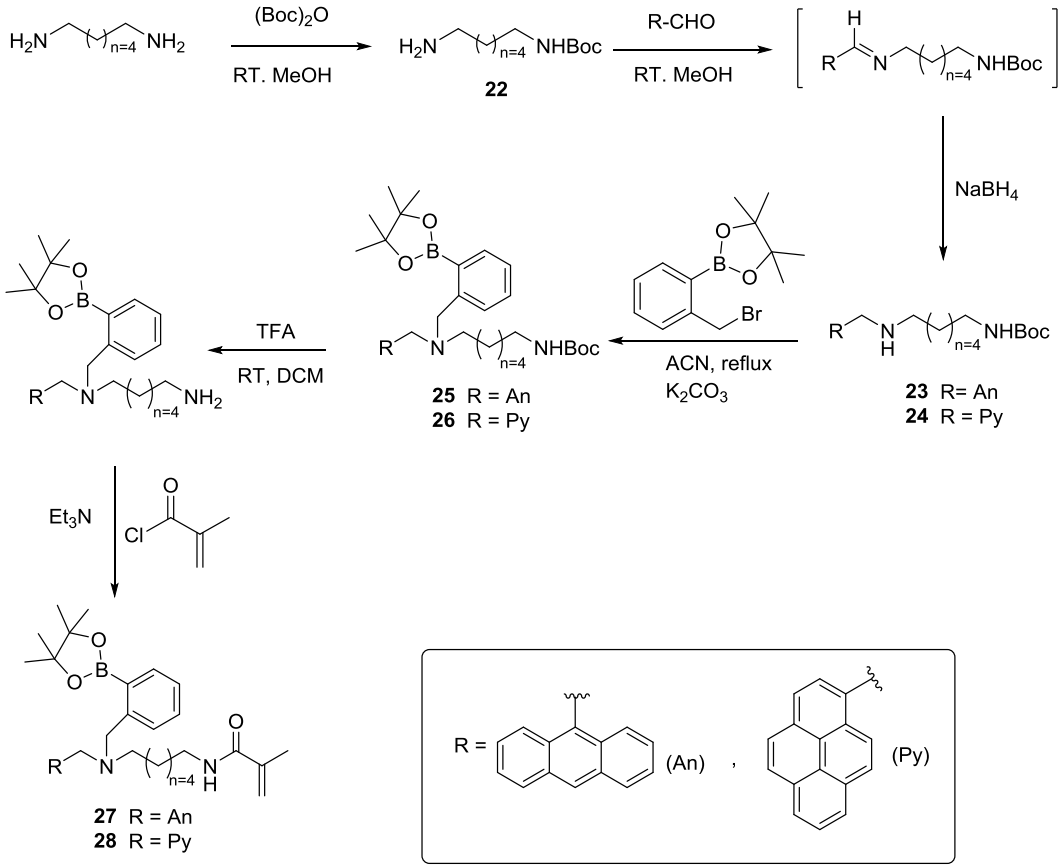

Scheme 23 Synthetic route for monomers containing fluorophore and boronic acid moiety

Compound **22** was obtained by adding 1 eq. of di-tert-butyl dicarbonate ($(Boc)_2O$) to 5 eq. of 1,6-hexanediamine stirring overnight,[158] then purified by column

chromatography with a yield of 74%. As there are two free amine groups, the other starting material ($(Boc)_2O$) needs to be added drop-wise in order to avoid side reactions. Most of the by-products were the starting materials due to excess amount of 1,6-hexanediamine used. As 1,6-hexanediamine has better water solubility compared with compound **22** and other byproduct, it could be washed off by means of extraction. It is hard to spot compound **22** under UV lamp as it has no absorption. 2,2-dihydroxyindane-1,3-dione (Ninhydrin) dip was employed to a finished TLC plate. Compounds **23** and **24** were obtained by mixing 1.0 eq. of compound **22** and 0.9 eq. of the respective aldehydes, and stirred in MeOH at room temperature, with a yield of 48% and 67.2%, respectively. ^{1}H NMR was employed to trace this reaction as the chemical shift of the proton on carbonyl group changed greatly when the reaction proceeded, mechanism shown in Scheme 24. Proton ***a*** is attached to a carbonyl group, of which the chemical shift is around 10 ppm, whereas proton ***b*** attached to an imine group, which has less electron-withdrawing ability than the carbonyl group, thus proton ***b*** is more shielded, showing an up-field chemical shift. Thus, the disappearance of the peak at 10.0 ppm and the emergence of the peak around 9.0-10.0 ppm shown in the ^{1}H NMR spectrum implied the completion of this reaction.

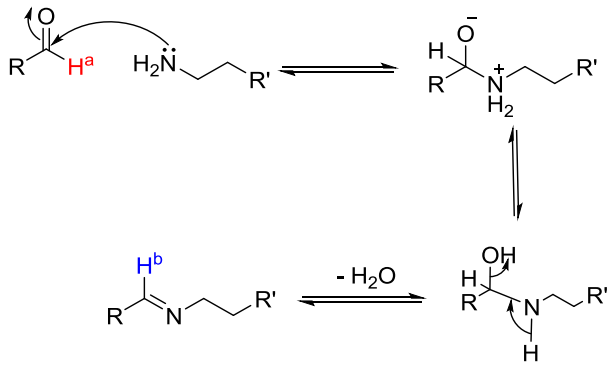

Scheme 24 Mechanism of the generation of intermediate

Compounds **25** and **26** were obtained under MeCN reflux in presence of K_2CO_3 for about 8 hours with almost quantitative yields 89% and 90%, respectively. In the case of stronger base being used or extended reaction time employed, the corresponding compounds without the pinacol protecting group would be obtained. After finishing

this reaction, condensing the mixtures under vacuum, crude products were precipitated out from water and then purified by chromatography if necessary. Compounds containing boronic acid groups are hard to purify, since the boronic acid moiety can interact with the hydroxyl surface groups in silica chromatography. Thus, low isolated yields often occurred due to streaking. In order to improve yields, the boronic acid moiety needs to be protected first with pinacol or 2,2-dimethyl-1,3-propanediol. However, for the formed boronated ester compounds, the protecting group could be removed during the column chromatography as well.

For the deprotection of di-*tert*-butyl-dicarbonate (BOC) group, it was found that the pinacol group was partially removed. However, since the binding event of boronic acid group and diols is a reversible process in the buffer solution, the pinacol group has little effect on the binding interaction between boronic acid and saccharide, thus compounds with pinacol moiety on have little effect in future investigation.

The final compounds **27** and **28** were not purely isolated, but NMR spectra showed the characteristic peaks. Monomethyl ether hydroquinone, used as stabiliser in acyl chloride reagent, adds extra peaks in NMR spectra, which make characterisation more difficulty. However, a quantitative reaction should be afforded as acyl chloride has a high reaction activity towards free amino moiety. Since the possible by-products would not be able to attend the further polymerisation step, the obtained compounds were used directly in the formation of hydrogel.

All the detailed synthetic procedures as well as characterisation data were collected in Chapter 6 (experimental part).

2.4 Investigations of saccharide sensing

2.4.1 Saccharide titrations in solution phase

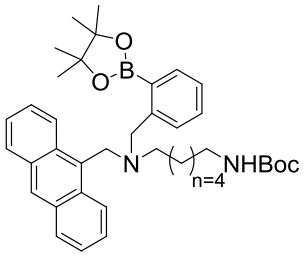

25

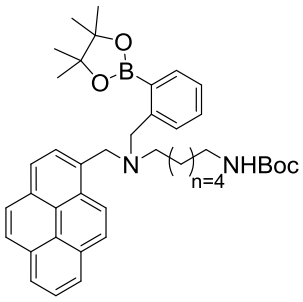

26

Saccharide titrations were carried out both in solution and hydrogel. Compounds **25** and **26** were chosen for the solution test, and only monosccharides were tested. The fluorescent titration of compounds **25** and **26** indicated that, upon adding the saccharides, an increase in fluorescent intensity was observed, shown in Figure 1 and Figure 2 respectively. This is consistent with previous PET sensors: binding between boronic acid and diols would decrease electron density of N atom as well as increase boron acidity, leading to a reduced PET processes. Typical anthracene emissions at 394 nm, 419 nm and 444 nm were observed for sensor **25**. The observed stability constants (K_{obs}) were calculated *via* Equation (13)[159] by employing emission intensity *versus* saccharides concentration. D-fructose showed the strongest binding stability with a value of 1381.7 ± 41.8 M^{-1} (R^2 = 0.999), for D-galactose K_{obs} = 221.4 ± 8.05 (R^2 = 0.999), for D-glucose K_{obs} = 221.4 ± 8.05 (R^2 = 1.00) and for D-mannose K_{obs} = 221.4 ± 8.05 (R^2 = 0.998). The binding stability constants follows the well-established order for binding between monoboronic acid and saccharides: D-fructose > D-galactose > D-mannose > D-glucose.[9] Titrations with senor **26** follows similar trend, but the observed stability constant for each saccharide is lower than that with sensor **25**, yet with larger fluorescent enhancement. The K_{obs}s and fluorescent enhancement are listed in Table 1 and Table 2, respectively. These results indicated that the fluorophore group did have an impact on the binding stability of boronic acid with saccharides. The lower K_{obs} of compound **26** toward monosaccharides may be due to the greater hydrophobic nature of the pyrene group as well as increased steric hindrance.[50]

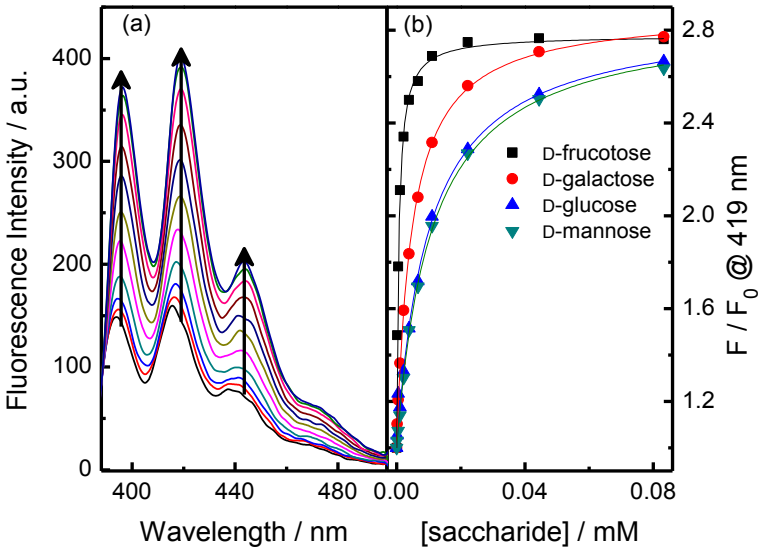

Figure 1 (a) Fluorescent spectral changes of compound **25** with different concentrations of D- fructose in pH 8.21 aqueous methanolic buffer solution [52.1 *wt*% methanol (KCl, 0.01000 M; KH_2PO_4, 0.002752 M and Na_2HPO_4, 0.002757 M)]; (b) Fluorescent intensity ratio (F / F_0) at 419 nm *versus* saccharide concentration

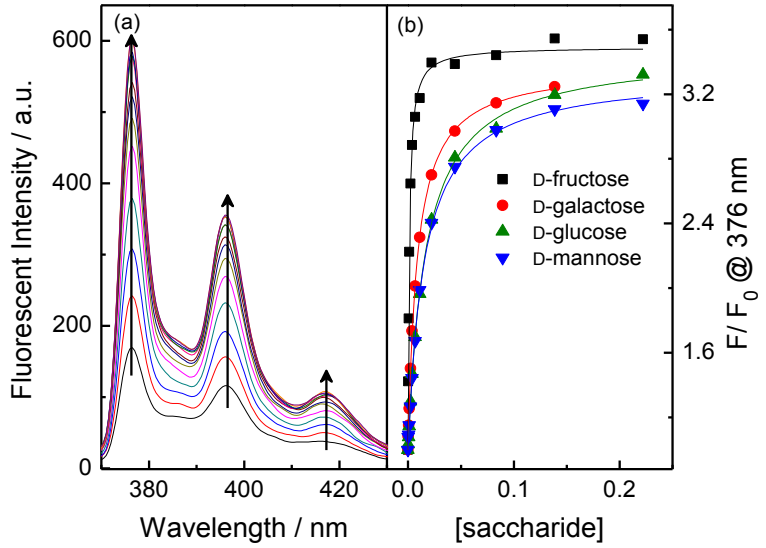

Figure 2 (a) Fluorescent spectral changes of compound **26** with different concentrations of D-fructose in solution as described in Figure 1. (b) Fluorescent intensity ratio (F / F_0) at 376 nm *versus* saccharide concentration

Table 1 Observed stability constants (K_{obs}), coefficient of determination (R^2) and fluorescence enhancements of compound **25**

	K_{obs} / dm^3 mol^{-1}	Fluorescence enhancement	R^2
D-Fructose	1381.7 ±41.80	2.54 ± 0.00	0.999
D-Galactose	221.4 ±8.05	2.82 ± 0.02	0.999
D-Glucose	87.18 ±1.80	2.82 ± 0.01	1.00
D-Mannose	92.48 ±3.79	2.87 ± 0.02	0.998

Table 2 Observed stability constants (K_{obs}), coefficient of determination (R^2) and fluorescence enhancements of compound **26**

	K_{obs} / dm^3 mol^{-1}	Fluorescence enhancement	R^2
D-Fructose	860.4 ±39.2	3.48 ± 0.02	0.997
D-Galactose	113.6 ±1.91	3.37 ± 0.01	1.00
D-Glucose	61.30 ±1.78	3.43 ± 0.02	0.999
D-Mannose	63.04 ±2.00	3.36 ± 0.02	0.999

2.4.2 Hydrogel formation and saccharide titrations

Hydrogel formation

The detail procedures of making acrylamide hydrogel was presented in experimental chapter (section 6.2.3). Following previous results, the polyacrylamide hydrogels were prepared, consisting of water (60% w/w), acrylamide (38% w/w), methylene bisacrylamide (1% w/w) and boron-containing acrylamide monomer (**27** or **28**, 1% w/w). However, it was found that due to the poor solubility of compounds **27** and **28**,

reduced amount of boron-additive acrylamide monomer is required in order to get clear hydrogels. 0.05 % compound **27** was finally used for gel formation. In fact, for compound **28**, the gel is still opaque even the percentage down to 0.025 wt%, and so most of the investigations were carried out with compound **27**.

Boron-additive hydrogel was first made in pure water environment. In order to test the factors that could affect the volume of hydrogel. Three hydrogel from the same batch were incubated overnight in pure water, pH 8.5 phosphate buffer and pH 8.21 phosphate buffer (containing 52.1 *wt* % methanol), respectively, of which size changes are shown in Picture 1. Compared with the size of hydrogel in pure water, hydrogel was swollen at pH 8.5 phosphate buffer and shrunk in pH 8.21 phosphate buffer containing 52.1 *wt* % methanol. In pure water solution, gel size can be affected by pH values, which were attributed to changes of the charges on boronic acid moiety. In alkali conditions, formation of boronate anion could efficiently increase the solubility of boro-additive and electro repulsion of the hydrogel. It is known organic solvents could partially dissolve hydrogel, causing the shrink. When in methanolic buffer solution (pH = 8.21, 52.1% wt MeOH), MeOH made the hydrogel shrink even with a pH value which was supposed to swell the gel. Thus buffer solutions without organic solvents were used in the following experiments.

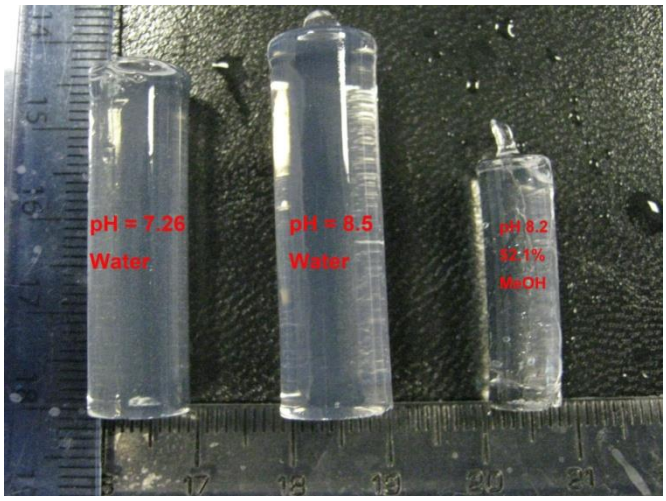

Picture 1 Size of gel after incubation in solution with different pH values for 16 hours

pH evaluation

As the binding stability between boronic acid and saccharide is greatly affected by pH values,[160] the hydrogel responses to pH were investigated. 0.05 M KH_2PO_4 was adjusted by 2 N NaOH to afford the buffer solutions with different pH values, 6.30, 7.31, 7.91, respectively. Since the buffer range of KH_2PO_4 / NaOH system is 5.6 to 8.0, the buffer was switched to Glycine / NaOH system, with a similar strategy to obtain the buffers with pH values of 8.60, 9.03, 9.49 and 10.17. D-fructose was utilised as model saccharide to evaluate the hydrogel responses with and without saccharides, the results shown in Figure 3. It was found that there was slightly higher saccharide response when pH > 8, which might be due to the enhanced binding affinity between boronic acid and saccharide. Another point to mention is that a hypsochromic shift of the maximum emission occurred for the hydrogel before and after addition of D-fructose from 448 nm to 409 nm.

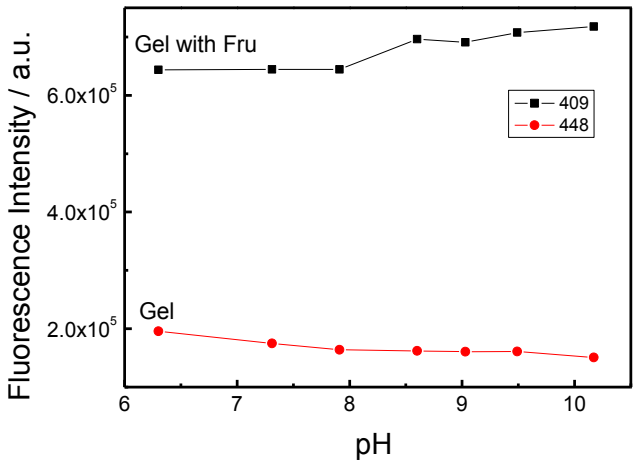

Figure 3 Fluorescent intensity changes of gel in buffer solution with different pH values

A micro-plate reader (12 × 8 wells) was used for the saccharide titration with hydrogels. The data for hydrogel-based saccharide titration was collected using a GILDON pλotonics fluoro-SENS fluorescence spectrometer. 0.2 mL gel precursor solution was added to each well and left for 40 minutes to set. Different volumes of saccharide solution were added and buffer was added to make the total liquid volume up to 0.1 mL. As binding in hydrogel is a diffusion based process, 2 hours of incubation time was

used to allow formation of boron-saccharide complex. Since the plate reader could offer high throughput analysis, saccharide titrations were carried out three times per concentration of saccharide, results shown in Figure 4. The selectivity orders for saccharides are consistent with that in solution, D-fructose > D-galactose > D- mannose > D-glucose. The binding constants of each saccharide, listed in Table 3, are much lower than that in solution phase. The binding constant with D-glucose is too low to be fitted. It is possible that the boronic acid moiety can't bind effectively with saccharides in hydrogel phase. One possible method is to reduce the size of hydrogel to even smaller, allowing faster diffusion process.

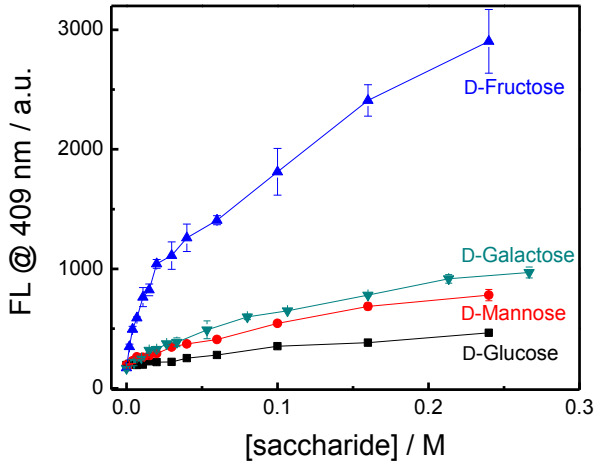

Figure 4 Fluorescent intensity ratios (F / F_0) at 409 nm *versus* saccharide concentration

Table 3 Observed stability constants (K_{obs}), fluorescence enhancements coefficient of determination (R^2) of compound **27**

	K_{obs} / $dm^3\ mol^{-1}$	Fluorescence enhancement	R^2
D-Fructose	52.6 ± 5.3	10.3 ± 0.4	0.992
D-Galactose	10.8 ± 1.3	6.4 ± 0.4	0.993
D-Glucose	--	--	--
D-Mannose	17.8 ± 4.8	3.1 ± 0.4	0.975

Both compounds **27** and **28** were used for electrophoresis in order to visualise the separation or detection of saccharides and glycated protein. It is proposed that the doping of compounds **27** and **28** could afford a boronic acid functionalised polyacrylamide hydrogel, which was used for the electrophoresis. The doped boronic acid moiety would bind with glycated protein, leading to a slower migration rate in electrophoresis, compared with the rates of normal proteins. Furthermore, the binding between boronic acid moiety and glycated protein would block the PET process, leading to the recovery of fluorophore emission. After finishing the electrophoresis, the plate could be visualised directly under a UV lamp. However, collaborators found it a bit difficult to use these two compounds in electrophoresis experiments as no results could be obtained due to that of compounds **27** and **28** having poor solubility, which are not suitable for electrophoresis.

2.5 Summary of Chapter 2

A series of boron-containing compounds **25**, **26**, **27** and **28** were synthesised which exhibited typical PET sensors activities. **27** and **28** contained a methyacrylamide moiety with a potential to form hydrogel polymer.

Secondly, saccharide titration in solution phase were carried with compounds **25** and **26**, sensor **25** has stronger binding with saccharides than that of sensor **26**, which may be due to the difference between fluorophores and steric effects.

Thirdly, a boron-additive hydrogel was formed by using compounds **27** and **28**. Due to poor solubility of compound **28**, only compound **27** has better performance to allow for further experiments. pH conditions and organic solvents were found to affect the volume of hydrogel, which were optimised before carrying out saccharide titrations. The binding stabilities of each saccharide in hydrogel are much lower than that in solution.

Compounds **27** and **28** were used by collaborators Marta P. Morais for electrophoresis and the results indicated that the compounds could not be used due to poor solubility.

Further optimisations by preparing of water soluble fluorophores are required before using in electrophoresis experiments.

CHAPTER THREE

Results and discussion

3 Results and discussion A dual response probe for fluoride and sugar recognition

3.1 Background

3.1.1 Overview of 1,8-naphthalimide based sensors

The 1,8-naphthalimide structure (Scheme 25) has been extensively explored as a versatile platform for biological sensing and imaging due to its unique photophysical properties such as absorption and emission in visible region, large Stokes shifts as well as high photostability.[16, 161] Additionally the photophysical properties could be modulated *via* modification on the fluorophore itself (3,4,6-positions) or on "*N*-imide site". Modification on 4-position with electron donating groups would induce a "push-pull" effect which leads to an internal charge transfer (ICT) character. Such ICT sensors displayed broad absorption around 450 nm and emission around 550 nm, respectively, allowing for designing of colorimetric sensors. Most 1,8-naphthalimide derivatives are sensitive to changes of microenvironment due to the ICT nature and also display solvent-dependency in their absorption and emission spectra.

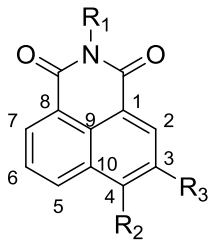

Scheme 25 Structure of 1,8-naphthalimide moiety

3.1.2 Fluoride detection based on 1,8-naphthalimide derivatives

4-amino-1,8-naphthalimide derivatives (**29a**) were first employed for anion recognition by Gunnlaugsson *et al* by modifying 4-NH_2 with aryl thiourea moiety, which could form strong hydrogen bonds with anions.[162] Small amounts of fluoride could cause fluorescence quenching with almost no change in absorption. The fluorescence quenching could be explained by a PET process from the aryl thiourea to the naphthalimide core, which was strengthened upon binding an anion, resulting in quenching of the 1,8-naphthalimide fluorescence. A 1:1 binding was shown between anion and receptor. An excess amount of fluoride could cause large absorption changes, which was believed to be caused by the deprotonation of the 4-amino moiety, confirmed by observations of a HF_2^- peak at 16 ppm in the ^{19}F NMR. The results indicated that not only the thiourea but also the -NH at 4-position of 1,8-naphthalimide were involved in the interaction with fluoride.

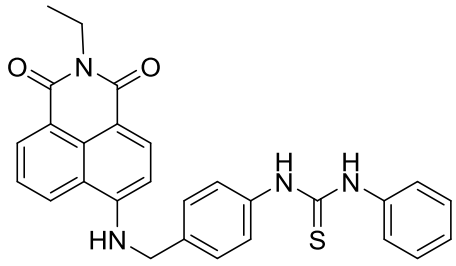

29a

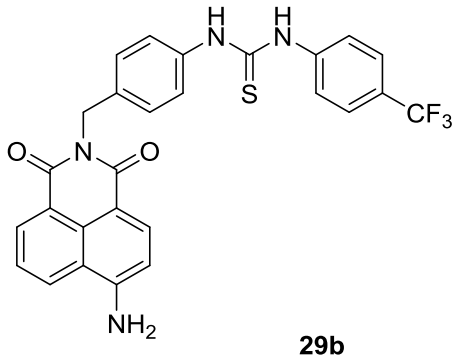

29b

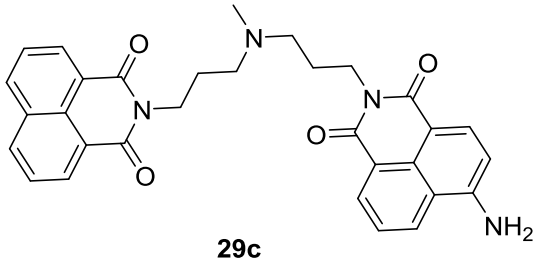

29c

Veale *et al* reported sensor **29b** by connecting aryl thiourea moiety to the *N*-imide part, where the fluorescence was also quenched upon addition of anions.[163] The observed

binding constants also indicated that the location of anion receptors (aryl thiourea moiety) has little effect on the sensing sensitivity towards anions; it was the deprotonation of 4-amino proton that caused the colour changes when fluoride added.

Pischel *et al* developed a bis-naphthalimide sensor **29c** to construct logic gates as the fluorescence emission of sensor **29c** could be tuned by protonation of tertiary amine and deprotonation by F^-.[164] The two naphthalimides (1,8-naphthalimide and 4-amino-1,8-naphthalimide) were linked through aliphatic spacer chain consisting of a tertiary amine. Protonation of the tertiary amine would selectively quench the PET process from amine to 1,8-naphthalimide, yet resulting in enhanced energy transfer between the 1,8-naphthalimide and -amino-1,8-naphthalimide parts. When the concentration of fluoride was in range of 0 to 20 μM, the protonated tertiary amine would be deprotonated, which then reactivated PET, leading to a fluorescence emission quenching. When more fluoride added (> 1 mM), deprotonation of 4-amino moiety would occur, resulting in a further quenching. Based on this, the author developed a ternary NOR logic gate mimic. This probe also proved that recognition of fluoride could be achieved solely on the deprotonation of the 4-amino position.

The 1,8-naphthalimide moiety offered a versatile platform for constructing fluoride sensors and there are several reviews in this regime.[14, 16, 17] The underlying mechanism is that the changes on the 4-amino of naphthalimide greatly affect its photophysical properties; and the fluoride anion is a strong Lewis base with small size, which made it an ideal candidate for tuning the photoproperties of naphthalimide.

3.1.3 Saccharide recognition based on 1,8-naphthalimide derivatives

Recognition of charge-neutral analytes such as saccharides is always a challenging issue and the boronic acid moiety was extensively explored for constructing saccharide probes as it can form boronate esters with 1,2- or 1,3-diols through covalent bonds. On the other hand, 1,8-naphthalimide moiety is extensively used in cation or anion sensors due to its unique photophysical properties. By combining these two parts, researchers

developed new saccharide probes *via* boronic acid modified naphthalimide derivatives. The Lakowicz and Heagy groups reported a series of naphthalimide-based mono-boronic acid probes **30a-f** with C_0 spacers.[165-167] **30a** was the first reported sensor and its fluorescence was quenched upon addition of saccharides, which was attributed to the photoinduced electron transfer mechanism as there are no fluorescence lifetime changes from the neutral form of boronic acid to its anionic form. **30b** displayed a dual response to saccharides and with selectivity towards D-glucose, though with a low quantum yield while **30c** was selective to D-galactose. This unusual selectivity indicated that there were other factors, such as conformational dynamics, that affected the binding affinity. **30d-30f** showed higher quantum yield and better solubility in water, however, not much enhanced sensitivity toward monosaccharides.

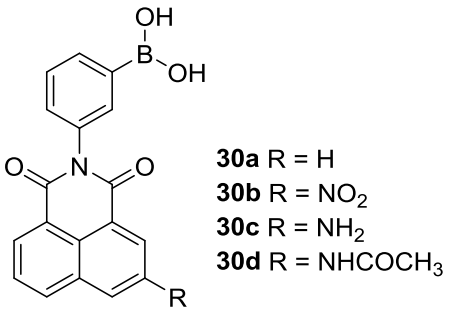

30a R = H
30b R = NO_2
30c R = NH_2
30d R = $NHCOCH_3$

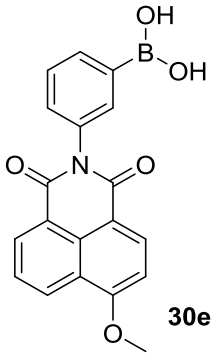

30e

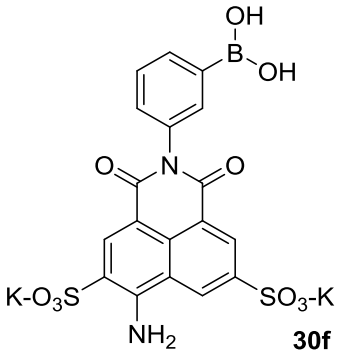

30f

The Trupp group designed a water soluble probe (**31**) for saccharides by attaching the boronic acid moiety in the 4-position with an ethylene as a linker.[168] By borrowing the B-N interaction, pronounced spectral changes were observed with the addition of saccharides. The sensor showed highest selectivity towards D-fructose with a limit detection of 0.1 mM. Most importantly, it gave a fluorescence turn-on response to saccharides, which is more desirable in designing fluorescent sensors. Another desirable feature is that the Stokes' shift is about 120 nm upon exposure to saccharides.

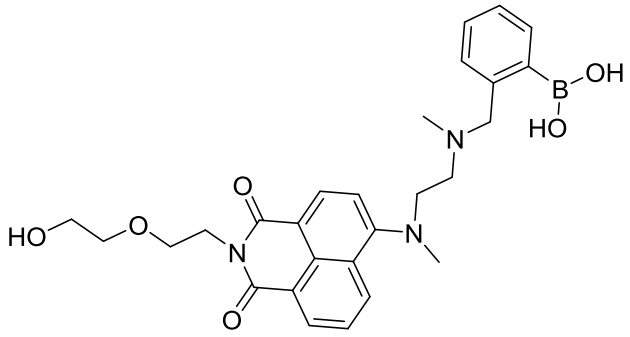

31

Later, based on the probe **31**, the Wang group reported a series of sensors synthesised by modifying the 4-amino group directly with a phenylboronic acid group. With various substituent groups on the 4-amino or on the *para*-position of phenylboronic acid moiety, they investigated the substitution effect on the saccharide sensing and also the underlying mechanism.[169, 170] However, results indicated that the variation of the substitution only produced a limited effect on saccharide binding.

3.2 Aim and Objective

Though the 1,8-naphthalimide moiety has been shown to be a good reporter for chemosensing applications, few of boron-modified naphthalimide compounds were reported for fluoride recognition. Within this project, a boron-containing 1,8-naphthalimide probe and its according control compounds were synthesised. By attaching the boronic acid group to the naphthalimide through a hydrazone bond, the degree of conjugation in the entire system would extend due to the "amino conjugation",[171] which, it was hypothesised, would facilitate charge transfer, resulting in longer wavelength of spectral changes. The response toward fluoride can be studied as both 4-amino proton and boron are binding sites to fluoride.[14] In addition, saccharide recognition could also be investigated by comparing with previous work.

3.3 Investigations on fluoride sensing

*3.3.1 Syntheses of compounds **33**,**34** and **35***

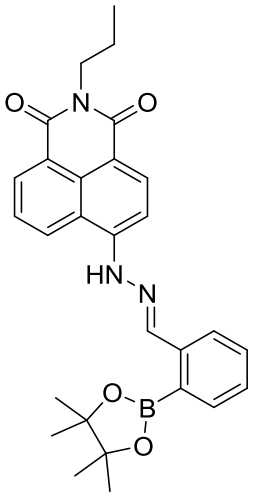

33

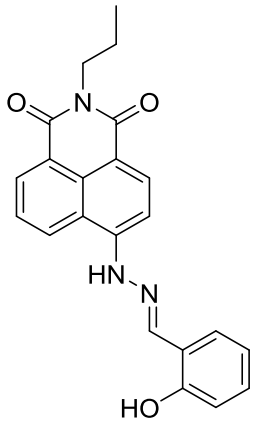

34

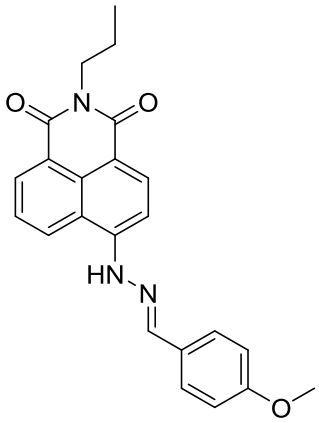

35

Compounds **33**, **34**, **35** were synthesised following procedures in literatures,[172] synthetic route shown in Scheme 26. Compound **32a** was synthesised by reacting propylamine with 4-bromo-1,8-naphthalimide anhydride. The propylamine could attack both anhydride part and 4-bromo position, thus the ratio of the reactants should keep close to 1:1. The reactant mixture was stirred in ethanol under reflux for 6 hours before condensed under vacuum. Then the resulted suspension was poured into ice water to precipitate out the crude product. Crystallisation was performed for purifying products with a yield of 89%. Compound **32** was obtained by treating compound **32a** with hydrazine, a yellow colour observed once compound **32** formed. After stirring in 2-methyoxylethanol for 3 hours, yellow solid was observed and TLC results indicated the disappearance of starting material compound **32a**. The precipitate was filtered and washed with cold ethanol. The yield was 71%. Compounds **33**, **34** and **35** were then synthesised under the same experimental conditions with different aldehyde reactants. Compound **33** has a poor yield, as the crude product required purification *via* flash

chromatography followed by recrystallisation, leading to a large amount of product loss. Compound **34** was synthesised as control compound of compound **33**, which had a phenol group at *para* position of corresponding aldehyde reactants. Compound **35** was obtained by mixing compound **32** with *p*-methoxylbenzaldehyde in ethanol, reacting for 6 hours under reflux. The resulting solid has two different morphologies, one powder whilst the other cotton-like. The two solids were purified separately; however, they were confirmed to be the same expected compound **35**. The underlying reasons for generating two different morphologies are still unclear yet. Detail experimental reaction conditions and full characterizations of all these compounds were listed in Chapter 6 of the thesis (Experimental).

The formed hydrazones are stable since they participate in electron delocalization of the conjugated systems. Meanwhile the conjugation effect also leads to planar conformations of these compounds. Theoretical calculations discovered that the optimized planar geometries were similar both in gas phase and in acetonitrile solution, with the *trans* form of the C=N double bond being more energetically favoured type.[173]

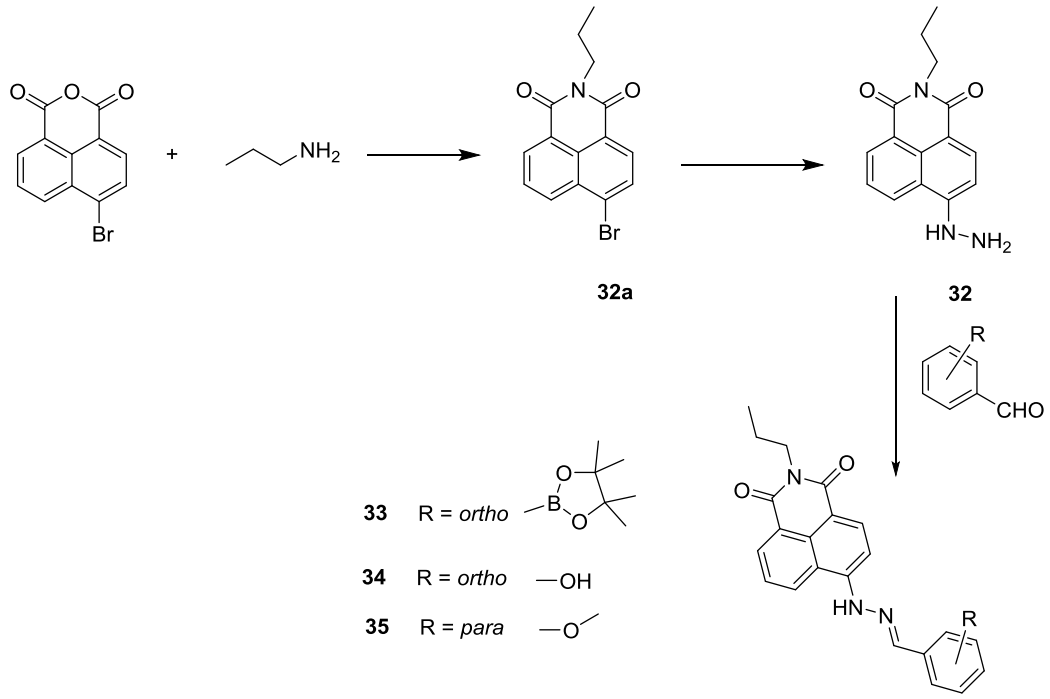

Scheme 26 Synthesis route of compounds **33**, **34** and **35**

3.3.2 Solvent effect

For 1,8-naphthalimide derivatives, an ICT photochemical character is often displayed, especially when the functional group was directly attached on the naphthalimide core. The optical properties of ICT-based probes are sensitive to the surrounding environment, thus a solvent screen was carried out to find out the most suitable solvent for fluoride sensing. The emission of compound **33** showed a bathochromic shift from 498 nm to 541 nm with decreasing solvent polarity (shown in Figure 5), which indicated an ICT characteristics of this probe.

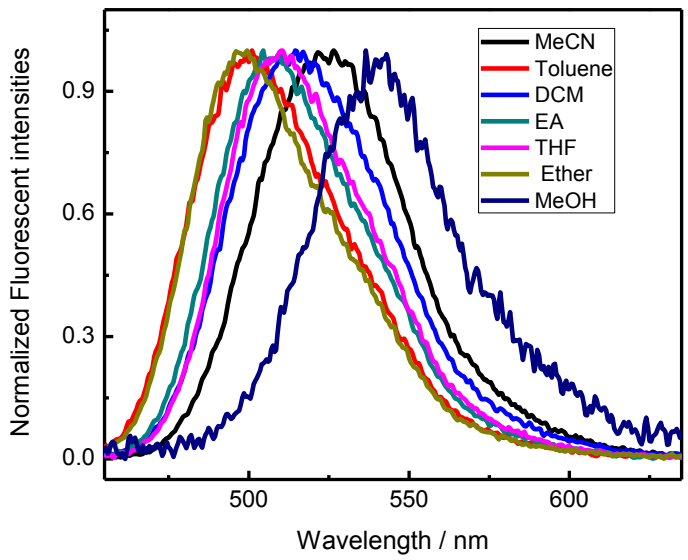

Figure 5 Normalised fluorescent spectra of compound **33** in different solvents. The polarities of solvent are shown in terms of dielectric constants: toluene 2.38, diethyl ether (Ether) 4.3, ethyl acetate (EA) 6.02, tetrahedrofuran (THF) 7.5, dichloromethane (DCM) 9.1, acetonitrile (MeCN) 37.5 and methanol (MeOH) 33. [**33**] = 2 μM

Furthermore, the responses of compound **33** toward fluoride were studied in each solvent in order to understand the solvent effect on the binding between fluoride and compound **33**. It was found that 4.6 equivalents of fluoride would induce different degrees of spectral absorption decrease as well as red-shifts of emission for compound

33 in all tested solvents except methanol, in which the addition of fluoride barely caused any changes (Figure 6). The behaviours of compound **33** in methanol could be attributed to the strong interaction between fluoride and methanol reducing the binding affinity between fluoride and compound **33**.

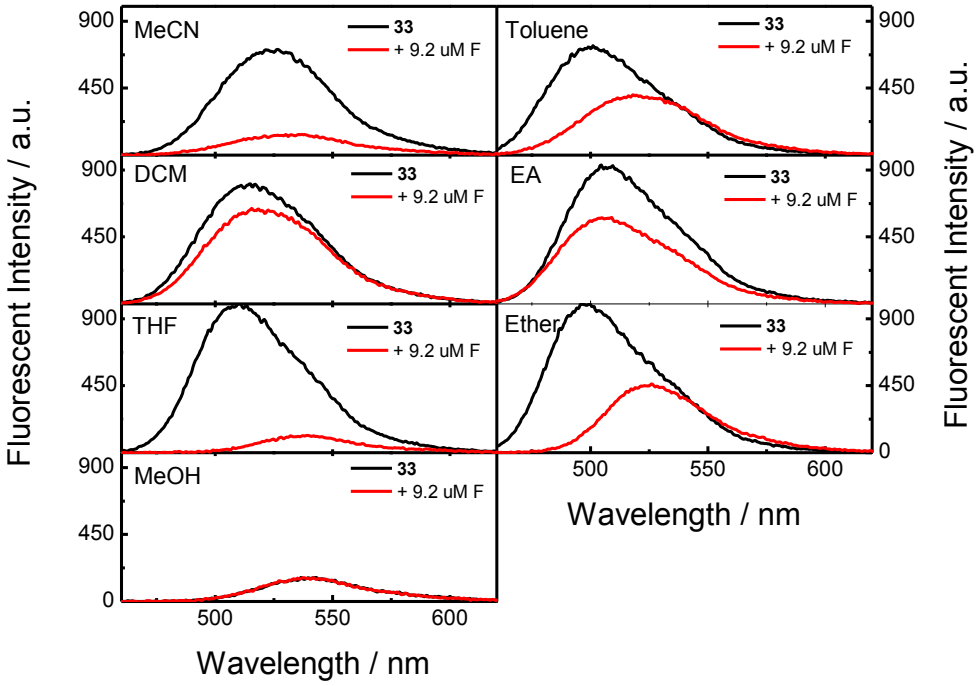

Figure 6 Fluorescent spectral changes of compound **33** in different solvents upon addition of 4.6 eq. of fluoride. [**33**] = 2 μM Note: as in different solvents the fluorescent emission intensities of compound **33** vary a lot, here all spectra were listed separately.

Considering the phenol group on control compound **34**, solvent effect together with responses toward fluoride in different solvents indicated that the absorption of compound **34** in each solvent is the same (two absorption peaks at 331 nm and 455 nm, respectively), but responses to fluoride are different as shown in Figure 7 and Figure 8. Upon addition of fluoride, the absorption peak of compound **34** stayed the same when in methanol. However, a new peak appeared at around 600 nm with a clear isobestic point at 500 nm in other solvents after addition of fluoride. The new peak splits into two different distinct peaks in THF and toluene. In ethyl acetate, the new peak was also observed, but with reduced intensity.

Experiments also showed that addition of methanol to other organic solvents would effectively reverse the binding between compounds **33**, **34** and fluoride. With regard to this, the test of fluoride sensing ability was limited to aprotic solvents. Considering the emission intensity, maximum emission wavelength and also the degree of spectral changes after addition of fluoride, acetonitrile was determined to be the optimal solvent for all the following investigations.

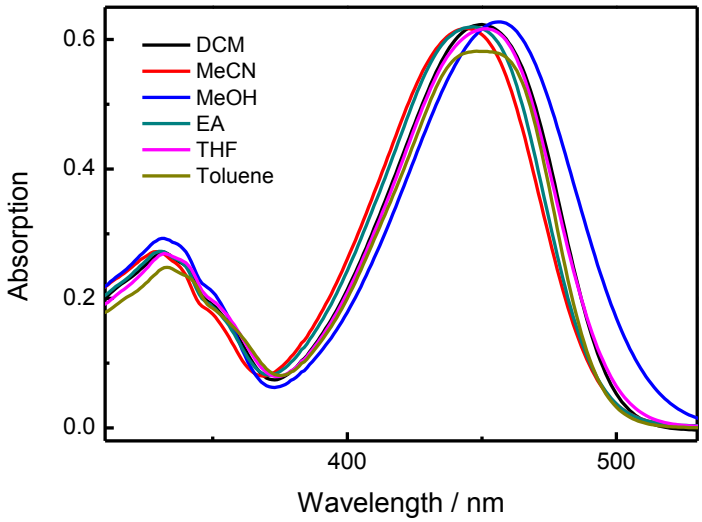

Figure 7 Absorption spectral changes of compound **34** in different solvents. [**34**] = 2.14×10^{-5} M

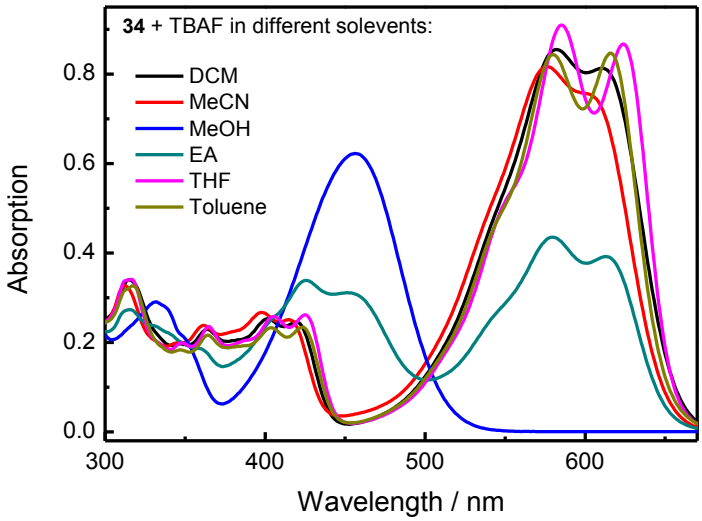

Figure 8 Absorption spectra of compound **34** with 4.6 eq. TBAF in different solvents. [**34**] = 2.14×10^{-5} M

3.3.3 Selectivity screen

Fluoride is a strong Lewis base and the design of fluoride sensors normally relies on the Lewis base-Lewis acid interaction. However, there are several other competitive anions, which are normally the interferences for fluoride detection. Thus a series of Lewis bases in their tetrabutyl ammonium salts format were used to test the selectivity of compounds **33** and **34**. For compound **33**, only F^-, OAc^- and $H_2PO_4^-$ produced changes in the absorption, a new peak at 589 nm formed with an isobestic point at 480 nm, while other anions caused almost no spectral changes (Figure 9). Comparing the spectral changes caused by F^-, OAc^- and $H_2PO_4^-$, it can be seen that fluoride causes the most pronounced difference at 589 nm. Meanwhile, a red-shift of absorption from 448 nm to 474 nm was observed upon addition of 5 equivalents of fluoride, whereas such red-shift was not seen for $H_2PO_4^-$ and OAc^-. The red-shift behaviour was also observed for the emission of fluorescent spectra of compound **33** (Figure 10).

On the addition of different anions to compound **34**, again only F^-, OAc^- and $H_2PO_4^-$ induced spectra changes. Nevertheless, F^- caused almost the same degree of changes as OAc^-, leading to a poor selectivity between these two anions, seen in Figure 11.

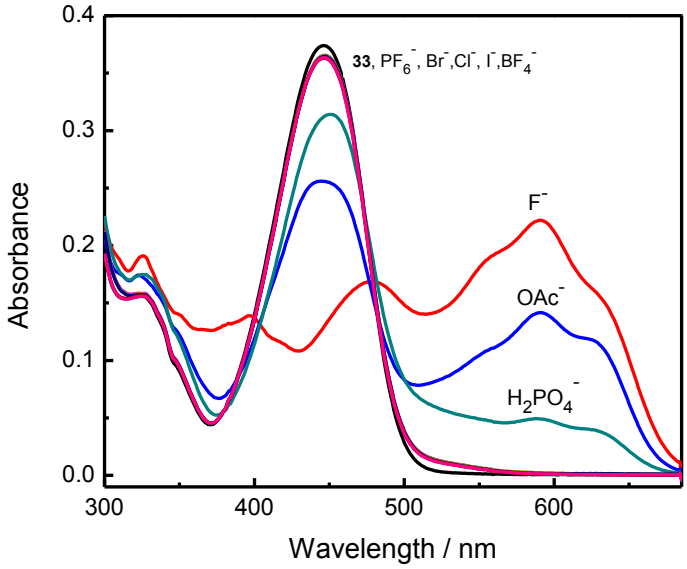

Figure 9 Absorption spectral changes of compound **33** upon addition of 5 eq. of each anion in MeCN. [**33**] = 12 uM

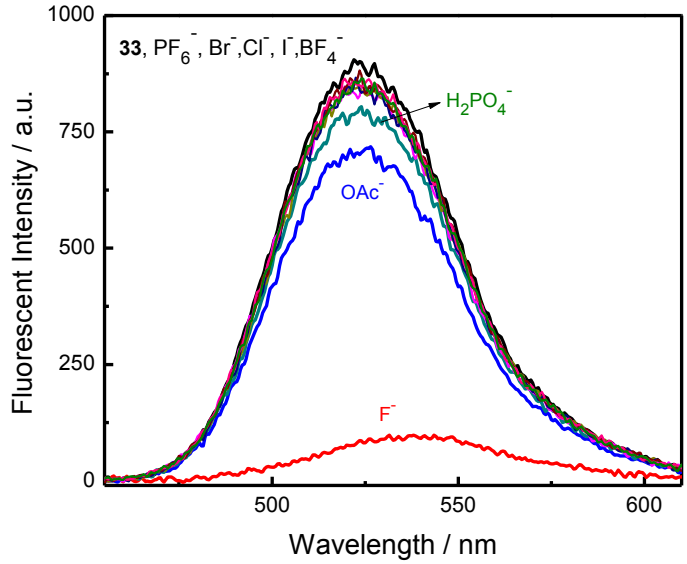

Figure 10 Fluorescent spectral changes after addition of 10 μM of different anions in MeCN. [**33**] = 3 uM

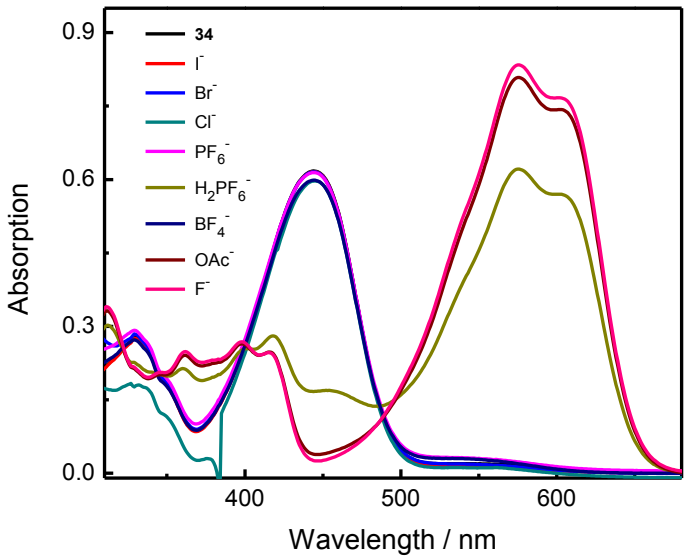

Figure 11 Absorption spectral changes of compound **34** upon addition of 4.6 eq. of each anion in MeCN. [**34**] = 21.4 uM

3.3.4 Anion titrations

*Compound **33** investigations*

There are two potential binding sites on compound **33**, the 4-amino position and boron atom position. Initial design concept was that these two binding sites would work co-operatively to interact with fluoride ion in order to achieve high sensitivity and selectivity. The anion selectivity results have already demonstrated that this probe could effectively discriminate different anions. The detail anion titration experiments, however, found that the two binding sites were not always working cooperatively as we expected. Actually, incorporation of a boronate ester moiety leads to a rather complicated interaction between compound **33** and fluoride.

Absorption spectral changes of compound **33** went through several stages when binding with TBAF, shown in Figure 12 and Figure 13. When the concentration of fluoride was below 30 μM, that is, less than 3 equivalents, the decreased peak at 448 nm shifted

with small increase of absorption at 590 nm. As the formation of absorption at 590 nm is mainly due to the interaction between fluoride and 4-amino proton, the spectral shift changes indicate that the boron moiety has priority to bind with fluoride, and the formed boron species induced the red-shift of the absorption peak at 448 nm. With increasing of fluoride, significant increase of absorption at 590 nm as well as continuously peak-shift at 448 nm were both observed. When the concentration of fluoride was over 120 μM (12 eq.), the absorption at 590 nm reached a plateau, leading to an "S" shape profile. While in fluorescent titration of compound **33**, a much more sensitive response was observed, requiring only 3 equivalents of fluoride to quench almost all the fluorescence (Figure 15). In addition, along with decrease of fluorescence, a red-shift of emission from 524 nm to 545 nm was displayed. The high sensitivity might be due to the B-F species providing more non-emissive relaxation pathways for the excited state of compound **33**.

A Job's plot analysis, shown in Figure 14, was carried out to investigate the binding interaction between fluoride and compound **33**, however, the results implied a complicated binding mode, which is partly due to the coordination between boron and fluoride anion and indicated a large deviation.

Based on the absorption titrations, binding constants were calculated using modified Hill equation,[174] which gave the binding constant K value as $(1.6 \pm 0.03) \times 10^4\ M^{-1}$ with $R^2 > 0.995$ (seen Appendix Fig. 1). The Hill coefficient n has a value of 2, indicating a cooperative binding.

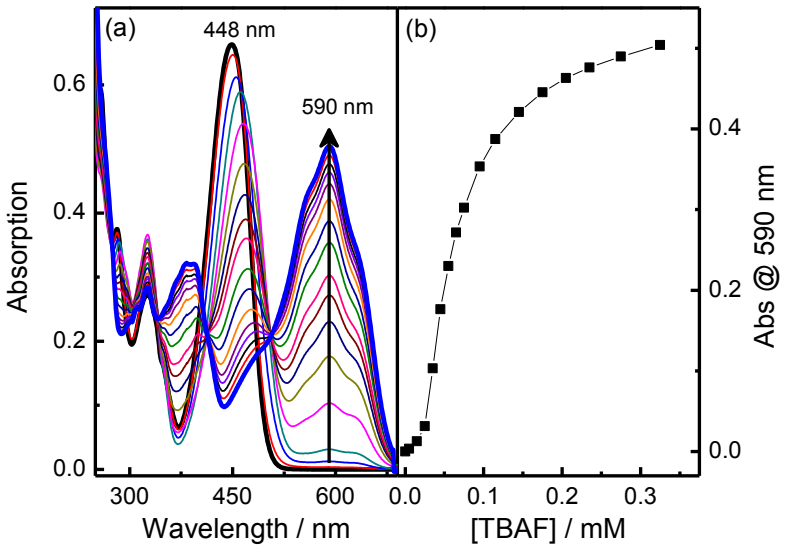

Figure 12 (a) Absorption spectral changes of compound **33** along with addition of TBAF in MeCN. [**33**] = 10 μM (b) absorption changes at 590 nm of compound **33** with different concentrations of TBAF

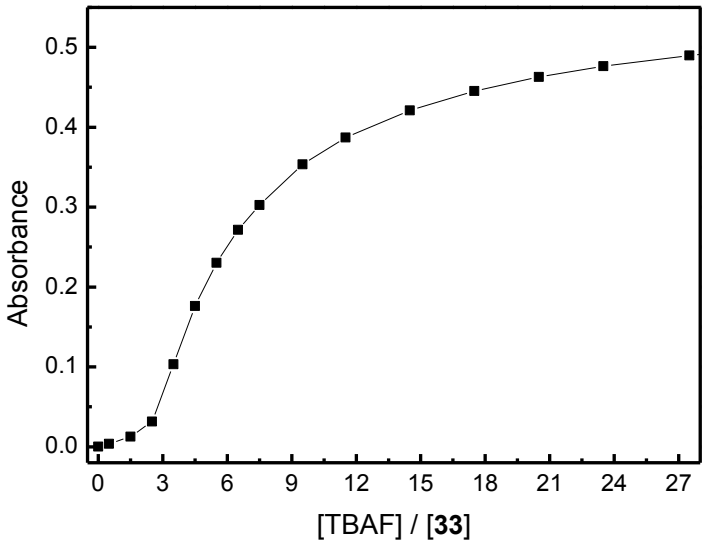

Figure 13 Absorption changes at 590 nm of compound **33** *versus* the ratio of the concentrations of TBAF to that of compound **33**

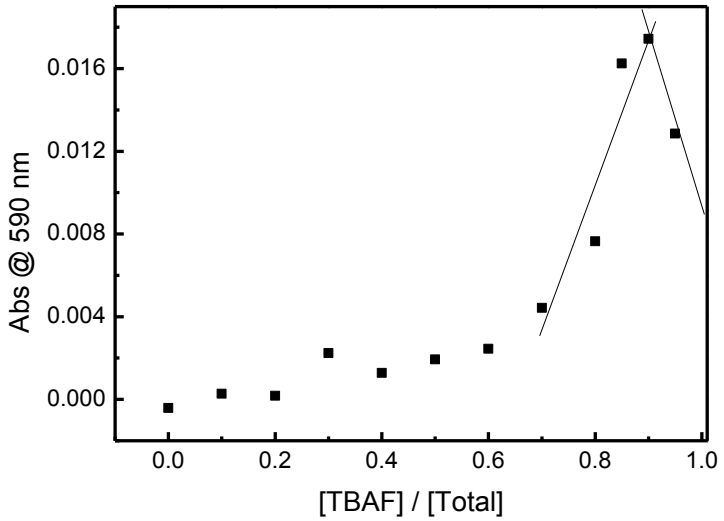

Figure 14 Job's plot diagram for binding interaction between compound **33** and TBAF in MeCN. Absorption of compound **33** at 590 nm were employed

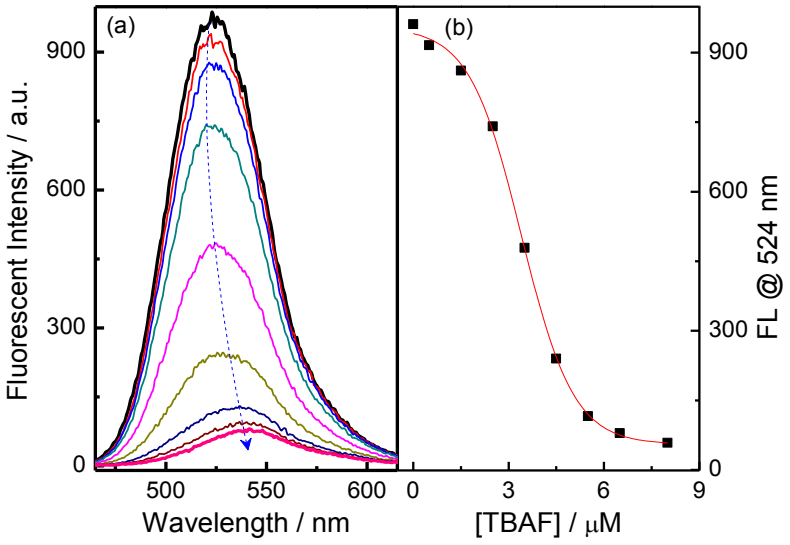

Figure 15 (a) Fluorescent spectral changes of compound **33** along with addition of TBAF in MeCN. [**33**] = 2×10^{-6} M, excited wavelength 450 nm; (b) emission changes at 524 nm of compound **33** with different concentrations of TBAF

The titrations of compound **33** with acetate anion were also carried out both in terms of absorption and fluorescence emission, a much weaker binding affinity was displayed compared with that of fluoride. As much as 16 eq. of acetate anion is needed to arrive at equilibrium state in the absorption titration and as for fluorescence titration, 6 eq. of

acetate were added to quench the original fluorescence by half. To our delight, the binding constant calculation fits the Hill equation, with K value of 7158 ± 424 M^{-1} and R^2 value of 0.998 (Appendix Figure 2). The Hill coefficient n is 1, suggesting an independent binding event. Judging from the binding constants, compound **33** has one magnitude higher of sensitivity toward F^- than that of OAc^-.

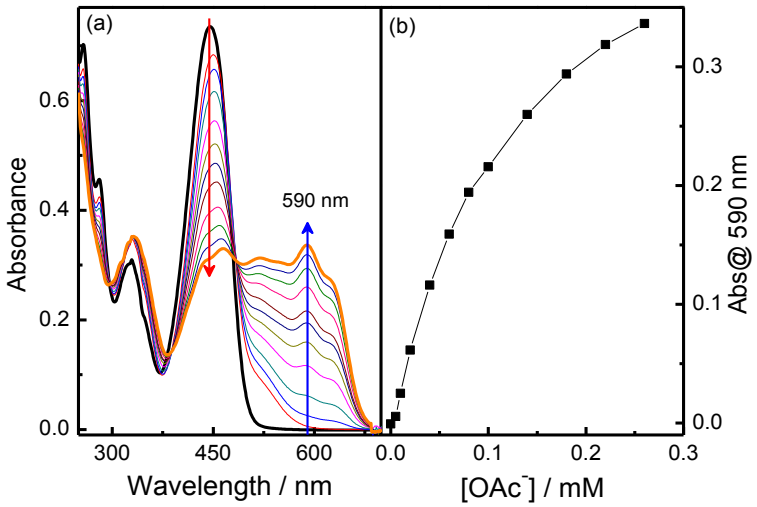

Figure 16 (a) Absorption spectral changes of compound **33** along with addition of TBA OAc in MeCN. [**33**] = 12 μM (b) absorption changes of compound **33** at 590 nm with different concentrations of TBA OAc

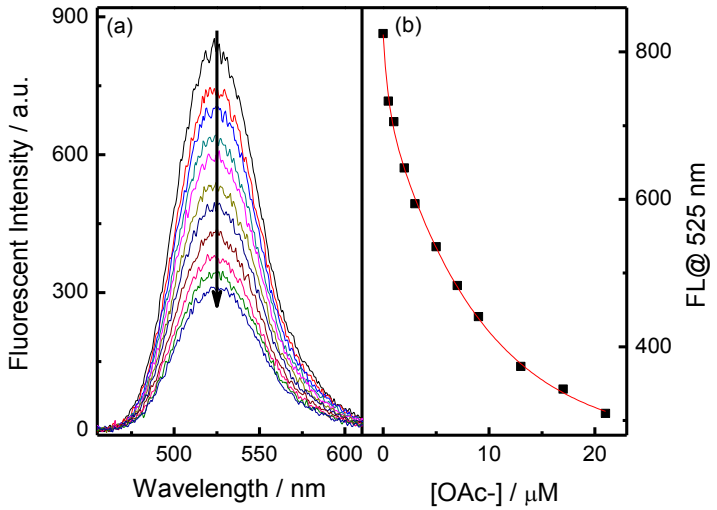

Figure 17 (a) Fluorescent spectral changes of compound **33** along with addition of TBA OAc in MeCN. [**33**] = 3×10^{-6} M, excited wavelength at 450 nm; (b) emission changes of compound **33** at 525 nm with different concentrations of TBA OAc

Compound **33** has a higher selectivity toward fluoride compared to acetate. Two factors account for this: one is that fluoride anion is a stronger base, which is able to form stronger hydrogen bonds; the other is that fluoride could coordinate with boron atom, acting in a cooperative manner to selectively discriminate anions.

*Compound **34** investigation*

Compared with compound **33**, compound **34** has a phenol group instead of boronate ester moiety at the *ortho*-position, which could elucidate the role of boronate ester in anion sensing. Compound **34** has absorption at 442 nm and 520 nm, respectively. Addition of fluoride induced a new absorption peak at around 575 nm with a shoulder peak at 605 nm and a decrease of fluorescent emission at 520 nm, seen in Figure 18 and Figure 19. Furthermore, compound **34** is much more sensitive to fluoride. 3 eq. of fluoride produced a plateau in the absorption spectra, where compound **33** required 13 eq. of fluoride. As for fluorescent titration, about 4 eq. of fluoride was needed for compound **34** to fully quench its emission, which has the same degree of sensitivity as that observed for compound **33**. The Job's plot analysis indicates a 2:1 binding mode (Figure 20), a binding constant based on Hill equation is $(4.3 \pm 0.19) \times 10^4\ M^{-1}$ with R^2 as 0.992 (Appendix figure 3). A Hill coefficient value of 2 was determined indicating that cooperative binding exists. A higher binding constant $(2.2 \pm 1.7) \times 10^5\ M^{-1}$ with R^2 value as 0.998 was obtained when using nonlinear least squares analysis for 2:1 anion-to-host complex formation (Appendix figure 4). Nonlinear least square analysis (Equation (24), deduced procedures listed in section 1.6 in chapter one) could afford stepwise binding constants K_1 and K_2, obtained for 2:1 binding. The observed binding constants by nonlinear least squares analysis were generally referred to K_2.

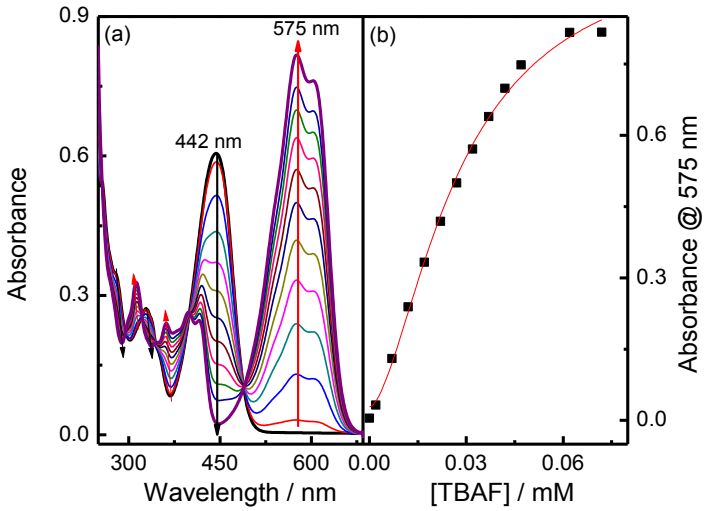

Figure 18 (a) Absorption spectral changes of compound **34** along with addition of TBAF in MeCN. [**34**] = 21.4 μM (b) absorption changes at 575 nm of compound **34** with different concentrations of TBAF

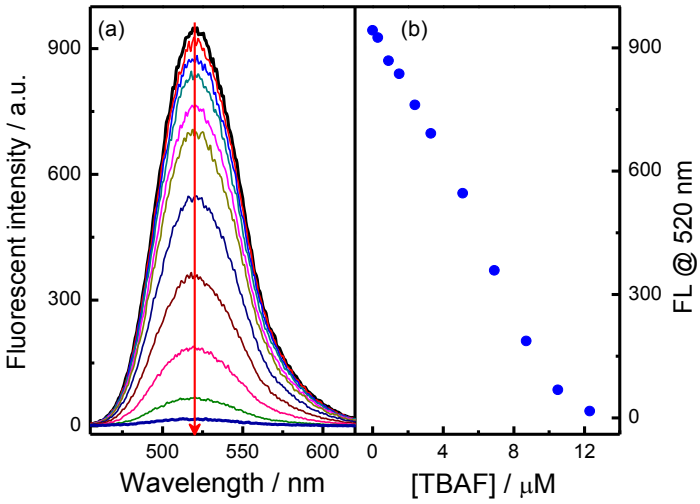

Figure 19 (a) Fluorescent spectral changes of compound **34** along with addition of TBAF in MeCN. [**34**] = 2.14×10^{-6} M, excited wavelength 445 nm; (b) emission changes at 520 nm of compound **34** with different concentrations of TBAF

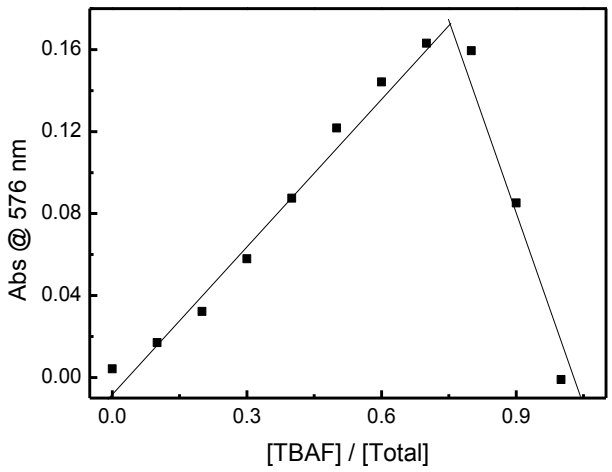

Figure 20 Job's plot diagram for binding interaction between compound **34** and TBAF in MeCN. Absorptions of compound **34** at 576 nm were employed

In order to fully understand the binding affinity difference, a spectral investigation with acetate was also performed. Upon addition of acetate to compound **34**, an absorption peak at 575 nm was observed, similar to that seen with fluoride. Although compound **34** showed enhanced sensitivity toward fluoride, here another issue is that it showed similar even slightly better sensitivity toward acetate as well, indicating a poor selectivity between anions, shown in Figure 21. The Job's plot analysis (Figure 22) also indicated a 2:1 binding ratio. Similarly, binding constants were obtained *via* Hill equation and nonlinear least square fitting with binding constants K $(7.7 \pm 0.25) \times 10^4$ M^{-1} (R^2 =0.994) and $(1.6 \pm 0.29) \times 10^5$ M^{-1} (R^2 =0.999), respectively, seen in Appendix Figure 5 and 6. These results indicate that the Lewis acidic 4-amino proton and the phenol group at *ortho* position can effectively interact with both fluoride and acetate ions.

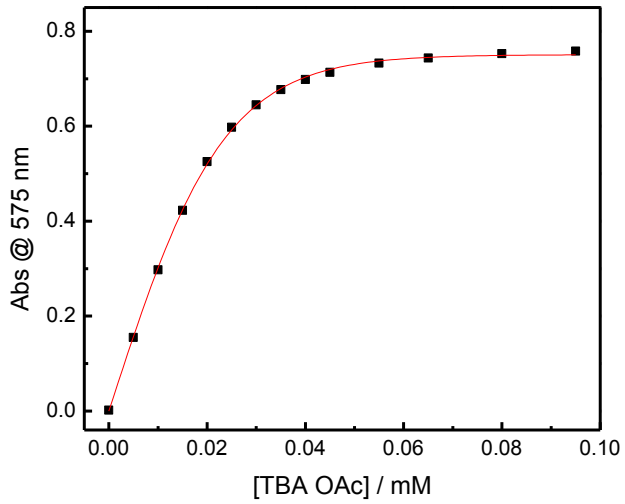

Figure 21 Absorption changes at 575 nm of compound **34** with different concentrations of TBA OAc MeCN, [**34**] = 2.14×10^{-5} M.

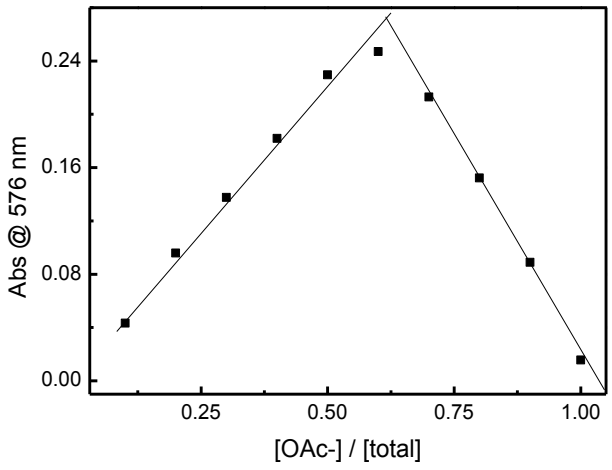

Figure 22 Job's plot diagram for binding interaction between compound **34** and TBAOAc in MeCN. Absorptions of compound **34** at 576 nm were employed

*Compound **35** investigation*

The absorption of compound **35** at 452 nm decreased upon addition of TBAF, along with increase at 588 nm, of which the trend is similar to those observed with compounds **33** and **34**, seen in Figure 23. Also 3.5 eq. of fluoride was required to reach the equilibrium state, which has the same degree of sensitivity as that observed for

compound **35** and a higher sensitivity than that of compound **33**. The Job's plot analysis (Figure 24) results again indicated a 2:1 binding ratio and the binding constant of compound **35** with TBAF is $(3.0 \pm 0.07) \times 10^4$ M^{-1} with R^2 as 0.997 (Appendix Figure 7). Compounds **34** and **35** showed similar sensitivities towards fluoride, both higher than that of compound **33**. These results indicated that the 4-NH is the predominate binding site for fluoride.

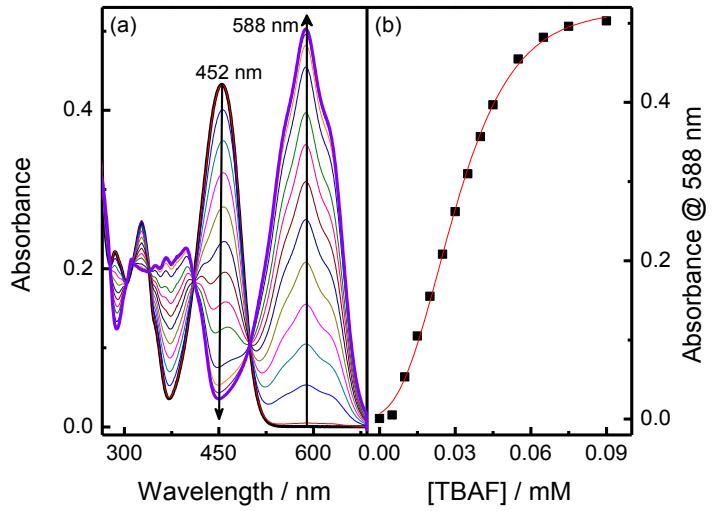

Figure 23 (a) Absorption spectral changes of compound **35** along with addition of TBAF in MeCN. [**35**] = 20 μM (b) absorption changes at 588 nm of compound **35** with different concentrations of TBAF

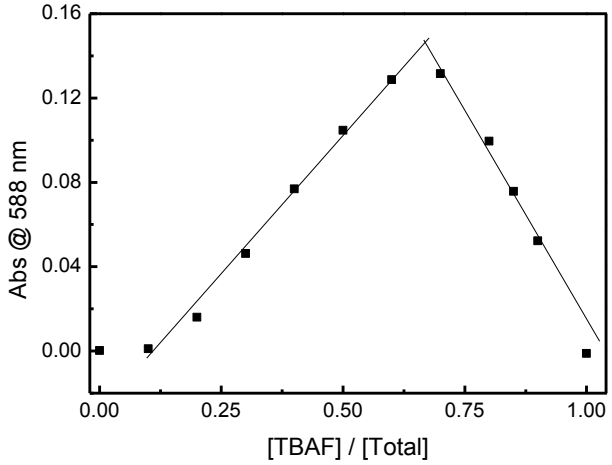

Figure 24 Job's plot diagram for binding interaction between compound **35** and TBAF in MeCN. Absorptions of compound **35** at 588 nm were employed

*Comparisons between compounds **33**, **34** and **35***

All three compounds had responses to anions with formation of new absorption peaks at around 600 nm together with a decrease of fluorescent emission. Furthermore, binding between compound **33** and fluoride also induced a red-shift of both absorption and emission, which were neither observed for interaction between acetate and compound **33** or any other anions with compounds **34** and **35**. The observed red-shifts of absorption and emission peaks is proposed to originate from the coordination between boron and fluoride. And the newly formed absorption peak came from the hydrogen bonding interaction between anion and the host acceptors, which also induce obvious colour changes and NMR chemical shifts, discussed later in this chapter.

In terms of absorption spectra, compounds **33** showed poor sensitivity towards both fluoride and acetate, compared with that of compound **34** (Figure 25(a) and Figure 26). However, an interesting observation is that, the fluorescent emission changes of compound **33** displayed an improved selectivity between fluoride and acetate (Figure 25 (b)). What's more, when compared with the binding constants obtained from absorption titration, listed in Table 4, compound **33** displayed a better selectivity between fluoride and acetate ions than that of compound **34**.

In the other words, compound **33** sacrifices the sensitivity toward fluoride and acetate to obtain a better selectivity between them.

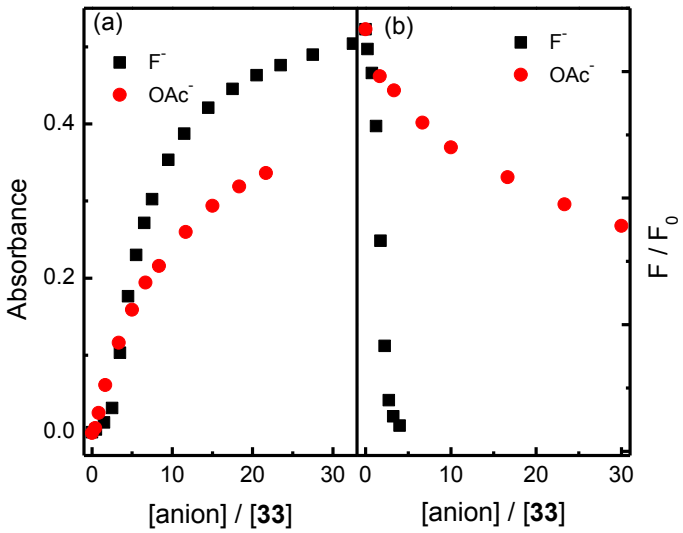

Figure 25 (a) Absorptions of compound **33** with fluoride and acetate anion *versus* ratios of anion to compound **33**; (b) Fluorescent intensities of compound **33** with fluoride and acetate *versus* ratios of anion to compound **33**

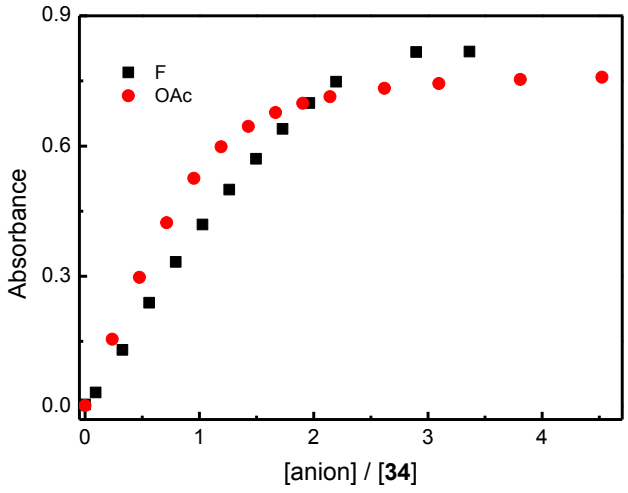

Figure 26 Absorptions of compound **34** with fluoride and acetate anions *versus* ratios of anion to compound **34**

Table 4 Binding constants of compounds **33** and **34** towards fluoride and acetate, calculated by Hill equation

	Binding constant (M^{-1}) fluoride	Binding constant (M^{-1}) acetate (M^{-1})
Compound **33**	$(1.60 \pm 0.03) \times 10^4$	7158 ± 424
	$R^2 = 0.995$	$R^2 = 0.998$
Compound **34**	$(4.35 \pm 0.19) \times 10^4$	$(7.72 \pm 0.25) \times 10^4$
	$R^2 = 0.992$	$R^2 = 0.994$

Based on the behaviours of compound **33** with different anions, the binding mode with anions could be proposed as shown in Scheme 27. There are two binding sites for fluoride on compound **33**, whereas there is only the one binding sites, 4-NH moiety, for other anions like OAc^- and $H_2PO_4^-$. The coordination between boron atom and fluoride could induce the spectral changes of compound **33** in terms of absorption peak shift as well as new peak formation. While other anions could only induce the formation of new absorption peak. Besides, the additional binding site increased the selectivity ability of compound **33** between fluoride and competitive anions, though the sensitivity toward fluoride is not as high as compound **34** and **35** do.

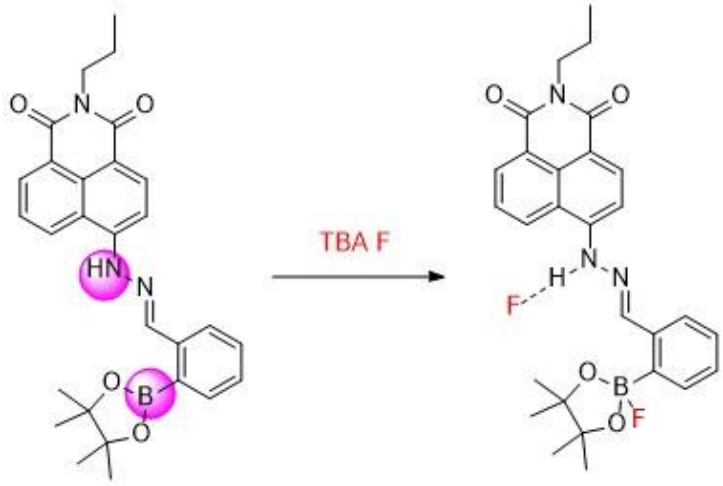

Scheme 27 Proposed binding scheme of compound **33** with fluoride

3.3.5 NMR investigations

*NMR evidences for binding between compound **33** and TBAF*

The binding of anions was also verified from ^{1}H NMR spectroscopy (DMSO-d_6) by monitoring the aromatic N-H proton that initially appears at 11.65 ppm and imine proton at 8.98 ppm. Upon addition of fluoride, a new peak emerged at 11.6 ppm along with the decrease of peak of the aromatic N-H proton, shown in Figure 27. After addition of 1 eq. of fluoride, the original peak decreased, which was further broadened and eventually disappeared when the concentration of fluoride arrived at 3.0 eq. The initial peak of the imine proton also had a down-field shift to 9.07 ppm and gradually overlapped with a double peak from another proton. Then it was shifted up-field to 8.97 ppm after over 3 eq. of fluoride being added.

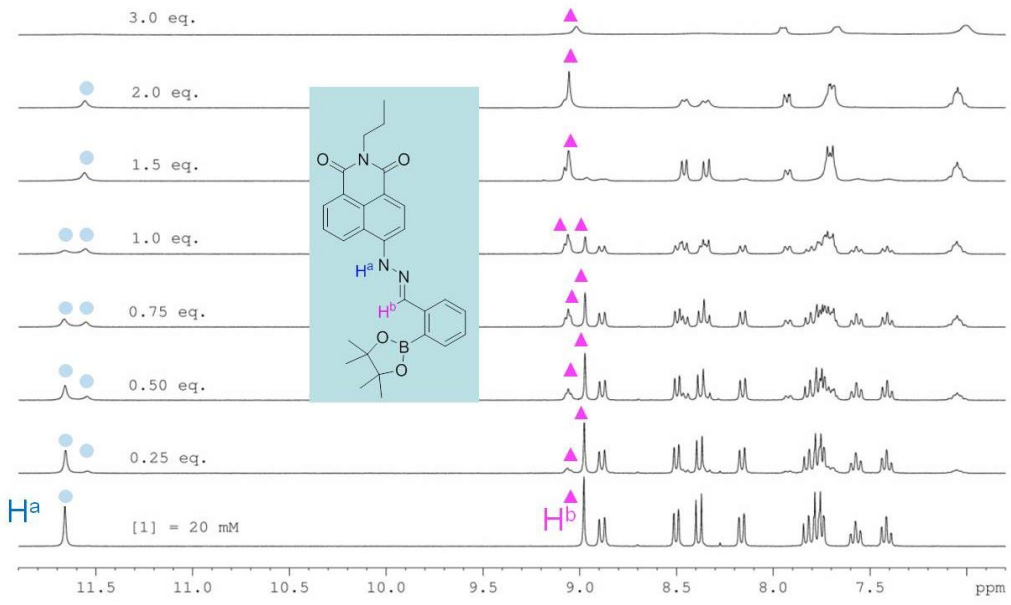

Figure 27 Stack plot of ^{1}H NMRs of compound **33** on addition of TBAF (0-3.0 eq.) in DMSO- d_6, [**33**] = 20 mM

Unlike the behaviour of compound **33** in ^{1}H NMR, no split proton was observed with compound **34** (Figure 28). The peaks of aromatic N-H and phenol proton broaden and

disappeared upon addition of fluoride. No further changes were observed when the concentration of fluoride was over 2.4 eq. Instead a new peak came out at around 16 ppm, supporting the formation of HF_2^-, shown in Figure 29. And for other proton peaks, the binding between fluoride and compound **34** induced an up-field shift, listed as Figure 30, since the binding between anion and compound **34** would increase the electron density of naphthalimide core, leading to the increase of electron shielding on the proton.

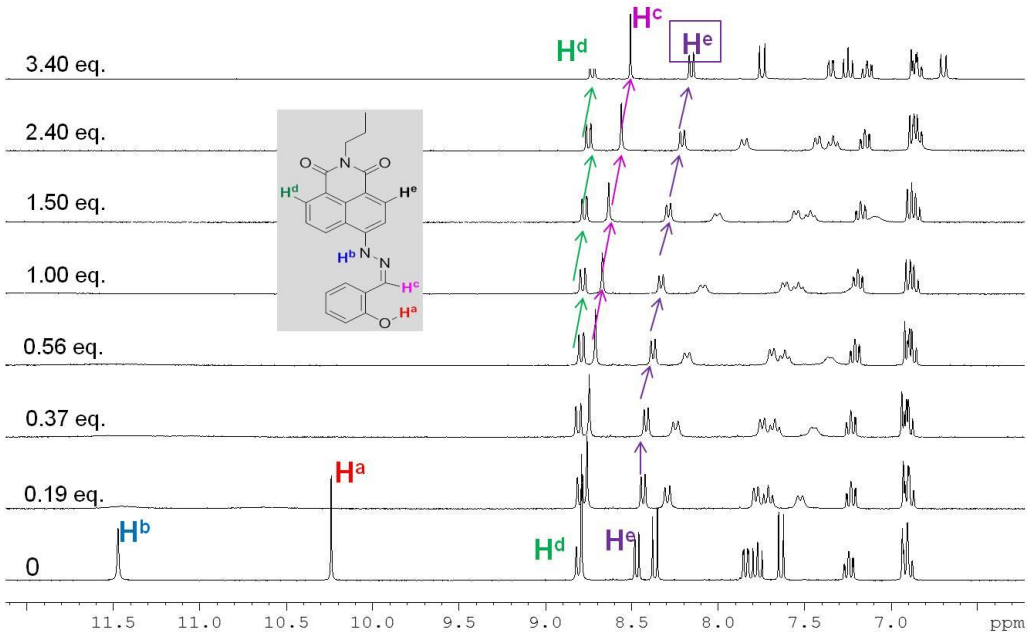

Figure 28 Stack plot of ^{1}H NMRs of compound **34** on addition of TBAF (0-3.4 eq.) in DMSO- d_6

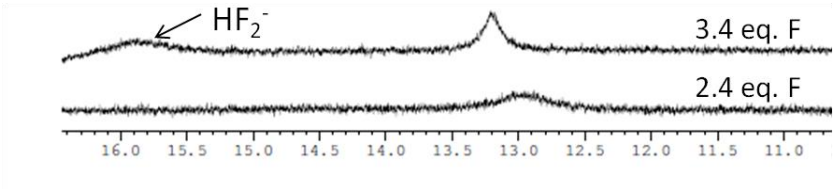

Figure 29 Stack plot of ^{1}H NMRs of compound **34** on addition of TBAF (2.4-3.4 eq.) in DMSO- d_6

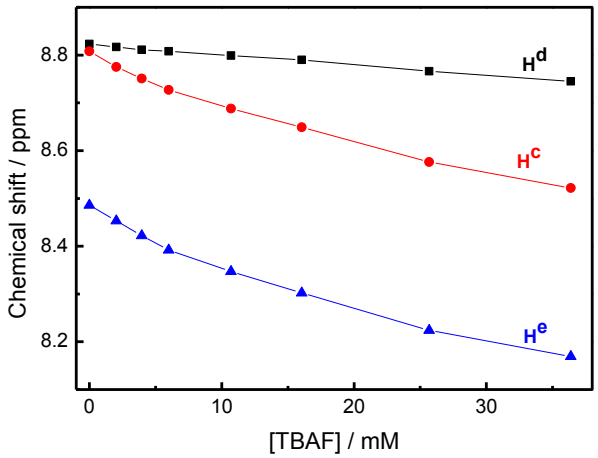

Figure 30 Chemical shifts of protons on compound **34** *versus* concentrations of fluoride

^{1}H NMR titrations of compound **35** with fluoride shared similar behaviours to that of compound **34** with fluoride. The aromatic N-H proton immediately disappeared after addition of fluoride (Figure 31). All the proton peaks shift to up-field along with increase concentration of fluoride, which did not go through further changes after addition of *ca.* 2.6 eq. of fluoride. The chemical shifts of typical protons are shown in Figure 32.

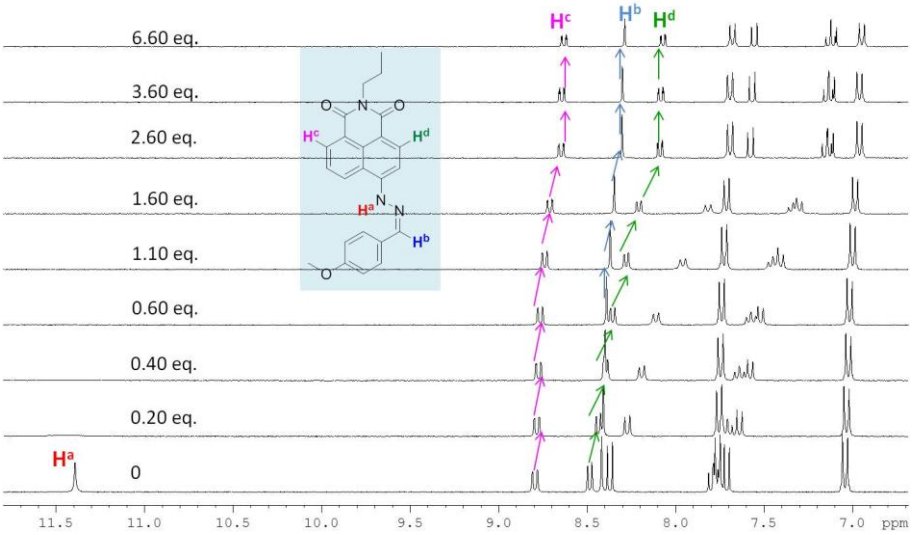

Figure 31 Stack plot of ^{1}H NMRs of compound **35** on addition of TBAF (0-6.6 eq.) in DMSO- d_6

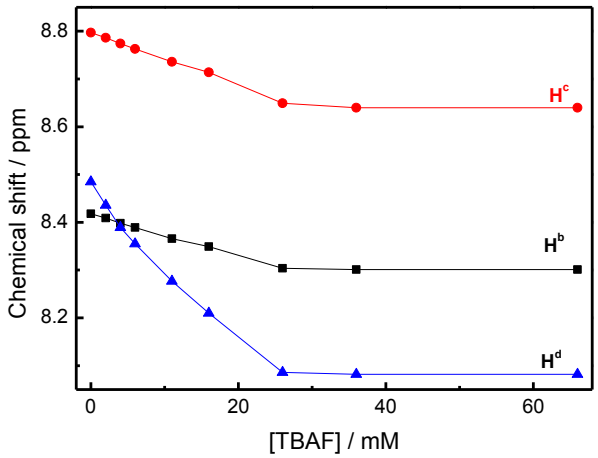

Figure 32 Chemical shifts of protons on compound **35** *versus* concentrations of fluoride

3.3.6 Anions recognition via visualisation

Fluoride sensing with clear colour changes are always desirable, as they have potential to develop into quick, simple and naked-eye detection methods. Thanks to the unique photoproperties of 4-amino-1,8-naphthalimide, another significant character of probes **33**, **34** and **35** is that recognition of anions could be visualised due to the deprotonation process of the aromatic N-H proton. The initial colours of compounds **33**, **34** and **35** are similar with a bright yellow colour and addition of fluoride results in a dark blue colour (Figure 33). As for compound **33**, different anions could induce different colour changes as well. When 5 eq. of each anion were added to 12 μM of compound **33**, the colour of the solutions changed to a slightly dark yellow (Figure 34). After addition of 13 eq. of each anion, it was found that different anions could display different colours, shown in Figure 35, with fluoride producing a dark blue, OAc^- giving a steel blue and $H_2PO_4^-$ an orange. It was assumed that different binding affinities of these anions induced different degrees of deprotonation, which accounted for the different colours.

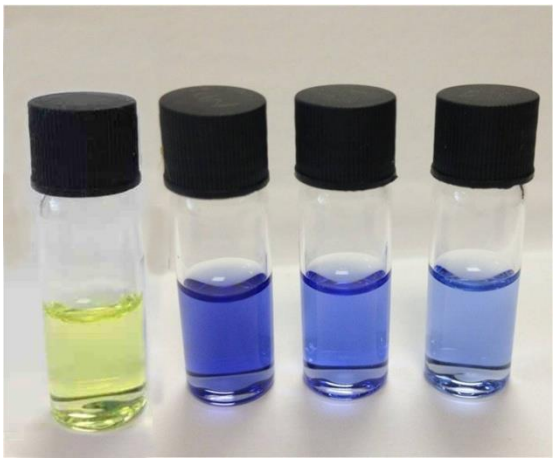

Figure 33 Colour changes of 20 μM compounds with 27 eq. fluorides, from left to right: compounds **33**, compounds **33** + F^-, **34** + F^- and **35** + F^-

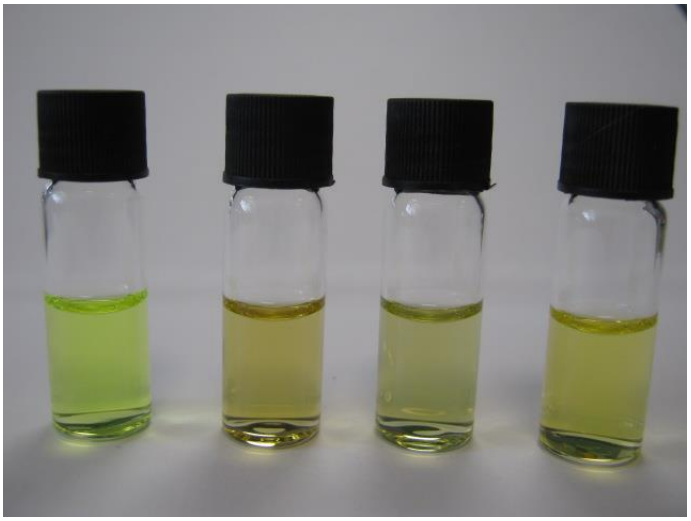

Figure 34 Colour changes of 12 μM compounds **33** with 5 eq. of anions, from left to right: compound **33**, + F^-, + OAc^- , + $H_2PO_4^-$

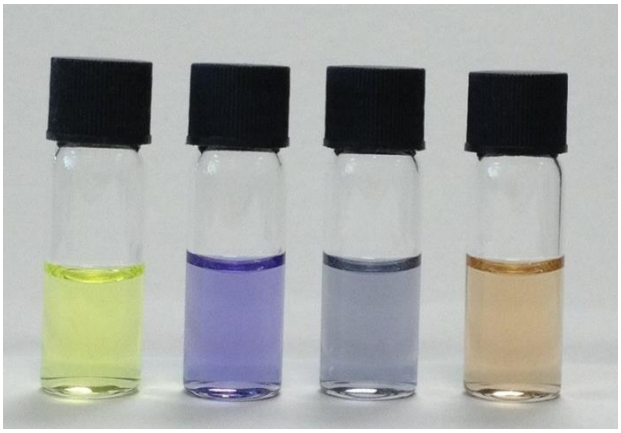

Figure 35 Colour changes of 12 μM compounds **33** with 13 eq. of anions, from left to right: compound **33**, + F^-, + OAc^- , + $H_2PO_4^-$

3.4 Investigations on saccharide sensing

While compound **33** was designed for fluoride detection, the saccharide sensing ability is still worth being investigated. With regard to this aspect, several boron modified naphthalimide derivatives have already been reported.[166-170]

3.4.1 Stability investigations and pH optimisations

Compound **33** has a poor solubility in aqueous environment since precipitate would form from pure water buffer solution. The fluorescent intensity changes of compound **33** along with time were tested in methanol - water co-solvent buffer system, shown in Figure 36. It was found out that compound **33** could remain stable with water content less than 17% in the system. Thus investigations were carried out in a buffer system with water content of 17%.

It's well known that the interaction affinity between boronic acid and diols are dependent on the pH values of the system. The pH profile were ploted by recording fluorescent intensites of compound **33** at different pH values with and without presence of saccharide, see Figure 37. The fluorescent intensity of compound **33** stays stable in

slightly acidic condition, which will decrease along with increasing of pH of the system. The fluorescence was almost totally quenched when pH was 11. While in the presence of D-fructose, the pH titration profile shifts to a lower pH, compared with that of compound **33** itself. It is believed that the binding between boronic acid and saccharide would induce formation of bornate ester, which could easily convert to its anionic form, leading to the quenching of fluorescence. The boronic acid on compound **33** was already protected by a pinacol group; therefore, a competitive binding process existed in this system. The binding stability between D-fructose and boronic acid is much higher than that of pinacol with boronic acid moiety, which was believed to overwhelm the pinacol. The pH titration suggested that saccharide could result in the largest fluorescent difference at around pH 7.4.

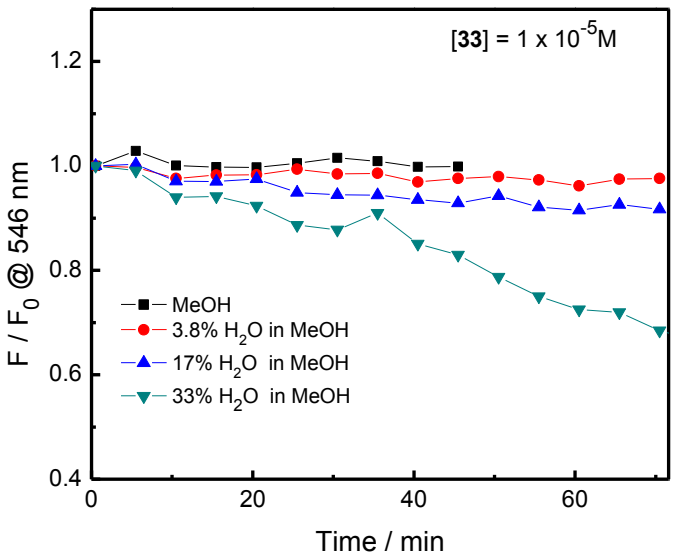

Figure 36 Stabilities of compound **33** in co-solvents system: Black (pure methanol), Red (3.8% water in MeOH), Blue (17% water in MeOH), Cyan blue (33% water in MeOH) [**33**] = 1×10^{-5} M; λ_{ex} = 470 nm;

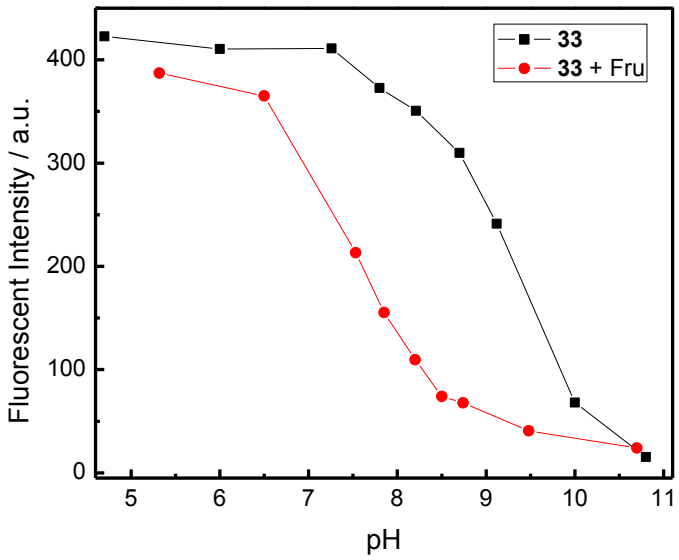

Figure 37 pH profiles of compound **33** with and without presence of D-fructose; [**33**] = 1×10^{-5} M; λ_{ex} = 470 nm; (D-fructose was utilised as it showed strongest binding affinity with monoboronic acid probe in previous results)

Based on all these observations, the following experiments were carried out in pH 7.4 PBS buffer solutions with 83 % *vol* content of methanol. To ensure full equilibrium of the system, the solution was also left for 30 minutes before used for further experiments.

3.4.2 Saccharide titrations

The boronic acid moiety on compound **33** was protected by a pinacol group, the dynamic equilibrium process between boronic acid and diol can lead to the formation of more stable boronate ester if two different types of diols existed, as the binding constant between pinacol and boronic acid is far less than that with saccharide.

All the tested monosaccharides induced a steady decrease of fluorescent intensity of compound **33**, similar to the D-fructose titration shown in Figure 38. The calculated binding constants indicated quite low values, following the well-established selectivity

orders for monoboronic acid deirvatives: D-fructose > D-galacotose > D-mannose > D-glucose.

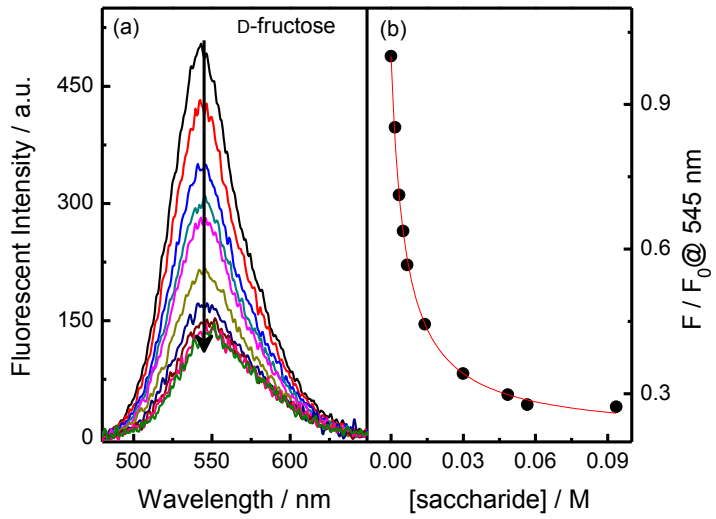

Figure 38 (a) Fluorescent spectral changes of compound **33** along with addition of D-fructose; (b) Ratio of F/ F_0 at 545 nm of compound **33** *versus* concentration of D-fructose; [**33**] = 1×10^{-5} M; λ_{ex} = 470 nm; λ_{em} = 545 nm;

Table 5 The observed binding stabilities and R^2 of compound **33** with different saccharides

	K_{obs}	R^2
D-fructose	170.6 ± 7.52	0.997
D-galacotose	39.15 ± 2.33	0.998
D-mannose	19.04 ± 1.82	0.994
D-glucose	9.76 ± 2.79	0.981

3.5 Summary of Chapter 3

The photophysical properties of 1,8-naphthalimide core and its applications in fluoride and saccharide recognition were reviewed.

A boron-containing 1,8-naphthalimide probe (**33**) and its according control compounds **34** and **35** were synthesised, which were fully characterised. The potential abilities of these compounds for recognising anions were investigated. It was found that compounds **34** and **35** showed higher sensitivities towards fluoride in terms of absorption, yet compound **33** had better selectivity between fluoride and acetate. It was proposed that the dual binding sites on compound **33** for fluoride anion accounts for the enhanced selectivity, though such structure rendering binding process complicated. The recognition process could also be visualised by naked-eye due to the deprotonation of 4-amino proton. These assumptions were supported by the NMR spectral results.

Compound **33** was also used for saccharide detection. Both stability and pH optimisation were carried out prior to measurement. It was found that compound **33** showed the most pronounced spectral changes at pH 7.4 with 17 % *vol* water content. Fluorescent titrations with different monosaccharides revealed that the fluorescent intensity of compound **33** could be quenched, and the degree of quenching follows the trend: D-fructose > D-galacotose > D-mannose > D-glucose.

CHAPTER FOUR

Results and discussion

4 Results and discussion Colorimetric enantioselective recognition of chiral secondary alcohols

4.1 Background

4.1.1 Chiral alcohol sensing

For two stereoisomers with mirror images, they are normally called enantiomers. With regard to the chemical and physical properties, enantiomers are almost identical, yet, with different opposite chirality. The differences in charility, in some enantiomers, would greatly affect their pharmacological efficacy and induce the side effect. Thus this century has seen an increasing demand for determining the concentration and purity of enantiomers due to the importance of enantiopurity in the pharmaceutical industry.[175, 176] Chiral molecular recognition systems have been employed to assess enantiopurity, that exploit both covalent interactions,[54, 177-181] and non-covalent interactions.[182] Among non-covalent recognition systems reported ionic interactions, hydrogen bonding,[183-185] π-π interactions,[186] metal coordination[187-189] and hydrophobic interactions have all been shown to be effective, and these interactions have attracted great interests as they were employed for many applications such as self-assembly[190-192] and molecular recognition.[45, 193-202] The hydrogen bond is an important directional inter- or intra-molecular interaction, which is crucial for controlling molecular conformation and molecular aggregation.[185] In the area of molecular recognition, the strength of binding between ligands and receptor could be determined by hydrogen bonding, when the hydrogen binding is the controllable factors. For example, in biological systems, the binding between a substrate and an enzyme, as well as cell surface recognition, in great degree, depend on the hydrogen bond interactions.[203]

As for those reported examples for chiral molecular recognition, chiral carboxylic acids

and amino acids are the common analytes, which is reasonable as the strong hydrogen binding capability would endow them unique characteristics when binding with receptors. In regard to chiral alcohol sensing, the much weaker interactions with receptors make it difficult to achieve enantioselective recognition, thus most of this part remains undeveloped.

Zehnacker and co-workers reported a chiral alcohol probe based on laser induced fluorescence excitation spectra of naphthyl fluorophore (**36**) formed in a continuous supersonic expansion of helium. The fluorescent spectrum of (*R*)-**36** with (*S*)-2-chloro-1-propanol displayed different peaks from that of (*S*)-**36** with (*R*)-2-chloro-1-propanol. Besides, other chiral alcohols could also be discriminated by compound **36**. The problem is that this sensing strategy requires complicated techniques.

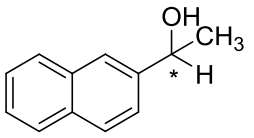

36

Steiner outlined the palette of hydrogen bonding patterns available including O-H ··· N and N-H ···O/N interactions.[185] These interactions have been extensively explored in the crystal engineering of supramolecular structures,[204, 205] catalytic reactions and molecular recognition.[193, 196, 206-208] Shinkai introduced chiral acids as templates to create enantiomerically pure aggregated structures using N-H·· ·O/N hydrogen bonding interactions, yet this is only capable of the enantioselective sensing of chiral acids.[193] Ghosh *et al* employed a series of pyridine derivatives for distinguishing carboxylic acids from non-hydroxyl analogues through such hydrogen bonding interactions as well.[196, 206] Fang and Lu also utilised this interaction for developing saccharide derivatives.[207, 208] Among the aforementioned examples, only the one reported by Fang *et al* demonstrated the enantioselective ability of the receptor for those saccharide derivatives diols. Addition of octyl *β*-D-glucopyranoside to compound **37** produced a positive CD signal, which was believed to be the result of an inward conformation of the two indole rings after binding with a chair-like pyranoside. Meanwhile, the enantiomer of octyl *β*-D-glucopyranoside (octyl *β*-L-glucopyranoside) induced an almost mirror image spectrum.

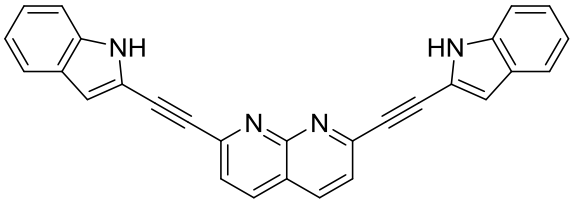

37

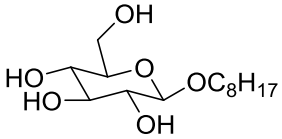

Octyl β-D-Glucopyranoside

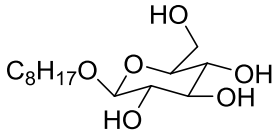

Octyl β-L-Glucopyranoside

*4.1.2 Previous studies of compounds **38** and **39***

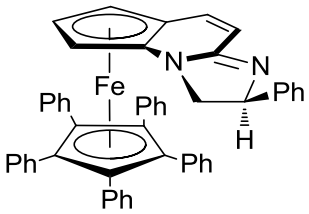

38

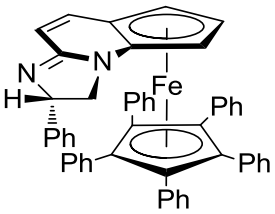

39

Planar chiral ferrocene compounds **38** and **39**, containing both central and planar chiral elements, were previously designed and synthesised as an enantioselective catalyst for the kinetic resolution of secondary alcohols.[209, 210] An enantioselectivity factor up to 1892 was confirmed. The strong hydrogen bond interaction together with the cation-π interaction was believed to be the promoting effect for effective catalysis, depicted in Scheme 28. It was especially noteworthy that whilst diastereoisomer **39** functioned exquisitely as a catalyst for kinetic resolution of secondary alcohol acylation, diastereoisomer **38** was completely inactive (an open *top face* was reasoned to be

required for the acylated catalyst to be able to effectively deliver its cargo).

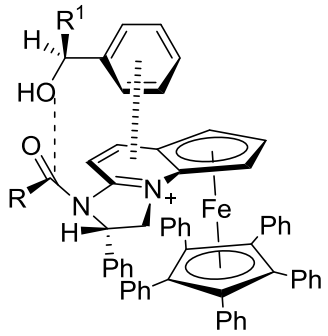

Scheme 28 Proposed transition state and the interactions between **39** and substrate

4.2 Aim and Objective

Previous studies have demonstrated the enantioselective ability for kinetic resolution of secondary alcohol acylation. The imidazole nitrogens on **38** and **39** are strong Lewis bases and can themselves form hydrogen bonds with alcohols.[211-213] Furthermore, the nitrogen (*N*) - hydroxyl (C-OH) hydrogen bonding interaction is crucial for achieving enantioselective detection of chiral alcohols. All of these factors promoted us to explore the potential of compounds **38** and **39** for the enantioselective sensing. As the ferrocene core has absorption in the visible region, it was wondered if compounds **38** and **39** were able to enantioselectively discriminate chiral alcohols *via* visible colorimetric sensing. Both compounds **38** and **39** were kindly supplied by collaborators from Eastern Central University of Science and Technology (ECUST).

4.3 Investigation of chiral alcohols

Solvent determination

In a dynamic supramolecular system, the interaction between substrate and guest molecules can be affected by various factors, such as solvents, temperature and phase,

especially the influences of solvents on the hydrogen bond in the studied system. Therefore, the hydrogen bond interactions between **38** and chiral alcohols (dimethyl D-tartrate as model chiral alcohol) were studied in various solvents, spectral changes in various solvents indicating a strong dependence on the solvent. Spectral changes, shown in Figure 39, are almost identical before and after addition of 6 equivalents of dimethyl D-tartrate (D-DT) in toluene, THF, diethyl ether and ethyl acetate, while methanol itself could induce spectral changes of **38** and addition of 6 eq. of D-DT could only induce small changes at short wavelength. The changes in hexane could largely be attributed to the increase of baseline resulting from the insolubility issues. Though changes were also observed in DCM, the changes in acetonitrile are the most pronounced, and the absorption values are shown in Table 6. Thus all the subsequent investigations were carried out in acetonitrile.

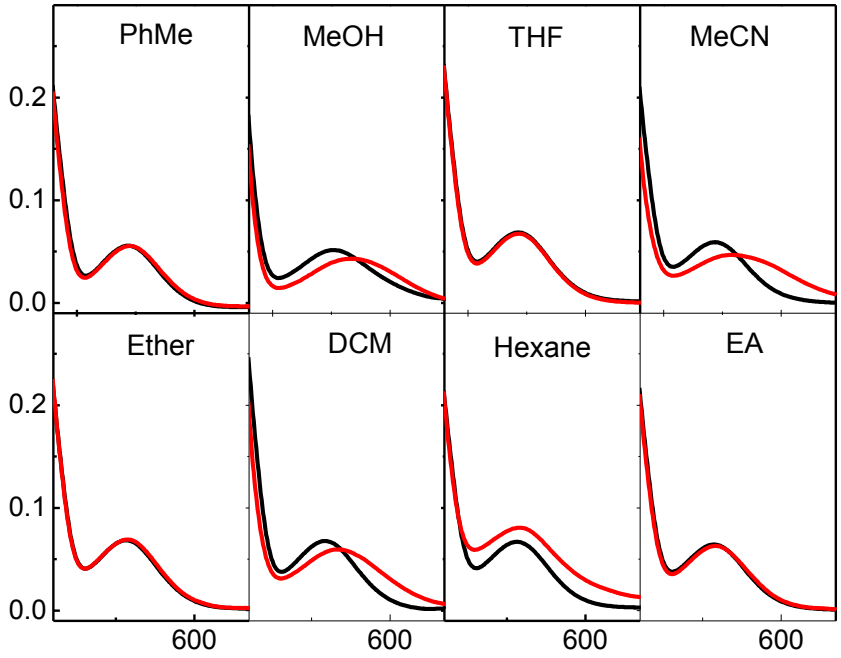

Figure 39 Absorption changes of **38** before (black line) and after (red line) addition of dimethyl-D-tartrate (D-DT) in different solvents

Table 6 The ratio values of absorption at 576 nm to 516 nm of compound **38** in different solvents before and after addition of dimethyl D-tartrate

	Δ[a]	A1[b]	A2[c]
Toluene	0.046	0.246	0.292
Methanol	0.456	0.650	1.106
THF	-0.009	0.331	0.322
Acetonitrile	0.571	0.354	0.925
Diethyl ether	0.018	0.319	0.337
Dichloromethane	0.438	0.363	0.801
Hexane	0.210	0.328	0.538
Ethyl acetate	0.042	0.331	0.373

[a] Δ = A2-A1

[b] A1: ratio values of absorption at 576 nm to 516 nm when **38** was 0.1 mM in each solvent

[c] A2: ratio values of absorption at 576 nm to 516 nm when 0.6 mM dimethyl-D-tartrate was added to the prepared solution

*Optical behaviours of **38** and **39** with different alcohols*

As fluorescent intensities of **38** and **39** are very low, spectral studies were investigated using UV-*vis* spectroscopy. Compounds **38** and **39** have an absorption peak at 516 nm, which was red-shifted to 576 nm upon addition of dimethyl D/L-tartrates (L-DT and D-DT) , shown in Figure 40. Here enantioselectivity was observed as dimethyl D-tartrate produced larger spectral shifts with **38** and **39** than that of dimethyl L-tartrate (Figure 40 and Figure 41). One thing to point out is that different enantiomers only affect the CD absorption without inducing the Cotton effect. The observed binding constants for dimethyl D/L -tartrates with **38** and **39,** as in Figure 42, are 392.5 ± 63.2 / 112.5 ± 29.3 dm^3 mol^{-1} and 298.3 ± 84.7 / 141.4 ± 26.1 dm^3 mol^{-1} respectively by using Equation (16), the deduction process of which was presented in Chapter one (section 1.6).[53] Meanwhile enantioselective recognition could be observed colorimetrically, since after the addition of six equivalents of dimethyl D-tartrate to a solution of **38,** a colour difference was observed as shown in Figure 43.

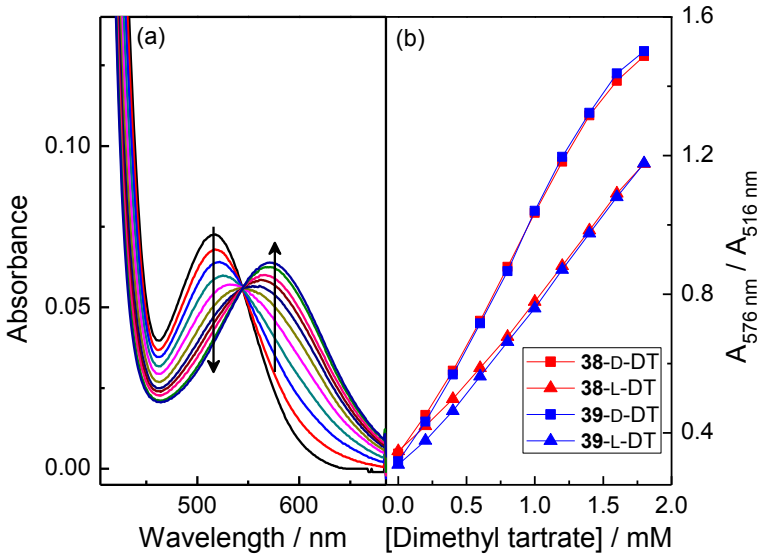

Figure 40 (a): UV-*vis* spectral changes of 0.1 mM **38** in MeCN upon addition of dimethyl D-tartrate; (b): The ratio of absorbance at 576 nm to 516 nm *versus* concentrations of D/L- tartrate for **38** and **39**

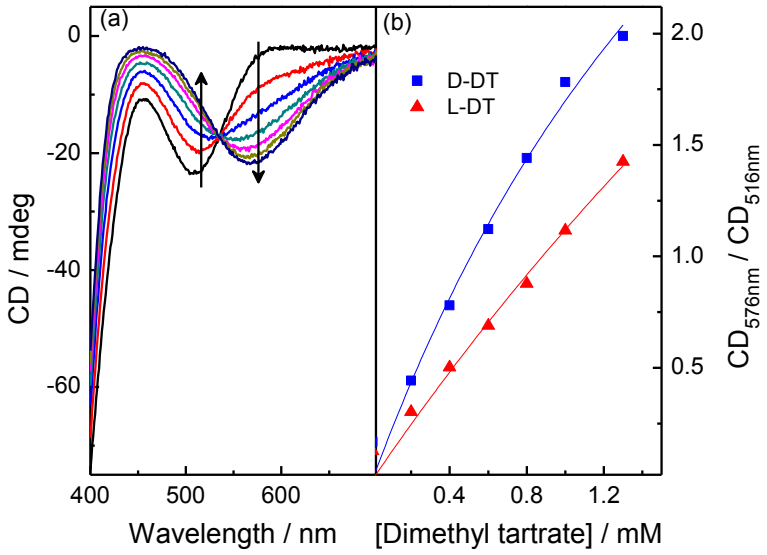

Figure 41 (a): CD spectral changes of 0.1 mM **38** in MeCN upon addition of dimethyl D-tartrate; (b): The ratio of absorbance at 576 nm to 516 nm *versus* concentrations of dimethyl D/L-tartrate.

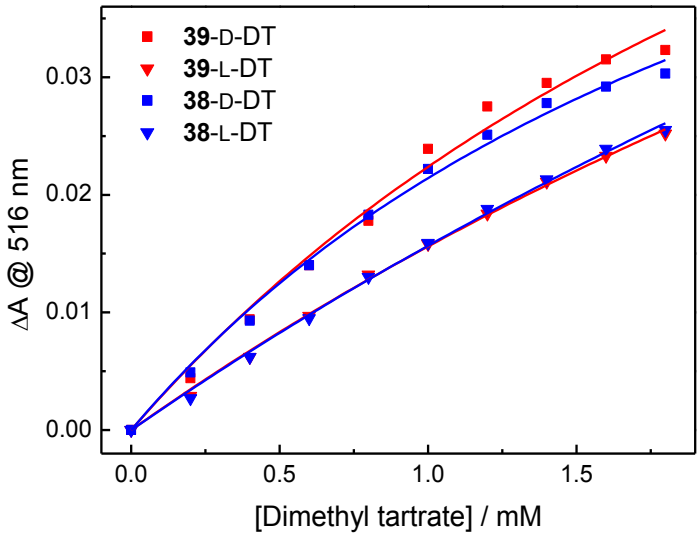

Figure 42 Absorption differences at 516 nm of compounds **38** and **39** in MeCN *versus* concentrations of dimethyl tartrate; [**38**] = [**39**] = 0.1 Mm; $\Delta A = A_0 - A$

Table 7 Calculated binding constants for **38** and **39**

	39-D-DT	**39**-L-DT	**38**-D-DT	**38**-L-DT
b	0.0974 ± 0.019	0.126 ± 0.020	0.0760 ± 0.008	0.155 ± 0.035
K	298.3 ± 84.7	141.4 ± 26.1	392.5 ± 63.2	112.5 ± 29.3
R^2	0.988	0.998	0.994	0.998

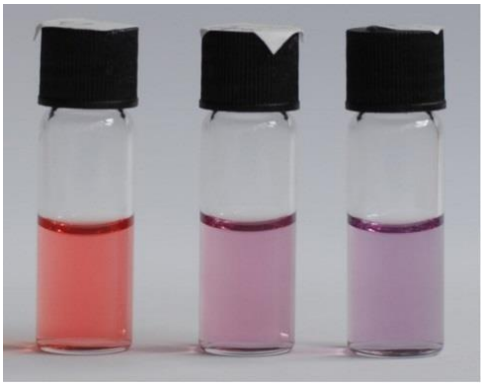

Figure 43 From left to right: 0.1 mM **38**, 6 eq. of dimethyl L-tartrate, 6 eq. of dimethyl D-tartrate in MeCN

The sensing behaviours of the diastereoisomers **38** and **39** with dimethyl D/L-tartrates

were identical, demonstrating a divergence between applications to alcohol recognition as opposed to acylation catalysis, i.e. the inactive catalyst, **38**, works equally well as a sensor. As such we chose to make further use of the *inactive* catalyst and continued our investigations with compound **38** only.

A series of chiral alcohols were studied. It was found that chiral alcohols with $pK_a \leq 12$ displayed higher chiral discrimination $\Delta \geq 0.1$ (Δ is the difference between (A_{576nm} / A_{516nm}) for each pair of enantiomers with 0.1 mM **38** and, 0.6 mM of the chiral alcohol)[214], shown in Table 8. It is reasonable as with lower pK_a, the proton is more acidic, which would have stronger hydrogen binding than those with larger pK_a values. D/L – tartaric acids were also investigated and while pronounced spectral and colorimetric changes were observed, no enantioselectivity was detected (Figure 44 and Figure 45). The observed binding constants for D/L –tartaric acid with **38** are 3131 ± 1157 dm^3 mol^{-1} and 4636 ± 1755 dm^3 mol^{-1}, respectively (Figure 46), which is much higher than that with alcohol since the pK_a of tartaric acids are much lower, indicating the stronger strength in hydrogen bonding.

It seems that the hydrogen bonding strength plays a crucial role in chiral alcohol recognition. When the analytes are secondary alcohols, the stronger the hydrogen bonds between analytes and substrate, the better the performance of the enantioselectivity. However, at a certain stage, increase of the hydrogen bonding strength would lead to loss of the potential of enantioselectivity, for example, the use of tartaric acids. One possible explanation is that the substrates were protonated when tartaric acids were utilised. In order to further justify this assumption, the following NMR spectra studies were carried out.

Table 8 Structures of the chiral secondary alcohols tested in this study and the ratio of absorption at 576 nm to 516 nm of compound **38** after addition of 6 equivalents of each chiral alcohol

Chiral alcohols (A_{576nm} / A_{516nm})[a]		Δ[b]	pK_a[215]
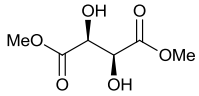 (-)-Dimethyl D-tartrate 0.982	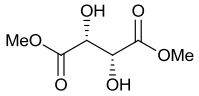 (+)-Dimethyl L-tartrate 0.742	0.240	11.44 ± 0.20
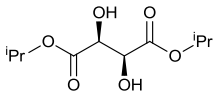 (-)-Diisopropyl D-tartrate 0.641	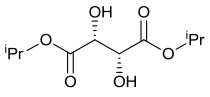 (+)-Diisopropyl L-tartrate 0.446	0.195	11.70 ± 0.20

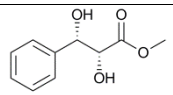 (2*R*,3*S*)-methyl 2,3-dihydroxy-3-phenylpropanoate 0.366	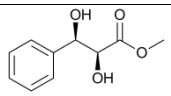 (2*S*,3*R*)-methyl 2,3-dihydroxy-3-phenylpropanoate 0.350	0.016	12.33 ± 0.20
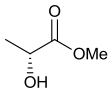 (+)-Methyl D-lactate 0.626	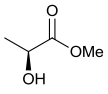 (-)-Methyl L-lactate 0.555	0.071	13.07 ± 0.20
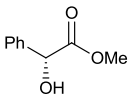 Methyl (R)-(-)-mandelate 0.580	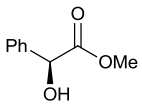 Methyl (S)-(+)-mandelate 0.457	0.123	12.19 ± 0.20
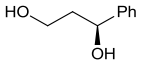 (*S*)-1-phenylpropane-1,3-diol 0.334	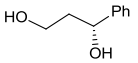 (*R*)-1-phenylpropane-1,3-diol 0.333	0.001	13.93 ± 0.20
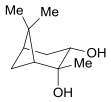 (1*R*,2*R*,3*S*,5*R*)-(-)-Pinanediol 0.348	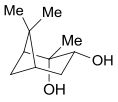 (1*S*,2*S*,3*R*,5*S*)-(+)-Pinanediol 0.333	0.015	14.68 ± 0.60

[a] Ratios of absorption at 576nm to 516 nm, [**38**] = 0.1 mM, [chiral alcohols] = 0.6 mM

[b] Δ is the differences between (A_{576nm} / A_{516nm}) for each pair of enantiomers

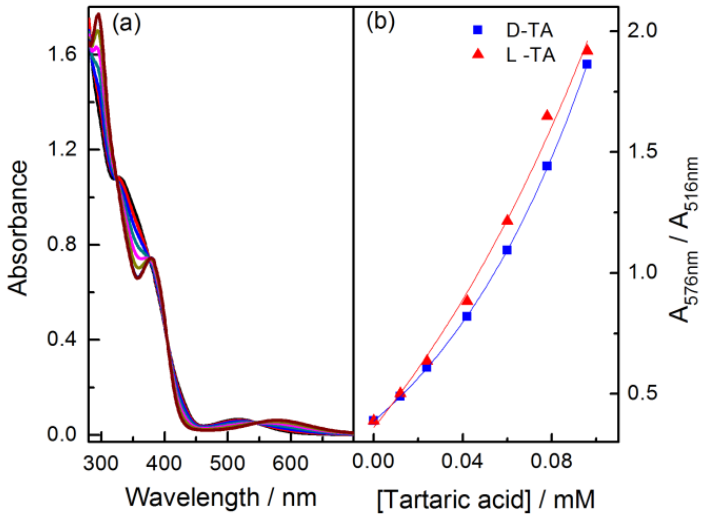

Figure 44 (a): Absorption changes of **38** with addition of D-tartaric acid; (b): ratios of absorbance of compound **38** at 576 nm to 516 nm against concentrations of D/L-tartaric acids

Figure 45 From left to right: 0.1 mM compound **38**; with 1 eq. L-tartaric acid; with 1 eq. D-tartaric acid

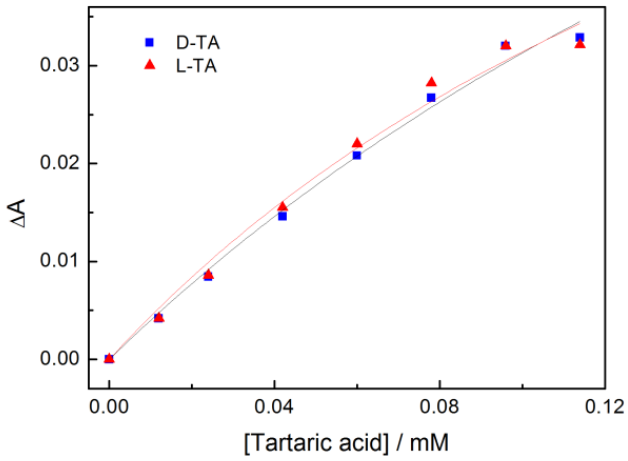

Figure 46 Absorption differences at 516 nm of compound **38** in MeCN *versus* concentrations of tartaric acids; [**38**] = 0.1 mM; $\Delta A = A_0 - A$

4.4 NMR studies

The nature of the interaction between compound **38** and chiral alcohols can easily be investigated by NMR spectra, as the protonation and hydrogen bonding have very different behaviours on the chemical shift of NMR spectra. The induced hydrogen bonding was illustrated by the chemical shift changes of proton *a* and *b*, which was defined at two dimension NMR correlation spectroscopy, COSY (Figure 47). For compound **38** itself, the doublet peak proton *a* has a correlation with proton *b* covered

by peaks of other protons. Such a cross peak indicated that proton *a* and proton *b* belong to two neighbouring carbon atoms respectively. After addition of 4.8 eq. D-DT, both had a down-field shift, which revealed the doublet peak of proton *b* as well. Based on these observations, proton *a* and *b* could be assigned.

(a)

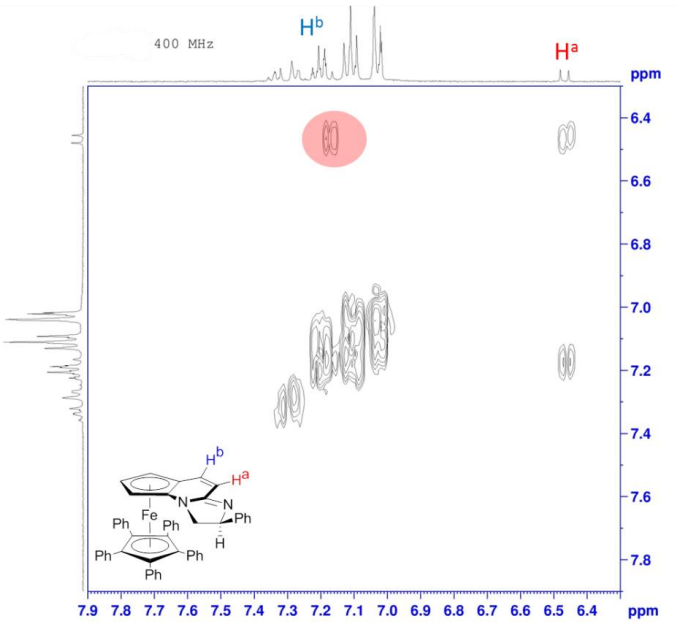

(b)

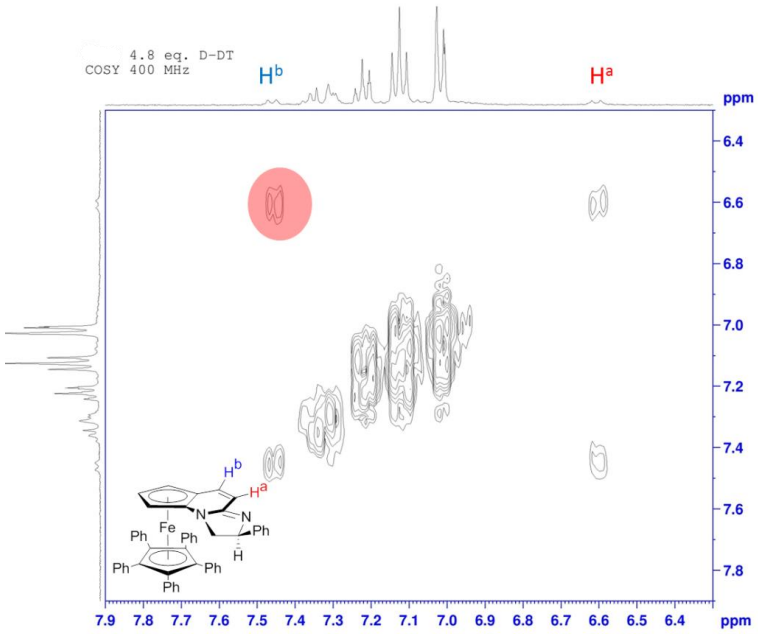

Figure 47 (a) COSY NMR of compound **38** in MeCN-d_3; (b) COSY NMR of compound **38** with 4.8 eq. of dimethyl D-tartrate

^{1}H NMR titrations of **38** with dimethyl D-tartrate and D-tartaric acid indicate that similar hydrogen bonding species are responsible for the observed spectral changes, shown in Figure 48 and Figure 49. The down-field shift of both proton *a* and *b* upon addition of D-DT and D-TA results from the hydrogen bond between nitrogen (*N*) - hydroxyl (*OH*), which would reduce the electron density on the N atom, leading to less electron-shielding effect on nearby protons. By comparing the chemical shifts of protons *a* and *b*, it is easily found that on addition of same amounts of D-TA and D-DT, chemical shifts induced by former are much more than that induced by latter. It means the stronger the hydrogen bond, the more down-field shift of the protons. On the other hand, the changes induced by addition of D-DT and D-TA could also be observed by the colour changes as well, shown in Figure 50.

The enantioselectivity ability of compound **38** towards chiral alcohols could also be seen from NMR spectral differences, shown in Figure 51. With the same amounts of dimethyl tartrates, chemical shifts of proton *a* and *b* induced by D-DT are larger, which means that D-DT could form stronger hydrogen bond with compound **38** than L-DT. This indicated that the configurations of chiral alcohols could also affect the strength of the formed hydrogen bond.

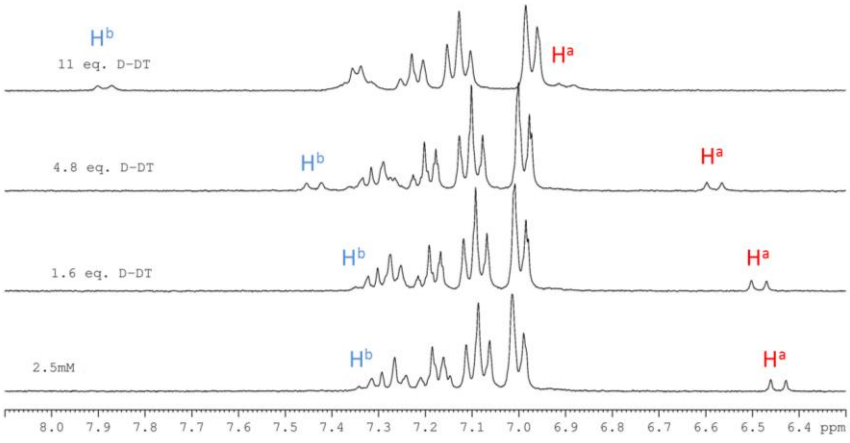

Figure 48 Stacked NMR plots of compound **38** with different concentrations of D-DT in MeCN-d_3. [**38**] = 2.5 mM

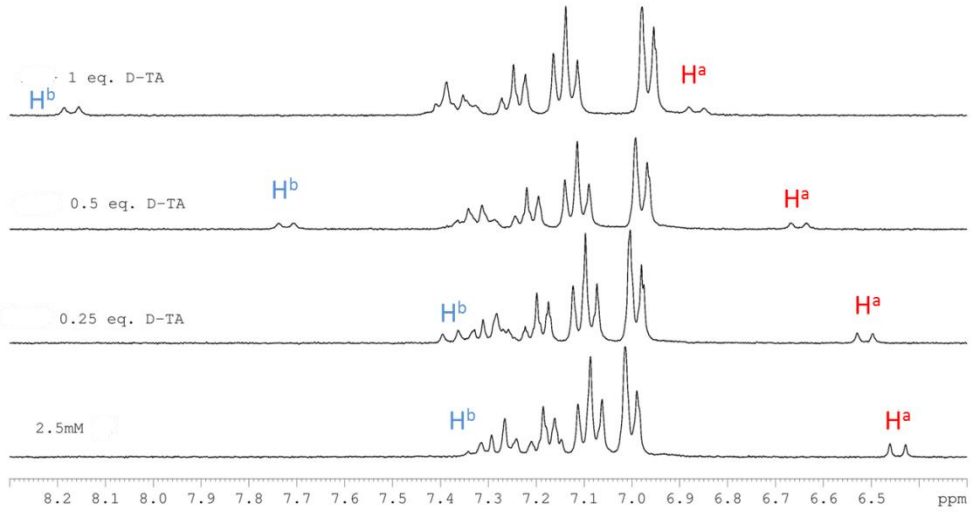

Figure 49 Stacked NMR plots of compound **38** with different concentrations of D-TA in MeCN-d_3. [**38**] = 2.5 mM

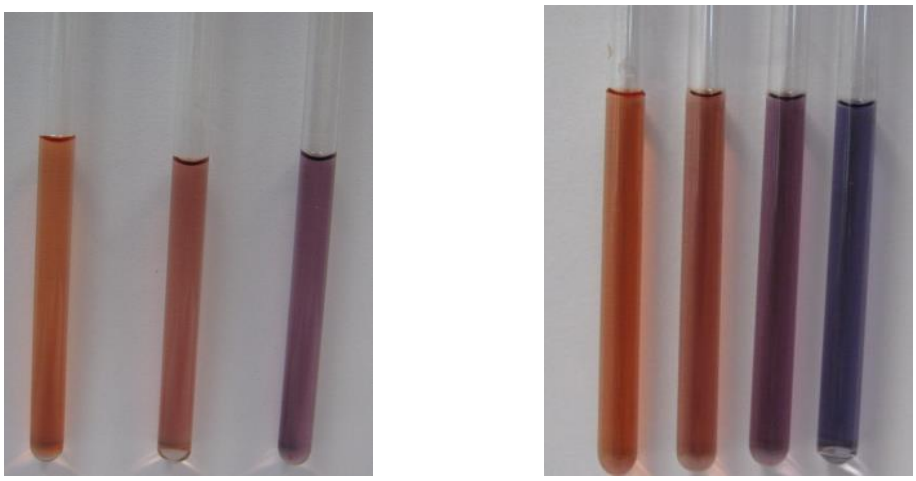

(a) (b)

Figure 50 (a) Colour changes of compound **38** with different concentrations of D-DT, from left to right: [**38**] = 2.5 mM, [**38**] + 4.8 eq. D-DT, [**38**] + 11 eq. D-DT; (b) Colour changes of compound **38** with different concentrations of D-TA, from left to right: [**38**] = 2.5 mM, [**38**] + 0.25 eq. D-TA, [**38**] + 0.5 eq. D-TA, [**38**] + 1 eq. D-TA

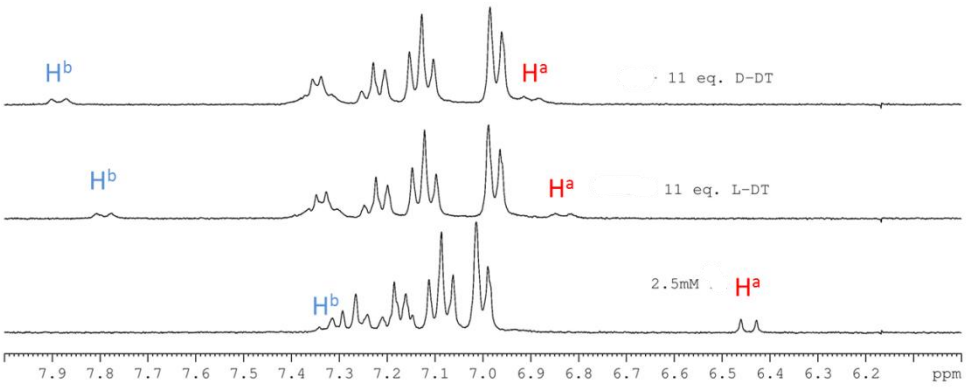

Figure 51 Stacked NMR plots for compound **38** itself and with D-DT and L-DT, respectively

The NMR spectral changes originate from the hydrogen bond between compound **38** and the guest (acid or alcohol) other than previous hypothesis of protonation. For tartaric acid, with lower pK_a values, stronger hydrogen bonds formed, yet, without enantioselectivity. For chiral alcohols, like D-DT and L-DT, the configurations could also play a role on the strength of the formed hydrogen bond. Thus we believe that enantioselectivity is controlled by steric demands within the hydrogen bonding complexes formed between the guest (acid or alcohol) and compound **38**.

4.5 Summary of Chapter 4

Enantioselective recognition of alcohols is under explored and also more difficult compared with the detection of carboxylic acids. Compounds **38** and **39** were initially used as enantioselective catalysts for kinetic resolution study of the acylation of secondary alcohols. The concern of the widely explored N···OH hydrogen bond interaction lead to investigations on the potential application for chiral alcohol sensing.

The hydrogen bonding interactions between host (**38** and **39**) and alcohols are strongly dependent on the solvents. Acetonitrile was chosen as the ideal solvent. UV-*vis* spectra results indicated that **38** and **39** have almost identical responses towards chiral alcohols. The lower pK_a values of chiral alcohols displays better enantioselectivity, however, the

enantioselectivity ability is lost when treated with chiral acids (smaller pK_a than alcohols),though pronounced spectral changes were achieved with chiral acids.

Further NMR studies revealed that similar hydrogen bonding species are responsible for the observed spectral changes of **38** with dimethyl D-tartrate and D-tartaric acid, which ruled out the hypothesis that protonation occurred when tartaric acids were added to **38**. The observed enantioselectivity of **38** could partially be due to the steric effect of the formed hydrogen bond complexes, which was proposed as in Scheme 29. Therefore, the increased distance between **38** and the chiral centres for the hydrogen bonding complexes formed with the tartaric acid (3 bonds, Scheme 29 (b)) over the alcohols (2 bonds, Scheme 29 (b)) explains the lack of enantioselectivity observed between the D/L-tartaric acids.

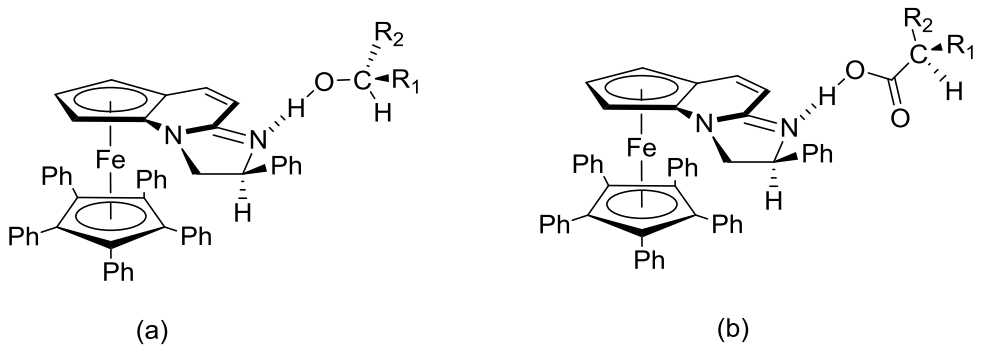

Scheme 29 Proposed hydrogen binding structures of compound **38** with (a): chiral secondary alcohols and (b): chiral acids

CHAPTER FIVE

Results and discussion

5 Results and discussion Suzuki-Miyaura reaction based saccharide recognition

5.1 Background

5.1.1 Brief introduction about reaction based saccharide sensing

Saccharide recognition has been extensively explored in the last few decades. Various methods were developed in order to meet different requirements for saccharide sensing.[216] Electrochemical methods are the most well established, especially in glucose monitoring. Currently, only small quantities of blood are needed to detect blood sugar level by (sub)micro dimension sensors. Optical strategies are still in their infancy.[65, 217, 218] However, lots of attention is focused on developing optical based saccharide probes due to the various potential advantages of these methods, like non-invasive continuous monitoring sugar levels and free of reference electrode.

Optical molecular sensors are one of the largest class of saccharide sensors, by either using the affinity of boronic acid moiety towards diols[40, 219] or hydrogen bond interaction between a sensor and saccharides. Such types of sensors lie in the field of host-guest sensing system, which has been well discussed in Chapter one. Boronic acid based sensors suffer from low solubility or low sensitivity due to low affinity with saccharides.

Another type of saccharide sensors are enzyme based methods, involving catalytic reactions. The incorporated enzymes are mainly glucose oxidase (GOx) and glucose dehydrogenase which can convert glucose into products that are more easily detected. GOx could catalyse the convertion of glucose to D-glucono-1,5-lactone, which is then converted to gluconactone. By measuring the amount of oxygen consumption (reaction (**4**)), H_2O_2 (reaction (**4**)) or formed protons (reaction (**5**)), the concentration of glucose

could be determined as well. Glucose dehydrogenase could catalyse the reaction in reaction (**6**) and the formed NADH is proportional to the concentration of glucose, which offered another indirect way to measuring saccharide concentration.

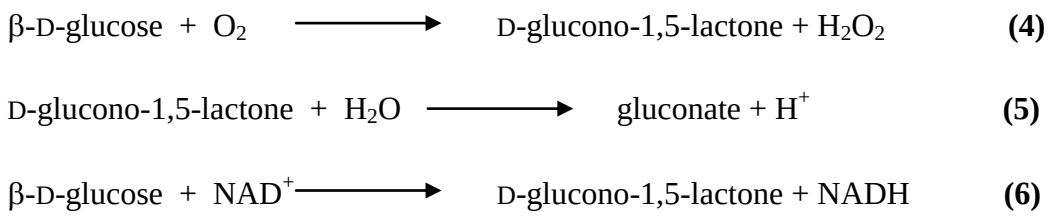

These enzyme involved saccharide sensors are generally catalytic in nature, thus normally with high sensitivity. While great success has been achieved based on this method, some drawbacks still exist. The most common problem is the stability, which are lied in the nature of the enzyme. For example, harsh pH values or higher temperature can cause fatal damages to the GOx enzyme.[220]

One possible solution for tackling these problems without losing high sensitivity is to find alternative saccharide involved reactions. Judging from the structure of saccharides, which are charge neutral molecules and have different conformations in solution, are difficult to be involved with in chemical reaction, other than those enzyme catalysed reactions. In view of these facts, we wondered if reactions with indirect involvement of saccharide could be used for developing novel saccharide sensing methods.

5.1.2 Initial studies on Suzuki- Miyaura homo-coupling reaction based saccharide detection method

Boronic acid derivatives were originally used in organic synthesis before its exploration for saccharide recognition. The Nobel Prize winning Suzuki-Miyaura reaction is one of the leading reactions with boronic acid derivatives as the starting material. The boron atom is an electron deficient centre and prone to coordination with atoms having a lone

pair of electrons. The formed complex easily undergoes the transmetalation process, which affords a new chemical bond, leading to formation of new compounds. Most of the usages originate from the cross-coupling, where halides and organoboron compounds are cross-linked by forming new C-C bonds. The reaction conditions are normally high temperature, with organic solvents in an inert atmosphere. However, the homo-coupling reaction can be carried out at room temperature under an open atmosphere.

In the Suzuki-Miyaura reaction, provided a certain amount of saccharide is present, it was proposed that the binding between boronic acid and saccharide might affect the Suzuki-Miyaura reaction, as the formed boronate ester complex would have a different reaction rate compared with that of the initial boronic acid. As is known, once the boronate ester is formed, the boron centre will be more acidic, thus less nucleophilic, which makes the transmetalation step more difficult to proceed.

In 2010, by employing simple arylboronic acid (phenylboronic acid) this hypothesis was verified.[221] The results demonstrated that saccharide recognition could be achieved using this method. The proposed sensing strategy was illustrated in Scheme 30, where the boronate ester was formed by saccharide interacting with free boronic acid. The formed boronate esters have a slower reaction rate towards formation of the biphenyl product than that of free boronic acid. Thus by studying the kinetic profiles of the Suzuki homo-coupling reaction, the effect of saccharide on this reaction could be investigated.

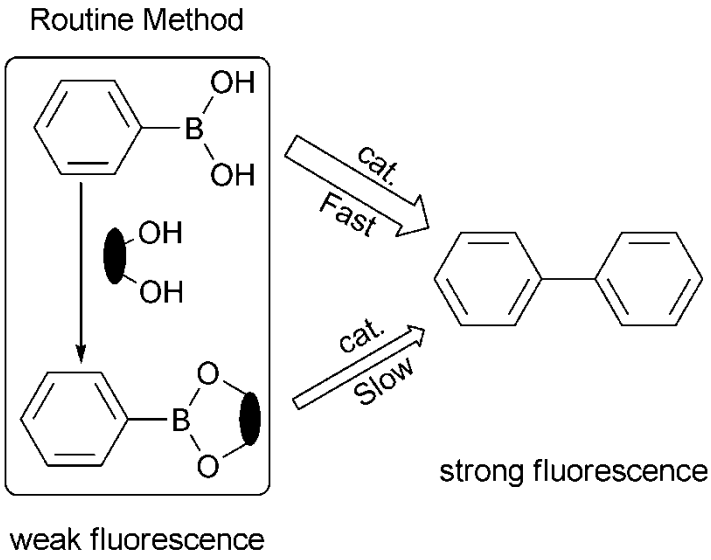

Scheme 30 Proposed strategy for saccharide sensing coupled with catalytic Suzuki homo-coupling reaction, Scheme in the "box" represents classic sensing strategy based on the saccharide-boronic interaction

Phenylboronic acid (PBA) has a very weak fluorescence itself, the observed fluorescent emission came from the formed product, biphenyl. By recording the fluorescent intensity at a certain time, we found that the formed product, represented by the observed fluorescent intensity, has a linear relationship with the amount of added saccharide. Based on these results, we established a Suzuki homo-coupling reaction based saccharide sensing strategy, where the presence of saccharide acted as an inhibitor for this reaction. What's more, sensitivity towards saccharides had been improved by employing the catalytic reaction as well, which contributed to the different reaction rates of free boronic acid and the formed boronate ester complex.

However, when employing phenylboronic acid (PBA) as the substrate, the corresponding excitation wavelength is 250 nm, where intrinsic fluorescence interference will impede this sensing strategy. Therefore, we decided to investigate different boronic acids in order to optimize this protocol.

5.1.3 Issues with the proposed sensing mechanism

In 2011, the Kay Severin group reported a Pd-based indicator displacement assay for saccharide recognition. They observed that palladium could form moderately stable complexes with the chosen fluorescent dye, which also lead to quenching of fluorescence. By adding competitive analyte, monosaccharide, the fluorescent dye could be released, resulting in recovery of fluorescence (Scheme 31).

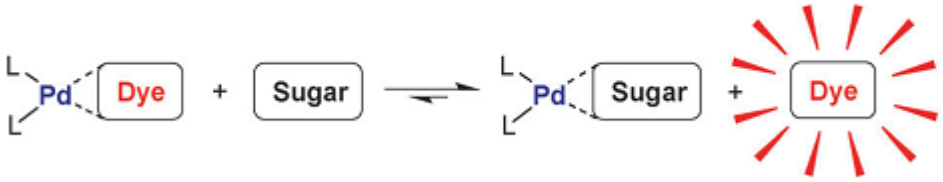

Scheme 31 Representation of sensing strategy based on indicator displacement assay

Their work led us to rethink about the mechanism we had proposed in our previous work. If palladium species can form complexes with carbohydrates, then the formation of boronate ester is not the only factor that affects the reaction rate of the Suzuki homo-coupling reaction, since palladium is the catalyst in this reaction and any changes to the catalyst, before and after addition of saccharide, can also control the sensing of carbohydrates.

In order to fully understand the sensing mechanism in our previous work, the interaction between palladium and saccharides under the experimental conditions should be investigated.

5.2 Aim and Objective

First, as in the previous study, the system suffers from possible interferences; here alternative boronic acids should be employed to construct new sensing platforms. Therefore, naphthalene-1-boronic acid and 1,4-phenyldiboronic acid were chosen, which have simple structures like phenylboronic acid, but could generate products with longer wavelength emission.

Secondly, in order to study the interaction between palladium and saccharide, the prerequisites are that the new substrate should not bear any group that could interact with saccharides; palladium should be able to act as a catalyst in the new system and investigations should be carried out under the same experimental conditions as our previous work. In order to meet these requirements, another palladium-catalysed reaction, Tsuji-Trost reaction, was investigated.

5.3 Investigations on saccharide sensing

5.3.1 Naphthalene-1-boronic acid as substrate

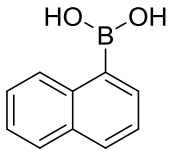

40

First the compound naphthalene-1-boronic acid (**40**) was employed in Suzuki-Miyaura homo-coupling reaction in Na_2CO_3-$NaHCO_3$ buffer system at room temperature. The fluorescence spectra quickly changed upon adding catalyst and the peak at around 330 nm decreased with the emergence of a new peak at around 380 nm, showing a clear isostilbic point at 346 nm, shown in Figure 52. The emission at 330 nm belongs to intrinsic fluorescence of naphthalene-1-boronic acid (**40**), while the new emission originates from newly formed product.[222] The kinetic study was performed by adding different concentrations of D-fructose and comparing changes of the ratio I_{380nm} / I_{330nm} over time, shown in Figure 53. It was found that the fluorescence ratio grew steadily along with time while no changes were observed, given the concentration of D-fructose reduced to a certain point. When with a fixed concentration of D-fructose, the response is greater at longer time. However, from a practical point, long analysis time means a time consuming method, which is not practical. Therefore, the 25th minute point was chosen for all experiments.

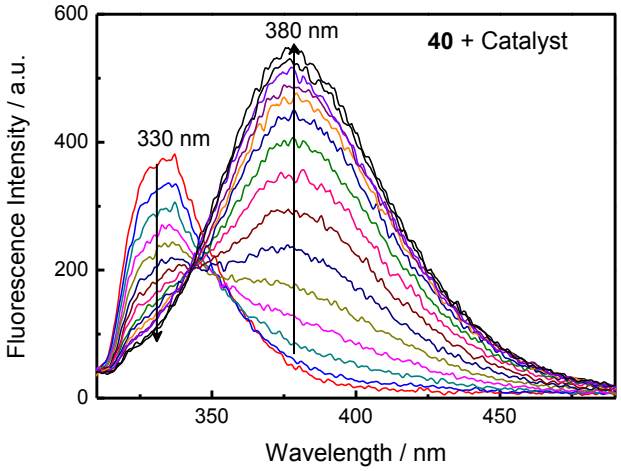

Figure 52 Fluorescent spectral changes of **40** under the catalytic reaction in buffer solution. [**40**] = 3×10^{-6} M

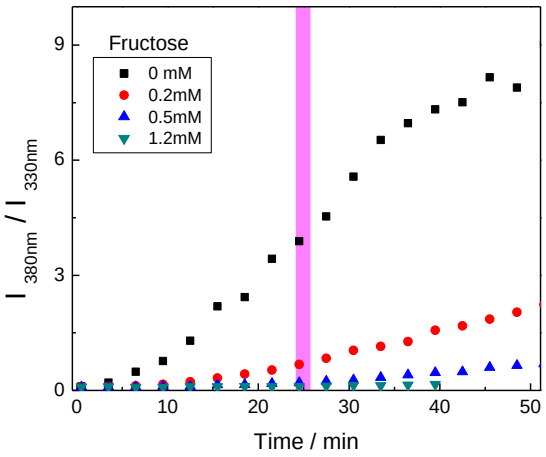

Figure 53 Ratio changes of fluorescence intensities at 380 nm and 330 nm along with time, with different concentrations of fructose under the catalytic reaction in buffer solution. [**40**] = 3×10^{-6} M

Based on these observations, the titration with fructose was carried out by adding different concentrations of D-fructose to a series of solutions and collecting the fluorescence spectra at 25th minute, shown in Figure 54. The $3\sigma/k$ based detection limit of D-fructose is estimated to be 1.8×10^{-5} M, the detection limit of which is in the same order of magnitude, compared with that of phenylboronic acid. When naphthalene-1-

boronic acid (**40**) employed, a ratiometric fluorescent sensor achieved, which can effectively eliminate most or all interference from the environment with built-in correction and also avoid the instrument fluctuation. If applying non-linear least square binding fit equation, it was found that the binding constant is 5716 ± 536 M^{-1} with R^2 value of 0.990 (Appendix Figure 8).

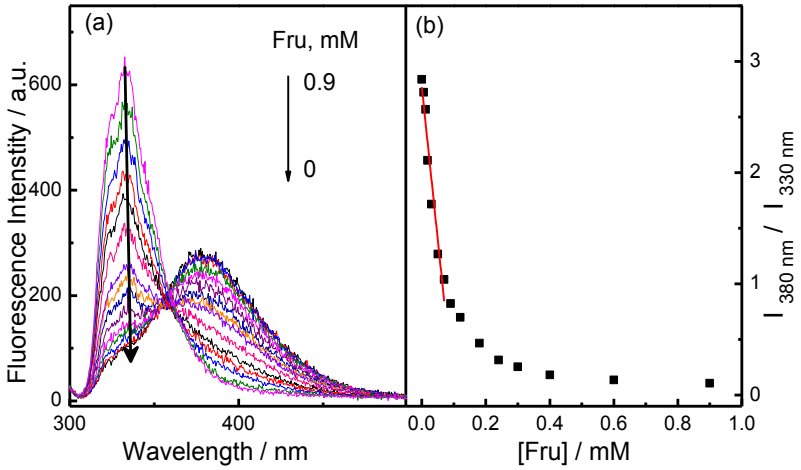

Figure 54 (a) Fluorescent spectra at 25th minute in the presence of increasing concentration of fructose; (b) Plot of the fluorescent intensity ratios (I_{380nm} / $I_{330\,nm}$) *versus* saccharide concentration.

Using the same protocol, the saccharide titration with D-galactose and D-glucose were also investigated. The limit of detection (LOD) is shown in Table 9, compared with previous work. The LODs are in same order of magnitude with different reporting signals. It is reasonable since the underlying sensing mechanism is the same; the only change is the signal reporter, which won't greatly affect the sensitivity

Table 9 Comparison of limit of detection of different saccharides with naphthalene-1-boronic acid and phenylboronic acid, respectively

	Limit of detection, mol / L		
	D-fructose	D-galactose	D-glucose
40 (I_{380nm} / I_{330nm})	1.8×10^{-5}	2.0×10^{-4}	1.2×10^{-3}
PBA (I_{311nm})	2.4×10^{-5}	3.3×10^{-4}	6.1×10^{-3}

5.3.2 1,4-phenylenediboronic acid as substrate

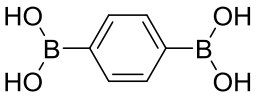

41

The investigation was further extended to other boronic acid compounds. One interesting example is 1,4-phenylenediboronic acid (**41**). When 1,4-phenyldiboronic acid was used in Suzuki homocoupling reaction under the same condition as described above, the fluorescence intensity increases quickly, followed by decrease over time, which was quite different from the former compounds investigated. One possible reason was that the product had underwent polymerisation, as each 1,4-phenylenediboronic acid has two boronic acid moieties. The decrease of fluorescence may result from the poor solubility of generated polymer in pure water. Under this assumption, the effect of solvent was investigated. It was found that the solvent plays an important role in the coupling reaction, not only on the fluorescent intensity changes but also the maximum emission peak wavelength, shown in Figure 55. Addition of organic solvents would impede the reaction rate, indicated by the slow increase of fluorescent emission. In THF, the emission was at around 370 nm, which is at 350 nm in other systems.

For the same solvent, different amounts of the added solvent can also affect the total reaction kinetics, shown in Figure 56, which indicated that the increased amount of MeCN would impede the reaction rate. The observed phenomenon also showed some underlying factors on the Suzuki coupling reaction, of which the exact mechanism is still unclear.

The Na_2CO_3-$NaHCO_3$ buffer solution was utilised in the sensing system in order to compare with the other two systems. The spectra were collected after 6 minutes, considering that in buffer solution, the fluorescent intensity at 350 nm decreased after 6 minutes. Then the saccharide titration of **41** was carried out with D-fructose, shown in Figure 57. The reaction displayed a better linear fitting curve than that of **40**, however, the fluctuation of the spectra were much stronger. The co-solvent systems have not been optimised for the saccharide sensing, based on compound **41**, which will need to be explored in the future.

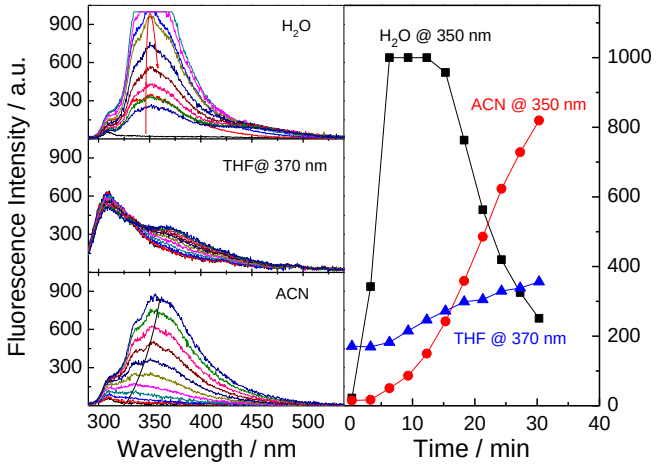

Figure 55 Fluorescence intensity changes with different solvents, the total volume is 3 mL, of which the buffer solution is 2.6 mL, [**41**] = 5×10^{-6}M, [Pd] = 1.0×10^{-5} M (Note: the spectra are over-scale when carried out in H_2O system.)

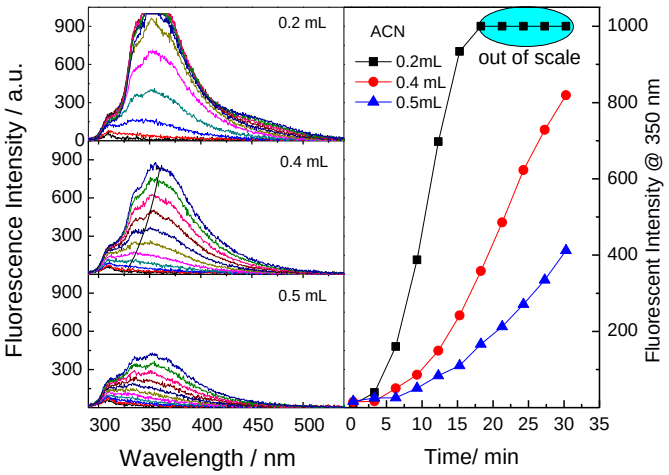

Figure 56 Fluorescent spectra with different amounts of MeCN in system and fluorescent intensity changes at 350 nm with time.

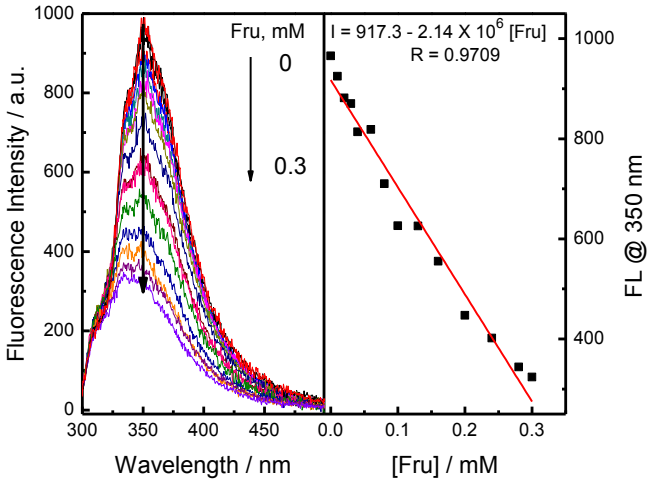

Figure 57 Changes of fluorescent intensities at 350 nm with different concentrations of fructose at 6th minute. [**41**] = 5 × 10^{-6} M.

5.4 Extended mechanism discussion

*5.4.1 Synthesis of compound **43***

The Kazunori Koide group [128] firstly built up a palladium detection platform *via* the Tsuji-Trost reaction, where the palladium catalysed reaction could cleavage the allyl group, resulting in a free hydroxyl group, which was then deprotonated to afford high quantum yield species.

Compound **43** was obtained in following procedures shown in Scheme 32. The allylation step could afford compound **42** quantitatively, and then went through the next step to obtain compound **43**. All the syntheses procedures and compound characterizations are listed in experimental chapter.

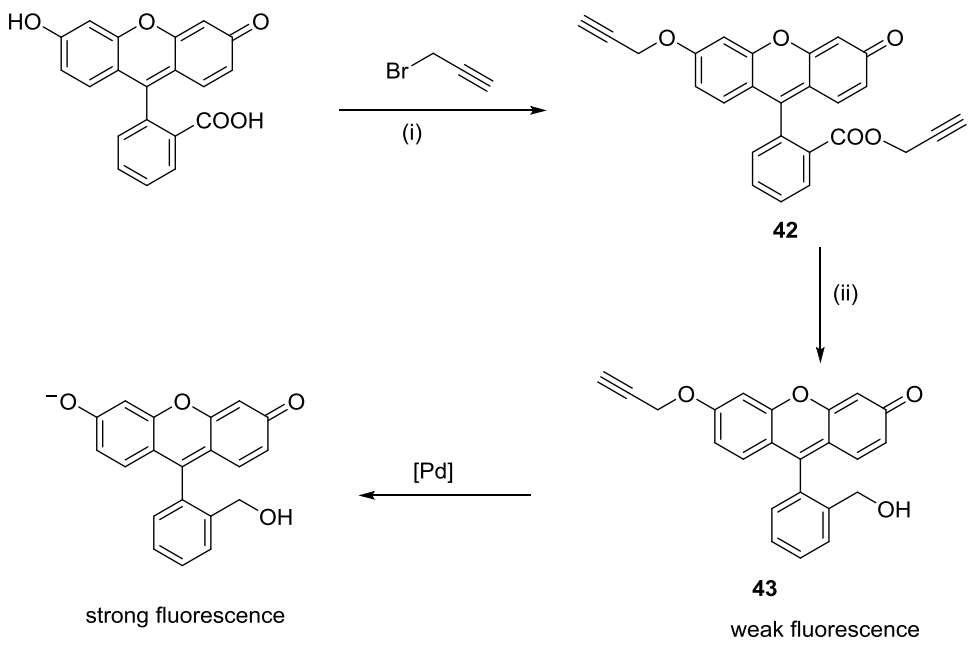

Scheme 32 Synthesis route of compound **43** and the illustration of palladium catalysed Tsuji-Trost reaction. (i) DMF, K_2CO_3, 40 °C, 99%; (ii) (a), DCM, DIBALH, -78 °C, N_2; (b), Et_2O, DDQ, 0 °C, 23%

5.4.2 Study of saccharide effect on palladium catalysis

All the experimental conditions stayed the same as those used in the Suzuki homo-coupling reaction for easier comparison of saccharide effect on the efficiency of the palladium catalyst.

A new fluorescent emission at 511 nm was observed once compound **43** was mixed with the palladium catalyst, shown in Figure 58. The kinetic profiles of this catalytic reaction were monitored with and without presence of saccharide; the results suggested that saccharide impede the reaction rate, shown in Figure 59. Addition of 11 mM D-fructose could result in a slower reaction rate. Meanwhile, investigations on the kinetics of catalytic reaction also revealed that the fluorescence intensity has the largest difference at the 20th minute before and after addition of 11 mM D-fructose. Therefore, fluorescence intensities at the 20th minute were collected for further comparison.

It was also found that for the same concentration of different saccharides, D-fructose showed the strongest effect on impeding reaction rate, followed by D-galactose and D-glucose (Figure 60), which has the same order as boronic acid based probes. No clear reasons were found to explain such a coincidence.

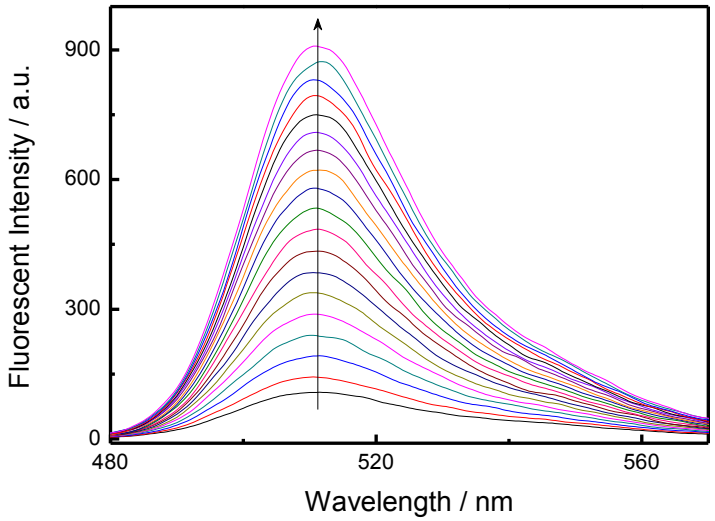

Figure 58 Fluorescent spectral changes along with time. [**43**] = 1×10^{-5} M, [catalyst] = 1×10^{-5} M

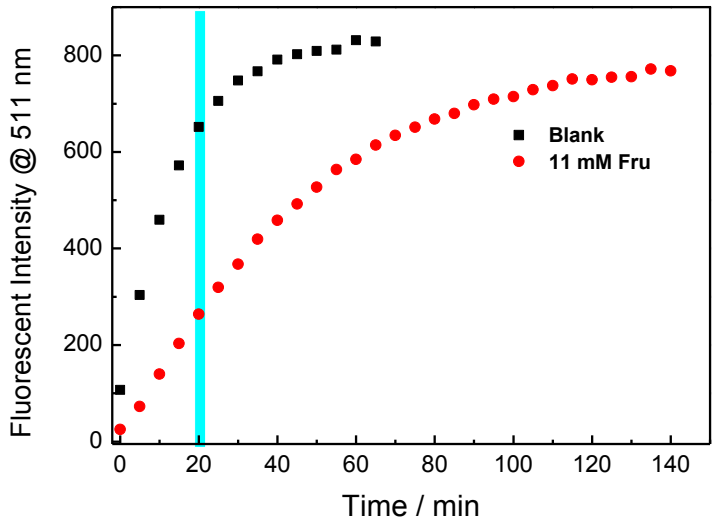

Figure 59 Fluorescent intensity changes along at 511 nm along with time in the presence / absence of D-fructose. . [**43**] = 1×10^{-5} M, [catalyst] = 1×10^{-5} M

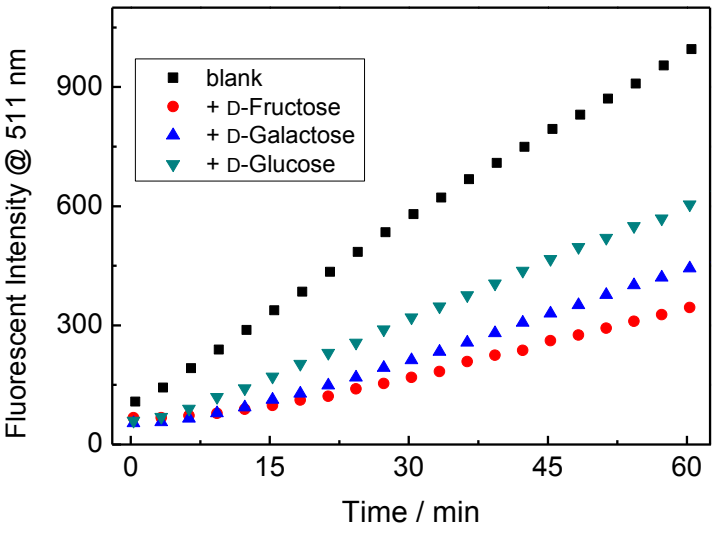

Figure 60 Fluorescent intensity changes of compound **43** at 511 nm along with time in the presence of different saccharides (■ blank, ▽ blank + D-glucose, △ blank + D-galactose, ● blank + D-fructose,) [**43**] = 1×10^{-5} M, [catalyst] = 4×10^{-6} M

Though saccharide could affect the catalytic reaction rate, the effect was only to a limited degree, as over 40 mM D-fructose was needed to arrive at the plateau state of the titration curve, given in Figure 61. By comparing the titration curve of compounds

40 and **43** with D-fructose, respectively, it is easy to see that with compound **40**, only 0.4 mM D-fructose is needed to reach the equilibrium state, however, for compound **43**, more than 100 times higher of saccharide was required to arrive at the same outcomes. When Equation (13) applied, the obtained binding constant is 378 ± 51 M^{-1} with R^2 value of 0.967 (Appendix Figure 9).

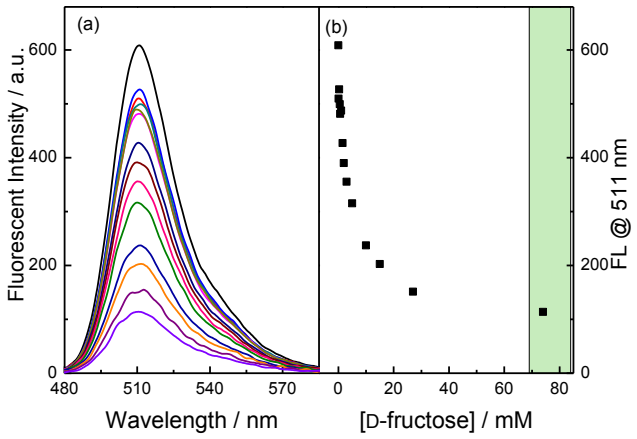

Figure 61 (a) Fluorescent spectral changes of compound **43** at 20th min after adding different concentrations of D-fructose in Na_2CO_3-$NaHCO_3$ buffer solution; (b) fluorescent intensity changes at 511 nm in the presence of different concentrations of D-fructose. [**43**] = 1×10^{-6} M, [Pd] = 1×10^{-6} M.

5.5 Summary of Chapter 5

Boronic acid derivatives were used as versatile candidates in organic synthesis for constructing new C-C bonds. Meanwhile, they were also extensively explored in saccharide recognition as the boronic acid moiety can form cyclic boronate ester with diols through covalent bonds. The interesting finding was that these applications have yet to be combined and reported in the literature. Inspired by the molecular sensing strategies based on reactions, we developed a Suzuki homo-coupling reaction based saccharide recognition platform. The formed boronate ester complex *via* the binding between boronic acid and saccharide has a slower reaction rate towards the Suzuki

homo-coupling reaction. The different reaction rate of free boronic acid and formed boronate ester towards the Suzuki homo-coupling reaction accounted for the fluorescence differences that were recorded at a specific time. The potential of saccharide sensing was investigated by using phenylboronic acid as substrate. Both selectivity and sensitivity were improved, compared with using the traditional method.

Other boronic acid derivatives were employed to extend this sensing system. A ratiometric sensor was developed by using naphthalene-1-boronic acid, with longer wavelength emission and improved sensitivity. 1,4-phenyldiboronic acid showed a longer wavelength and quicker responses, however, suffered from solubility issues. Future work needs to focus on the optimisation of solvent employed.

Studies of the palladium catalysed Tsuji-Trost reaction under the same experimental conditions as for the Suzuki homocoupling reaction indicated that the palladium catalyst may also interact with saccharides as well, but only to a limited degree.

CHAPTER SIX

Experimental

6 Experimental

6.1 General reagents and techniques

6.1.1 Solvents and reagents

Solvents and reagents were purchased from Sigma-Aldrich company Ltd, Lancaster Synthesis Ltd and Fisher Scientific UK and used without further purification, unless stated otherwise.

6.1.2 Instruments

Fluorescence Measurement

Fluorescence measurements were recorded in this project using a Perkin-Elmer Luminescence Spectrophotometer LS 50B, utilising cuvettes with 10 mm path lengths, four faces polished. This instrument was operated using FL Winlab software. For gel based saccharide titration, spectra were measured on Fluoro SENS GILDEN with 96 (12 x 8) wells plate reader devices. All solvents used in fluorescence measurement were HPLC grade and the water was second distilled.

UV-vis Measurement

Absorption measurement was performed using Perkin-Elmer UV-*vis* spectrometer Lambda20 with 10 mm path length of cuvettes. Baseline correction using blank solvent was carried out every time running machine. This instrument was operated using UV Winlab software.

pH measurement

Hanna Instruments HI 9321 Microprocessor pH meter was used and routinely calibrated by Fisher Chemicals standard buffer solutions (pH 4.0 - phthalate, 7.0 - phosphate, and 10.0 - borate).

Nuclear Magnetic Resonance Spectra (NMR)

NMR spectra were collected on Bruker ultrashield NMR spectrometer. ^{1}H spectra were recorded at 300.22 MHz, ^{11}B spectra at 96.32 MHz and ^{13}C spectra at 75.499 MHz. Where a Bruker AVANCE 400 was used, ^{1}H spectra and $\{^{1}H - ^{1}H\}$ were recorded at 400.13 MHz. Tetramethylsilane (Me_4Si) was used as internal standard and chemical shifts (δ) are expressed in parts per million. For boron spectra, boron trifluoride diethyl etherate ($BF_3.OEt_2$) was performed as a standard. General assignments of the spectroscopic data are denoted as: singlet (s), doublet (d), triplet (t) and multiplet (m).

Mass Spectra (MS)

Mass Spectra was measured on a Bruker microTOF mass spectrometer with an electrospray ionization (ESI) source. Samples were made up in HPLC grade methanol. The spectrometer was coupled to an Agilent Technologies 1200 LC system. 10μL of sample was injected into a 30:70 flow of water/acetonitrile at 0.3 mL/min to the mass spectrometer. Data acquisition and automated processing were controlled via Compass Open Access 1.2 software. Corresponding theoretical values are calculated using the Bruker data processing software, Data Analysis 3.4.

Melting point

Melting points of compound were obtained from Stuart Melting point SMP10. By selecting a plateau temperature *via* the digital display and press "start" button, the measurement can be started. The unit quickly heats up and remains at the selected plateau temperature until the user is ready to start the test. Insert the sample tubes and press "start". The unit then heats at a fixed rate of 2°C per minute for the SMP10. When the sample is seen to melt, note the temperature on the display. Press "stop" to end heating and cool the block.

Solid state infrared (IR) spectroscopy

Measurement was performed using Perkin Elmer 1000 FT-IR Express spectrometer. Products were placed directly onto the spectrometer diamond plat and compressed. The spectrum was displayed and then could be processed in the software. Characteristic absorption peaks are reported in wavelength (cm^{-1}).

Thin Layer Chromatography (TLC)

Thin layer chromatography was got using commercially available Merck aluminium backed plates coated with a 0.20 mm layer of silica gel 60 with fluorescent indicator UV254. Plates were visualized using either ultraviolet light of 254 nm or 365 nm wavelength or by staining the plates with Ninhydrin solution or "Curry" solution. Silica gel column chromatography was carried out using Davisil LC 60A silica gel.

6.2 Experimental measurement conditions

6.2.1 Fluorescent measurement of hydrogel

Buffer

The fluorescent titrations for compounds **25** and **26** were carried out in a pH 8.21 aqueous methanolic buffer. The buffer was prepared following the literature method of Perrin and Dempsey [223] and contained:

52.1 *wt*% HPLC grade methanol in deionised water with KCl, 0.01000 mol / L, KH_2PO_4, 0.002752 mol / L and Na_2HPO_4, 0.002757 mol / L.

Fluorescence titrations

In each case the tested compound was weighed out in a small volumetric flask and then made up to the required volume with HPLC grade methanol to obtain a stock solution of known concentration. Considering the test limit of fluorescence spectrometer, certain volume of stock solution were transferred to a volumetric flask and use the already made buffer solution to make up to the required volume, for example 100 mL. Then a solution with known molarity was obtained. When carrying out the fluorescent titration, the dilute solution needs to be transferred into a conical flask with a stir bar inside and a lid to cover. Each time after adding a certain amount of saccharide, 10 minutes of stirring are needed to make the saccharide dissolve and interact with substrate. Table 10 shows the concentration, emission and excited wavelength of each compound.

For the fluorescent spectrometer, the parameters are fixed as: slit, 5.0 nm / 3.0 nm, scan speed: 600 nm / min.

Table 10 Fluorescence measurement condition for compounds **25** and **26**

Fluorophore	Concentration, mol / L	λ_{ex} / nm	λ_{em} / nm
Anthracene	6.0×10^{-7}	370	419
Pyrene	1.0×10^{-7}	342	376

Data analysis

Data was collected *via* the Perkin-Elmer Winlab software package. The observed stability constants (K_{obs}) with coefficient of determination (γ^2) were calculated by the fitting of emission intensity *versus* saccharide concentration using non-linear(Levenberg-Marquardt algorithm) curve fitting.[224]

6.2.2 Hydrogel fluorescence measurement

The hydrogel fluorescence measurement was based on a plate reader, employing the assay methodology of the fluoroSENS GILDON pλotonics instrument. Excited

wavelength is 370 nm and maximum emission 409 nm. The buffer solution is made according to GSK laboratory data book: 50 mL 0.1M KH_2PO_4 was mixed with 46.1 mL 0.1M NaOH and adding water to make up to 100 mL. The saccharide solutions used were also made from the buffer solution in order to keep pH value the same in the test system, since the total volume for gel titration is only 0.3 mL, of which 0.2 mL is hydrogel.

6.2.3 Procedure of hydrogel formation

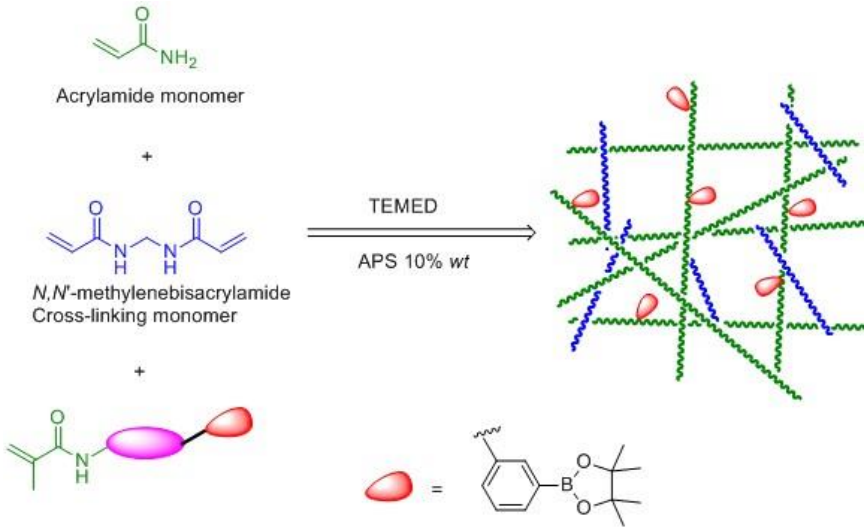

Scheme 33 Acryalmide hydrogel formation procedure

The acrylamide hydrogel was formed by copolymerisation of acrylamide and bisacrylamide in water through the free radical polymerisation, as shown in Scheme 33. Ammonium persulfate (APS) afford free radicals under catalysis of tetramethylethylenediamine (TEMEDA).[157] Detail make-up procedures were listed in several steps:

1) Aqueous ammonium persulfate (APS) stock solution (10% *wt*/vol) was freshly prepared and kept below 4°C until required.
2) Methlylene bisacrylamide (0.040 g) and acrylamide (1.52 g) were added to water (8

mL) and stirred well until all have dissolved.

3) 2 mg boro-additive was dissolved in 0.2 ml MeOH first and then added into the above mixture in step 2.
4) Tetramethylethylenediamine (TMEDA) (20 μl) and APS (60 μl) were then also added. 3 ml syringes were used to suck up the mixture and allowed to set, it took roughly 30 minutes. As for plate reader based saccharide titration, 0.2 ml mixture was taken into each well.

When making gel for saccharide titration, the water in step 2 was replaced by buffer solution, which ensured the titration was carried out in a buffered solution environment, since the overall volume for each well is approximately 0.3 ml.

6.3 Compounds characterisation

6.3.1 Precursors for hydrogel monomers

step 1:

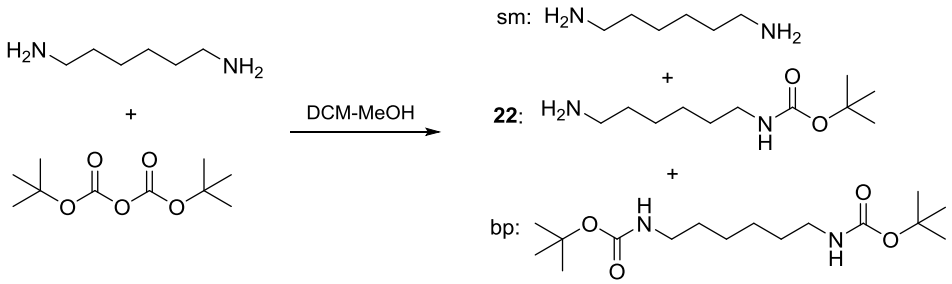

tert-butyl (6-aminohexyl)carbamate

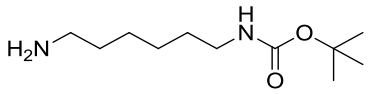

22

1,6-hexanediamine (2.95 g, 25 mmol) was dissolved in minimum amount of MeOH and di-tert-butyl dicarbonate (1.09 g, 5 mmol) in 20 mL MeOH. The latter solution was added dropwise into 1,6-hexanediamine solution. TLC (DCM: CH_3OH 9:1.5 with five drops of triethylamine) was used to track the reaction once every two hour. MeOH was removed under reduced pressure and then DCM added, and Na_2SO_4 was used to dry the DCM layer after washed up by water for three times (3 x 100 ml). Most of the starting material could be washed off, which was indicated by the TLC. The solvent removed *in vacuum* to afford yellow oil. Silica gel column chromatography was utilised to obtain pure compound **22** (1.6 g, 74%). Using elute with DCM: Hexane 9:1 to remove 1,6-hexanedi-tert-butyldicarbonate, followed by pure DCM, DCM: MeOH 20:1 and at last DCM:MeOH 5:1.

^{1}H NMR (300 MHz, $CDCl_3$, ppm, Me_4Si) δ 1.26 (m, 4H), 1.37(m,11H), 1.46 (m, 2H), 2.59-2.63 (t, 2H, *J* = 6, -CH_2-NH_2), 3.00-3.07 (dt, 2H, *J* = 6,9, -CH_2-NHBoc)

^{13}C NMR (75.499 MHz, $CDCl_3$, ppm, Me_4Si) δ 26.5, 26.6, 28.39 (3C), 30.0, 33.6, 40.4, 42.0, 78.9, 156.0

ESI-Mass [M + H^+] $C_{11}H_{26}N_2O_2^+$ calculated 217.1916, Found 217.1993

Step 2:

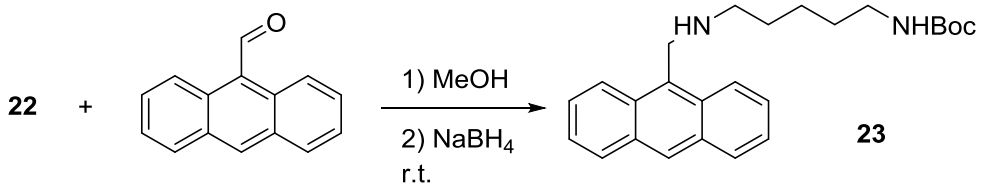

tert-butyl (6-((anthracen-9-ylmethyl)amino)hexyl)carbamate

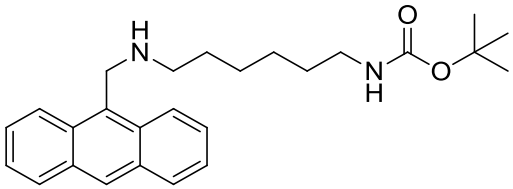

23

Compound **22** (2.0 g, 9.2 mmol) and 9-anthracene aldehyde (1.7 g, 8 mmol) were dissolved in DCM and stirred at room temperature overnight. The intermediate compound is imine. The chemical shift of proton on imine group has a significant difference from that of aldehyde. The reaction could be traced by monitoring the disappearance of proton peak of aldehyde at around 10 ppm on NMR spectrum. Then $NaBH_4$ (0.3499 g, 9 mmol) was added gently followed by being stirred for 4h. Then 3 mL H_2O was added to quench the reaction. The reaction mixture was condensed under reduced pressure then dissolved in 20 mL DCM again. The solution was washed with water (4 x 100mL) and dried over anhydrous magnesium sulphate. A yellow solid was obtained by column chromatography with yield (1.8g, 48 %). The elute ratio follows the order of DCM: Hexane10:1, pure DCM, DCM: CH_3OH 20:1 and DCM: CH_3OH 10:1,

^{1}H NMR (300 MHz, $CDCl_3$, ppm, Me_4Si) δ 1.17-1.27 (m, 4H), 1.33-1.36 (s, 9H), 1.38-1.60 (m, 4H), 2.84-2.88 (t, *J* = 6 Hz, 2H), 3.06-3.10 (q, 2H,) 4.62 (s, 2H), 7.44-7.49 (m, 2H), 7.51- 7.57 (m, 2H), 7.99-8.02 (d, *J* = 9 Hz, 2H), 8.32-8.35 (d, *J* = 9 Hz, 2H), 8.40 (s, 1H)

^{13}C NMR (75.499 MHz, $CDCl_3$, ppm, Me_4Si) δ 26.7, 27.1,28.5(3C), 30.0, 40.6, 45.8, 50.4, 53.4, 79.0, 124.1, 124.9, 126.1, 126.2, 127.2, 129.2, 130.3, 156.02(C=O)

ESI-Mass [M + Na^+] $C_{26}H_{34}N_2O_2$ Na^+ calculated 429.2517 Found 429.2545

tert-butyl (6-((pyren-1-ylmethyl)amino)hexyl)carbamate

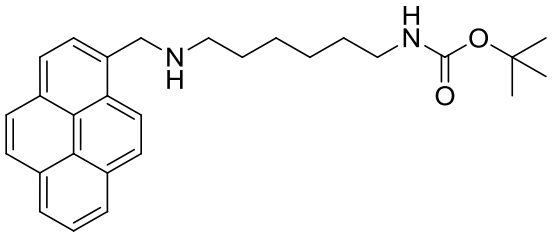

24

Compound **22** (2.1 g, 9.7 mmol) and 1-pyrene aldehyde (2.0 g, 8.7 mmol) were dissolved in DCM and stirred at room temperature for overnight. Then reaction was moved to next step when NMR spectra showed the disappearance of proton peak on aldehyde. Then $NaBH_4$ (0.37 g, 9.7 mmol) was added gently followed by being stirred for 4 hours. Then 5 mL H_2O was added to quench the reaction. The reaction mixture was condensed under reduced pressure and dissolved in 25 mL DCM again. An off-white compound was afforded after removing solvent. Then solid was dissolved in 10 ml DCM. 1 N HCl was used to wash off the starting material then solid come out between the water and DCM layer. The collected DCM layer and solid was washed by 1 N NaOH. The DCM layer was collected and dried over Na_2SO_4. Compound **24** was purified by silica chromatograph with yield 67.2 %.

^{1}H NMR (300 MHz, $CDCl_3$, ppm, Me_4Si) δ 1.24-1.39 (m, 4H), 1.42-1.45 (m, 9H), 1.48-1.66 (m, 4H), 2.62-2.66 (t, *J* = 6 Hz, 2H), 3.03-3.05 (t, J = 6 Hz, 2H), 4.32 (s, 2H), 8.02-8.12 (m, 4H), 7.89-7.95 (m, 4H), 8.23-8.26 (d, *J* = 9 Hz, 1H),

^{13}C NMR (75.499 MHz, $CDCl_3$, ppm, Me_4Si) δ 26.8, 27.1, 28.6, 30.1, 40.6, 49.9, 51.8, 53.5, 78.9, 123.1, 124.6, 124.8, 124.9 (2C), 125.0, 125.8, 126.8, 127.0, 127.4, 127.5, 128.9, 130.5, 130.8, 131.3, 134.0, 156.1,

ESI-Mass [M + Na^+] $C_{28}H_{34}N_2O_2Na^+$ calculated 453.2517, found 453.2512

IR 3331.38 cm^{-1}, 3350 cm^{-1}, 3373 cm^{-1}, (NH bond stretch), 2926.08 cm^{-1}, 2853.99 cm^{-1} (alkane)1682.60 cm^{-1} (NH-CO), 1514 cm^{-1}, 1443 cm^{-1}, 1364.7 cm^{-1}, 1248 cm^{-1}, 1161 cm^{-1}, 993.91 cm^{-1}, 844.88 cm^{-1},708.40 cm^{-1}

The attachment of boronate ester:

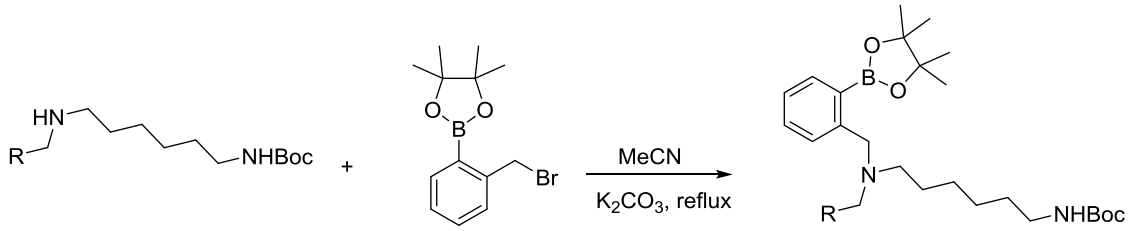

tert-butyl(6-((anthracen-9-ylmethyl)(2-(4,4,5,5-tetramethyl-1,3,2-dioxaborolan-2-yl)benzyl)amino)hexyl)carbamate

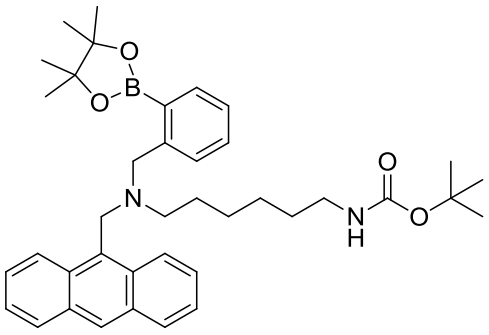

25

Compound **23** (1.8 g, 4.4 mmol, 1.0 eq) and 2-bromomethylphenylboronic acid pinacol ester (1.45 g, 4.6 mmol, 1.05 eq) were dissolved in 30 mL MeCN. Potassium carbonate

(1.82 g, 13.2 mmol, 3 eq.) was then added. The reaction was heated to reflux and stirred for 12 h. Solvent was removed under reduced pressure.1.5 mL acetone was added into the mixture to afford a clear liquid. The solution was added dropwise into 300 mL water whilst shaking the flask vigorously in order to form light yellow flocculent precipitate. The solid was then dried *in vacuum* and washed with 100mL water .The yield of compound **25** is 89% (2.46 g).

^{1}H NMR (300 MHz, CD_3OD, ppm, Me_4Si) δ 0.88-0.98(m, 4H), 1.12-1.23 (m, 9H), 1.28-1.30 (m, 2H)1.41-1.43 (m, 12H), 1.49-1.91 (m, 2H), 2.72-2.77 (t, *J* = 6 Hz, 2H), 2.81-2.85 (t, *J* = 6 Hz, 2H), 4.44 (s, 2H), 5.00 (s, 2H), 7.28-7.58 (m, 8H), 8.07-8.10 (d, *J* = 9 Hz, 2H), 8.18-8.21 (d, *J* = 9 Hz, 2H), 8.62 (s, 1H)

^{13}C NMR (75.499 MHz, CD_3OD, ppm, Me_4Si) δ 14.4, 15.5, 21.1, 23.8, 25.4, 25.7, 25.9, 28.6, 29.3, 48.9, 53.5, 59.3,60.1,65.3, 67.4, 77.7, 83.6, 121.4, 123.5, 125.9, 128.0, 129.5, 129.9, 131.0, 131.1, 133.4, 135.2, 136.3, 155.9, 170.7

ESI-Mass [M + H^+] $C_{39}H_{52}BN_2O_4^+$ calculated 623.40, found 623.40

IR: 3354 cm^{-1}, 2976.38 cm^{-1}, 2933 cm^{-1},1691.89 cm^{-1}, 1599 cm^{-1}, 1509 cm^{-1}, 1443 cm^{-1}, 1345.39 cm^{-1}, 1166 cm^{-1}, 1143 cm^{-1},730.73 cm^{-1}

tert-butyl(6-((pyren-1-ylmethyl)(2-(4,4,5,5-tetramethyl-1,3,2-dioxaborolan-2-yl)benzyl)amino)hexyl)carbamate

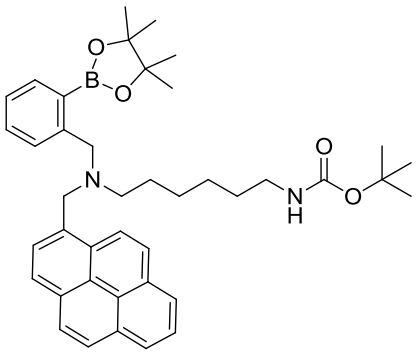

Compound **24** (0.18 g, 0.41 mmol, 1.0 eq.) and 2-bromomethylphenylboronic acid pinacol ester (0.13 g, 0.43 mmol, 1.05 eq) were dissolved in 20 mL MeCN. Potassium carbonate (0.173 g, 1.25 mmol, 3 eq) was then added. The reaction was heated to reflux and stirred for overnight. Solvent was removed under reduced pressure.1.0 mL acetone was added into the mixture to afford a clear liquid. The solution was added dropwise into 100 mL water while shaking the flask vigorously. Emulsion solid was formed when the mixture was dropped in the water and left the mixture overnight. The solid was then dried *in vacuum* and washed with 100 mL water. The yield of compound **26** is 90 % (0.213 g).

^{1}H NMR (300 MHz, CD_3OD,) 0.91-1.09 (m, 7H), 1.19 (m, 9H), 1.28-1.42 (m, 12H), 1.61 (broad peak, 2H), 2.76-2.81 (m, 4H), 4.40 (s, 2H), 4.72 (s, 2H), 7.24-7.38 (m, 3H), 7.73-7.75 (d, *J* = 9, 1H), 8.03-8.11 (m, 9H)

^{13}C NMR (75.499 MHz, CD_3OD, ppm, Me_4Si) 24.9, 27.4, 27.9, 29.2, 30.9, 41.4, 61.9, 80.2, 123.6, 125.8, 126.0, 128.1, 127.0, 127.2, 127.8, 128.6, 129.3, 129.5, 130.4, 131.4, 132.1, 132.8, 133.4, 136.6, 158.8

ESI-Mass [M + H^+] $C_{41}H_{52}BN_2O_4^+$ 647.67 not found

Without pinacol group $C_{35}H_{42}BN_2O_4^+$ calculated 565.32 found 565.32

N-(6-((anthracen-9-ylmethyl)(2-(4,4,5,5-tetramethyl-1,3,2-dioxaborolan-2-yl)benzyl)amino)hexyl)methacrylamide

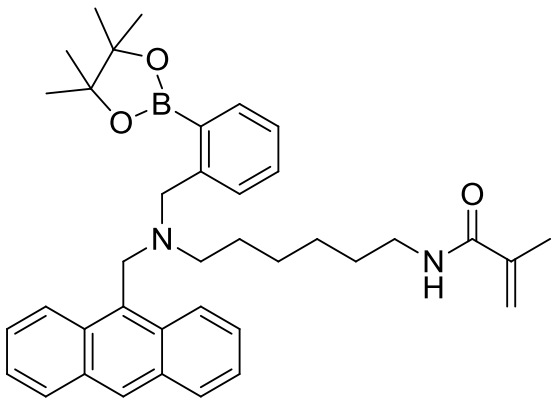

27

The compound **25** (1.54 g, 2.9 mmol) was dissolved in 20 mL DCM and with 2 eq. of triethylamine (0.58 g, 0.81 mL, 5.8 mmol) and the round-bottom flask was put in ice bath before addition of methacryloyl chloride (0.58 mL, 5.9 mmol, 2.0 eq.). The mixture was stirred for 5 h and then washed with saturated sodium hydrogen carbonate aqueous solution (2 x 100 mL). The organic phase was washed with saturated sodium chloride solution (3 x 100 mL) until the water layer was neutral, then dried with Na_2SO_4 before removing organic solvents. A yellow powder was obtained. NMR showed partial of the products without pinacol moiety.

^{1}H NMR (300 MHz, $CDCl_3$): 8.61-8.40 (2H, s), 8.08-7.96 (5H, m), 7.73-7.42 (6H, m) , 6.50-4.20 (4H, m), 3.41-2.50 (3H, m), 2.15-0.51 (19H, m)

ESI-MS: [M + H^+] $C_{38}H_{48}BN_2O_3^+$ calcu. 591.3753, found: 547.3779; [M + Na^+] $C_{38}H_{47}BN_2O_3\,Na^+$, calculated 613.3572, found: 613.3038

For formula without pinacol group

[M +H^+] $C_{32}H_{38}BN_2O_3^+$, calcu. 509.2970 found: 509.2975; [M +Na^+] $C_{32}H_{37}BN_2O_3\,Na^+$, calcu. 531.2789, found: 531.2814

N-(6-((pyren-1-ylmethyl)(2-(4,4,5,5-tetramethyl-1,3,2-dioxaborolan-2-yl)benzyl)amino)hexyl)methacrylamide

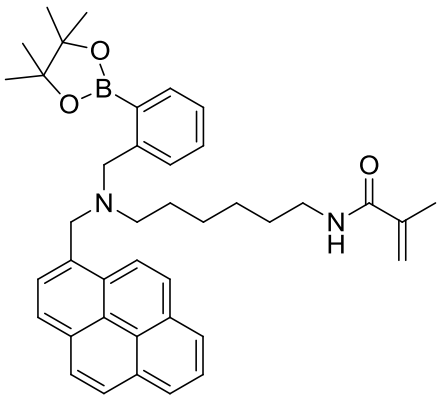

28

The compound **26** (1.65 g , 2.68 mmol) was dissolved in 20 mL DCM with 0.75 ml tiethylamine (5.37 mmol, 2.0 eq.) and put in ice bath before addition of methacryloyl chloride (0.53 mL, 5.37 mmol, 2.0 eq.). The mixture was stirred for 5 h and then washed with saturated sodium hydrogen carbonate aqueous solution (2 x 50 mL). The organic phase was washed with saturated sodium chloride solution (3 x 50 mL) until the water layer was neutral, followed by drying with Na_2SO_4. A yellow powder was obtained after condensed under vacuum. The acrylamide monomer is easy to go polymerisation with temperature above 35 °C, therefore, all the procedures needs to be carried out under this temperature. Pure NMR spectrum is also not available for this compound, but typical NMR peaks were found in ^{1}H NMR spectrum, which was listed here.

^{1}H NMR (300 MHz, $CDCl_3$): 8.51-7.75 (10H, m), 7.74-7.25 (3H, m), 6.08-5.10 (2H, m), 4.26 (1H, s), 3.93 (1H, s), 3.30-2.91 (2H, m), 2.72-2.40 (1H, m), 2.03-1.88 (4H, m), 1.62-1.04 (12H, m)

ESI-MS: [M + H^+] $C_{40}H_{48}BN_2O_3^+$ calcu. 615.3753, found: 615.3801; For formula without pinacol group [M + H^+] $C_{34}H_{38}BN_2O_3^+$, calcu. 533.2970 found: 533.2999

6.3.2 Naphthalimide derivatives

6-bromo-2-propyl-*1H*-benzo[*de*]isoquinoline-1,3(*2H*)-dione

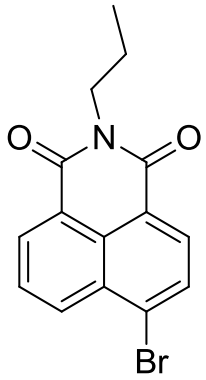

32a

1.0 g (3.6 mmol) 4-bromo-1,8-naphthalic anhydride and *n*-propylamine (0.3 ml, 3.6 mmol) were dissolved in 50 mL ethanol, heated to reflux for 6 hours. The suspension was poured into 100 mL ice water after removing part of the ethanol *in vacuum*. The crude product was filtered and purified by column chromatography. Pure compound **32a** was obtained as a slightly gray solid (1.03 g, yield: 89%).

^{1}H NMR (300 MHz, $CDCl_3$): 8.50 (d, *J* = 7.29 Hz, 1H), 8.39 (d, *J* = 8.7 Hz, 1H), 8.25 (d, *J* = 7.8 Hz, 1H), 7.89 (d, *J* = 7.5 Hz, 1H), 7.71 (t, *J* = 7.5 Hz, 1H), 4.03 (t, *J* = 7.5 Hz, 2H), 1.73–1.61 (m, 2H) and 0.93 (t, *J* = 7.5 Hz, 3H).

^{13}C NMR (75.499 MHz, $CDCl_3$): 163.5, 163.5, 133.1, 131.9, 131.1, 131.0, 130.5, 130.1, 128.8, 128.0, 123.0, 122.2, 42.1, 21.4, 11.6

ESI-Mass $[M + H^+]$ $C_{15}H_{13}BrNO_2^+$ calcu. 319.1728, found 319.1413

6-hydrazinyl-2-propyl-*1H*-benzo[*de*]isoquinoline-1,3(*2H*)-dione

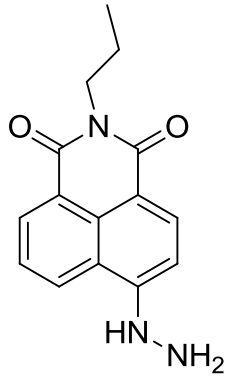

32

1.03 g compound **32a** (3.24 mmol) and 0.3 ml hydrazine (0.306 g, 9.5 mmol) were dissolved in 4 ml 2-methyoxylethanol and heated to reflux for 3 hours. After cooling to room temperature, precipitation was washed with ethanol. Silica chromatography (95% MeOH in DCM) was employed to purify and a yellow solid **32** was obtained (0.62g, 71.3%).

^{1}H NMR (300 MHz, $(CD_3)_2SO$): 9.09 (s, 1H), 8.59 (d, *J* = 7.8 Hz, 1H), 8.40 (d, *J* = 7.8 Hz, 1H), 8.28 (d, *J* = 9 Hz, 1H), 7.60 (t, *J* = 7.2 Hz, 1H), 7.23 (d, *J* = 9 Hz, 1H), 3.96 (t, *J* = 6 Hz, 2H), 1.68-1.55 (m, 2H), 0.90 (t, *J* = 6 Hz, 3H)

^{13}C NMR (75.499 MHz, $(CD_3)_2SO$): 164.2, 163.3, 153.5, 134.6, 130.9, 129.7, 128.6, 124.5, 122.1, 118.8, 107.7, 104.4, 41.2, 21.3, 11.8

ESI-Mass [M + Na^+] $C_{15}H_{15}N_3O_2\,Na^+$ calculated 292.1062, found 292.1031

2-propyl-6-(2-(2-(4,4,5,5-tetramethyl-1,3,2-dioxaborolan-2-yl)benzylidene)hydrazinyl)-*1H*-benzo[*de*]isoquinoline-1,3(*2H*)-dione

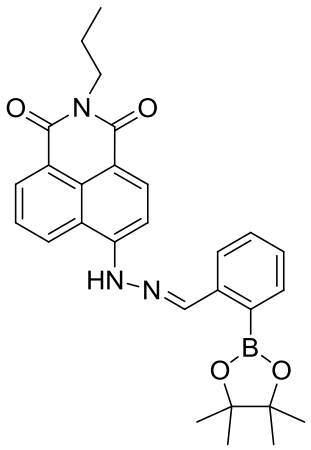

33

0.287g (1.06 mmol) compound **32** dissolved in MeOH / DMF and 0.252g (1.08 mmol) 2-aldehyde-pinacol-boronate ester was added, stirring at room temperature for 12 hours. Solid was precipitated out after pouring mixture into ice-water. The crude product were first to purify by recrystallisation then with flash column chromatography to afford compound **33** (0.04g) with a yield of 8%.

^{1}H NMR (300 MHz, $(CD_3)_2SO$) 11.67 (s, NH, 1H), 8.98 (s, 1H), 8.49 (d, *J* = 7.2 Hz, 1H), 8.37 (d, *J* = 8.5 Hz, 1H), 8.15 (d, *J* = 7.8 Hz, 1H), 7.78 (m, 3H), 7.57 (t, *J* = 7.4 Hz, 1H), 7.41 (t, *J* = 7.3 Hz, 1H), 3.98 (d, *J* = 7.3 Hz, 2H), 1.63 (m, 2H), 1.36 (s, 12H), 0.93 (t, *J* = 7.4 Hz, 3H)

^{13}C NMR (75.5 MHz, $(CD_3)_2SO$) 164.0, 163.4, 147.0, 144.9, 140.3, 136.0, 133.8, 131.5, 131.3, 129.5, 129.2, 128.8, 125.6, 125.3, 122.3, 119.1, 111.5, 107.7, 84.3, 25.0, 21.3, 11.8

ESI Mass [M + H^+] $C_{28}H_{30}B_1N_3O_4$ Calculated 484.2363, found 484.2343;

Melting point: 240 °C

6-(2-(2-hydroxybenzylidene)hydrazinyl)-2-propyl-*1H*-benzo[*de*]isoquinoline-1,3(*2H*)-dione

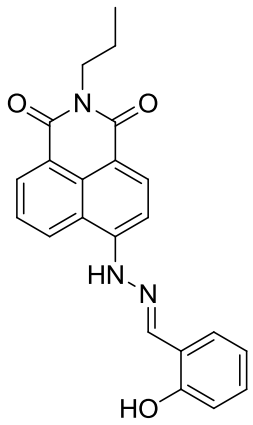

34

0.135 g (0.50 mmol) compound **32** and salicylaldehyde (0.073g, 0.6 mmol) were refluxed in ethanol (30 ml) for 5 h. Then the mixture was cooled and recrystallised from ethanol in the yield of 75% (0.186 g).

^{1}H NMR(300 MHz, $(CD_3)_2SO$) 11.47 (s, 1H), 10.24 (s, 1H), 8.81 (ds, *J* = 8.6 Hz, 2H), 8.47 (d, *J* = 6.6 Hz, 1H), 8.37 (d, *J* = 8.5 Hz, 1H), 7.80 (m, 2H), 7.64 (d, *J* = 8.5 Hz, 1H), 7.25 (m, 1H), 6.91 (m, 2H), 3.98 (t, *J* = 7.4 Hz, 2H), 1.62 (m, 2H), 0.90 (t, *J* = 7.4 Hz, 3H)

^{13}C NMR (75.5 MHz, $(CD_3)_2SO$ 164.1, 163.3, 156.6, 146.7, 142.4, 134.0, 131.2, 129.5, 128.6, 126.8, 125.3, 122.3, 120.9, 119.9, 119.0, 116.5, 111.1, 106.8, 41.2, 21.3, 11.8

ESI-Mass [M + H^+] $C_{22}H_{20}N_3O_3^+$ found 374.1518; [M - H] $C_{22}H_{18}N_3O_3^-$ found 372.1412,

Melting point: 254 °C

Elemental Analysis, theory C:70.7, H: 5.13, N: 11.2; found C: 70.1. H: 5.15, N:11.1;

6-(2-(4-methoxybenzylidene)hydrazinyl)-2-propyl-*1H* benzo[*de*]isoquinoline-1,3(*2H*)-dione

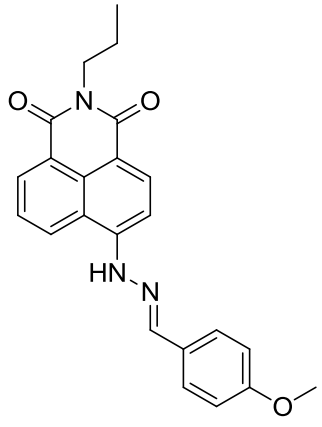

35

0.11 g (0.37 mmol) compound **32** and 0.055g (0.40 mmol) *p*-methoxybenzaldehyde were stirred in 30 ml ethanol for 6 hours. After cooling down the mixture to room temperature, precipitation came out which was filtered through to afford wine red solid with a yield of 80%. One point needs to mention that the solid has two different morphologies. One is cotton like and the other is powder like. Both were confirmed to be compound **35**.

^{1}H (300 MHz, $(CD_3)_2SO$) 11.32 (1H, s, NH), 8.73 (1H, d, *J* = 7.8 Hz), 8.43 (1H, d, *J* = 7.2 Hz), 8.37 (1H, s), 8.3 (1H, d, *J* = 8.5 Hz), 7.73 (3H, m), 7.65 (1H, d, *J* = 8.5 Hz), 7.01 (2H, d, *J* = 8.8 Hz), 3.95 (2H, t, *J* = 7.4 Hz), 3.80 (3H, s), 1.61 (2H, m), 0.89 (3H, t, *J* = 7.4 Hz)

^{13}C (75.5 MHz, $(CD_3)_2SO$): 164.0, 163.3, 160.9, 147.0, 144.4, 133.9, 131.1, 129.5, 128.7, 128.6, 127.6, 125.1, 122.3, 118.9, 114.7, 110.8, 106.9, 55.7, 55.3, 21.3, 11.8,

ESI-Mass positive $C_{23}H_{22}N_3O_3^+$ calculated: 388.1661, found: 388.1660

Melting point: 246 °C

6.3.3 Substrates for the Tsuji-Trost reaction

prop-2-yn-1-yl-2-(3-oxo-6-(prop-2-yn-1-yloxy)-*3H*-xanthen-9-yl)benzoate

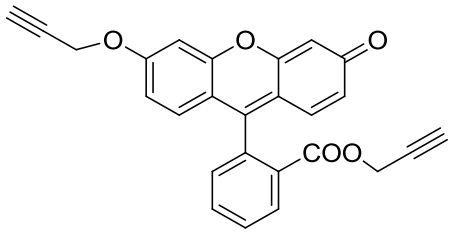

42

0.5 g (1.5 mmol) fluorescein and 0.62 g (4.4 mmol) K_2CO_3 was dissolved in 6 mL DMF. 0.35 mL (3.9 mmol, 2.6 eq.) propargyl bromide was added dropwise over 10 minutes. The reaction mixture was heated to 60 °C for 6 hours, followed by cooling down to room temperature and poured into ice-water. The reaction was monitored by TLC until all the fluorescein was converted. The formed precipitation was filtered and washed with water then hexane. The material obtained was by column using a gradient of 1-5% MeOH in DCM. 0.61 g compound **42** was obtained in 99% yield.

^{1}H NMR (300 MHz, $(CD_3)_2SO$): 8.22 (d, *J* = 9 Hz, 1H), 7.73-7.61 (m, 2H), 7.28 (d, *J* = 1.2 Hz, 1H), 7.03 (s, 1H), 6.89-6.74 (m, 3H), 6.51 (d, J = 12 Hz, 1H), 6.46 (s, 1H), 4.74 (d, J = 2.4 Hz, 2H), 4.53 (m, 2H), 2.56 (s, 1H,), 2.27 (s, 2H).

^{13}C NMR (300 MHz, $(CD_3)_2SO$): 184.3, 164.4, 161.9, 158.7, 153.7, 149.9, 134.2, 133.9, 131.2, 131.1, 130.8, 130.5, 129.9, 129.3 (2C), 117.5, 115.2, 114.3, 105.0, 101.9, 79.6, 78.7, 78.3, 77.7, 56.7, 53.1.

MS (ESI): *m*/*z* calculated for $C_{26}H_{17}O_5^+$: 409.1076; found: 409.1107, calculated for $C_{26}H_{17}O_5Na^+$: 431.0895 [$M + Na^+$]; found: 431.0901

9-(2-(hydroxymethyl)phenyl)-6-(prop-2-yn-1-yloxy)-*3H*-xanthen-3-one

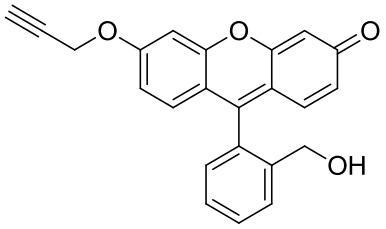

43

A solution of DIBALH (1.7 ml, 20% *wt* in toluene) was added dropwise to a solution of compound **42** (0.204 g in 10 ml DCM) at -78 °C under N_2 atmosphere and allowed to stir at the same temperature for 15 minutes before leaving it to stir for another 2 hours at room temperature (25 °C). At this point, the colour of the solution was bright red. Then the resulting mixture was diluted with Et_2O (7ml) after cooling to 0 °C, followed by addition of saturated aqueous NH_4Cl (2 ml). The solution colour changed from red to yellow, along with formation of precipitate. The suspension was stired for a further hour after removing ice-bath. Another 20 ml Et_2O was added in order to dissolve the formed solid before treatment with DDQ (114 mg, 0.5 mmol). The addition of DDQ turned the colour of the solution to dark green. After 2 hours stirring, the resulting solution was filtered through a pad of Celite. EtOAc (30 ml) was used to wash the pad and the filtrate was dried over Na_2SO_4. The solvent was removed under vacuum and product was purified by silica gel chromatography (25 % EtOAc in hexane) to provide compound **43** in 23 % yield.

^{1}H NMR (300 MHz, $(CD_3)_2SO$) 9.85 (s, 1H), 7.43 (d, *J* = 6Hz, 1H), 7.33 (t, *J* = 6Hz, 1H), 7.22 (t, *J* = 6Hz, 1H), 6.80-6.84 (m, 2H), 6.71-6.76 (m, 2H), 6.65-6.69 (dd, *J* = 3 Hz, 1H), 6.58 (d, *J* = 3 Hz, 1H), 6.48-6.52 (dd, *J* = 3 Hz, 1H), 5.22 (s, 2H), 4.82 (s, 2H), 3.59 (t, *J* = 3 Hz, 1H).

^{13}C NMR (300 MHz, $(CD_3)_2SO$) 158.5,158.0, 150.8, 150.7, 145.6, 138.8, 130.2, 130.1, 128.6, 128.3, 123.5, 121.5, 118.4, 116.1, 112.4, 112.0, 101.9, 101.5, 82.8, 79.4, 78.9, 72.0, 56.0.

ESI-MS: *m/z* calculated for $C_{23}H_{17}O_4^+$: 357.1126 [$M + H^+$]; found: 357.1156, calculated for $C_{23}H_{16}O_4Na^+$: 379.0946 [$M + Na^+$]; found: 379.0948

CHAPTER SEVEN

Conclusion and Future work

7 Conclusion and future work

7.1 Conclusion

There are four projects included in this thesis, following the same concept of developing optical responsive systems for molecular recognition. Traditional molecular recognition strategy is based on the design of a molecule which can display responses in the presence of different concentrations of analyte. Usually, extensive organic synthesis is required to obtain the probe molecule. The design of the substrate structures as well as the choices of signalling reporters used are the crucial factors for achieving high selective and sensitive probes. Such strategy has seen enormous development especially with employment of fluorescence.

The supramolecular concept can be used to develop new sensing protocols such as the indicator-displacement-assay. The development of nanotechnology and bioscience has promoted the formation of smart materials for ultrasensitive detection of biological species. Some health-related molecular recognition can be achieved both *in vitro* and *in vivo*. One of the new sensing protocols is reaction-based probes, so called, chemodosimeters. Such probes rely on reaction specificity but can be designed to achieve high selectivity and sensitivity.

In the first chapter of this thesis, detail of molecular recognition in the area of optical sensing as well as the function and importance of target molecules were introduced. The mechanisms of fluorescence changes and common design strategies for chemosensor were also illustrated along with the introduction of Suzuki coupling reaction and Tsuji-Trost reaction. A summary of the recent developments in saccharide and fluoride were presented.

A brief summary of the work carried out by our group, was also listed, which focused on exploring boronic acid based saccharide and fluoride sensors. Recently, efforts were also spent on designing functionalised material for detection of protein glycation as well as saccharide separation. Based on these achievements, the first project was aimed

at designing boronic acid modified fluorescent hydrogels for saccharide sensing and also for separation of glycated proteins *via* electrophoresis, which was expected to be visualised under a UV lamp without using a staining process. Two boronic acid modified acrylamide monomers were synthesised, of which the responses to monosaccharides were investigated both in solution and in gel. However, due to poor solubility of these monomers, the project was put on hold.

In the third chapter, a series of naphthalimide derivatives were synthesised in order to achieve a fluoride sensor. As expected, all three compounds had responses to fluoride, with compounds **34** and **35** having similar degree of sensitivity towards fluoride, yet both higher than that of compound **33** did. One problem was that compound **34** had poor selectivity between fluoride and acetate, whereas compound **33** had a clear spectral difference between fluoride and acetate. Compound **33** scarified sensitivity towards fluoride in order to obtain a better selectivity between anions. The observed results were a consequence of the coordination with boron.

In the fourth chapter, compounds **38** and **39** were initially expected to use for interacting with boronic acid compounds in order to form a chiral selective assembly. It was found that they had strong interaction with chiral alcohols even without the boronic acid moiety. Based on this observations, an enantioselectivity platform towards secondary alcohols could be achieved by employing compounds **38** and **39**. Although D/L-tartaric acids induced more pronounced spectral changes, no enantioselectivity was observed. The hydrogen bond formed between **38**, **39** and chiral molecules were believed to be crucial in recognising the chiral diols. The enantioselectivity was controlled by steric demands within the formed hydrogen bonding complexes.

When designing saccharide sensors, the most common problems occurred are that the probe requires extensive synthetic efforts and has poor solubility. In the fifth chapter, saccharide recognition was achieved by employing simple boronic acids in Suzuki homo-coupling reactions, where no extensive synthetic efforts are required. Those, phenylboronic acid, naphthalene-1-boronic acid and 1,4- phenyldiboronic acid, were employed and each of them showed unique spectra responses toward saccharides. In order to understand the sensing mechanism, the Tsuji-Trost reaction was used to check if there was interaction between the catalyst [palladium] and the substrate under

identical experimental conditions. The results indicated that saccharides did affect the catalytic efficiency of palladium, however, only to a limited degree. It was assumed that both the interaction between boronic acid and diols and the coordination between palladium and diols contributed to the final effect of diols on the reaction rate.

The thesis is composed of four sub-projects, all of which focussed on the recognition of diols and/or fluoride. The hydrogel project was based on the conventional strategy, an attempt to extend the application field of the boronic acid moiety. The naphthalimide project focused on the impact of the coordination between boron and fluoride on the sensing of fluoride. The Suzuki homo-coupling project was aimed at exploring new strategy for saccharide sensing.

7.2 Future work

Though the research results presented in this thesis did answer some questions we have met, some other new questions arise from these results at the same time, which needs to be addressed in future.

In the boron containing hydrogel project, poor solubility is the big issue for extending the applications. Therefore, further optimisations by preparing water soluble fluorophores are required before using in electrophoresis experiments. Besides, the binding affinities between boronic acid and saccharides are also controlled by the diffusion process in hydrogel, which can be solved by reducing the gel size investigated.

Though the boron-modified naphthalimide probe had proved its potential ability for fluoride recognition, yet, such ability was greatly impaired in aqueous environment as the interaction between fluoride ion and the acceptor was dominated by weak interaction. An alternative strategy is employing siliphilic property of fluoride as well as the coordination ability to boron to design a suitable fluoride sensor.

The Suzuki coupling reaction based saccharide sensing strategy offers a quick and sensitive platform for constructing saccharide probes. 1,4-phenyldiboronic acid (**41**) showed its unique property for saccharide sensing, however, the experimental condition

needs to be further optimised, like employing co-solvent systems. Additionally, the catalyst could be replaced by other formats of palladium as well to investigate the ligand effect on the catalytic efficiency.

CHAPTER EIGHT

BIBLIOGRAPHY

8 BIBLIOGRAPHY

1. J. M. Berg, *Biochemistry, 5th edition*, W. H. Freeman and Co., New York 2001.
2. D. L. Nelson, *Principles of Biochemistry, Fourth Edition*, W. H. Freeman,, 2008.
3. W. G. Adams, K. A. Deaver, S. L. Cochi, B. D. Plikaytis, E. R. Zell, C. V. Broome, J. D. Wenger, D. S. Stephens, M. M. Farley and C. Harvey, *J. A. M. A.*, 1993, **269**, 221-226.
4. S. J. Angyal, in *Adv. Carbohydr. Chem. Biochem.*, ed. H. Derek, Academic Press, 1991, pp. 19-35.
5. N. S. Oliver, C. Toumazou, A. E. G. Cass and D. G. Johnston, *Diabetic Medicine*, 2009, **26**, 197-210.
6. V. R. Sørensen, E. R. Mathiesen, T. Watt, J. B. Bjorner, M. V. N. Andersen and B. Feldt-Rasmussen, *Diabetologia*, 2007, **50**, 2254-2262.
7. Z. Kejík, T. Bříza, J. Králová, P. Martásek and V. Král, *Anal. Bioanal. Chem.*, 2010, **398**, 1865-1870.
8. S. Shinkai, ed. S. Shinkai, Royal Society of Chemistry,, 2005, pp. i-174.
9. J. P. Lorand and J. O. Edwards, *J. Org. Chem.*, 1959, **24**, 769-774.
10. R. R. S. P. C. Burns, *Acta. Cryst. Section C*, 2003, **C59**.
11. S. P. Draffin, P. J. Duggan and G. D. Fallon, *Acta Crystallogr., Sect. E: Struct. Rep. Online*, 2004, **60**, O1520-O1522.
12. J. H. Hartley, M. D. Phillips and T. D. James, *New J. Chem.*, 2002, **26**, 1228-1237.
13. P. D. Beer and P. A. Gale, *Angew. Chem. Int. Ed.*, 2001, **40**, 486-516.
14. T. Gunnlaugsson, M. Glynn, G. M. Tocci, P. E. Kruger and F. M. Pfeffer, *Coord. Chem. Rev.*, 2006, **250**, 3094-3117.
15. C. Suksai and T. Tuntulani, *Chem. Soc. Rev.*, 2003, **32**, 192-202.
16. R. M. Duke, E. B. Veale, F. M. Pfeffer, P. E. Kruger and T. Gunnlaugsson, *Chem. Soc. Rev.*, 2010, **39**, 3936-3953.
17. M. Cametti and K. Rissanen, *Chem. Commun.*, 2009, 2809-2829.
18. T. Gunnlaugsson, H. D. P. Ali, M. Glynn, P. E. Kruger, G. M. Hussey, F. M. Pfeffer, C. M. G. dos Santos and J. Tierney, *J. Fluoresc.*, 2005, **15**, 287-299.
19. E. Kissa, *Clinical Chemistry 1987; v., p*, 1987, **33**, 253-255.
20. M. S. Frant and J. W. R. Jr, *Science (Washington, DC, U. S.)*, 1966, **154**, 1553.
21. J. R. Lakowicz, *Principles of Fluorescence Spectroscopy*, 2006.
22. S. A. Hilderbrand and R. Weissleder, *Curr. Opin. Chem. Biol.*, 2010, **14**, 71-79.
23. T. Heyduk, Y. Ma, H. Tang and R. H. Ebright, *Methods Enzymol.*, 1996, **274**, 492-503.
24. W. R. a. R. Lapouyade, *Topics in Fluorescence Spectroscopy*, 2002, **4**, 109-149.
25. A. Czarnik, *Topics in Fluorescence Spectroscopy*, 2002, **4**.
26. T. D. James, *Top Curr Chem*, 2007, 107.
27. N. DiCesare and J. R. Lakowicz, *Journal of Biomedical Optics*, 2002, **7**, 538.
28. K. R. A. S. Sandanayake and S. Shinkai, *J. Chem. Soc., Chem. Commun.*, 1994, 1083.
29. K. R. A. S. Sandanayake, S. Imazu, T. D. James, M. Mikami and S. Shinkai, *Chem. Lett.*, 1995, **24**, 139-140.

30. S. Arimori, L. I. Bosch, C. J. Ward and T. D. James, *Tetrahedron Lett.*, 2002, **43**, 911-913.
31. N. DiCesare and J. R. Lakowicz, *Chem. Commun.*, 2001, 2022-2023.
32. T. D. James, K. R. A. S. Sandanayake and S. Shinkai, *J. Chem. Soc., Chem. Commun.*, 1994, 477.
33. T. D. James, K. R. A. S. Sandanayake, R. Iguchi and S. Shinkai, *J. Am. Chem. Soc.*, 1995, **117**, 8982-8987.
34. T. Füster, *Ann. Phys.(Leipzig)*, 1948, **2**, 55-75.
35. R. Freeman, L. Bahshi, T. Finder, R. Gill and I. Willner, *Chem. Commun.*, 2009, 764.
36. J. Wu, W. Liu, J. Ge, H. Zhang and P. Wang, *Chem. Soc. Rev.*, 2011, **40**, 3483-3495.
37. B. Liu and B. Z. Tang, *Macromol. Rapid Commun.*, 2013, **34**, 704.
38. Y. Liu, C. M. Deng, L. Tang, A. J. Qin, R. R. Hu, J. Z. Sun and B. Z. Tang, *J. Am. Chem. Soc.*, 2011, **133**, 660-663.
39. Z. Guo, I. Shin and J. Yoon, *Chem. Commun.*, 2012, **48**, 5956-5967.
40. M. D. P. Tony D James, Seiji Shinkai *Boronic Acids in Saccharide Recognition*, Royal Society of Chemistry, 2006.
41. R. Nishiyabu, Y. Kubo, T. D. James and J. S. Fossey, *Chem. Commun.*, 2011, **47**, 1106-1123.
42. J. S. Fossey, F. D'Hooge, J. M. H. van den Elsen, M. P. P. Morais, S. I. Pascu, S. D. Bull, F. Marken, A. T. A. Jenkins, Y.-B. Jiang and T. D. James, *Chem. Rec.*, 2012, **12**, 464-478.
43. E. Galbraith and T. D. James, *Chem. Soc. Rev.*, 2010, **39**, 3831-3842.
44. R. Nishiyabu, Y. Kubo, T. D. James and J. S. Fossey, *Chem. Commun.*, 2011, **47**, 1124-1150.
45. A. M. Kelly, Y. Perez-Fuertes, J. S. Fossey, S. L. Yeste, S. D. Bull and T. D. James, *Nature Protocols*, 2008, **3**, 215-219.
46. Y. Egawa, T. Seki, S. Takahashi and J.-i. Anzai, *Materials Science and Engineering: C*, 2011, **31**, 1257-1264.
47. T. R. Jackson, J. S. Springall, D. Rogalle, N. Masurnoto, H. C. Li, F. D'Hooge, S. P. Perera, A. T. A. Jenkins, T. D. James, J. S. Fossey and J. M. H. van den Elsen, *Electrophoresis*, 2008, **29**, 4185-4191.
48. B. Appleton and T. D. Gibson, *Sens. Actuators, B*, 2000, **65**, 302-304.
49. M. D. Phillips and T. D. James, *J. Fluoresc.*, 2004, **14**, 549-559.
50. S. Arimori, G. A. Consiglio, M. D. Phillips and T. D. James, *Tetrahedron Lett.*, 2003, **44**, 4789-4792.
51. S. Arimori, M. L. Bell, C. S. Oh and T. D. James, *Org. Lett.*, 2002, **4**, 4249-4251.
52. K. R. A. S. Sandanayake and S. Shinkai, *J. Chem. Soc., Chem. Commun.*, 1994, **0**, 1083-1084.
53. C. J. Ward, P. Patel and T. D. James, *J. Chem. Soc., Perkin Trans. 1*, 2002, **0**, 462-470.
54. J. Z. Zhao, M. G. Davidson, M. F. Mahon, G. Kociok-Kohn and T. D. James, *J. Am. Chem. Soc.*, 2004, **126**, 16179-16186.
55. J. Z. Zhao and T. D. James, *J. Mater. Chem.*, 2005, **15**, 2896-2901.
56. M. D. Phillips, T. M. Fyles, N. P. Barwell and T. D. James, *Chem. Commun.*, 2009, **0**, 6557-6559.

57. F. D'Hooge, S. A. Elfeky, S. E. Flower, S. I. Pascu, A. T. A. Jenkins, J. M. H. v. d. Elsen, T. D. James and J. S. Fossey, *RSC Adv.*, 2012, **2**, 3274-3280.
58. S. A. Elfeky, S. E. Flower, N. Masumoto, F. D'Hooge, L. Labarthe, W. Chen, C. Len, T. D. James and J. S. Fossey, *Chem. Asia. J.*, 2010, **5**, 581-588.
59. S. A. Elfeky, F. D'Hooge, L. Poncel, W. Chen, S. P. Perera, J. M. H. van den Elsen, T. D. James, A. T. A. Jenkins, P. J. Cameron and J. S. Fossey, *New J. Chem.*, 2009, **33**, 1466-1469.
60. A. Schiller, R. A. Wessling and B. Singaram, *Angew. Chem. Int. Ed.*, 2007, **46**, 6457-6459.
61. Y. Kanekiyo and H. Tao, *Chem. Lett.*, 2005, **34**, 196-197.
62. C. Yu and V. W. W. Yam, *Chem. Commun.*, 2009, **yan**, 1347-1349.
63. C. Y. S. Chung, K. H. Y. Chan and V. W. W. Yam, *Chem. Commun.*, 2011, **47**, 2000-2002.
64. C. Shimpuku, R. Ozawa, A. Sasaki, F. Sato, T. Hashimoto, A. Yamauchi, I. Suzuki and T. Hayashita, *Chem. Commun.*, 2009, 1709.
65. M. S. Steiner, A. Duerkop and O. S. Wolfbeis, *Chem. Soc. Rev.*, 2011, **40**, 4805-4839.
66. C. Nakai and J. A. Thomas, *J. Biol. Chem.*, 1974, **249**, 6459-6467.
67. L. S. Kaminsky, M. C. Mahoney, J. Leach, J. Melius and M. J. Miller, *Critical Reviews in Oral Biology and Medicine*, 1990, **1**, 261-282.
68. J. D. B. Featherstone, *Community Dentistry and Oral Epidemiology*, 1999, **27**, 31-40.
69. T. W. Hudnall, C.-W. Chiu and F. P. Gabbai, *Acc. Chem. Res.*, 2009, **42**, 388-397.
70. M. E. Jun, B. Roy and K. H. Ahn, *Chem. Commun.*, 2011, **47**, 7583-7601.
71. J. Du, M. Hu, J. Fan and X. Peng, *Chem. Soc. Rev.*, 2012, **41**.
72. A.-F. Li, J.-H. Wang, F. Wang and Y.-B. Jiang, *Chem. Soc. Rev.*, 2010, **39**, 3729-3745.
73. S. K. Kim and J. Yoon, *Chem. Commun.*, 2002, 770-771.
74. T. D. Thangadurai, C. J. Lee, S. H. Jeong, S. Yoon, Y. G. Seo and Y. I. Lee, *Microchem. J.*, 2013, **106**, 27-33.
75. B. Liu and H. Tian, *Chem. Lett.*, 2005, **34**, 686-687.
76. W. W. Huang, Z. Y. Yang, H. Lin and H. K. Lin, *J. Fluoresc.*, 2013, **23**, 21-29.
77. E. J. Cho, B. J. Ryu, Y. J. Lee and K. C. Nam, *Org. Lett.*, 2005, **7**, 2607-2609.
78. S. O. Kang, J. M. Llinares, D. Powell, D. VanderVelde and K. Bowman-James, *J. Am. Chem. Soc.*, 2003, **125**, 10152-10153.
79. P. Piatek and J. Jurczak, *Chem. Commun.*, 2002, **0**, 2450-2451.
80. A. F. D. de Namor, M. Shehab, R. Khalife and I. Abbas, *J. Phys. Chem. B*, 2007, **111**, 12177-12184.
81. A. Aydogan, D. J. Coady, V. M. Lynch, A. Akar, M. Marquez, C. W. Bielawski and J. L. Sessler, *Chem. Commun.*, 2008, 1455-1457.
82. X. H. Cheng, S. Li, G. H. Xu, C. G. Li, J. G. Qin and Z. Li, *ChemPlusChem*, 2012, **77**, 908-913.
83. J. Ren, Z. Wu, Y. Zhou, Y. Li and Z. X. Xu, *Dyes Pigm.*, 2011, **91**, 442-445.
84. T. H. Kim and T. M. Swager, *Angew. Chem. Int. Ed.*, 2003, **42**, 4803-4806.
85. M. Xue, X. Wang, H. Wang, D. Chen and B. Tang, *Chem. Commun.*, 2011, **47**, 4986-4988.
86. J. F. Zhang, C. S. Lim, S. Bhuniya, B. R. Cho and J. S. Kim, *Org. Lett.*, 2011, **13**, 1190-1193.

87. B. Zhu, F. Yuan, R. Li, Y. Li, Q. Wei, Z. Ma, B. Du and X. Zhang, *Chem. Commun.*, 2011, **47**, 7098-7100.
88. Y. Bao, B. Liu, H. Wang, J. Tian and R. Bai, *Chem. Commun.*, 2011, **47**, 3957-3959.
89. J. Cao, C. Zhao, P. Feng, Y. Zhang and W. Zhu, *RSC Adv.*, 2012, **2**, 418-420.
90. X. Cao, W. Lin, Q. Yu and J. Wang, *Org. Lett.*, 2011, **13**, 6098-6101.
91. O. A. Bozdemir, F. Sozmen, O. Buyukcakir, R. Guliyev, Y. Cakmak and E. U. Akkaya, *Org. Lett.*, 2010, **12**, 1400-1403.
92. V. Bhalla, H. Singh and M. Kumar, *Org. Lett.*, 2010, **12**, 628-631.
93. H. E. Katz, *J. Org. Chem.*, 1985, **50**, 5027-5032.
94. S. Jacobson and R. Pizer, *J. Am. Chem. Soc.*, 1993, **115**, 11216-11221.
95. C. Dusemund, K. Sandanayake and S. Shinkai, *Journal of the Chemical Society-Chemical Communications*, 1995, 333-334.
96. S. Yamaguchi, S. Akiyama and K. Tamao, *J. Am. Chem. Soc.*, 2001, **123**, 11372-11375.
97. C. R. Cooper, N. Spencer and T. D. James, *Chem. Commun.*, 1998, 1365-1366.
98. K. M. K. Swamy, Y. J. Lee, H. N. Lee, J. Chun, Y. Kim, S.-J. Kim and J. Yoon, *J. Org. Chem.*, 2006, **71**, 8626-8628.
99. T. Nishimura, S. Y. Xu, Y. B. Jiang, J. S. Fossey, K. Sakurai, S. D. Bull and T. D. James, *Chem. Commun.*, 2013, **49**, 478-480.
100. M. Melaimi and F. P. Gabbaï, *J. Am. Chem. Soc.*, 2005, **127**, 9680-9681.
101. E. V. Anslyn, *Agnew. Chem. Int. Ed.*, 2006, **45**, 1190-1196.
102. P. Scrimin and L. J. Prins, *Chemical Society Reviews*, 2011, **40**, 4488.
103. S. T. Phillips, *Journal of the American Chemical Society*, 2011, **133**, 5170-5173.
104. N. Miyaura and A. Suzuki, *J. Chem. Soc., Chem. Commun.*, 1979, 866.
105. A. M. Suzuki, Norio, *Chem. Rev.*, 1995, **95**, 2457-2483.
106. A. Suzuki, *Chem. Commun.*, 2005, 4759.
107. A. Suzuki, *J. Organomet. Chem.*, 1999.
108. R. Rossi, F. Bellina and A. Carpita, *Synthesis*, 2004, **2004**, 2419-2440.
109. G. P. McGlacken and L. M. Bateman, *Chem. Soc. Rev.*, 2009, **38**, 2447.
110. Z. Z. Song and H. N. C. Wong, *J. Org. Chem.*, 1994, **59**, 33-41.
111. A. O. Aliprantis and J. W. Canary, *J. Am. Chem. Soc.*, 1994, **116**, 6985-6986.
112. A. S. Batsanov, J. C. Collings, I. J. S. Fairlamb, J. P. Holland, J. A. K. Howard, Z. Y. Lin, T. B. Marder, A. C. Parsons, R. M. Ward and J. Zhu, *J. Org. Chem.*, 2005, **70**, 703-706.
113. S. Kotha, K. Lahiri and D. Kashinath, *Tetrahedron*, 2002, **58**, 9633-9695.
114. J. P. Parrish, Y. C. Jung, R. J. Floyd and K. W. Jung, *Tetrahedron Lett.*, 2002, **43**, 7899-7902.
115. N. Wu and X. Chen, *Lett. Org. Chem.*, 2010, **7**, 11-14.
116. M. S. Wong and X. L. Zhang, *Tetrahedron Lett.*, 2001, **42**, 4087-4089.
117. M. MorenoManas, M. Perez and R. Pleixats, *J. Org. Chem.*, 1996, **61**, 2346-2351.
118. H. Yoshida, Y. Yamaryo, J. Ohshita and A. Kunai, *Tetrahedron Lett.*, 2003, **44**, 1541-1544.
119. C. Adamo, C. Amatore, I. Ciofini, A. Jutand and H. Lakmini, *Journal of the American Chemical Society*, 2006, **128**, 6829-6836.
120. C. Adamo, C. Amatore, I. Ciofini, A. Jutand and H. Lakmini, *J. Am. Chem. Soc.*, 2006, **128**, 6829-6836.
121. G. C. Fu, *Acc. Chem. Res.*, 2008, **41**, 1555-1564.

122. T. E. Barder, S. D. Walker, J. R. Martinelli and S. L. Buchwald, *J. Am. Chem. Soc.*, 2005, **127**, 4685-4696.
123. S. Carrettin, J. Guzman and A. Corma, *Agnew. Chem. Int. Ed.*, 2005, **44**, 2242-2245.
124. G. J. Cheng and M. M. Luo, *Eur. J. Org. Chem.*, 2011, 2519-2523.
125. J. Tsuji, Takahash.H and M. Morikawa, *Tetrahedron Lett.*, 1965, 4387-&.
126. B. M. Trost and T. J. Fullerton, *J. Am. Chem. Soc.*, 1973, **95**, 292-294.
127. B. M. Trost and D. L. Van Vranken, *Chem. Rev.*, 1996, **96**, 395-422.
128. F. L. Song, A. L. Garner and K. Koide, *J. Am. Chem. Soc.*, 2007, **129**, 12354-+.
129. K. Hirose, *J. Inclusion Phenom. Macrocyclic Chem.*, 2001, **39**, 193-209.
130. I. T. Ho, K. C. Haung and W. S. Chung, *Chem. Asia. J.*, 2011, **6**, 2738.
131. b. wang, *Tetrahedron*, 2002.
132. N. Y. Edwards, T. W. Sager, J. T. McDevitt and E. V. Anslyn, *J. Am. Chem. Soc.*, 2007, **129**, 13575-13583.
133. S. Gamsey, A. Miller, M. M. Olmstead, C. M. Beavers, L. C. Hirayama, S. Pradhan, R. A. Wessling and B. Singaram, *J. Am. Chem. Soc.*, 2007, **129**, 1278-1286.
134. K. F. Arndt, *Hydrogel senor and acutor*, 2009.
135. T. Miyata, T. Uragami and K. Nakamae, *Adv. Drug Delivery Rev.*, 2002, **54**, 79-98.
136. C. P. McCoy, F. Stomeo, S. E. Plush and T. Gunnlaugsson, *Chem. Mater.*, 2006, **18**, 4336-4343.
137. Y. J. Lee and P. V. Braun, *Advanced Materials*, 2003, **15**, 563-566.
138. K. Lee and S. A. Asher, *J. Am. Chem. Soc.*, 2000, **122**, 9534-9537.
139. C. Alvarez-Lorenzo and A. Concheiro, *J. Controlled Release*, 2002, **80**, 247-257.
140. J. D. Debord and L. A. Lyon, *J. Phys. Chem. B*, 2000, **104**, 6327-6331.
141. J. H. Kim and T. R. Lee, *Chem. Mater.*, 2004, **16**, 3647-3651.
142. K. Deligkaris, T. S. Tadele, W. Olthuis and A. van den Berg, *Sens. Actuators, B*, 2010, **147**, 765-774.
143. R. A. Siegel, Y. D. Gu, M. Lei, A. Baldi, E. E. Nuxoll and B. Ziaie, *J. Controlled Release*, 2010, **141**, 303-313.
144. L.-Y. Chu, Y. Li, J.-H. Zhu, H.-D. Wang and Y.-J. Liang, *J. Controlled Release*, 2004, **97**, 43-53.
145. A. J. T. Miyata, K. Nakamae, A.S. Hoffman, *Macromol. Chem. Phys.*, 1996.
146. K. Kataoka, H. Miyazaki, M. Bunya, T. Okano and Y. Sakurai, *J. Am. Chem. Soc.*, 1998, **120**, 12694-12695.
147. A. Doring, W. Birnbaum and D. Kuckling, *Chem. Soc. Rev.*, 2013.
148. V. L. Alexeev, A. C. Sharma, A. V. Goponenko, S. Das, I. K. Lednev, C. S. Wilcox, D. N. Finegold and S. A. Asher, *Anal. Chem.*, 2003, **75**, 2316-2323.
149. S. A. Asher, V. L. Alexeev, A. V. Goponenko, A. C. Sharma, I. K. Lednev, C. S. Wilcox and D. N. Finegold, *Journal of the American Chemical Society*, 2003, **125**, 3322-3329.
150. S. A. A. Asher, V. L., S. Das and D. N. Finegold, *Clinical Chemistry*, 2004, **50**, 2353-2360.
151. X. Zhang, Y. Guan and Y. Zhang, *Biomacromolecules*, 2011, **13**, 92-97.
152. W. Wu, N. Mitra, E. C. Y. Yan and S. Zhou, *ACS Nano*, 2010, **4**, 4831-4839.
153. H. Vlassara, *Ann. N. Y. Acad. Sci.*, 2005, **1043**, 452-460.
154. G. F. Hu, *J. Chromatogr. A*, 1995, **705**, 89-103.

155. P. Jackson, *Mol. Biotechnol.*, 1996, **5**, 101-123.
156. M. P. P. Morais, J. D. Mackay, S. K. Bhamra, J. G. Buchanan, T. D. James, J. S. Fossey and J. M. H. van den Elsen, *Proteomics*, 2010, **10**, 48-58.
157. W. M. J. Ma, M. P. Pereira Morais, F. D'Hooge, J. M. H. van den Elsen, J. P. L. Cox, T. D. James and J. S. Fossey, *Chem. Commun.*, 2009, 532.
158. C. Dardonville, C. Fernandez-Fernandez, S.-L. Gibbons, G. J. Ryan, N. Jagerovic, A. M. Gabilondo, J. J. Meana and L. F. Callado, *Bioorg. Med. Chem.*, 2006, **14**, 6570-6580.
159. y = (1+ P1* P2 * x)/ (1+ P1 * x), of which P1 is binding stability constant and P2 is the values of F/F0
160. J. Yan, G. Springsteen, S. Deeter and B. Wang, *Tetrahedron*, 2004, **60**, 11205-11209.
161. X. Qian, Y. Xiao, Y. Xu, X. Guo, J. Qian and W. Zhu, *Chem. Commun.*, 2010, **46**, 6418-6436.
162. T. Gunnlaugsson, P. E. Kruger, T. C. Lee, R. Parkesh, F. M. Pfeffer and G. M. Hussey, *Tetrahedron Lett.*, 2003, **44**, 6575-6578.
163. E. B. Veale and T. Gunnlaugsson, *J. Org. Chem.*, 2008, **73**, 8073-8076.
164. R. Ferreira, P. Remón and U. Pischel, *J. Phys. Chem. C*, 2009, **113**, 5805-5811.
165. H. Cao, D. I. Diaz, N. DiCesare, J. R. Lakowicz and M. D. Heagy, *Org. Lett.*, 2002, **4**, 1503-1505.
166. H. Cao, T. McGill and M. D. Heagy, *J. Org. Chem.*, 2004, **69**, 2959-2966.
167. N. DiCesare, D. P. Adhikari, J. J. Heynekamp, M. D. Heagy and J. R. Lakowicz, *J. Fluoresc.*, 2002, **12**, 147-154.
168. S. Trupp, A. Schweitzer and G. J. Mohr, *Org. Biomol. Chem.*, 2006, **4**, 2965-2968.
169. S. Jin, J. Wang, M. Li and B. Wang, *Chem. Euro. J.*, 2008, **14**, 2795-2804.
170. J. Wang, S. Jin, S. Akay and B. Wang, *Eur. J. Org. Chem.*, 2007, 2091-2099.
171. J.-A. Gan, Q. L. Song, X. Y. Hou, K. Chen and H. Tian, *J. Photochem. Photobiol. A*, 2004, **162**, 399-406.
172. Y. Zhou, H. Zhou, T. Ma, J. Zhang and J. Niu, *Spectrochim. Acta, Part. A*, 2012, **88**, 56-59.
173. D. Cheshmedzhieva, P. Ivanova, S. Stoyanov, D. Tasheva, M. Dimitrova, I. Ivanov and S. Ilieva, *Phys. Chem. Chem. Phys.*, 2011, **13**, 18530-18538.
174. E. M. Pérez, L. Sánchez, G. Fernández and N. Martín, *J. Am. Chem. Soc.*, 2006, **128**, 7172-7173.
175. S. C. Stinson, *Chem. Eng. News*, 2000, **78**, 55-78.
176. A. Thayer, *Chem. Eng. News*, 2005, **83**, 49-53.
177. J. Z. Zhao, T. M. Fyles and T. D. James, *Angew. Chem. Int. Ed.*, 2004, **43**, 3461-3464.
178. X. Zhang, L. N. Chi, S. M. Ji, Y. B. Wu, P. Song, K. L. Han, H. M. Guo, T. D. James and J. Z. Zhao, *J. Am. Chem. Soc.*, 2009, **131**, 17452-17463.
179. Y. B. Wu, H. M. Guo, T. D. James and J. Z. Zhao, *J. Org. Chem.*, 2011, **76**, 5685-5695.
180. F. Han, L. N. Chi, X. F. Liang, S. M. Ji, S. S. Liu, F. K. Zhou, Y. B. Wu, K. L. Han, J. Z. Zhao and T. D. James, *J. Org. Chem.*, 2009, **74**, 1333-1336.
181. T. D. James, K. R. A. S. Sandanayake and S. Shinkai, *Nature*, 1995, **374**, 345-347.
182. G. A. Hembury, V. V. Borovkov and Y. Inoue, *Chem. Rev.*, 2008, **108**, 1-73.
183. R. G. Desiraju, Oxford university Press, 1999.

184. M. C. Etter, *Acc. Chem. Res.*, 1990, **23**, 120-126.
185. T. Steiner, *Angew. Chem. Int. Ed.*, 2002, **41**, 48-76.
186. C. G. Claessens and J. F. Stoddart, *J. Phys. Org. Chem.*, 1997, **10**, 254-272.
187. G. R. Whittell, M. D. Hager, U. S. Schubert and I. Manners, *Nat. Mater.*, 2011, **10**, 176-188.
188. J. H. Jia, P. Hubberstey, N. R. Champness and M. Schroder, in *Molecular Networks*, ed. M. W. Hosseini, 2009, pp. 135-161.
189. B. Moulton and M. J. Zaworotko, *Chem. Rev.*, 2001, **101**, 1629-1658.
190. G. M. Whitesides and B. Grzybowski, *Science*, 2002, **295**, 2418-2421.
191. J. Seo, J. W. Chung, E. H. Jo and S. Y. Park, *Chem. Commun.*, 2008, 2794-2796.
192. M. D. Yilmaz and J. Huskens, *Soft Matter*, 2012, **8**, 11768-11780.
193. T. Ishi-i, M. Crego-Calama, P. Timmerman, D. N. Reinhoudt and S. Shinkai, *J. Am. Chem. Soc.*, 2002, **124**, 14631-14641.
194. R. Nandhakumar, J. Ryu, H. Park, L. Tang, S. Choi and K. M. Kim, *Tetrahedron*, 2008, **64**, 7704-7708.
195. H. Watarai, K. Mitani, N. Morooka and H. Takechi, *Analyst*, 2012, **137**, 3238-3241.
196. K. Ghosh, T. Sen and R. Frohlich, *Tetrahedron Lett.*, 2007, **48**, 2935-2938.
197. L. Pu, *Acc. Chem. Res.*, 2012, **45**, 150-163.
198. L. Cavallo, M. E. Cucciolito, A. De Martino, F. Giordano, I. Orabona and A. Vitagliano, *Chem. Euro. J.*, 2000, **6**, 1127-1139.
199. M. M. Wanderley, C. Wang, C.-D. Wu and W. Lin, *J. Am. Chem. Soc.*, 2012, **134**, 9050-9053.
200. Y. Liu, B. Li, T. Wada and Y. Inoue, *Tetrahedron*, 2001, **57**, 7153-7161.
201. H. Y. Cun, Y. L. Wang, B. Yang, L. Zhang, S. X. Du, Y. Wang, K. H. Ernst and H. J. Gao, *Langmuir*, 2010, **26**, 3402-3406.
202. A. Mravik, Z. Bocskei, K. Simon, F. Elekes and Z. Izsaki, *Chem. Euro. J.*, 1998, **4**, 1621-1627.
203. R. E. Hubbard and M. Kamran Haider, in *Encyclopedia of Life Sciences (ELS)*, John Wiley & Sons, Ltd, 2010.
204. E. Kolomiets, V. Berl and J. M. Lehn, *Chem. Euro. J.*, 2007, **13**, 5466-5479.
205. V. Berl, I. Huc, R. G. Khoury, M. J. Krische and J. M. Lehn, *Nature*, 2000, **407**, 720-723.
206. K. Ghosh and S. Adhikari, *Tetrahedron Lett.*, 2006, **47**, 3577-3581.
207. W. Lu, L.-H. Zhang, X.-S. Ye, J. Su and Z. Yu, *Tetrahedron*, 2006, **62**, 1806-1816.
208. J.-M. Fang, S. Selvi, J.-H. Liao, Z. Slanina, C.-T. Chen and P.-T. Chou, *J. Am. Chem. Soc.*, 2004, **126**, 3559-3566.
209. B. Hu, M. Meng, Z. Wang, W. T. Du, J. S. Fossey, X. Q. Hu and W. P. Deng, *J. Am. Chem. Soc.*, 2010, **132**, 17041-17044.
210. B. Hu, M. Meng, J. S. Fossey, W. Mo, X. Hu and W.-P. Deng, *Chem. Commun.*, 2011, **47**, 10632-10634.
211. V. B. Birman, E. W. Uffman, J. Hui, X. M. Li and C. J. Kilbane, *J. Am. Chem. Soc.*, 2004, **126**, 12226-12227.
212. M. Wang, Y.-H. Shi, J.-F. Luo, W. Du, X.-X. Shi, J. S. Fossey and W.-P. Deng, *Catalysis Science & Technology*, 2011, **1**, 100-103.
213. M. Wang, Z. Wang, Y.-H. Shi, X.-X. Shi, J. S. Fossey and W.-P. Deng, *Agnew. Chem. Int. Ed.*, 2011, **50**, 4897-4900.

214. K. N. Kim, K. C. Song, J. H. Noh and S.-K. Chang, *Bull. Korean Chem. Soc*, 2009, **30**, 197.
215. Calculated using advanced chemistry development (ACD/Labs) software V11.02 ACD/Labs, 1994-2013.
216. Y. Egawa, T. Seki, S. Takahashi and J.-i. Anzai, *Mater. Sci. Eng., C*, 2011, **31**, 1257-1264.
217. J. C. Pickup, F. Hussain, N. D. Evans, O. J. Rolinski and D. J. S. Birch, *Biosens. Bioelectron.*, 2005, **20**, 2555-2565.
218. H. S. Mader and O. S. Wolfbeis, *Microchim. Acta*, 2008, **162**, 1-34.
219. T. D. James, in *Creative Chemical Sensor Systems*, ed. T. Schrader, Springer-Verlag Berlin, Berlin, 2007, pp. 107-152.
220. S. Park, H. Boo and T. D. Chung, *Anal. Chim. Acta*, 2006, **556**, 46-57.
221. S.-Y. Xu, Y.-B. Ruan, X.-X. Luo, Y.-F. Gao, J.-S. Zhao, J.-S. Shen and Y.-B. Jiang, *Chem. Commun.*, 2010, **46**, 5864-5866.
222. L. Ismail and M. Abdel-Mottaleb, *International Journal of Photoenergy*, 2003, **5**, 249-254.
223. B. D. D. D. Perrin, *Champan & Hall*, 1974.
224. C. R. Cooper and T. D. James, *J. Chem. Soc., Perkin Trans. 1*, 2000, **0**, 963-969.

CHAPTER NINE

Appendix

9 Appendix

9.1 Non-linear curve fitting for anion titration

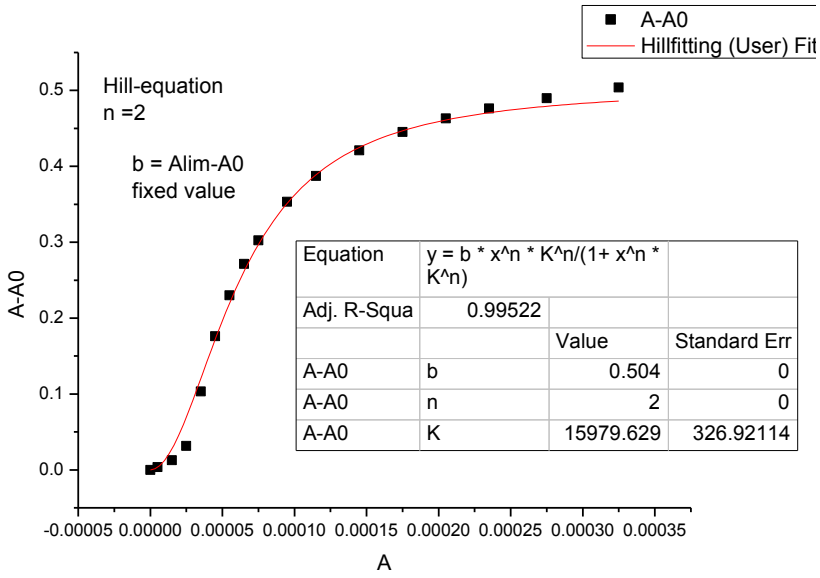

Equation	y = b * x^n * K^n/(1+ x^n * K^n)		
Adj. R-Squa	0.99522		
		Value	Standard Err
A-A0	b	0.504	0
A-A0	n	2	0
A-A0	K	15979.629	326.92114

Appendix Figure 1 Non-linear fitting curve of compound **33** with TBAF by Hill equation

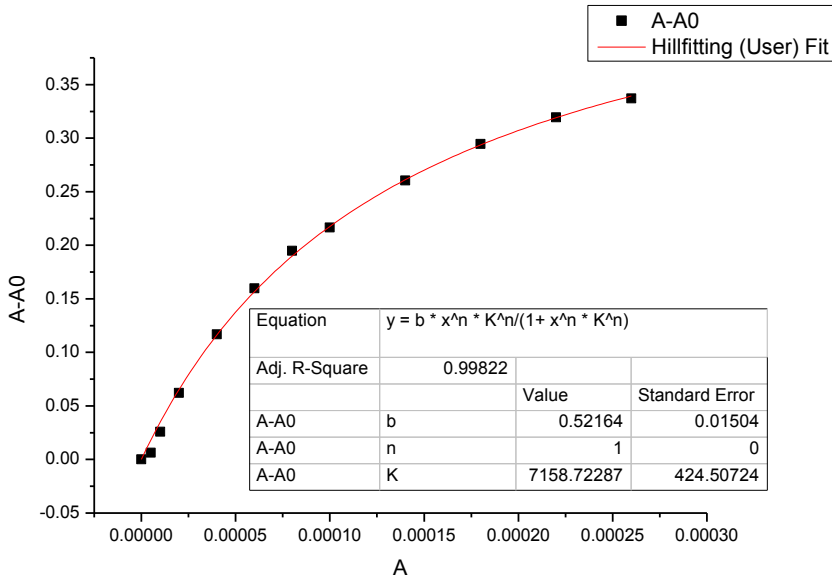

Appendix Figure 2 Non-linear fitting curve of compound **33** with TBA OAc by Hill equation

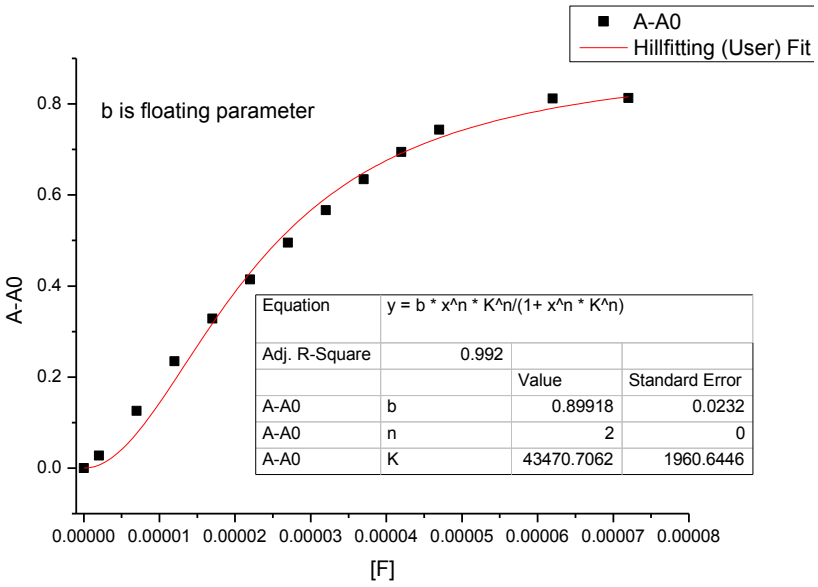

Appendix Figure 3 Non-linear fitting curve of compound **34** with TBAF by Hill equation

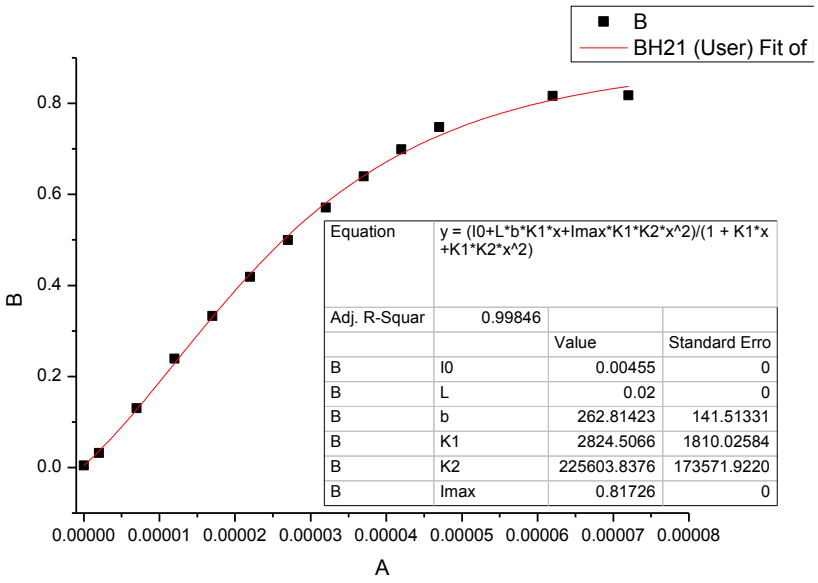

Appendix Figure 4 Non-linear least square fitting curve of compound **34** with TBAF

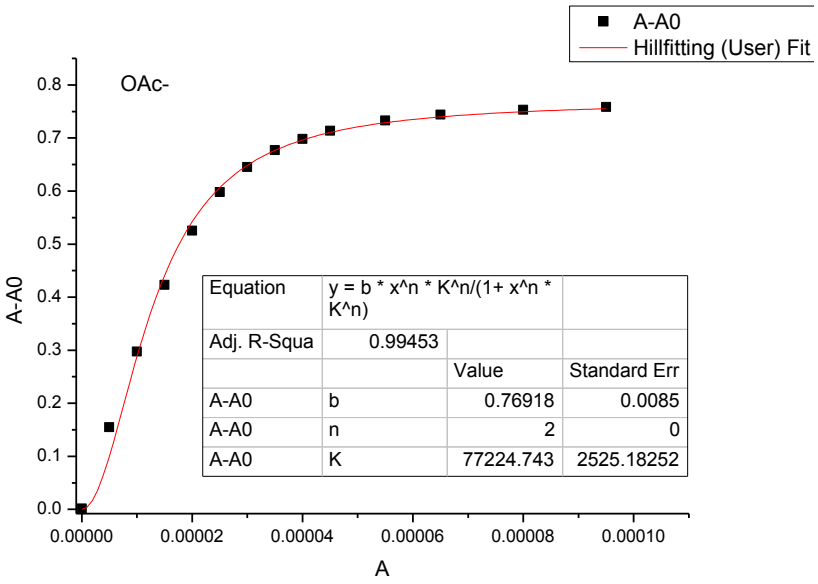

Appendix Figure 5 Non-linear fitting curve of compound **34** with TBA OAc by Hill equation

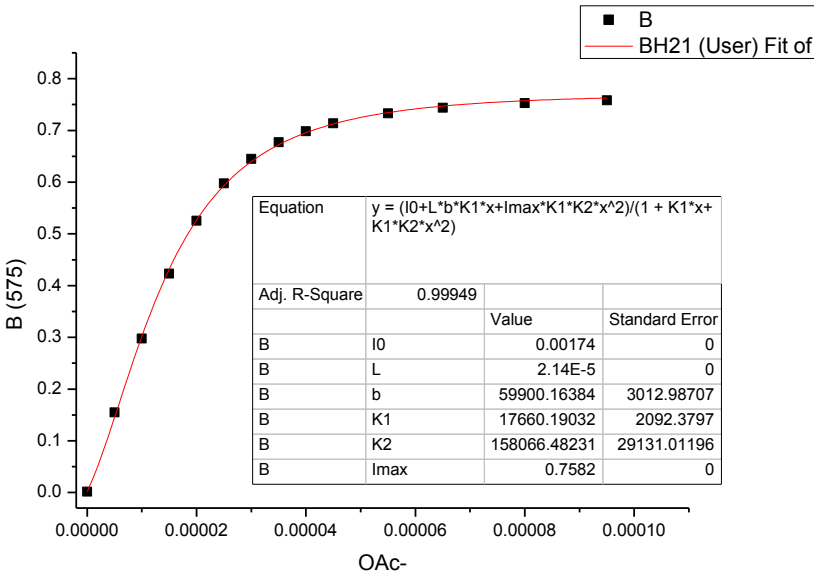

Appendix Figure 6 Non-linear least square fitting curve of compound **34** with TBA OAc

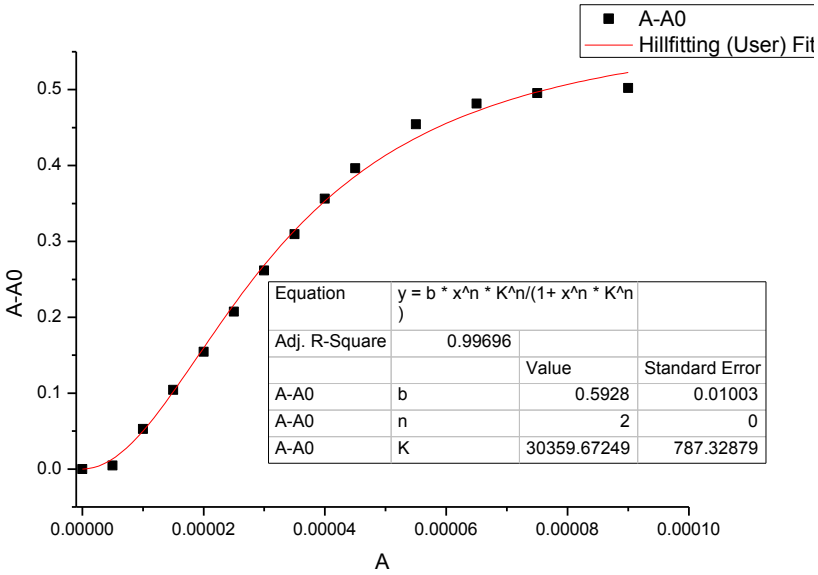

Appendix Figure 7 Non-linear fitting curve of compound **35** with TBAF by Hill equation

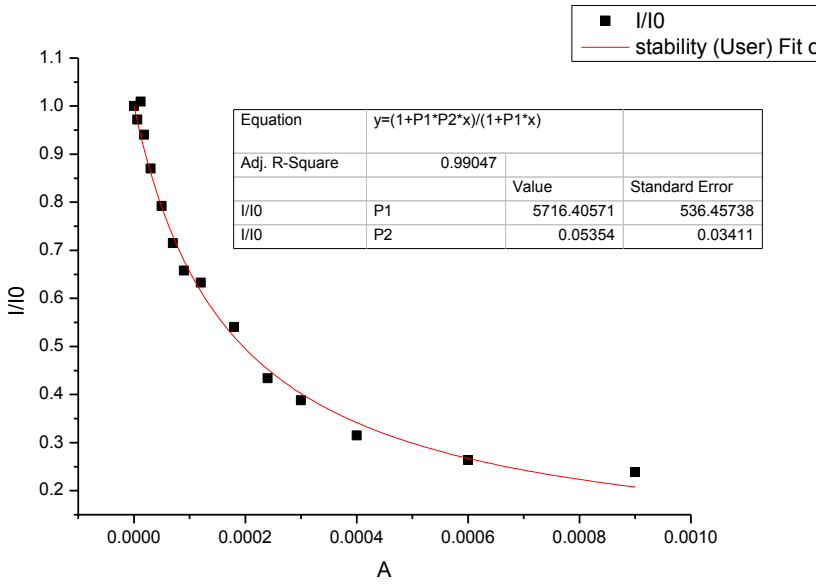

Appendix Figure 8 Non-linear fitting curve of compound **40**

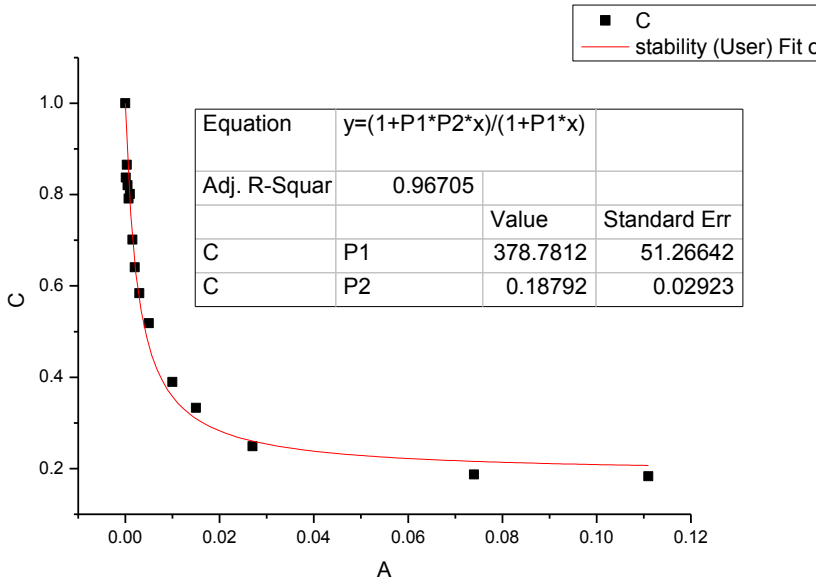

Appendix Figure 9 Non-linear fitting curve of compound **43**

9.2 List NMR spectra

9.2.1 NMR for hydrogel project

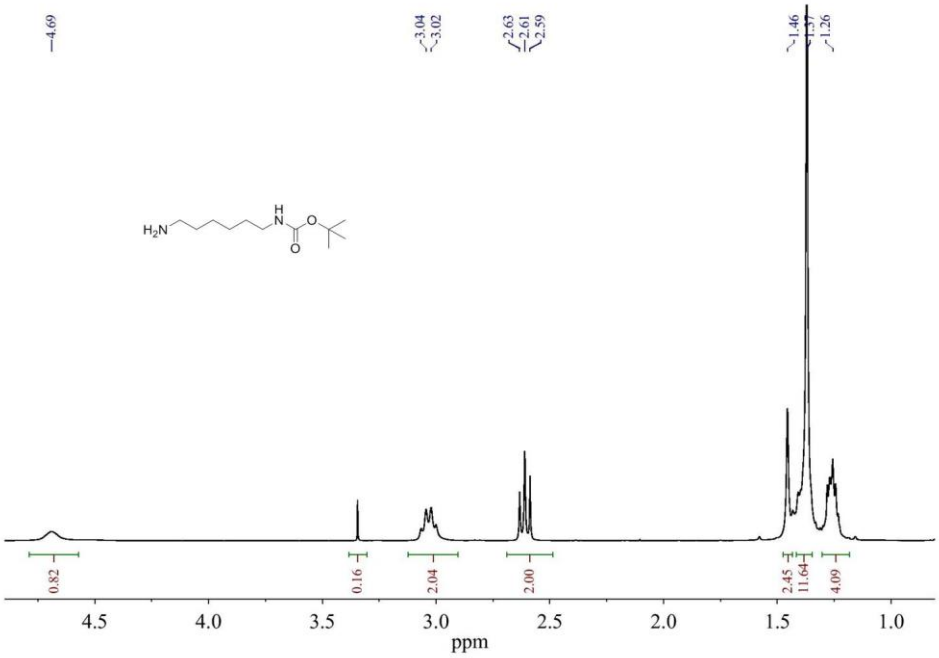

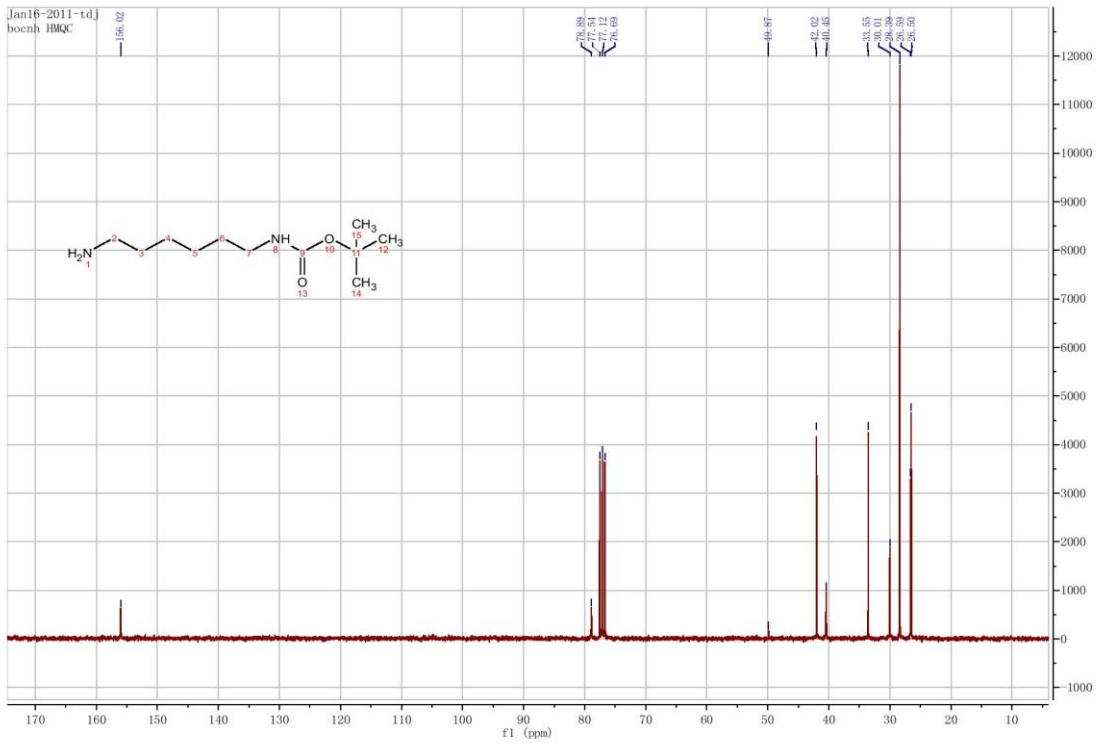

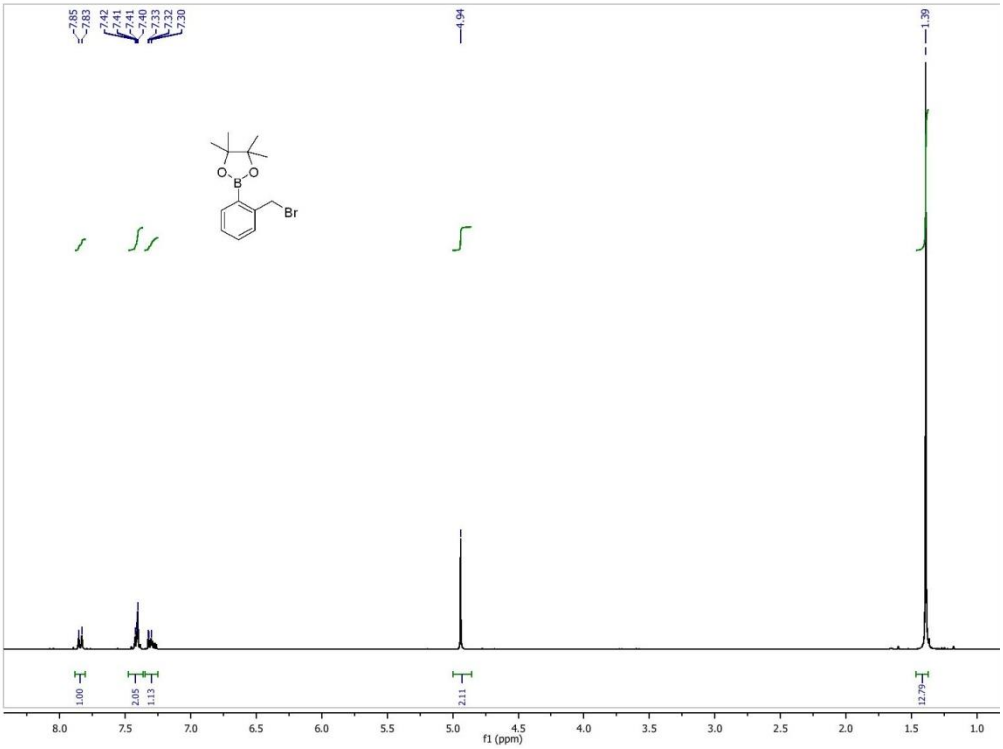
7.85
7.83
7.42
7.41
7.41
7.40
7.33
7.32
7.30
4.94
1.39
Br
1.00
2.05
1.13
2.11
12.79
8.0
7.5
7.0
6.5
6.0
5.5
5.0
4.5
4.0
3.5
3.0
2.5
2.0
1.5
1.0
f1 (ppm)

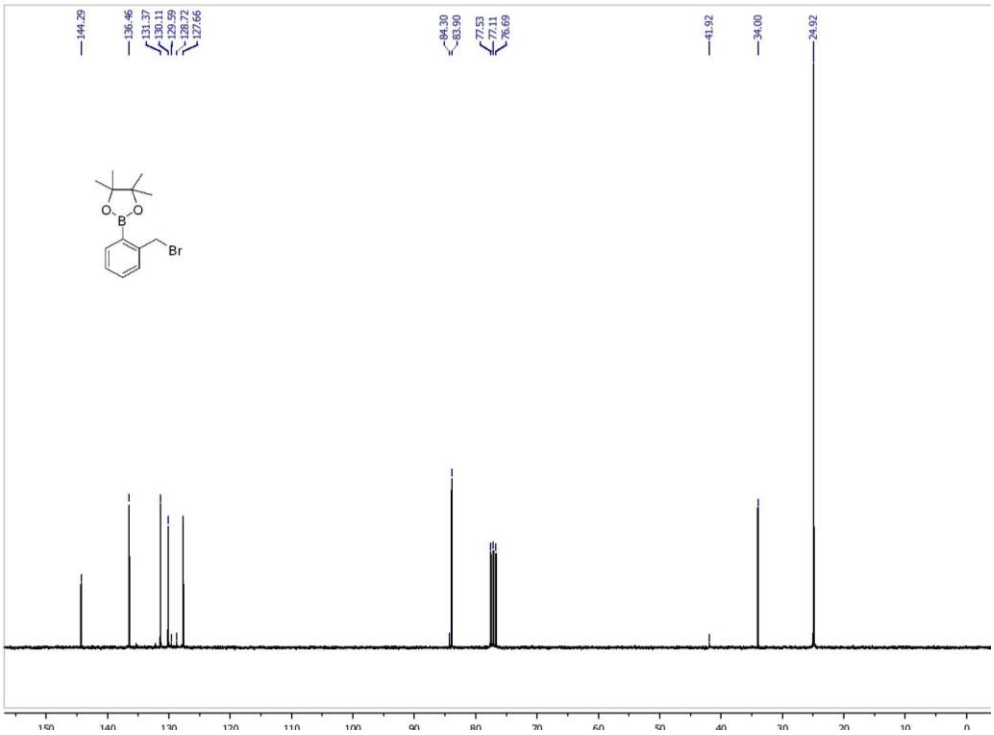
144.29
136.46
131.37
130.11
129.59
128.72
127.66
84.30
83.90
77.53
77.11
76.69
41.92
34.00
24.92
Br

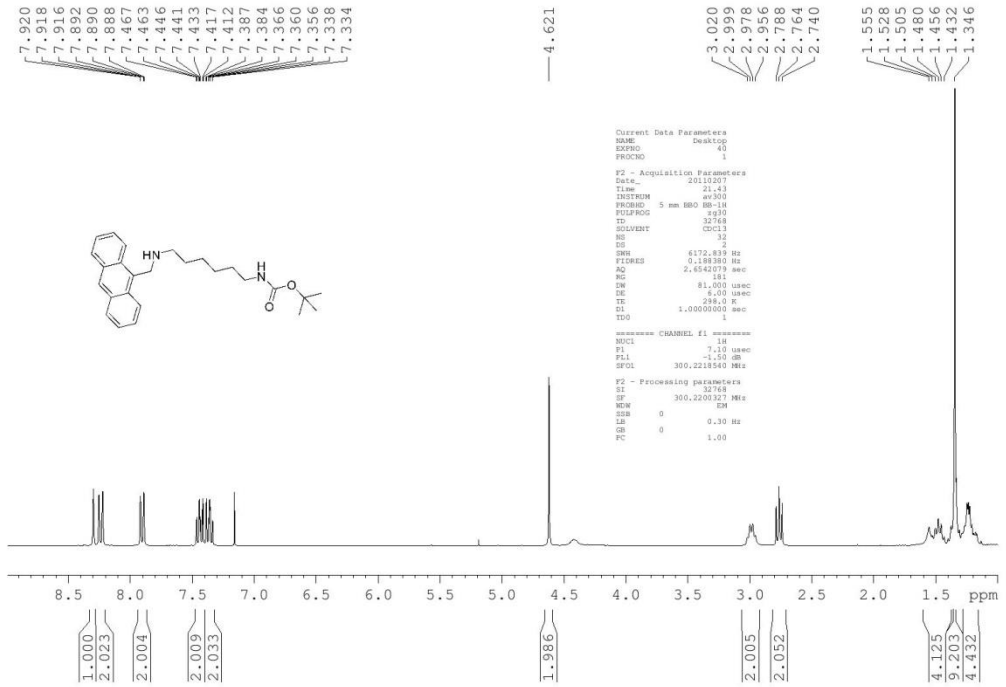
7.920
7.918
7.916
7.892
7.890
7.888
7.467
7.463
7.446
7.441
7.433
7.417
7.412
7.387
7.384
7.366
7.360
7.356
7.338
7.334
4.621
3.020
2.999
2.978
2.956
2.788
2.764
2.740
1.555
1.528
1.505
1.480
1.456
1.432
1.346
HN
H
N
O
O
8.5
8.0
7.5
7.0
6.5
6.0
5.5
5.0
4.5
4.0
3.5
3.0
2.5
2.0
1.5
ppm
1.000
2.023
2.004
2.009
2.033
1.986
2.005
2.052
4.125
9.203
4.432

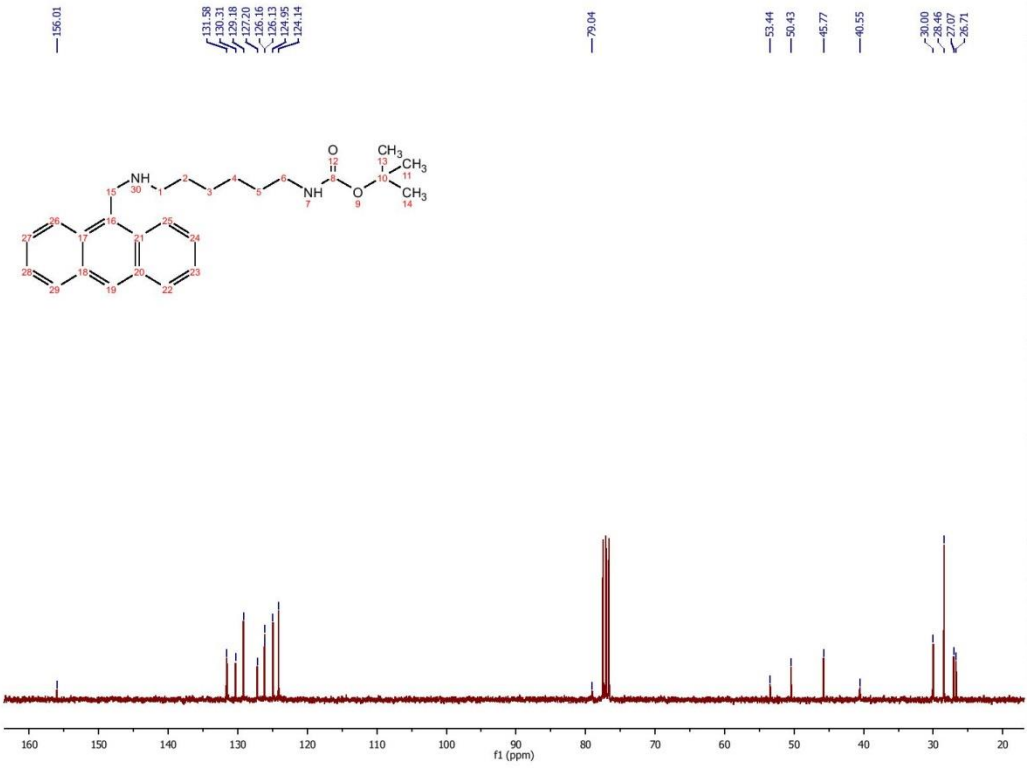
156.01
131.58
130.31
129.18
127.20
126.16
126.13
124.95
124.14
79.04
53.44
50.43
45.77
40.55
30.00
28.46
27.07
26.71
NH
NH
O
O
CH3
CH3
CH3
160
150
140
130
120
110
100
90
80
70
60
50
40
30
20
f1 (ppm)

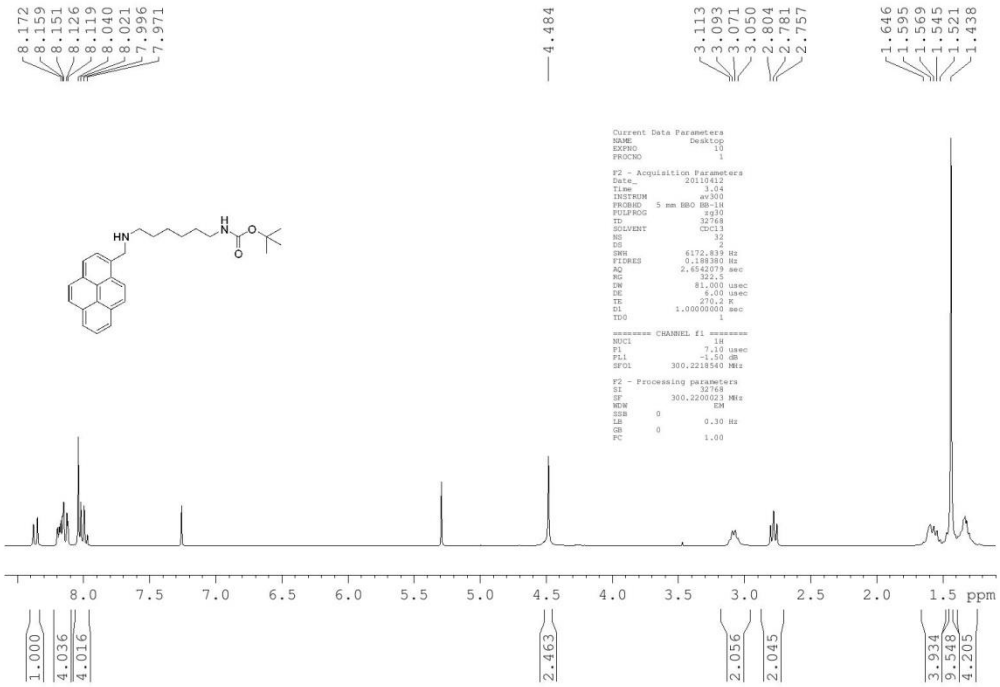
8.172
8.159
8.151
8.126
8.119
8.040
8.021
7.996
7.971
4.484
3.113
3.093
3.071
3.050
2.804
2.781
2.757
1.646
1.595
1.569
1.545
1.521
1.438
HN
O
O
8.0
7.5
7.0
6.5
6.0
5.5
5.0
4.5
4.0
3.5
3.0
2.5
2.0
1.5 ppm
1.000
4.036
4.016
2.463
2.056
2.045
3.934
9.548
4.205

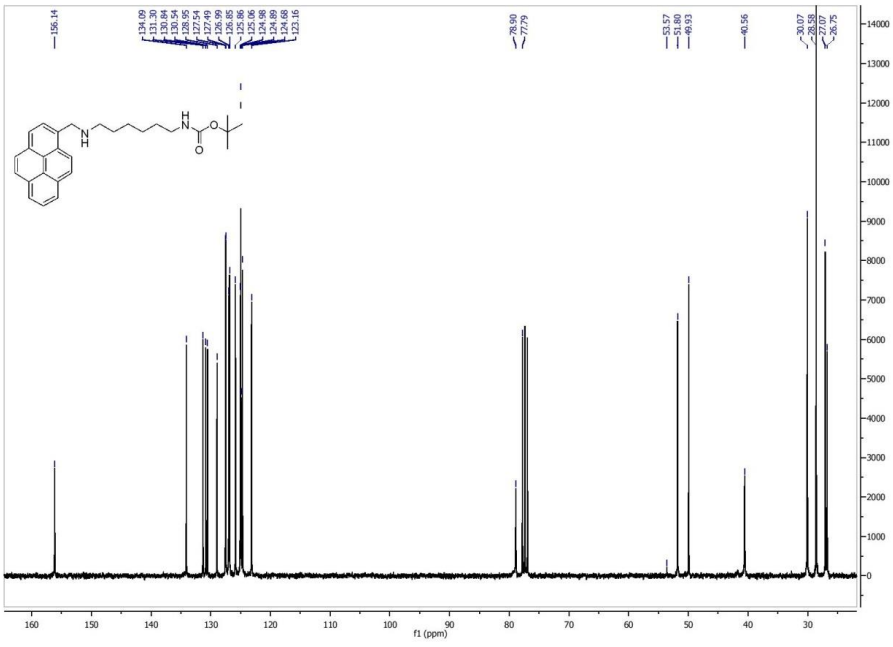
156.14
134.09
131.30
130.84
130.54
129.95
127.54
127.49
126.99
125.85
125.86
125.06
124.98
124.89
124.68
123.16
78.90
77.79
53.57
51.68
40.93
40.56
30.07
28.58
27.07
26.75
HN
O
O
160
150
140
130
120
110
100
90
80
70
60
50
40
30
f1 (ppm)
14000
13000
12000
11000
10000
9000
8000
7000
6000
5000
4000
3000
2000
1000
0

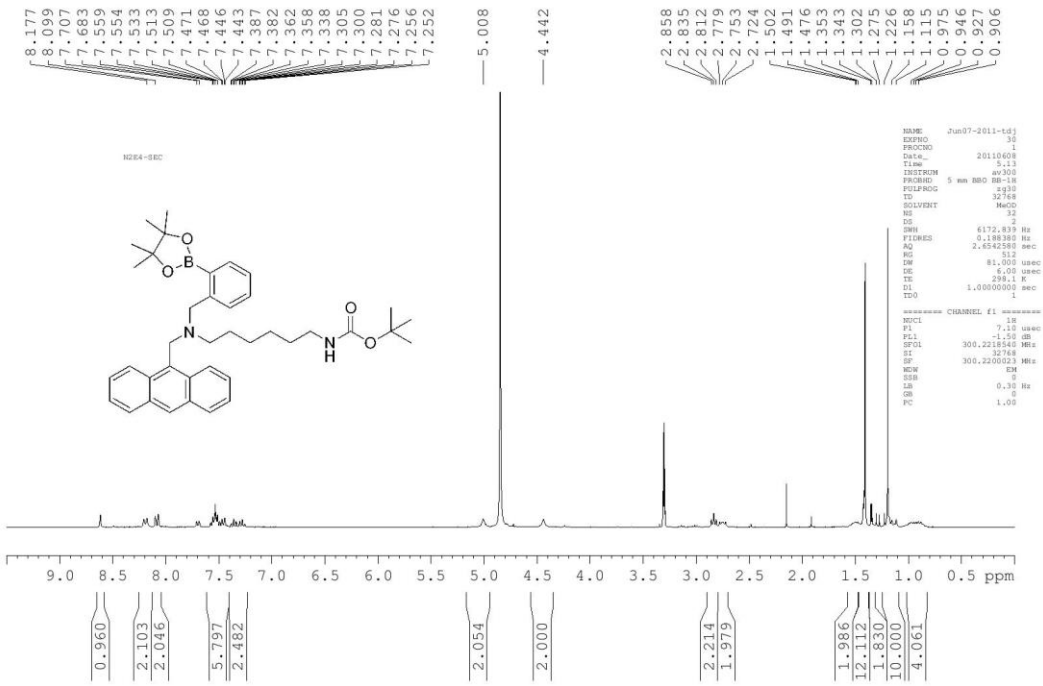

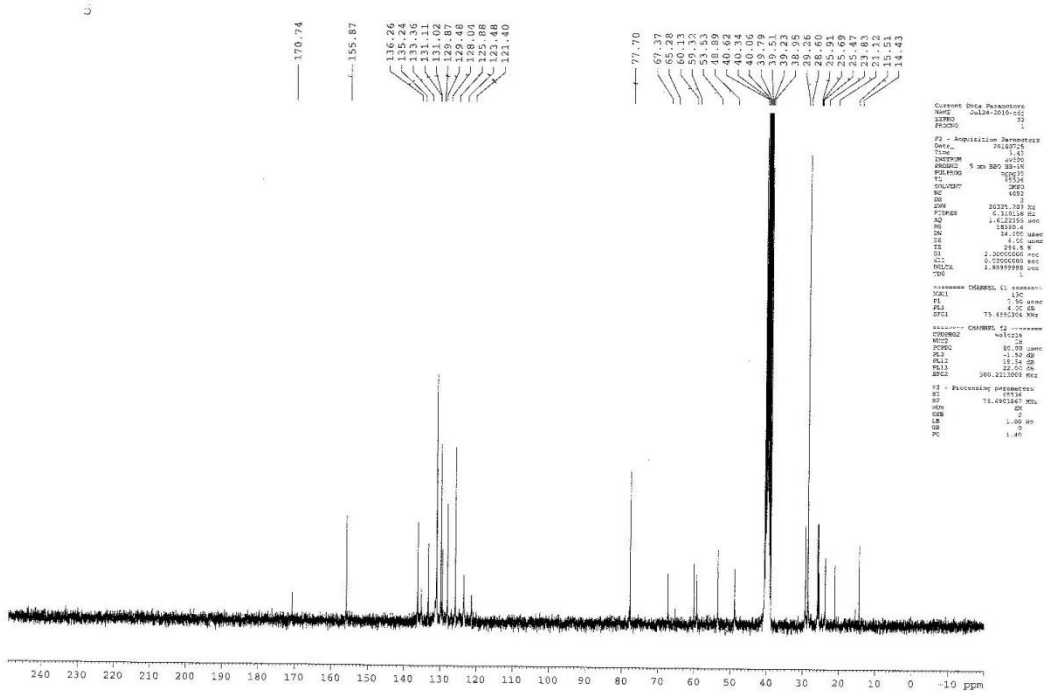

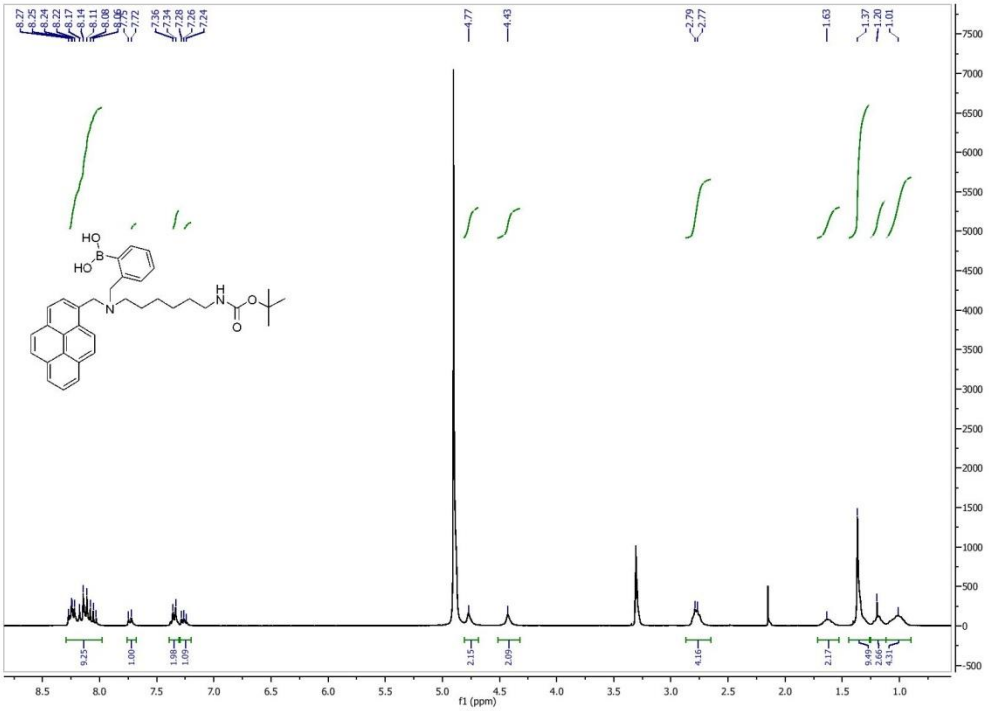

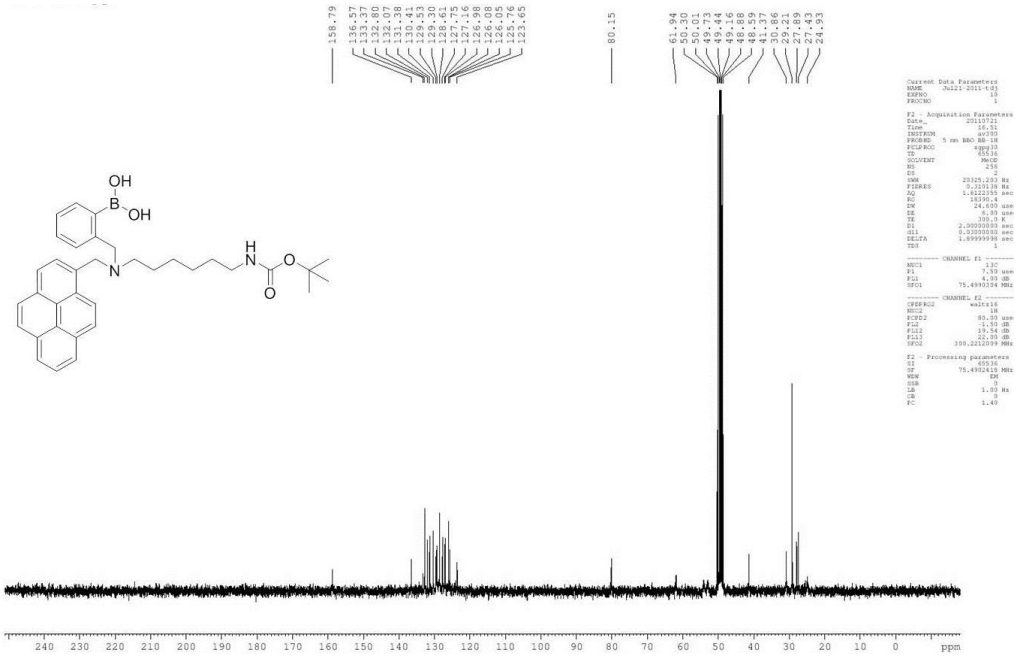

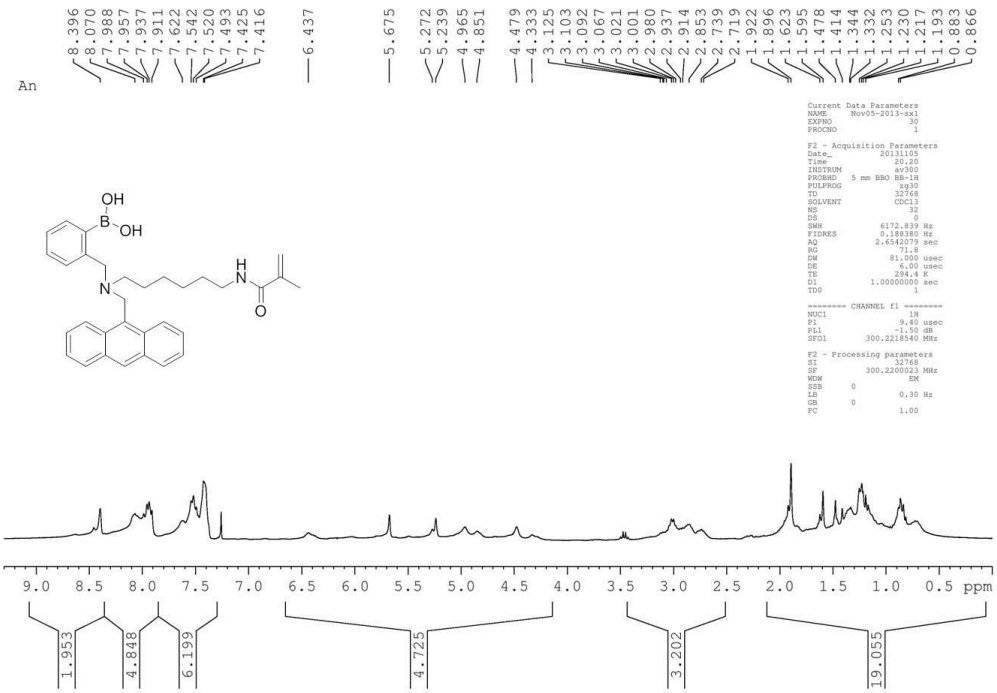
An
8.396
8.070
7.988
7.957
7.937
7.911
7.622
7.542
7.520
7.493
7.425
7.416
6.437
5.675
5.272
5.239
4.965
4.851
4.479
4.333
3.125
3.103
3.092
3.067
3.021
3.001
2.980
2.937
2.914
2.853
2.739
2.719
1.922
1.896
1.623
1.595
1.478
1.414
1.344
1.332
1.253
1.230
1.217
1.193
0.883
0.866
OH
B
OH
H
N
N
O
9.0 8.5 8.0 7.5 7.0 6.5 6.0 5.5 5.0 4.5 4.0 3.5 3.0 2.5 2.0 1.5 1.0 0.5 ppm
1.953
4.848
6.199
4.725
3.202
19.055

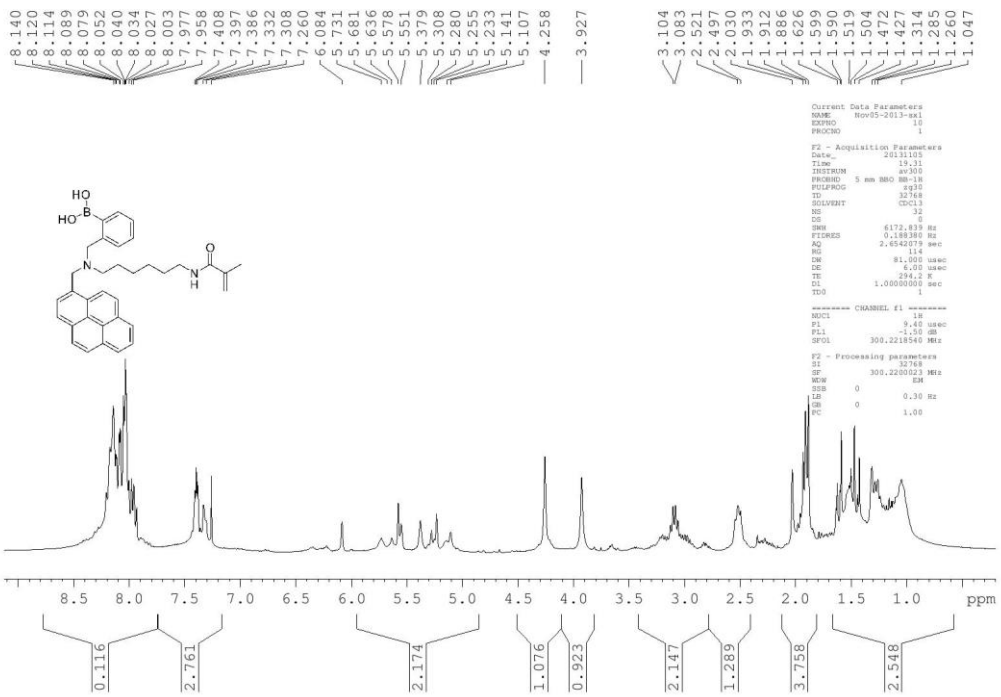
8.140
8.120
8.114
8.089
8.079
8.052
8.040
8.034
8.027
8.003
7.977
7.958
7.408
7.397
7.386
7.332
7.308
7.260
6.084
5.731
5.681
5.636
5.578
5.551
5.379
5.308
5.280
5.255
5.233
5.141
5.107
4.258
3.927
3.104
3.083
2.521
2.497
2.030
1.933
1.912
1.886
1.626
1.599
1.590
1.519
1.504
1.472
1.427
1.314
1.285
1.260
1.047
HO
B
HO
N
H
N
O
8.5 8.0 7.5 7.0 6.5 6.0 5.5 5.0 4.5 4.0 3.5 3.0 2.5 2.0 1.5 1.0 ppm
0.116
2.761
2.174
1.076
0.923
2.147
1.289
3.758
2.548

9.2.2 NMR for naphthalimide derivatives

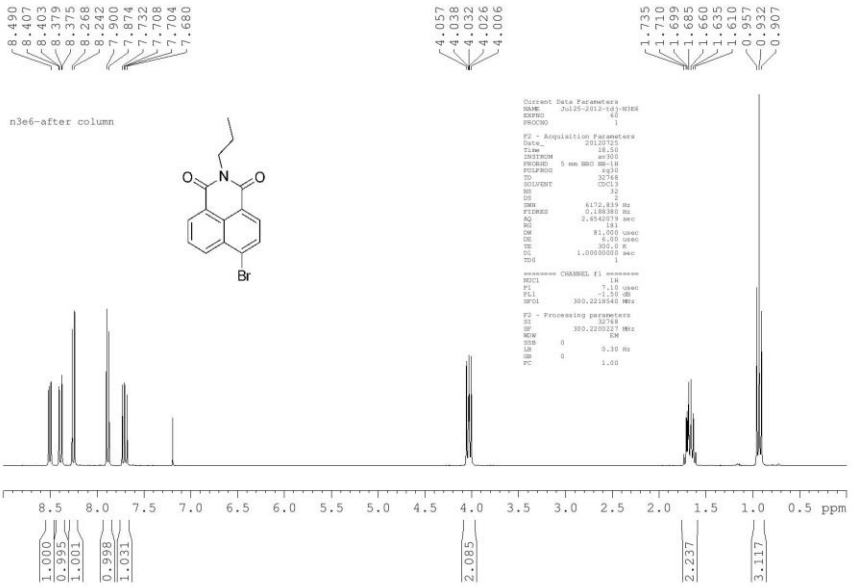

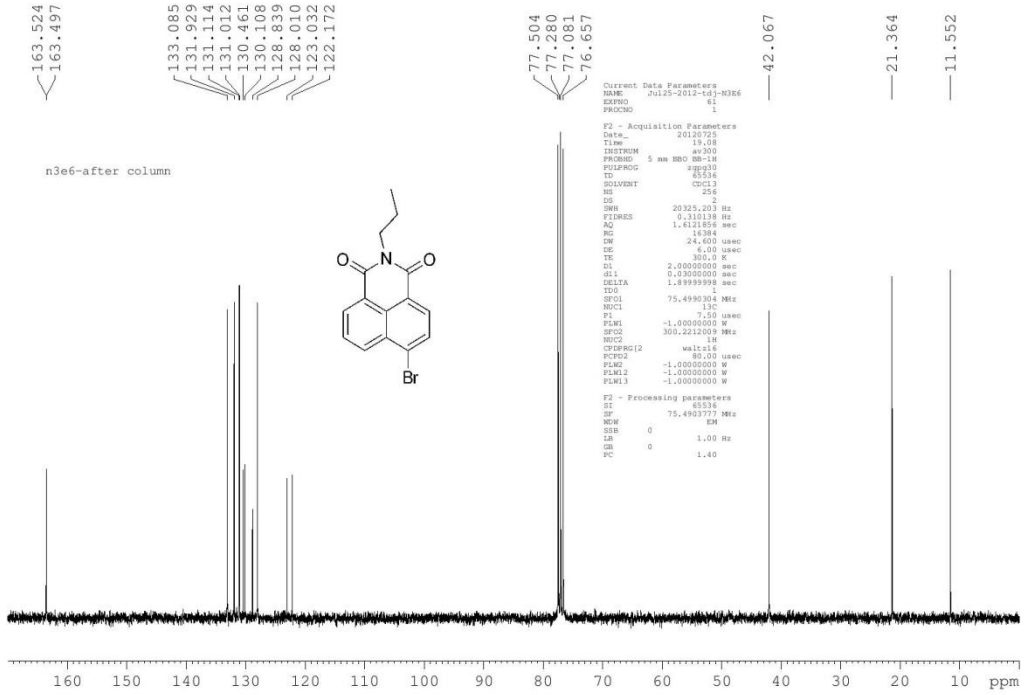

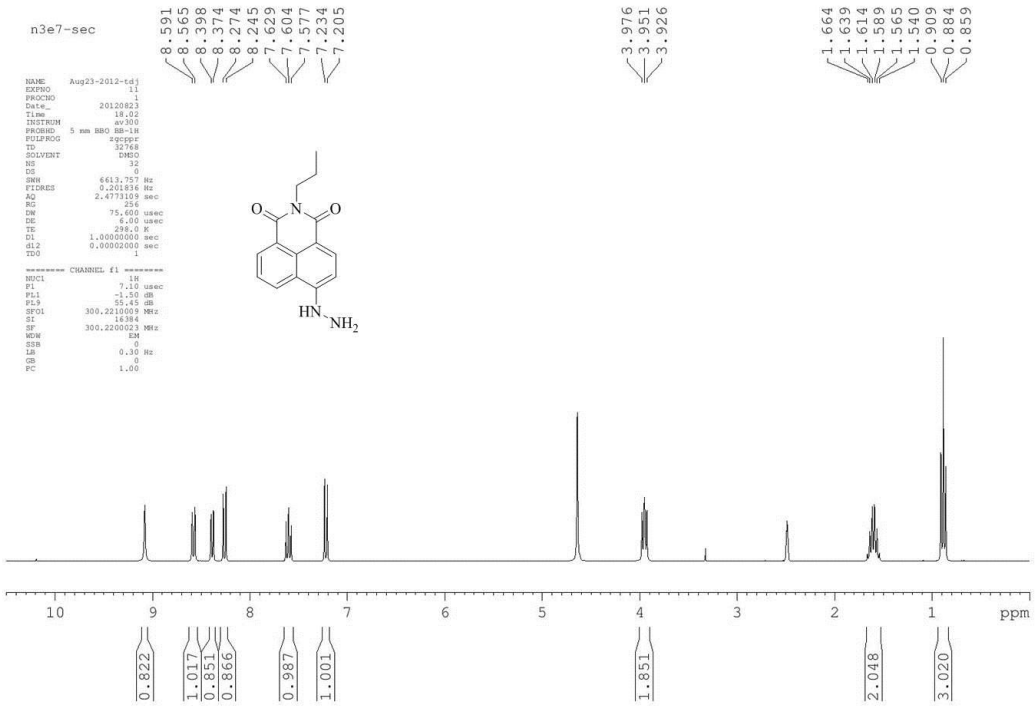
n3e7-sec
8.591
8.565
8.398
8.374
8.274
8.245
7.629
7.604
7.577
7.234
7.205
3.976
3.951
3.926
1.664
1.639
1.614
1.589
1.565
1.540
0.909
0.884
0.859
HN
NH2
10
9
8
7
6
5
4
3
2
1
ppm
0.822
1.017
0.851
0.866
0.987
1.001
1.851
2.048
3.020

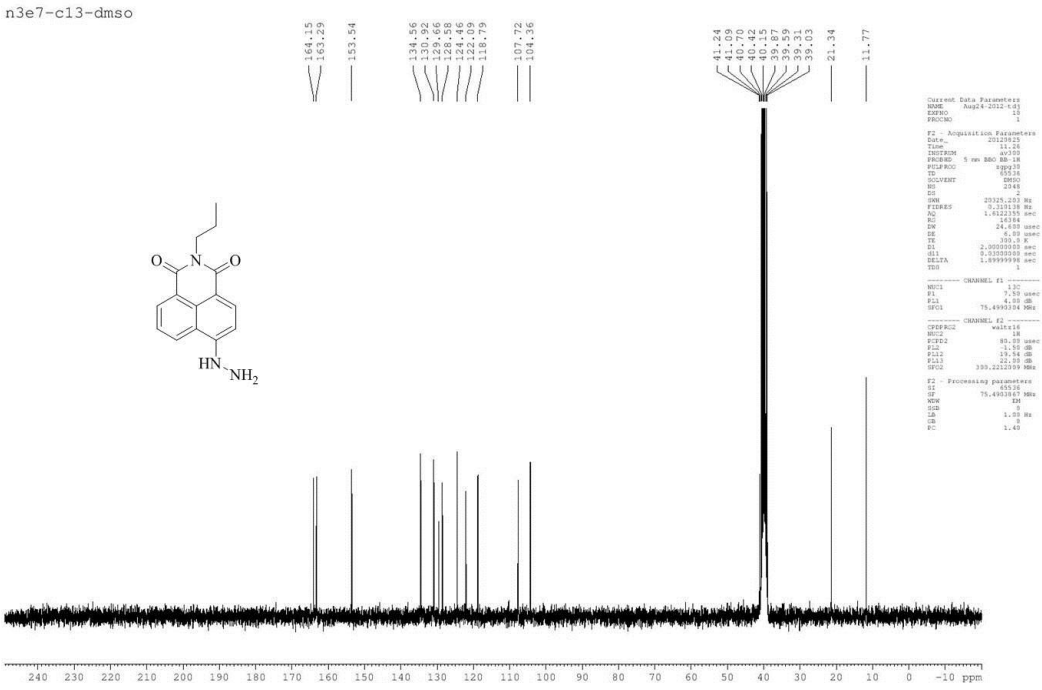
n3e7-c13-dmso
164.15
163.29
153.54
134.56
130.92
129.66
128.58
124.46
122.09
118.79
107.72
104.36
41.24
41.09
40.93
40.42
40.15
39.87
39.59
39.31
39.03
21.34
11.77
HN
NH2
240
230
220
210
200
190
180
170
160
150
140
130
120
110
100
90
80
70
60
50
40
30
20
10
0
-10 ppm

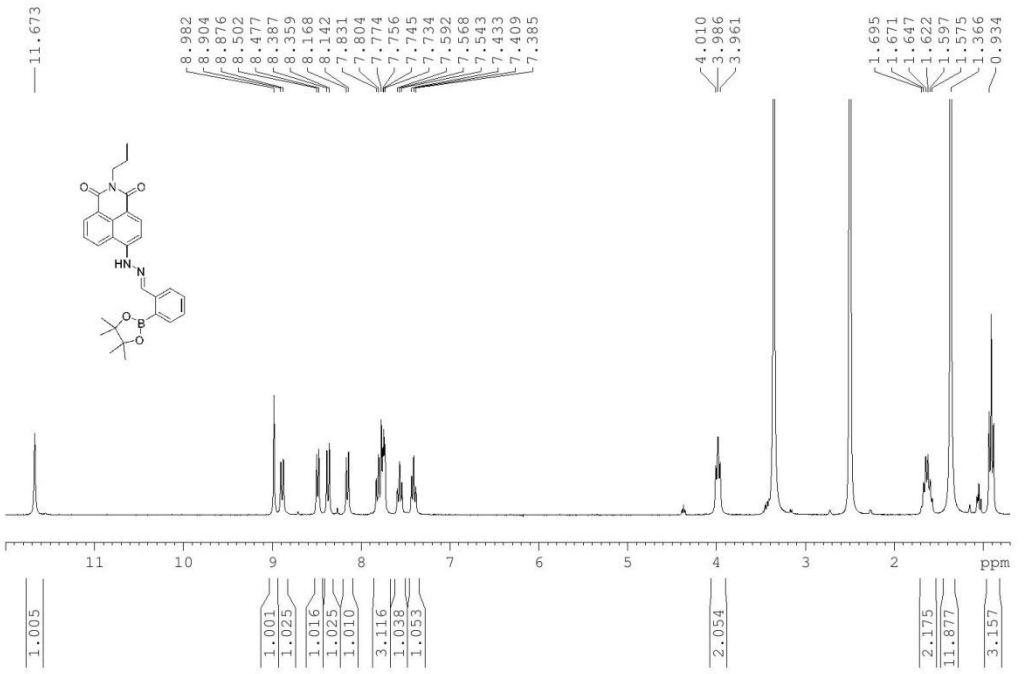
11.673
8.982
8.904
8.876
8.502
8.477
8.387
8.359
8.168
8.142
7.831
7.804
7.774
7.756
7.745
7.734
7.592
7.568
7.543
7.433
7.409
7.385
4.010
3.986
3.961
1.695
1.671
1.647
1.622
1.597
1.575
1.366
0.934
HN
N
O
B
11
10
9
8
7
6
5
4
3
2
ppm
1.005
1.001
1.025
1.016
1.025
1.010
3.116
1.038
1.053
2.054
2.175
11.877
3.157

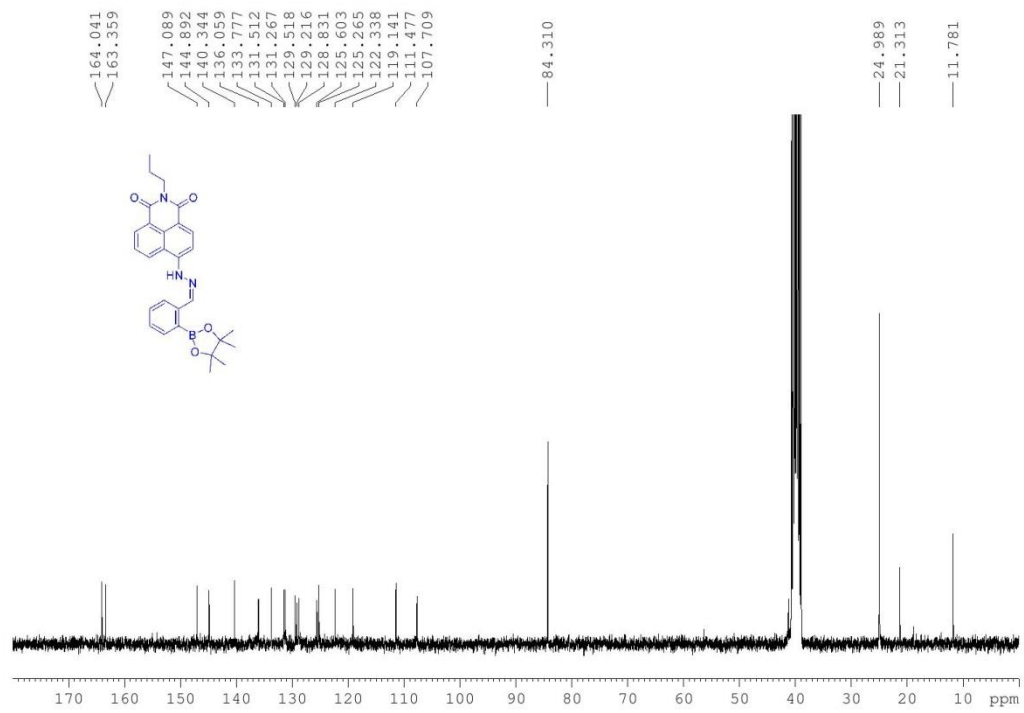
164.041
163.359
147.089
144.892
140.344
136.059
133.777
131.512
131.267
129.518
129.216
128.831
125.603
125.265
122.338
119.141
111.477
107.709
84.310
24.989
21.313
11.781
HN
N
O
B
170
160
150
140
130
120
110
100
90
80
70
60
50
40
30
20
10
ppm

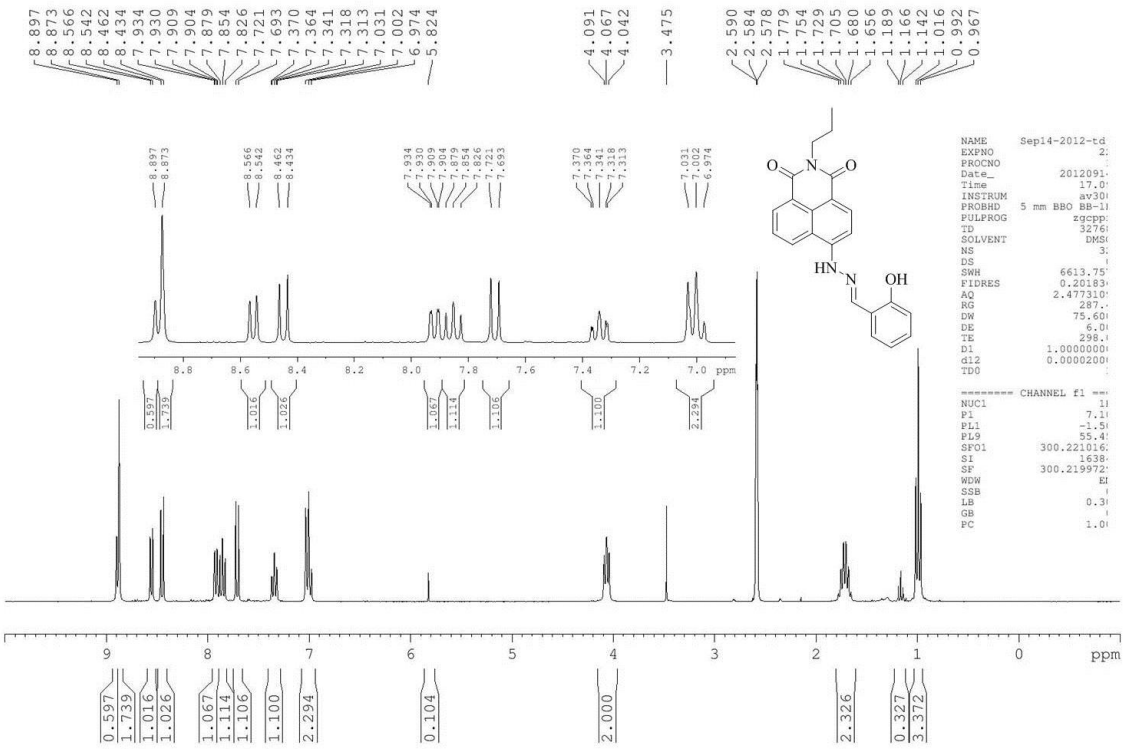

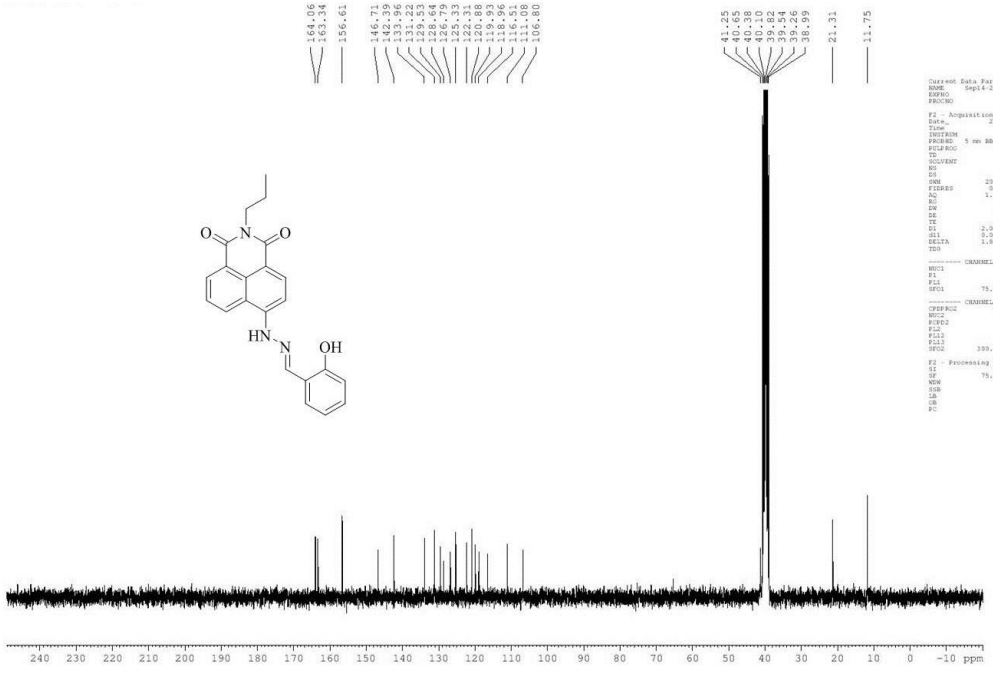

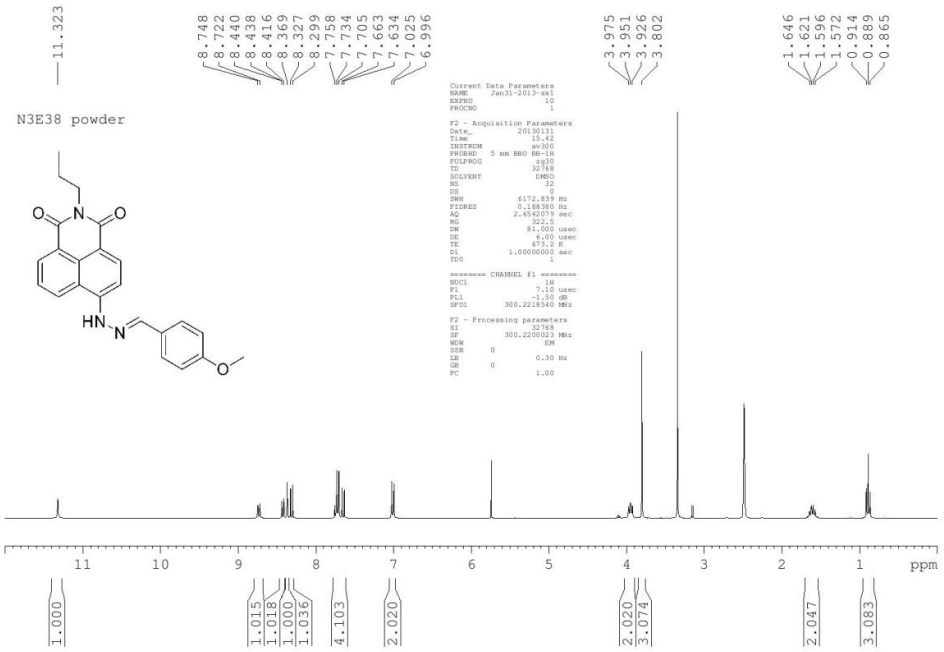
11.323
8.748
8.722
8.440
8.438
8.416
8.369
8.327
8.299
7.758
7.734
7.705
7.663
7.634
7.025
6.996
3.975
3.951
3.926
3.802
1.646
1.621
1.596
1.572
0.914
0.889
0.865
N3E38 powder
HN
N
O
O
O
11
10
9
8
7
6
5
4
3
2
1
ppm
1.000
1.015
1.018
1.000
1.036
4.103
2.020
2.020
3.074
2.047
3.083

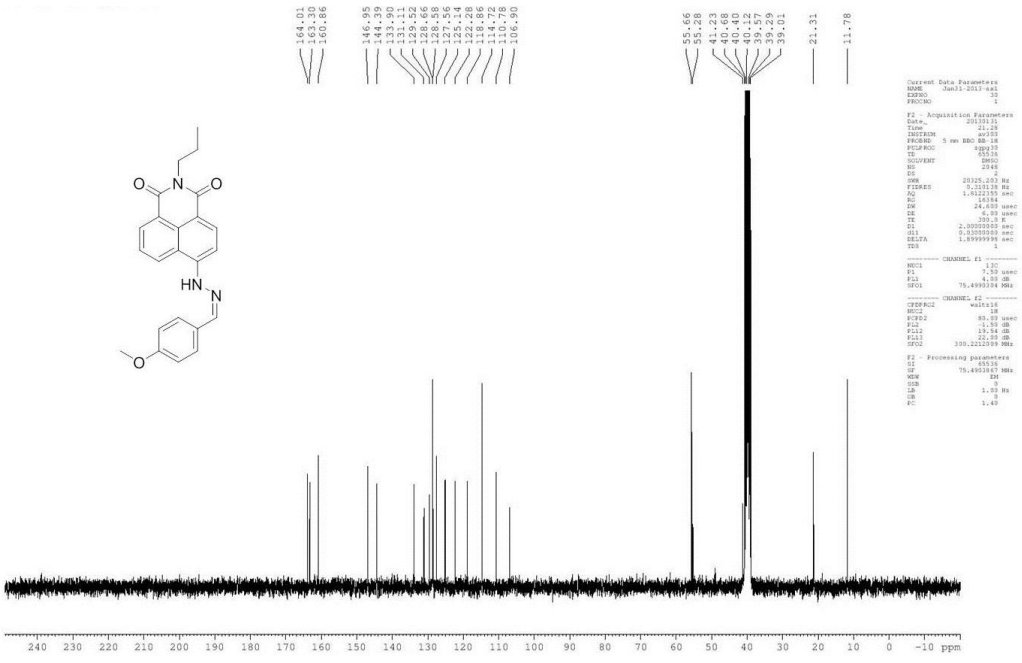
164.01
163.30
160.86
146.95
144.39
133.90
131.11
129.26
128.96
128.58
127.56
125.14
122.88
118.68
114.72
110.78
106.90
55.66
55.28
41.23
40.68
40.40
40.12
39.57
39.29
39.01
21.31
11.78
HN
N
O
O
O
240
230
220
210
200
190
180
170
160
150
140
130
120
110
100
90
80
70
60
50
40
30
20
10
0
-10
ppm

*9.2.3 NMR for compounds **42** and **43***

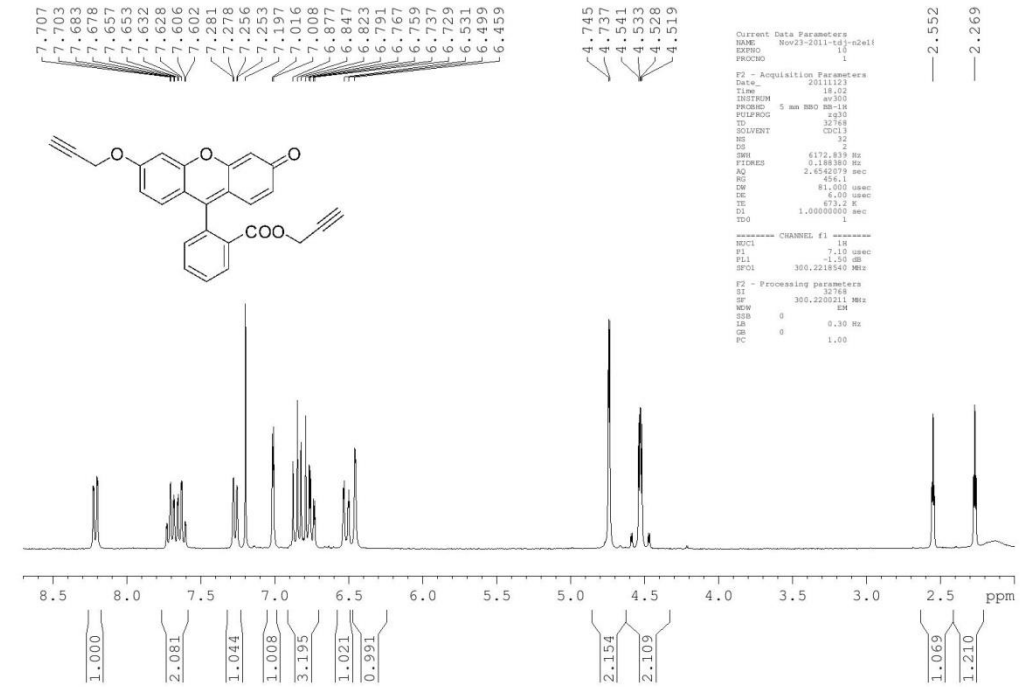

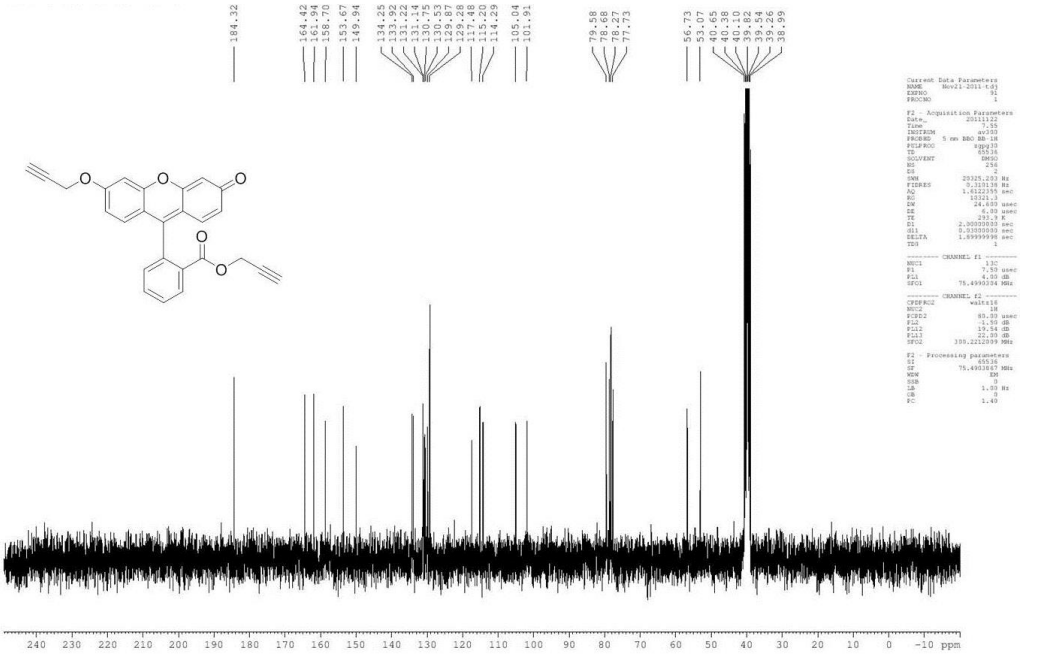

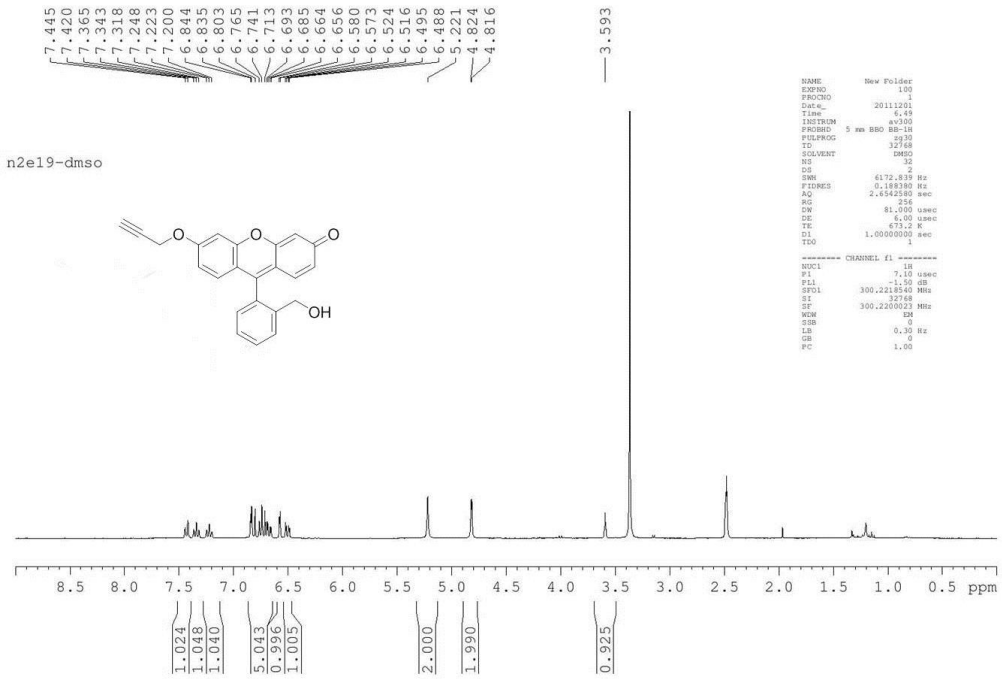
7.445
7.420
7.365
7.343
7.318
7.248
7.223
7.200
6.844
6.835
6.803
6.765
6.741
6.713
6.693
6.685
6.664
6.656
6.580
6.573
6.524
6.516
6.495
6.488
5.221
4.824
4.816
3.593
n2e19-dmso
O
O
O
OH
NAME New Folder
EXPNO 100
PROCNO 1
Date_ 20111201
Time 6.49
INSTRUM av300
PROBHD 5 mm BBO BB-1H
PULPROG zg30
TD 32768
SOLVENT DMSO
NS 32
DS 0
SWH 6172.839 Hz
FIDRES 0.188380 Hz
AQ 2.6542580 sec
RG 256
DW 81.000 usec
DE 6.00 usec
TE 673.2 K
D1 1.00000000 sec
TD0 1
======= CHANNEL f1 =======
NUC1 1H
P1 7.10 usec
PL1 -1.50 dB
SFO1 300.2218540 MHz
SI 32768
SF 300.2200023 MHz
WDW EM
SSB 0
LB 0.30 Hz
GB 0
PC 1.00
8.5 8.0 7.5 7.0 6.5 6.0 5.5 5.0 4.5 4.0 3.5 3.0 2.5 2.0 1.5 1.0 0.5 ppm
1.024
1.048
1.040
5.043
0.996
1.005
2.000
1.990
0.925

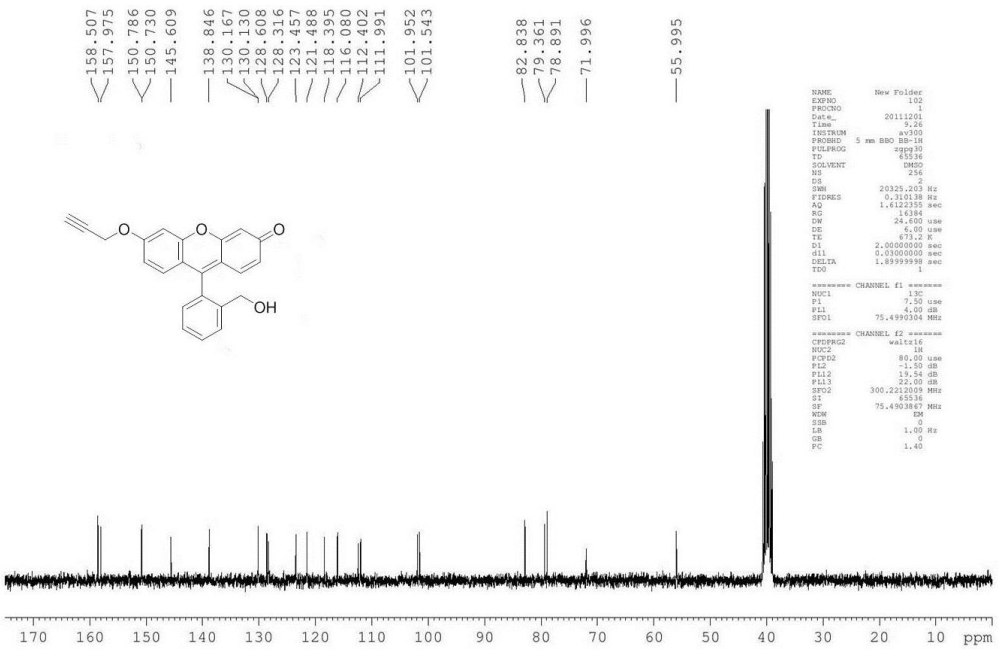
158.507
157.975
150.786
150.730
145.609
138.846
130.167
130.130
128.608
128.316
123.457
121.488
118.395
116.080
112.402
111.991
101.952
101.543
82.838
79.361
78.891
71.996
55.995
O
O
O
OH
NAME New Folder
EXPNO 102
PROCNO 1
Date_ 20111201
Time 9.26
INSTRUM av300
PROBHD 5 mm BBO BB-1H
PULPROG zgpg30
TD 65536
SOLVENT DMSO
NS 256
DS 2
SWH 20325.203 Hz
FIDRES 0.310138 Hz
AQ 1.6122355 sec
RG 16384
DW 24.600 use
DE 6.00 use
TE 673.2 K
D1 2.00000000 sec
d11 0.03000000 sec
DELTA 1.89999998 sec
TD0 1
======= CHANNEL f1 ======
NUC1 13C
P1 7.50 use
PL1 4.00 dB
SFO1 75.4990304 MHz
======= CHANNEL f2 ======
CPDPRG2 waltz16
NUC2 1H
PCPD2 80.00 use
PL2 -1.50 dB
PL12 19.54 dB
PL13 22.00 dB
SFO2 300.2212009 MHz
SI 65536
SF 75.4903867 MHz
WDW EM
SSB 0
LB 1.00 Hz
GB 0
PC 1.40
170 160 150 140 130 120 110 100 90 80 70 60 50 40 30 20 10 ppm